SCREW THEORY BASED DYNAMIC BALANCE METHODS

JAN DE JONG

Screw theory based dynamic balance methods

Jan de Jong

De promotiecommissie is als volgt samengesteld:

Voorzitter en secretaris:	
prof. dr. G.P.M.R. Dewulf	Universiteit Twente
Promotoren:	
prof. dr. ir. D.M. Brouwer PDEng	Universiteit Twente
prof. dr. ir. J.L. Herder	Technische Universiteit Delft
Assistent promotor:	
dr. ir. V. van der Wijk	Technische Universiteit Delft
Leden:	
prof. dr. M. Carricato	Università di Bologna, Italy
dr. ir. M.H.M. Ellenbroek	Universiteit Twente
prof. dr. ir. H.J.F.M. Koopman	Universiteit Twente
Prof. Dr.-Ing. habil A. Müller	Johannes Kepler Universität Linz, Austria

Screw theory based dynamic balance methods
Jan Johannes de Jong
PhD Thesis, University of Twente, Enschede, The Netherlands
February 2020

This work was part of the project 'IN-BALANCE: Inherent Dynamic Balancing for Fast and Accurate Manipulators', number12848, funded by NWO-TTW.

ISBN: 978-90-365-4937-0
DOI 10.3990/1.9789036549370
Cover designed by albertwieringa.nl
Printed by Gildeprint Drukkerijen, Enschede, The Netherlands

SCREW THEORY BASED DYNAMIC BALANCE METHODS

PROEFSCHRIFT

ter verkrijging van
de graad van doctor aan de Universiteit Twente,
op gezag van de rector magnificus,
prof. dr. T.T.M. Palstra,
volgens besluit van het College voor Promoties
in het openbaar te verdedigen
op vrijdag 7 februari 2020 om 14:45 uur

door

Jan Johannes de Jong

geboren op 14 september 1986
te Bellville, Zuid-Afrika

Dit proefschrift is goedgekeurd door de promotoren:
prof. dr. ir. D.M. Brouwer PDEng
prof. dr. ir. J.L. Herder

en door de assistent promotor:
dr. ir. V. van der Wijk

Summary

High-speed robots induce large fluctuating reaction forces and moments on their supports, inducing disruptive vibrations and limiting the precision at the end-effector. *Dynamic balance* targets these fluctuating reaction forces and moments to enable robots that are both fast and precise. This can be achieved by adding counter-mechanisms such as counter-rotating balance shafts or duplicate mirrored mechanisms, potentially leading to an unfavourable increase in complexity, mass and motor torque. Fortunately, a few parallel mechanisms are known that may be balanced by a specific design of the mass distribution, potentially enabling simple, low-weight and cost-effective balance solutions. The design process of this particular class of mechanisms is however impeded by the intricacy of the dynamic balance conditions. These conditions typically contain complex kinematic models to ensure that dynamic balance holds for all poses, velocities and accelerations of parallel mechanisms. Especially for spatial mechanisms with multiple degrees of freedom (DOF), it is difficult to find new dynamically balanced solutions. Another obstacle in the balance process is that it is not fully known which types of mechanisms can be dynamically balanced by design of the mass distribution, i.e. without resorting to complex and costly counter-mechanisms.

This thesis therefore aims to provide analytic tools to extract and solve the dynamic balance conditions in a uniform manner and find mechanisms that can be balanced in a favourable way. To that end, screw theory is used throughout this thesis as it combines a geometric, spatial interpretation of rigid body motion with a concise and systematic description of differential kinematics and dynamics.

This resulted in three screw theory based dynamic balance methods. The *instantaneous dynamic balance method* solves the necessary conditions for dynamic balance in a direct and geometric manner, resulting in parallel, spatial and multi-DOF mechanisms that are dynamically balanced in a single pose. In this pose the robot accelerations will not induce shaking forces and moments. Further away from this pose, the balance quality, typically worsens. Yet, when combined with partial balancing, the dynamic balance is extended over multiple paths that intersect in this pose, leading to wider choice of dynamically balanced motion. Based on this, a 2-DOF demonstrator is designed, the Fuga I, which is dynamically balanced for motion over two paths that intersect perpendicularly in the middle of the workspace. Measurements confirm the path balance as well as the instantaneously dynamically balanced pose of this demonstrator.

The *higher-order dynamic balance method* expands dynamic balance over the complete workspace by including a sufficient number of higher-order partial derivatives of the dynamic balance conditions. The resulting necessary

and sufficient conditions are linear in the inertial parameters such that null space algorithms provide all possible dynamically balanced designs for any type of nonsingular linkage. To aid the designer, a partitioning and multipole-interpretation of the resulting design space is presented, leading to the design of a spatially moving 3-RSR mechanism that is dynamically balanced for 2-DOF motion on three symmetric planes.

The *pure-inertia method* treats a specific class of mechanisms, the symmetric subspace motion generators. It is shown that two prominent examples in the dynamic balance literature share kinematic mirror symmetry and a mass distribution of the links that is equivalent to pure moments of inertia. Based on these observations, a novel 2-DOF planar dynamically balanced mechanism is presented.

These three dynamic balance methods provide the means to solve the dynamic balance conditions of arbitrary linkages and a direction for the search of new kinematic structures that permit simple and efficient dynamic balance solutions.

Samenvatting

Frametrillingen zijn ongewenst voor hoge-precisie robotica. Echter, hoe sneller een robot beweegt, des te groter deze ongewenste trillingen worden. Dit komt voornamelijk doordat robots zich tijdens de beweging afzetten tegen het basisframe; het frame gaat vervolgens trillen en geeft deze ongewenste trilling ook door aan de eindeffector, de vloer en eventuele precisie-instrumenten in de omgeving. Grotere versnellingen resulteren in grotere variërende reactiekrachten (schudkrachten) en reactiemomenten (schudmomenten) en dus in meer trillingen. Dit betekend dat hoge precisie en hoge doorvoersnelheid conflicterende ontwerpeisen zijn.

Door het robotmechanisme *dynamisch te balanceren* kunnen deze ongewenste frametrillingen tegen worden gegaan om de combinatie van hoge snelheid en hoge precisie mogelijk te maken. Bij een dynamisch gebalanceerd mechanisme zijn de onderdelen zo ontworpen dat ze precies tegenovergestelde bewegingen maken waardoor het frame geen schudkrachten en schudmomenten hoeft te weerstaan. Dit kan door bijvoorbeeld door het mechanisme uit te breiden met contragewichten en contraroterende elementen. Dit leidt echter ook tot complexe, zware en economisch minder rendabele robots.

Gelukkig bestaan er ook enkele mechanismen met gesloten ketens die dynamisch gebalanceerd kunnen worden door een specifieke keuze van armlengtes en massaverdelingen zodat er geen extra contra-elementen nodig zijn. Het blijkt echter lastig om deze effectieve balansoplossingen te vinden, zeker voor ruimtelijk bewegende, parallelle mechanismen met meerdere vrijheidsgraden. Momenteel bestaat er geen systematische, algemene en volledige balansaanpak, waardoor de kinematische en dynamische vergelijkingen op een handmatige manier opgelost moeten worden. Daarnaast is het nog niet duidelijk welke typen mechanismen zonder extra, zware en complexe contraroterende elementen gebalanceerd kunnen worden. Dit maakt dynamisch balanceren tot een tijdrovend trial-and-error proces.

Dit proefschrift is gericht op een systematische methode om de dynamische balansvergelijkingen op te stellen en op te lossen zodat er eenvoudig nieuwe en efficiënt gebalanceerde ontwerpen gevonden kunnen worden. Daartoe wordt in dit proefschrift de schroeftheorie toegepast. De schroeftheorie is een wiskundig raamwerk dat een systematische en beknopte beschrijving geeft van de differentiële kinematica en dynamica. Bovendien geeft het daarbij een geometrische interpretatie van ruimtelijke bewegingen waardoor de gevonden oplossingen eenvoudig te visualiseren en te interpreteren zijn.

Dit resulteert in drie dynamische balansmethoden. De eerste, de *momentane dynamische balansmethode*, lost de noodzakelijke balansvoorwaarden op

door middel van de geometrische beschrijving van de schroeftheorie. Deze balansoplossing geldt echter maar in één gekozen stand. In deze stand wekken de versnellingen van de robot geen schudkrachten of schudmoment op. Voor andere standen is de dynamische balans niet gegarandeerd. In combinatie met trajectbalans wordt deze specifieke stand het snijpunt van meerdere gebalanceerde trajecten, zodat er een groter werkgebied op een gebalanceerde wijze bereikt kan worden. Op basis van deze methode is er een proefopstelling ontwikkeld met twee vrijheidsgraden, de Fuga I. Deze robot is dynamisch gebalanceerd voor bewegingen over twee trajecten die elkaar haaks snijden in het midden van het werkgebied. Metingen aan deze opstelling bevestigen zowel de trajectbalans als de stand waarin de momentane dynamische balans geldt.

De *hogere-orde dynamische balansmethode* breidt deze dynamisch gebalanceerde stand uit over het gehele werkgebied door een voldoende aantal hogere partiële afgeleiden van de balansvoorwaarden mee te nemen. Dit resulteert in de noodzakelijk en voldoende balansvoorwaarden die bovendien lineair zijn in de inertiële parameters. Met behulp van nulruimte-algoritmen geeft dit alle mogelijke dynamische balansoplossingen voor een willekeurig, niet-singulier mechanisme dat bestaat uit eenvoudige scharnieren. De resulterende ontwerpruimte, de nulruimte, wordt gesplitst aan de hand van de seriële kettingen waaruit het mechanisme is opgebouwd. Vervolgens wordt deze ontwerpruimte weergegeven met de veelpool-representatie zodat de oplossing eenvoudiger te interpreteren is. Dit leidt tot een 3-RSR mechanisme dat dynamisch gebalanceerd is voor bewegingen in drie spiegelsymmetrische vlakken.

De *methode van een puur traagheidsmoment* is gericht op de dynamische balans van een specifieke klasse van mechanismen, de bewegingsvoortbrengers van een symmetrische deelruimte. Spiegelsymmetrie blijkt de basis te zijn voor twee prominente voorbeelden van dynamisch gebalanceerde mechanismen uit de literatuur. Daarnaast blijkt dat de massaverdeling van de lichamen equivalent is aan een puur traagheidsmoment. Op basis van deze twee observaties wordt er een nieuw spiegelsymmetrisch mechanisme gepresenteerd dat dynamisch gebalanceerd is voor de twee vrijheidsgraden.

Deze drie dynamische balansmethoden bieden naast de oplossingswijze ook een richting voor de zoektocht naar nieuwe kinematische structuren die gebalanceerd kunnen worden op een simpele en efficiënte wijze.

Contents

Chapter 1

Introduction

Dynamic balance removes disruptive base vibrations of high-speed robots by eliminating the dynamic reaction forces and moments. This design principle aims to provide robots that combine a high throughput with a high end-effector accuracy. This chapter discusses the need for dynamic balance and the possibilities and limitations of current dynamic balance techniques, leading to the research objectives and the outline of this thesis.

1.1 Dynamic balance and its potential for industrial robots

High-speed robots have a problem: they induce large fluctuating reaction forces and moments on their base and surroundings, exciting vibrations and noise, and disrupting of neighbouring robot cells or precision equipment [67, 55, 73, 108]. These *shaking forces* and *shaking moments* are caused by rapid acceleration and deceleration of the load, links, motors and other components of the robot. Large and heavy support structures, additional dampers and passive or active vibration isolation are used to mitigate these vibration effects [39, 56].

Instead of dealing with the adverse effects, dynamic balance treats these vibrations at the source by reducing or eliminating the shaking forces and moments through a specific design of the mechanism, for example by addition of counter-mechanisms, mirrored mechanisms or by design of the mechanism's kinematics and mass distribution, i.e. the mass, centre of mass (COM) and moments of inertia (MOIs) of the moving links [67, 68, 5, 4]. In a dynamically balanced mechanism, all links counteract each other exactly, leading to stationary net interface forces and moments of the mechanism as whole. A mechanism is *force balanced* when the shaking forces are zero, *moment-balanced* when the shaking moments are zero, and *dynamically balanced* when both the shaking forces and moments are zero (Fig. 1.1). Note that in this definition the base is assumed fixed, such that relative motion of mechanism with respect to the base completely determines its dynamics.

Dynamic balance is of interest to high-speed robots for two reasons. Firstly, a dynamically balanced robot induces no vibrations of the base and surroundings

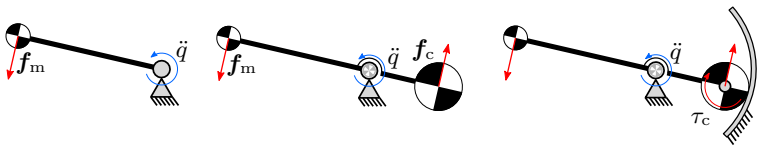

Figure 1.1: (a) A hinged lever arm induces a fluctuating reaction force $\boldsymbol{f}_m$ on the base during motion, joint acceleration $\ddot{q}$ in this case. (b) By addition of a countermass force is balanced by $\boldsymbol{f}_c$ and the common COM (depicted in grey) is made stationary. (c) The shaking moment may be cancelled by additional counter-rotating devices, such a counter-rotating countermass [47].

since the loads on the base are stationary [68, 2, 5]. Therefore, dynamic balance potentially increases the precision of the robot's end-effector as well as the sensors, and precision-mechanisms in the vicinity. Secondly, a dynamically balanced robot is also highly dynamically decoupled [107]. This means that — under the assumption of rigid body dynamics — the motion of the base will induce no or reduced internal forces and moments on the robot. A dynamically decoupled mechanism therefore moves with the base as if it were a rigid body, allowing for a precise positioning with respect to the moving base. For example, when a dynamically decoupled short stroke robot is placed on a high-speed long stroke robot, the accelerations of the long stroke will induce no disrupting forces and moments on the short stroke and vice versa, allowing for a fine end-effector positioning [55]. This is in contrast to vibration isolation techniques, such as active hard mount vibration isolation [94, 95], that maintain precision with respect to the inertial frame of reference. Moreover, these techniques due transmit shaking forces and moments depending on effective moving mass and the bandwidth of the vibration isolation.

Besides the application in high-speed robotics, dynamic balance is also of interest in other fields where vibrations are detrimental, such as telescopes [86], space manipulation [1, 63] and hand-held tools [107]. It should furthermore be noted that force balance leads to a fixed (or constant velocity of the) common COM of the mechanism [46].This is for example to increase the load-bearing capacity of slow-moving, heavy-duty robots [21, 37].

In the past, the dynamic balance principle has been applied to single degree of freedom (DOF), constant-speed machines such as steam locomotives (Fig. 1.2a), internal combustion engines (Fig. 1.2b), and industrial sewing machines [35]. Their cycle times could thereby be reduced without amplifying the dynamic loads that would lead to wear and uncomfortable vibrations. Motor cycles engines, for example, consist of several countermasses and counter-rotating balance shafts to balance the rectilinear, reciprocating motion of the pistons, allowing for a comfortable ride at high speeds [110] (Fig. 1.2c). With a similar trend in robotics [51, 82], i.e. a desired reduction of the cycle times without the adverse effects of vibrations, it is urgent to extend dynamic balance to these multi-DOF, spatially moving mechanisms with varying trajectories while keeping the structures simple and low in weight.

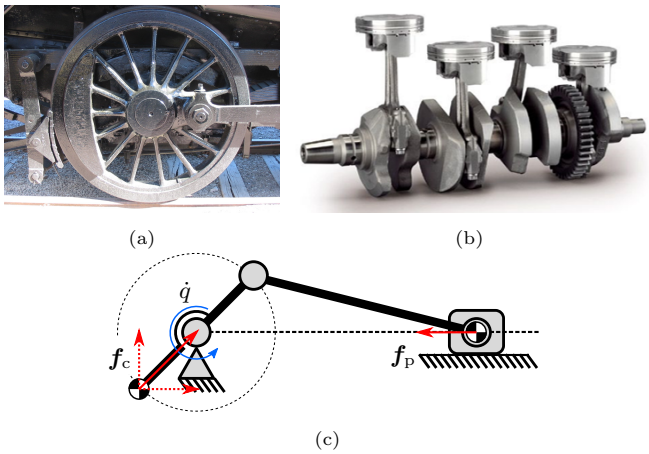

Figure 1.2: Balance masses (a) in the wheels of steam locomotives and (b) on the crankshafts of combustion engines partly balance the reciprocal motion of the pistons [110]. (c) The first harmonic, inline component of shaking forces $\boldsymbol{f}_\mathrm{p}$ of the piston is compensated by the inertial force $\boldsymbol{f}_\mathrm{c}$, induced by the rotational velocity $\dot{\boldsymbol{q}}$ of the countermasses. Other pistons and counter-rotating balance shafts, which are not shown here, balance the remaining shaking forces and moments. ((a) Photograph by Sean Lamb, distributed under a CC-BY-AS 2.0 license. (b) Yamaha YZF-R1 crossplane crankshaft, accessed on 23 December 2019 `www.yamaha-motor.eu`)

1.2 State-of-the-art dynamic balance methods

The dynamic balance methods may be divided according to their respective starting point, leading to two main categories. On the one hand, the *analysis methods* start from given a kinematic design and search for mass distributions that result in a dynamically balanced mechanism. The *synthesis methods* on the other hand, initially leave the kinematic design open, but start with a set of elementary dynamically balanced modules or concepts that are stacked, combined or modified, to come up with a dynamically balanced mechanism to fulfils the desired motion requirements. The analysis methods are therefore used when the kinematics are given and the mass distribution is open, while the synthesis methods are applicable when both the kinematics and mass distribution are free to choose. First, these two main categories are discussed, followed by several *intermediate methods* and *partial balancing methods*, which do not fall in either category.

Analysis methods for dynamic balance

The analysis methods for dynamic balance rely on satisfying force and moment balance conditions for a given mechanism in order to find sets of dynamically balanced mass distributions. Typically, these conditions prescribe a constant linear and angular momentum of the complete mechanism [116], thus elimin-

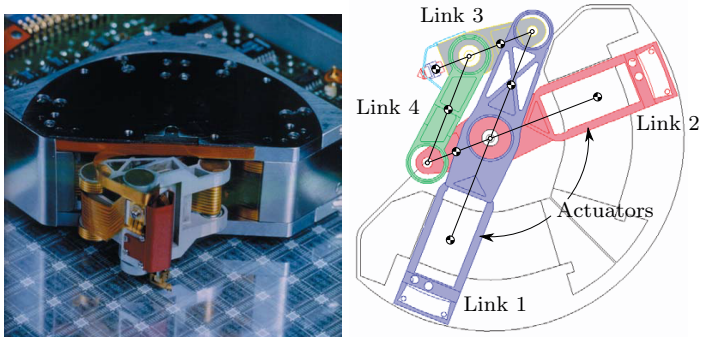

(a) (b)

Figure 1.3: (a) The dynamically balanced Hummingbird minipositioner was developed by IBM for high-speed, high-accuracy testing of chips [55]. Accelerations up to 50 g were achieved within 3 micron positioning accuracy. (b) Due to its hinged parallelogram structure, only countermasses at the base links are needed for force balance, which in this case are formed by the moving parts of the actuators. Moment balance was obtained by a reaction wheel placed on top of the mechanism, not shown here. (Figures are adapted from [70]. Courtesy of International Business Machines Corporation, © 2005 International Business Machines Corporation)

ating their derivatives, the shaking forces and moments. In practice, when the mechanism is initially at rest these conditions prescribe a zero linear and angular moment. Please note that the force balance conditions also imply a constant common COM of the mechanism [67] or a constant velocity of that COM. A mechanism's mass distribution that satisfies both the force and moment balance conditions is termed a *dynamic balance solution*, whereas the complete characterization of all dynamically balanced mass distributions is said to constitute the space of dynamical balanced designs; for simplicity called the *dynamically balanced design space*.

Robots consisting of revolute joint in a serial chain can be force balanced with relative ease by placing countermasses on each link. Starting from the end-effector, the movement of the last joint is force balanced when the COM of the last link is on this joint axis. For the second-to-last joint the aggregated COM — the combined COM of the last two links — is on the joint axis. When this is done for all joints in the chain, the mechanism is force balanced. For increasing number of DOFs, the total amount of balancing mass quickly escalates, resulting in a costly and unwieldy force balance solution. Moment balance of serial linkages requires additional structures, such as counter-rotating inertia wheels [14, 8, 47], cams [53] or duplicate mechanisms [67, 5] to generate an opposing angular momentum, further increasing the complexity, cost and required motor toques.

This 'serial' dynamic balancing solution also applies to parallel or closed loop mechanisms, since they can be regarded as a connection of several serial chains

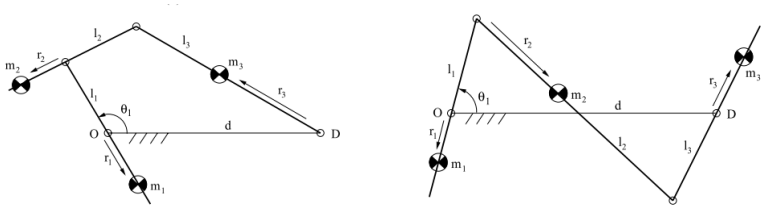

Figure 1.4: Dynamic balance of a planar $4R$ four-bar linkage is possible only for (a) the kite type and (b) anti-parallelogram type [75]. (Figures from [120])

[93], as formalized for the planar case in [125]. Similarly, the required number of balancing mass and counter-rotating devices lead to the disadvantages mentioned before [59, 104].

Fortunately, parallel mechanisms exhibit a larger dynamically balanced design space, due to the additional kinematic relations between the moving links, and thus require fewer balancing masses, as well as fewer counter-rotating devices (e.g. Fig. 1.3 and [73]). Some parallel mechanisms can, under specific conditions, even be dynamically balanced without additional structures [19] such as the $4R$ four-bar linkages of the kite and anti-parallelogram type. Ricard and Gosselin obtained this result in 2000 by starting from a known force balance solution [15, 86]. With this, they wrote the moment balance conditions in redundant coordinates. Consecutively, the dependent coordinates were eliminated by judicious incorporation of the kinematic loop-closure constraints and trigonometric identities, leading to the essential dynamic balance conditions. The pose-dependent parts in these rather lengthy expressions could be eliminated, resulting in a range of dynamically balanced masses, COMs, and MOIs (Fig. 1.4). Later it was proved that indeed only these two kinematic types of the four-bar linkage can be dynamically balanced without resorting to counter-rotating mechanisms [75].

The dynamic balance solution of the four-bar linkage shows that dynamic balance enforces specific kinematics, i.e. geometry and modes of assembly, on top of a specific mass distribution. These specific kinematic conditions that enable dynamic balance are termed the *essential kinematic conditions*. Furthermore, this case shows that it may be difficult to obtain the complete dynamically balanced design space for parallel linkages — even for relatively simple kinematic structures — as it invokes the loop-closure constraints to eliminate the dependent coordinates.

To deal with the kinematic complexity of parallel mechanisms, several systematic analysis methods were developed. The force balance of single-DOF planar linkages is facilitated by the 'linearly independent vector method' of Berkoff and Lowen [15]. This method systematically eliminates one dependent joint coordinate per kinematic loop from the force balance equations, simplifying the conditions significantly. Based on this, the 'complex mass method' and extensions have been presented that incorporates the loop-closure con-

straints implicitly, directly yielding the general force balance solution for planar [10, 114, 124] and spatial linkages [57, 23, 60].

These methods indeed result in the complete force-balanced design space for most mechanisms. However, in some special kinematic cases — such as the parallelogram type four-bar linkage — these methods are too strict, leading to a spurious set of force balance conditions and consequently to only a subset of the design space [43, 42]. This is because a specific relation exists between the link motions, in the parallelogram case an equal angular velocity of the crank and the rocker, which would permit a larger design space. With an incomplete kinematic model these special relations are not taken into account, and restricting the solution. Moreover, these methods are intrinsically limited to force balance as they start from a constant common COM condition.

Alternatively, Moore, Gosselin, and Schicho [75] used toric geometry and factorization of Laurent polynomials for the dynamic balance of planar $4R$ four-bar linkages. This generalization of [86] led to a system of symbolic polynomial equations which, through the use of polynomial division [44], resulted in the aforementioned balanceablity proof. Later, the algebraic method was extended to the force balance of the spatial $4R$ Bennett linkage [75] and the dynamic balance of the spherical $4R$ four-bar linkage [76]. It was shown that the latter cannot be dynamically balanced without additional counter-rotating devices. Although these algebraic methods seem generally applicable, they still need to be tailored to the kinematics at hand, and an extension to more complex multi-DOF mechanisms has not been reported yet. Furthermore, the algebraic nature of the balancing procedure limits the development of intuition, which is desired from the designer's point of view.

Synthesis methods for dynamic balance

The synthesis methods start from a set of dynamically balanced modules or concepts, which are combined, modified and stacked into dynamically balanced mechanisms. This is advantageous since dynamic balance can be considered directly at the beginning of the design process. Then, when the kinematics are still open, dynamic balance may be achieved with relative ease, whereas at a later stage it may be obtained only by additing of countermasses, counter-mechanisms or counter-rotating devices [97].

Ricard et al. used the dynamically balanced four-bar linkage as a module to create a 3-DOF planar parallel mechanism [86]. Six of these four-bars were stacked and modified to form three dynamically balanced arms connected at a platform. For the extension to spatial moving linkages, Wu et al. required two four-bars per dynamically balanced module [120]. This resulted in a 3-DOF and a 6-DOF dynamically balanced spatial mechanism, consisting of respectively 4 and 12 four-bar linkages. The large number of links and countermasses seem impractical and lead to an unfavourable mass-to-payload ratio [104].

Based on Fisher's 'principal vector method' for the study of the dynamics of the human gait [40], Van der Wijk et al. derived a method to constrain the motion of a set of bodies such that the common COM remains stationary [107]. This method provides a range of linkages, typically modified pantographs

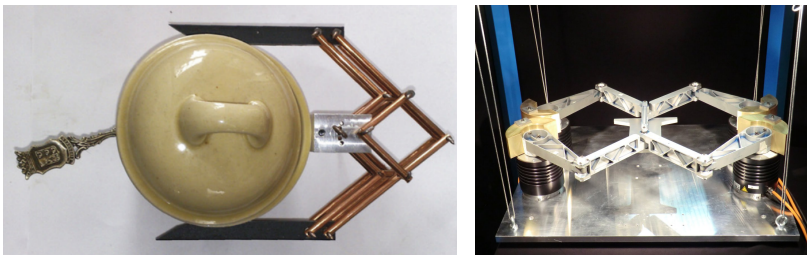

(a) (b)

Figure 1.5: The synthesis of multi-DOF dynamically balanced principal vector linkages. (a) The mirror symmetric dynamically balanced 2-DOF gripper (from [107]). (b) The 3-DOF DUAL-V, which is dynamically balanced along its symmetry axes (from [109]).

that trace the common COM location of a given initial (principal) set of linked bodies. By adding this linkage, the common COM becomes a physical point on the mechanism. Then, by fixing this point to the base, all remaining DOF of the mechanism will be force balanced. This method has subsequently been extended by treating not only bodies but also sub-linkages such as dyads [98] and triads [99] as mass equivalent [100], through relying on a graphical interpretation of the complex mass method [124]. As these synthesis methods solely enforce the essential kinematic requirements for force balance, i.e. a common COM, in principle all force-balanced mechanisms can be found. Indeed, a range of planar and spatial, multi-DOF, force-balanced mechanisms was synthesized through this method [100, 101].

These force-balanced principal vector linkages may also be dynamically balanced, for instance by means of an additional counter-rotating device [109], mirror symmetry [107] or reduction of the DOF [96]. Mirror symmetry resulted in a 2-DOF dynamically balanced gripper (Fig. 1.5a) and a planar 3-DOF, overactuated robot, the DUAL-V (Fig. 1.5b), which is dynamically balanced for motion along two perpendicular paths [109].

Yet, as shown in [96], not all results from the dynamic balance literature could be replicated using this principle. Furthermore, there is a fundamental difference between force balance and moment balance that hinders the generalization of this method to dynamic balance. In other words, the moment balance conditions are nonintegrable or nonholonomic conditions [80]. That means that the general moment balance condition are a function of pose and velocity and cannot be formulated as a set of admissible positions and orientations of bodies alone. Therefore, it is not readily clear which kinematic structure should be added to exactly enforce dynamic balance for an arbitrary set of bodies.

Other methods

Several intermediate methods can be found in literature that rely on a combination of synthesis and analysis methods. For example, the designer may start

from a kinematic structure for which dynamic balance is obtained by adding balancing linkages such as dyads [7] or counter-mechanisms [64, 63], or by replacing linkages by counter-mechanisms such as four-bars [45, 17] and crank-sliders [19, 17], or by using duplicate and mirrored mechanisms [59, 108].

Furthermore, several partial dynamic balance methods exist that use a reduced set of dynamic balance conditions to enable a larger design space and potentially more practical designs. Examples include frequency balancing, which eliminates only the first few harmonic loads [110], path balancing, which restricts the mechanism's motion to reactionless paths [84, 126, 1, 18], and optimal dynamic balancing [92, 36, 111, 25], which optimizes motor torques, bearing loads, or other requirements in conjunction with the shaking forces and moments.

Although these topics are outside the scope of this thesis, it may be expected that new insights from the synthesis or analysis methods will further these balancing methods as well.

1.3 Research objectives and approach

Dynamic balance through synthesis seems preferable to the analysis methods as it allows the mechanism designer to consider dynamic balance directly at the beginning of the design process when most of the kinematics and dynamics are not determined yet. This enables a larger design freedom and potentially more effective balance solutions. However, the state-of-the-art synthesis methods [86, 120] that rely on recombination of dynamically balanced modules have only a few of these modules at disposal. The principal vector method [97] on the other hand has shown to be a versatile method for synthesizing force-balanced mechanisms. Yet, the method itself cannot be readily extended to dynamic balance since it is not fully known what kinematic conditions a mechanism should enforce for additional moment balance.

To ultimately derive a comprehensive synthesis method, more insight is needed to fully understand the relation between the kinematic design and the dynamic balance conditions. However, the current analysis methods are either incomplete, limited to force balance, hindered by the kinematic and symbolic complexity, or provide limited intuition or interpretation, which seem essential to derive new synthesis methods.

This thesis therefore aims to strengthen the mathematical basis of dynamic balance and provide insight into the essential kinematic conditions of both planar and spatial linkages. Two research objectives are formulated:

1. To develop a holistic analysis method that provides all dynamically balanced mass distributions for any planar or spatial parallel linkage with single or multi-DOF.

2. To understand the underlying principles needed to achieve dynamic balance through mass distribution design.

This envisioned analysis method (*Objective 1*) should deal with the intrinsic kinematic and algebraic complexity associated with the loop closure without in-

tervention of the user. Additionally it should uniformly treat force and moment balance of planar and spatial linkages, and provide an intuitive description of the resulting solution space. Furthermore, since not all dynamically balanced solutions can be built as they might require negative masses or MOI, a check is needed to ensure the feasibility of the solution. Such a method would enable a systematic investigation (*Objective 2*) into the mechanisms that can be dynamically balanced by design of the mass distribution, i.e. without additional counter-devices, and as such, provide a basis for novel synthesis methods.

In search of this holistic, intrinsically spatial dynamic balance method that is applicable to arbitrary multi-DOF mechanism, screw theory [11] is applied throughout this thesis. Screw theory is a mathematical formulation for rigid body kinematics and dynamics. It treats the linear and angular velocity as a single 6-vector, termed twist. Likewise, the force and moment are unified as a wrench. This leads to a concise and frame-invariant description of spatially moving mechanisms. Furthermore, these 6-vectors are interpreted geometrically as lines in space. For example, a twist is equivalent to an infinitesimal rotation around a line in space and a translation along this line. A similar interpretation exist for wrenches, which can be represented as a force along a line and torque around this line, enabling a graphical representation of the dynamic balance conditions. Additionally, the derivatives of both the twists and the wrenches can be found in a concise and structured manner. This is used to find necessary and sufficient balance conditions that do not require a closed-form solution of the loop-closure constraint equations.

1.4 Contributions and thesis outline

This thesis is organized as follows: in *Chapter 2* the screw theory basis and notations as used in this thesis are presented in conjunction with an exploration of two fundamental differences between force and moment balance. Firstly, it is confirmed that moment balance is a nonholonomic condition. This poses challenges for synthesis methods, as indicated above, but also enables a wider choice of dynamically balanced paths than expected from the number of DOFs and number of dynamic balance conditions. Secondly, unlike what is assumed in literature, it is shown that, due to its definition, dynamic balance is a necessary but not a sufficient condition for dynamic decoupling. This means that a dynamically balanced robot placed on top of a rotating base, e.g. a satellite, vehicle or another robot, may still experience dynamic effects due to the motion of the base, potentially degrading its performance. This also indicates that dynamically balanced modules cannot always be simple stacked to form larger structures. This chapter therewith underlines two challenges faced by the synthesis approaches. This underpins the need for a uniform mathematical basis in order to advance the dynamic balance of higher DOF and spatially moving mechanisms.

Chapter 3 explores the geometric interpretation of the dynamic balance conditions as furnished by screw theory. Dynamic balance is represented by a set of spatial vectors whose sum is zero. This results in a zero-order, *instantaneous*

dynamic balance method for planar and spatial, multi-DOF mechanisms (Objective 1). This results in a specific pose in which the robot accelerations will not generate any shaking forces and moments. Further away from this pose, the robot's balance quality worsens. In combination with path balance this method yields a pose in which multiple dynamically balanced paths intersect. This might prove useful in pick-and-place applications where a part is to be placed very precisely at a single location while precision is of less important for the rest the workspace. The robot can then start from an arbitrary location and follow these reactionless paths in the approach of the placement point, resulting in less vibration when desired. The method is applied to a 2-DOF $5R$ five-bar linkage, yielding an experimental demonstrator with force balance over the complete workspace and moment balance along two perpendicular paths that intersect in the middle of the workspace, the instantaneously dynamically balanced pose. Measurements confirm the force balance of the mechanism and the existence of an instantaneously dynamically balanced pose.

In *Chapter 4 and 5* this instantaneous dynamic balance method is extended to the complete workspace, by using he higher-order derivatives of kinematics, dynamics and of the dynamic balance conditions. This results in a *higher-order dynamic balance method* that yields the design space of dynamically balanced inertial parameters for any given linkage (Objective 1). It is conjectured that with sufficient derivatives this comprise the complete design space of non-singular mechanisms. This balancing method depends on and is preceded by a screw theory based algorithm for higher-order derivatives of the solution to the loop-closure constraint equations, as presented Chapter 4. In Chapter 5 this higher-order kinematic approach is extended to rigid body dynamics, leading to the formulation of a generic dynamic balance method. Although serial mechanisms — and most parallel mechanisms — do not possess a feasible design space, i.e. demanding negative masses or negative MOIs, the complete description of the design space enables the selection of the favourable (minimal) number of counter-rotating devices. Moreover, this chapter confirms that special geometries exhibit a larger and even feasible design space (Objective 2). The method is illustrated by three examples, a 6-DOF serial robot, a planar $4R$ four-bar linkage, and a 3-DOF, spatially moving 3-RSR mechanisms. This last example shows a novel design which is dynamically balanced over three intersecting planes of motion. This allows for 2-DOF dynamically balanced motion on these planes of symmetry and a local 3-DOF motion on the intersection line.

The choice of kinematics, i.e. the topology and dimensions, completely determines whether a mechanism can be dynamically balanced by design of the mass distribution (Objective 2).The previous two balancing methods compute the design space for a given mechanism, yet yield little clues on the kinematics are favourable for dynamic balance. *Chapter 6* therefore investigates these essential kinematic conditions. More specifically, it is shown that several dynamically balanced planar mechanisms from literature share kinematic mirror symmetry and a mass distribution that can be represented by a single pure moment of inertia per link. Based on these insights, a *pure-inertia method* to dynamically balance symmetric, planar mechanisms is presented, resulting in

a 2-DOF planar mechanism that is dynamically balanced over its entire workspace.

This thesis closes with an overarching discussion (*Chapter 7*) and conclusion (*Chapter 8*).

Thesis note: Chapter 3-6 present the main contributions of this thesis. These chapters are reprints of published or submitted papers with minor adjustments. Due to this format, the introductions of the chapters may present some overlap whereas the chapter itself is not specifically framed within the flow of this thesis. Therefore, each of these chapters is accompanied with a footnote that describes the place and function of each chapter in the overall story of the thesis. The next chapter (Chapter 2), not in paper form, serves as an introduction to the bulk of the mathematics and notation that are used throughout this thesis. The discussion section (Chapter 7) highlights the connections and differences between the chapters to ensure the coherency of the thesis. In the appendix, supplementary information on the higher-order partial derivatives is found, which is used in Chapter 4 and 5. A combined bibliography and nomenclature is found at the end of the thesis.

1

Chapter 2

Fundamental concepts

Three fundamental concepts are treated to form the starting point of this thesis: 1) A screw theory based formulation of rigid body dynamics is used to obtain a tractable and concise description of dynamic balance. 2) Moment balance is, as opposed to the force balance, a path dependent or nonholonomic condition, meaning that this condition cannot be formulated in terms of pose alone. This fundamental difference, on the one hand, hinders the extension of current force balance methods to moment balance, but on the other hand also offers a wider choice of dynamically balanced paths. 3) Dynamic decoupling does not automatically hold for dynamic balance, as is suggested in literature. A mechanism is dynamically decoupled when the relative pose of mechanism is not affected by the motion of the base. Such a mechanism can therefore be treated as a virtual rigid body. These dynamically decoupled mechanisms form the basis of several synthesis methods as they can be stacked and combined to form larger DOF dynamically balanced mechanisms. Force balanced mechanisms are decoupled as the translations of the base do not influence the internal dynamics of the mechanism. Therefore no additional motor effort is required to maintain a relative position to a translating base. The same is not necessarily true for the rotational domain. Here it is shown that, beside dynamic balance, also a constant total moment of inertia is needed. These two fundamental differences between force and moment balance are derived formally and illustrated by simulations.

2.1 Introduction

The dynamics of rigid body systems is sometimes counter-intuitive. Especially in the rotational domain, unexpected effects may arise. Classical examples are the spinning top [119], the gyroscopic precession of a bicycle wheel [65] and the free-falling cat [54]. The latter example is of particular interest in the current context as a cat falling from a tree is by definition moment balanced. How is it possible that, although it experiences no external moment, it is still able to reorient itself in flight and land on its feet (Fig. 2.1a) without violating the law of conservation of angular momentum? If the cat were to be considered

as a single rigid body, it would certainly violate this law. If it simply counter-rotated its front part with respect to its back part, the cat might land on its feet, but it would end up with a twisted spine. Instead, the cat consecutively flexes and bends its spine to generate a net angular velocity [54]. Swapping this sequence leads to net rotation in another direction (Fig. 2.1b). This means that conservation of angular momentum dictates a condition depending on both the orientation and the angular velocity of the cat and not on the orientation alone. The cat can also reach any orientation depending on the sequence in which it bends and flexes the spine. The conservation of angular momentum and hence moment balance are therefore a nonintegrable, *nonholonomic* conditions [80]. That means that in general, these conditions cannot be integrated to be solely dependent on pose, they will also be depending on velocity. In contrast, force balance is a holonomic condition. This means that it can be alsways be formulated in terms pose alone, i.e on the location of COMs of the bodies. For that cat this means that it will hit the ground regardless of its internal motion.

As indicated in the previous chapter, the nonholonomicity of the moment balance condition challenges the extension of force balance techniques — e.g. the complex mass method [10], or the method of principal vectors [107] — to moment balance. Since force balance is a holonomic condition, it can be enforced by a condition on pose, namely by making the total centre of mass stationary. Based on this property, force balance can be intuitively achieved by adding a linkage to a set of bodies, typically pantograph-like structure, such that this added linkage physically traces the total COM location. The total COM, which is now a point of the linkages, is fixed in such away that the remaining motion of the system is force-balanced. This enables a synthesis method that, on outset, should yield all possible force-balanced linkages as it constrains only the essential kinematic conditions for force balance.

Now, for the generalization of this synthesis method to dynamic balance, a description is needed of the poses (i.e. positions and orientations) to which an arbitrary set of bodies can move to without inducing shaking forces and moments. If these bodies then were to be constrained to these poses by a suitable linkage, the whole system would be dynamically balanced. Since this is not possible on the pose level alone, alternative measures are needed to derive a comprehensive synthesis method. Fortunately, as the falling cat problem shows, moment balance may also permit unexpected motion. In this chapter, this nonholonomic behaviour of dynamically balanced mechanisms is investigated and illustrated by an example.

Another fundamental difference between force and moment balance is their relation with *dynamic decoupling*. A mechanism is dynamically decoupled[1] 1) when the motion of the mechanism does not induce forces and moments on a moving base, and 2) when the movement of the base does not require additional actuator forces or torques to execute an internal motion of the mechanism [97].

[1] Note the difference with another use of the term dynamic decoupling, which is the internal decoupling of the DOFs of the mechanisms from each other. In such mechanisms, the movement of a single DOF does not require actuation effort in other DOFs [3], potentially simplifying the control laws by minimizing cross talk.

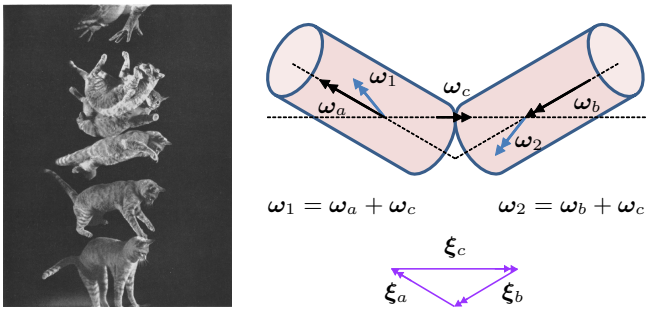

(a) (b)

Figure 2.1: (a) A falling cat reorients itself in midflight by consecutive forward flexion of the spine, then sideways bending, backward flexion and bending to the other side [54]. (b) Kane et al. [54] modelled the front and the back part of the cat as two rolling cylinders with angular velocities of $\boldsymbol{\omega}_1$ and $\boldsymbol{\omega}_2$ respectively. The angular momentum, respectively $\boldsymbol{\xi}_a$ and $\boldsymbol{\xi}_b$ induced by the internal rolling of the bodies, respectively $\boldsymbol{\omega}_a$ and $\boldsymbol{\omega}_b$, induces an opposite momentum $\boldsymbol{\xi}_c$ and a counter-rotation $\boldsymbol{\omega}_c$ of the cat as a whole. ((a) Photograph taken form [54])

Such mechanisms are important for dynamic balance as they behave as a single rigid body. Therefore, they are used as modules which can be recombined and stacked, as done by Ricard et al. [86] and Wu et al. [120]. These systems may also be used in space robotics. For example, by dynamically decoupling the motion of the robot arm from the moving base (e.g. space ship, satellite), the manipulation of the arm does not require corrective controls of the base [126].

Some literature suggests that dynamic balance will result in dynamic decoupling. For instance, in [97, p. 3] dynamic decoupling and its relation to dynamic balance is introduced as follows: "Because a dynamically balanced mechanism is dynamically decoupled from its base, dynamic behaviour of the base does not affect the relative motion of the mechanism. When the base is accelerated linearly or rotationally, e.g. by another device or due to external vibrations, a dynamically balanced mechanism behaves as a single rigid body with the base". Others imply that dynamic balance will result in constant total moment of inertia [86, 120], or that dynamically balanced mechanisms will conserve the momentum of a moving base [120, 63], and therefore behave as if dynamically decoupled. Yet no evidence is given to support these statements. In this chapter it will be shown that dynamic balance is a necessary but not sufficient condition for dynamic decoupling.

A rigorous description of rigid body dynamics is essential to describe these effects and to extend the current dynamic balance methods. A naive description of rigid body dynamics of spatially moving mechanisms quickly becomes unwieldy for mechanisms with a large number of bodies. The reference frames associated to each body, their kinematic transformations and the derivatives of these transformations all have to be systematically taken into account, poten-

tially leading to complicated sets of equations, and complicating the development of analytic dynamic balance methods.

In this thesis, the *screw theory* formulation is adopted. Screw theory is a systematic approach to describe spatial motion of rigid bodies and mechanisms [11]. It enables the use of mathematical tools such as the Lie bracket for rigid body motion [90, 91], resulting in a concise, frame-invariant description. Moreover, screw theory provides a geometrical interpretation of the linear and angular velocities and of the forces and moments acting on such systems. These properties are used in this chapter and throughout this thesis to obtain a better understanding of dynamic balance.

This chapter introduces screw theory and discusses the two fundamental differences between force and moment balance. More specifically, it shows that the nonholonomicity of the moment balance condition precludes a straightforward extension of forces balance synthesis methods, but also that it enables more motion possibilities than perhaps expected. Additionally, it shows that dynamic balance does not automatically lead to the dynamic decoupling of the mechanism from the base, i.e. the mechanism will still feel some of the motion of the base. This chapter aims to familiarize the reader with the concepts used in this thesis and sharpen the understanding of dynamic balance in the process. Governing equations are presented alongside examples and simulations.

This chapter is organized as follows: first a screw theory description of rigid body dynamics is introduced (Section 2.2), then the dynamic balance conditions are presented and integrated to show the nonholonomic behaviour of moment balance (Section 2.3), and finally the effect of dynamic balance on dynamic decoupling is investigated (Section 2.4).

2.2 Mathematical framework: screw theory

The description of dynamic balance of a collection of linked rigid bodies may rely on a mix of relative and absolute velocities. For instance, the dynamic balance conditions, i.e. zero shaking forces and moments are dependent on the absolute velocities and accelerations of bodies, whereas the possible motion of the mechanism is described by a minimal set of local coordinates, i.e. joint rates. In order to express the balance conditions in minimal coordinates several transformations are required. In screw theory these transformations may be described in a concise frame-invariant manner.

Here, a short overview is given to familiarize the reader with the screw theory and the notation used in this thesis. Starting from a conventional description of rigid body motion, the kinematics and dynamics in a screw theory context are revisited. This section is by no means a complete description of screw theory. It highlights only a few features of screw theory that will be used later on in this thesis. For a complete introduction into screw theory, proofs and details, consult the seminal books of R. Murray, Z. Li and S. Sastry [80] and of R. Featherstone [38].

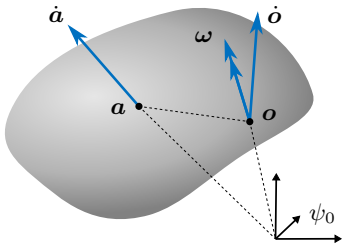

Figure 2.2: The velocity of all points $\boldsymbol{a}$ on a rigid body are determined by the velocity $\dot{\boldsymbol{o}}$ of a reference point $\boldsymbol{o}$ and the angular velocity $\boldsymbol{\omega}$. The inertial frame is denoted by ψ_0.

Rigid body motion

The velocities $\dot{\boldsymbol{a}}$ of the particles that form a rigid body can be expressed by the angular velocity $\boldsymbol{\omega}$ of the rigid body and velocity $\dot{\boldsymbol{o}}$ of a reference point $\boldsymbol{o}$ on that body, according to

$$\dot{\boldsymbol{a}} = \dot{\boldsymbol{o}} + \boldsymbol{\omega} \times (\boldsymbol{a} - \boldsymbol{o}) \tag{2.1}$$

in here the vectors $\boldsymbol{a}$ and $\boldsymbol{o}$, pointing respectively from the origin of the reference frame to the particle and from the origin to the point of reference (Fig. 2.2).

Now consider two bodies, hinged at $\boldsymbol{r}$, moving relative to each other and relative to the frame of reference (Fig. 2.3). In this case, body 2 is rotating with an angular velocity of $\boldsymbol{\omega}_2^1$, relative to body 1. The velocity of point $\boldsymbol{o}_2$ relative to the reference point on body 1 is $\dot{\boldsymbol{o}}_2^1$. The absolute angular velocity of body 1 is $\boldsymbol{\omega}_1^0$. The velocity of point $\boldsymbol{o}_1$ is $\dot{\boldsymbol{o}}_1$. It should be mentioned that the subscripts denote the reference frames or the bodies that twist belongs to. The superscripts denote the frame or body to which the twist is relative. Later on, a second superscript will be introduced to denote the frame of expression. If the situation permits, the subscripts and superscripts are dropped for the sake of convenience. For the computation of the absolute angular body 2 we may sum angular velocities directly

$$\boldsymbol{\omega}_2^0 = \boldsymbol{\omega}_1^0 + \boldsymbol{\omega}_2^1 \tag{2.2}$$

For computation of absolute velocity $\dot{\boldsymbol{o}}_2$, the rotation of the reference point $\boldsymbol{o}_2$ due to $\boldsymbol{\omega}_1$ has to be taken into account (Eq. 2.1), yielding

$$\dot{\boldsymbol{o}}_2^0 = \dot{\boldsymbol{o}}_2^1 + \dot{\boldsymbol{o}}_1^0 + \boldsymbol{\omega}_1^0 \times (\boldsymbol{o}_2^0 - \boldsymbol{o}_1^0) \tag{2.3}$$

If reference points $\boldsymbol{o}_1^0$ and $\boldsymbol{o}_2^0$ are chosen arbitrarily, the velocities cannot be summed directly since the angular velocity of the body 1 has to be taken into account. In the opposite case, when the reference points are chosen instantaneously coincident $\boldsymbol{o}_1^0 = \boldsymbol{o}_2^0$, the computation of the sum of instantaneous velocities simplify to

$$\dot{\boldsymbol{o}}_2^0 = \dot{\boldsymbol{o}}_1^0 + \dot{\boldsymbol{o}}_2^1 \tag{2.4}$$

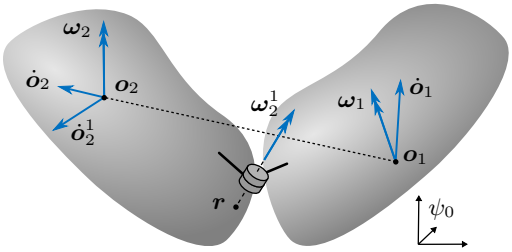

Figure 2.3: The summation of relative and absolute velocities in articulated bodies.

2

Consequently, the instantaneous velocities form a system of linear equations, just as the angular velocities (Eq. 2.3). These new velocities belong to the virtual particles, although attached to different bodies, which instantaneously pass through the same point of reference. During finite motion different particles may be identified with this velocity. Typically, this point is chosen as origin of the reference frame. In screw theory, the two 3-vectors of the linear and angular velocity are unified in a single 6-vector $\boldsymbol{t}$, termed *twist*. Now the instantaneous motion of body 2 reads

$$\underbrace{\begin{bmatrix}\boldsymbol{\omega}_2^0\\ \dot{\boldsymbol{o}}_2^0\end{bmatrix}}_{\boldsymbol{t}_2^0} = \underbrace{\begin{bmatrix}\boldsymbol{\omega}_1^0\\ \dot{\boldsymbol{o}}_1^0\end{bmatrix}}_{\boldsymbol{t}_1^0} + \underbrace{\begin{bmatrix}\boldsymbol{\omega}_2^1\\ \dot{\boldsymbol{o}}_2^1\end{bmatrix}}_{\boldsymbol{t}_2^1} \tag{2.5}$$

In the remainder, the velocities $\dot{\boldsymbol{o}}_i$ are the velocities of the frame of reference and simply referred to as the linear velocity $\boldsymbol{v}_i$ of body i.

A similar treatment holds for the forces and moments acting on a body. Conventionally, the forces $\boldsymbol{f}$ and moments $\boldsymbol{\tau}$ are expressed with respect to one application point per body. Now in order sum multiple forces and moments acting on a system, they first have to be transferred to the same point. In screw theory, the same point of reference is used for all bodies, unifying the treatment of forces and moments. This leads to a single 6-vector termed *wrench* $\mathbf{w}$. Both types of 6-vectors are termed *screws*.

Now, the power P generated by a twist and a wrench is simply their product, since they have the same application point, i.e. the origin of reference frame

$$P = \boldsymbol{f}^\top \boldsymbol{v} + \boldsymbol{\tau}^\top \boldsymbol{\omega} = \mathbf{w}^\top \boldsymbol{t} \tag{2.6}$$

The expression of different velocities and torques around a single point of reference is an important distinctive feature of screw theory that enables a uniform treatment of the translational and rotational domain.

Twists and wrenches

Another feature of screw theory is the geometrical interpretation of these 6-vectors or screws. Mozzi-Chasles' theorem states that the twist of the body can be decomposed into an angular velocity around a line in space and a linear

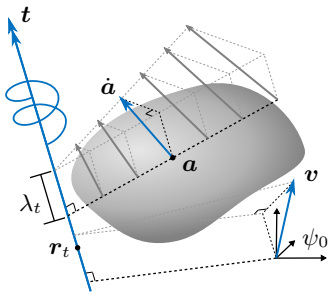

Figure 2.4: The linear and angular velocity of body form a helical velocity field for all particles $\boldsymbol{a}$ of a body. This twist $\boldsymbol{t}$ is denoted with a double arrow, with a helix representing the twist pitch λ_t. The velocity$\boldsymbol{v}$ is the velocity of the points instantaneously passing through the origin of reference ψ.

velocity along this line (Fig. 2.4). This screw-like interpretation of motion gives screw theory its name. This follows from the fact that the linear velocity of a body $\boldsymbol{v}$ can be decomposed into a part which is co-linear with the angular velocity, in the form of $\lambda_t\boldsymbol{\omega}$, and a part which is perpendicular to the angular velocity, in the form of $\boldsymbol{\omega} \times \boldsymbol{r}_t$. The scalar λ_t and vector $\boldsymbol{r}_t$ are computed via

$$\boldsymbol{r}_t = \frac{\boldsymbol{\omega} \times \boldsymbol{v}}{\|\boldsymbol{\omega}\|^2} + \delta_t \boldsymbol{\omega}, \qquad \lambda_t = \frac{\boldsymbol{\omega}^\top \boldsymbol{v}}{\|\boldsymbol{\omega}\|^2} \tag{2.7}$$

in which δ_t can be chosen freely. The λ_t is interpreted as the amount of translation per rotation, known as pitch. The point $\boldsymbol{r}_t$ can be any point on the twist axis. Finally the twist of any rigid body may be written as

$$\boldsymbol{t} = \begin{bmatrix} \boldsymbol{\omega} \\ \boldsymbol{v} \end{bmatrix} = \begin{bmatrix} \boldsymbol{\omega} \\ \boldsymbol{r}_t \times \boldsymbol{\omega} \end{bmatrix} + \lambda_t \begin{bmatrix} \boldsymbol{0} \\ \boldsymbol{\omega} \end{bmatrix} \tag{2.8}$$

In this interpretation two special cases exist: 1) Where the body is purely rotating the angular velocity is orthogonal to the linear velocity, so the pitch is zero ($\lambda_t = 0$). 2) Where the body is in pure translation its rotation axis lies at infinity and the pitch becomes infinite ($\lambda_t = \infty$). This corresponds with the notion that all points of a purely translating body have the same velocity. For the two cases the twist is given as

$$\boldsymbol{t}_0 = \begin{bmatrix} \boldsymbol{\omega} \\ \boldsymbol{r}_t \times \boldsymbol{\omega} \end{bmatrix}, \qquad \boldsymbol{t}_\infty = \begin{bmatrix} \boldsymbol{0} \\ \boldsymbol{v} \end{bmatrix} \tag{2.9}$$

For the wrench $\mathbf{w}$ a similar spatial interpretation exists. The Poinsot's theorem states that any combination of forces $\boldsymbol{f}$ and moments $\boldsymbol{\tau}$ acting on a body can be represented by a single force on a line passing through a point $\boldsymbol{r}_w$ and a pure torque around that line, the pitch λ_w

$$\mathbf{w} = \begin{bmatrix} \boldsymbol{\tau} \\ \boldsymbol{f} \end{bmatrix} = \begin{bmatrix} \boldsymbol{r}_w \times \boldsymbol{f} \\ \boldsymbol{f} \end{bmatrix} + \lambda_w \begin{bmatrix} \boldsymbol{f} \\ \boldsymbol{0} \end{bmatrix} \tag{2.10}$$

Similarly to the linear velocity, this torque $\boldsymbol{\tau}$ is specified as the torque around the origin of the reference frame. Here, the wrench axis location and pitch are given by

$$\boldsymbol{r}_w = \frac{\boldsymbol{f} \times \boldsymbol{\tau}}{\|\boldsymbol{f}\|^2} + \delta_w \boldsymbol{f}, \qquad \lambda_w = \frac{\boldsymbol{f}^\top \boldsymbol{\tau}}{\|\boldsymbol{f}\|^2} \tag{2.11}$$

where δ_w indicates the free coordinate along the wrench axis. Zero and infinity pitch screws exist for the wrenches as well. The former is a pure force through $\boldsymbol{r}_w$ and the latter is a pure moment. This corresponds to the notion that a pure couple has no point of application. The two special cases are given as

$$\mathbf{w}_0 = \begin{bmatrix} \boldsymbol{r}_w \times \boldsymbol{f} \\ \boldsymbol{f} \end{bmatrix}, \qquad \boldsymbol{t}_\infty = \begin{bmatrix} \boldsymbol{\tau} \\ \mathbf{0} \end{bmatrix}. \tag{2.12}$$

It should be noted that the two types of screws differ in the sense that for the twist the angular part $\boldsymbol{\omega}$ determines the screw axis direction, while for the wrench the linear part $\boldsymbol{f}$ determines the direction of the screw axis.

Mechanisms and Jacobians

The application of these two features, the uniform treatment of the translation and rotation domain and the geometric interpretation of the twist and wrench are now used for the velocity analysis of serial and parallel mechanisms.

Mechanisms are formed by a number of bodies connected through a set of joints, typically revolute (R), prismatic (P) or helical (H) joints. In serial chains the global twist of each body is determined by the joint velocities of the joints lower in the chain, i.e. between the body and the base (Fig. 2.5). If a single joint is actuated, all bodies higher in the chain experience the same twist. If multiple joints are actuated, the contribution of each joint is added since the linear and angular velocities are additive when expressed in the same frame of reference. The relative twist generated by actuation of each joint is termed instantaneous screw axis (ISA). These ISAs are denoted by $\boldsymbol{s}_i$ and are numbered from 1 to n, in which n is the most distal joint. For any body i, the ISAs lower in the chain completely determine the possible motion of that body, and therefore form its twist basis. This twist basis, or Jacobian — relating the joint velocities $\dot{\boldsymbol{q}}$ to the twist of that body — is therefore found by stacking all preceding twist axes

$$\boldsymbol{t}_i = \sum_{j=1}^{i} \boldsymbol{s}_j \dot{q}_j = \begin{bmatrix} \boldsymbol{s}_1 & \cdots & \boldsymbol{s}_i & \mathbf{0} \end{bmatrix} \dot{\boldsymbol{q}} = \boldsymbol{J}_i \dot{\boldsymbol{q}} \tag{2.13}$$

The geometrical interpretation of the previous section (Eq. 2.8) directly gives the ISAs, based on the joint type, axis and location. For example, the end-effector Jacobian of a 6-DOF industrial robot (Fig. 2.5) consisting solely of revolute joints is directly written as

$$\boldsymbol{J}_{\mathrm{ee}} = \begin{bmatrix} \boldsymbol{s}_1 & \cdots & \boldsymbol{s}_6 \end{bmatrix}, \qquad \boldsymbol{s}_i = \begin{bmatrix} \boldsymbol{n}_i \\ \boldsymbol{r}_{\mathrm{i}} \times \boldsymbol{n}_{i.} \end{bmatrix} \tag{2.14}$$

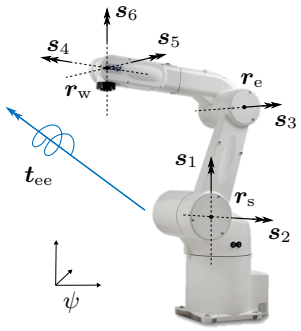

Figure 2.5: The end-effector twist $\boldsymbol{t}_{\text{see}}$ of an industrial 6-axis robot is formed by a linear combination of the instantaneous screw axis of each joint ($\boldsymbol{s}_i$, for $i = [1...6]$), passing through the shoulder $\boldsymbol{r}_{\text{s}}$, elbow $\boldsymbol{r}_{\text{e}}$, and wrist $\boldsymbol{r}_{\text{w}}$, expressed in the inertial frame of reference ψ. (Figure adapted from Adept: Viper Six-Axis Robot (s1300 Series), accessed on 23 December 2019, `www.e-motionsupply.com`)

in which $\boldsymbol{n}_i$ is the unit vector of the joint axis and $\boldsymbol{r}_i$ the joint location, all expressed in the inertial frame of reference (See Fig. 2.5):

$$\boldsymbol{r}_i = \begin{cases} \boldsymbol{r}_{\text{s}} & \text{for } i = [1,2] \\ \boldsymbol{r}_{\text{e}} & \text{for } i = [3] \\ \boldsymbol{r}_{\text{w}} & \text{for } i = [4,5,6] \end{cases} \tag{2.15}$$

For parallel mechanism, the twist basis of a may be deducted by regarding it as a set of connected serial chains. The twist of such closed loops can therefore be analyzed by cutting one body per loop, leaving multiple pairs of serial chains of which the end links must have equal twists. For example, a single loop system is opened by cutting a single body, inducing two virtual bodies, a and b, of which the twists must be equal

$$\boldsymbol{t}_a = \boldsymbol{t}_b, \qquad \boldsymbol{J}_a\dot{\boldsymbol{q}} = \boldsymbol{J}_b\dot{\boldsymbol{q}} \tag{2.16}$$

By selecting the proper amount of dependent $\boldsymbol{u}$ and independent $\boldsymbol{d}$ coordinates with respect to the number of constraints, this system is solvable for the dependent joint velocities.

$$\dot{\boldsymbol{q}} = \boldsymbol{C}\dot{\boldsymbol{u}} \tag{2.17}$$

in which $\boldsymbol{C}$ is referred to as the loop-closure Jacobian. The body twists may now be obtained by

$$\boldsymbol{t}_i = \boldsymbol{J}_i\boldsymbol{C}\dot{\boldsymbol{u}} \tag{2.18}$$

It should be noted that the columns of the $\boldsymbol{J}_i\boldsymbol{C}$-matrix are again geometric entities, termed unit twist is Chapter 3. Such a $\hat{\boldsymbol{t}}_{i.j}$ is the twist of body i as

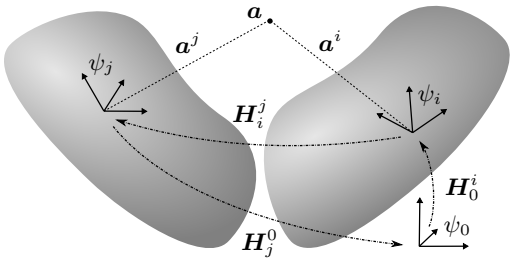

Figure 2.6: To each body a reference frame ψ is associated to express points, twists, wrenches, etc. A coordinate transformation, denoted by $\boldsymbol{H}_i^j$ changes the reference frame of expression.

a consequence of unit velocity of DOF j. Please note the distinction between $\hat{\boldsymbol{t}}_{i.j}$ and $\boldsymbol{s}$, the former is dependent on the choice of independent coordinates whereas $\boldsymbol{s}$ are associated to physical entities, that are joint type, location and orientation.

Transformations and derivatives

Up to now all screws were expressed in (or seen by) an inertial reference frame. Sometimes, especially in differential kinematics, it is convenient to express twists in a local, body-fixed reference frame. For example, ISA $\boldsymbol{s}_i$ is rigidly attached to the two connecting bodies i and $i+1$. This means that this ISA is constant when expressed in the local frames of these bodies, potentially leading to simpler equations. To encode this finite coordinate transformation, a reference frame ψ_i is attached to each body i (Fig. 2.6). A rotation matrix $\boldsymbol{R}$ and translation vector $\boldsymbol{o}$ encode the relative rotation and translation between these frames, such that point $\boldsymbol{a}$ changes its frame of expression from frame i to frame j according to

$$\boldsymbol{a}^j = \boldsymbol{R}_i^j \boldsymbol{a}^i + \boldsymbol{o}_i^j \tag{2.19}$$

The subscripts and superscripts denote the respective frames of reference. This successive rotation and translation is combined in a single operation through a transformation matrix $\boldsymbol{H}_i^j$

$$\check{\boldsymbol{a}}^j = \begin{bmatrix} \boldsymbol{a}^j \\ 1 \end{bmatrix} = \boldsymbol{H}_i^j \check{\boldsymbol{a}}^i, \qquad \boldsymbol{H} = \begin{bmatrix} \boldsymbol{R} & \boldsymbol{o} \\ \boldsymbol{0} & 1 \end{bmatrix} \tag{2.20}$$

The $\check{\boldsymbol{a}}$ denotes that the $\boldsymbol{a}$ vector is appended with a 1 to account for the translation. This notation is dropped when it is unambiguous. The matrix inverse yields the inverse transformation, i.e. form frame j to i

$$(\boldsymbol{H}_i^j)^{-1} = \boldsymbol{H}_j^i \tag{2.21}$$

This transformation matrix encodes the relative pose between two frames. It is therefore not surprising that the derivative of the transformation matrix

may be expressed through the relative twist of these frames

$$\dot{\boldsymbol{H}}_i^j = \begin{bmatrix} \dot{\boldsymbol{R}}_i^j & \dot{\boldsymbol{o}}_i^j \\ \boldsymbol{0} & 0 \end{bmatrix} = \big[\boldsymbol{t}_i^{j,j}\times\big]\boldsymbol{H}_i^j, \qquad \big[\boldsymbol{t}\times\big] = \begin{bmatrix} \big[\boldsymbol{\omega}\times\big] & \boldsymbol{v} \\ \boldsymbol{0} & 0 \end{bmatrix} \tag{2.22}$$

The $\big[\boldsymbol{\omega}\times\big]$ denotes the 3×3 skew symmetric matrix of the angular velocity vector. With a slight abuse of notation the 4×4 twist matrix also has the same symbol. Here a second superscript is used to denote the frame of expression of the twist. In this notation a twist $\boldsymbol{t}_i^{k,j}$ of body i is with respect to body j and expressed in frame k. For convenience the subscript and superscripts are omitted when unambiguous. For example, the ISA $\boldsymbol{s}_i^{k,i-1}$ of joint i is always with respect to the lower body $i-1$, such that this second superscript is dropped

$$\boldsymbol{t}_i^{k,i-1} = \boldsymbol{s}_i^k \dot{q}_i \tag{2.23}$$

When the twist is constant Eq. 2.22 has a uniform solution for the finite motion of a body

$$\boldsymbol{H}_i^j(t) = \exp(\big[\boldsymbol{t}_i^{j,j}\times\big]t)\boldsymbol{H}_i^j(0) \tag{2.24}$$

in which $\boldsymbol{H}_i^j(0)$ and $\boldsymbol{H}_i^j(t)$ are transformation matrices at the initial and final time respectively. The $\exp(\boldsymbol{A})$ denotes the matrix exponential of $\boldsymbol{A}$. This expression gives rise to an elegant formulation of the forward kinematics of serial chains [20]

$$\boldsymbol{H}_n^0(t) = \boldsymbol{H}_1^0\boldsymbol{H}_2^1\cdot\ldots\cdot\boldsymbol{H}_n^{n-1} = \prod_i^n \exp(\big[\boldsymbol{s}_i^0\times\big]q_i)\boldsymbol{H}_n^0(0) \tag{2.25}$$

Additionally, the twists are expressed in another frame by the adjoint transformation matrix $\mathrm{Ad}\big(\boldsymbol{H}\big)$ of $\boldsymbol{H}$

$$\boldsymbol{t}_\bullet^{j,\bullet} = \mathrm{Ad}\big(\boldsymbol{H}_i^j\big)\boldsymbol{t}_\bullet^{i,\bullet}, \qquad \mathrm{Ad}\big(\boldsymbol{H}\big) = \begin{bmatrix} \boldsymbol{R} & \boldsymbol{0} \\ \big[\boldsymbol{o}\times\big]\boldsymbol{R} & \boldsymbol{R} \end{bmatrix} \tag{2.26}$$

in which the $\bullet$ denotes frame numbers which are not altered by the transformation. The time derivative of this adjoint transformation is formed by an adjoint twist matrix, denoted by $\mathrm{ad}(\boldsymbol{t})$, as follows from the inclusion of Eq. 2.22 in Eq. 2.26

$$\frac{d}{dt}(\mathrm{Ad}\big(\boldsymbol{H}_i^j\big)) = \mathrm{ad}(\boldsymbol{t}_i^{j,j})\mathrm{Ad}\big(\boldsymbol{H}_i^j\big), \qquad \mathrm{ad}(\boldsymbol{t}) = \begin{bmatrix} \big[\boldsymbol{\omega}\times\big] & \boldsymbol{0} \\ \big[\boldsymbol{v}\times\big] & \big[\boldsymbol{\omega}\times\big] \end{bmatrix} \tag{2.27}$$

This adjoint twist matrix dictates how a twist changes under the influence of another twist. For example, the ISA higher in a serial chain change under actuation of the lower chain according to

$$\frac{\partial}{\partial q_i}\left(\boldsymbol{s}_j^0\right) = \mathrm{Ad}\big(\boldsymbol{H}_{i-1}^0\big)\frac{\partial}{\partial q_i}\left(\mathrm{Ad}\big(\boldsymbol{H}_i^{i-1}\big)\right)\boldsymbol{s}_j^i = \mathrm{ad}(\boldsymbol{s}_i^0)\boldsymbol{s}_j^0 \quad \text{for } i<j. \tag{2.28}$$

In this derivation the chain of Eq. 2.25 is decomposed into constant and varying part. By inclusion of Eq. 2.27 and Eq. 2.26 these partial derivatives are

expressed in the inertial frame. This operation — also termed the adjoint representation of the Lie bracket[2] — enables the concise description of the derivatives of kinematics and dynamics as used in Chapter 4 and 5.

A wrench changes its expression through the transposed inverse of the joint transformation matrix, since the power (Eq. 2.6) is invariant under transformation:

$$P = (\mathbf{w}^i)^\top \boldsymbol{t}^i = (\mathbf{w}^j)^\top \boldsymbol{t}^j \tag{2.29}$$

$$(\mathbf{w}^i)^\top \mathrm{Ad}\big(\boldsymbol{H}^i_j\big)\boldsymbol{t}^j = (\mathbf{w}^j)^\top \boldsymbol{t}^j \tag{2.30}$$

from which the transformation rule for wrenches is deduced

$$\mathbf{w}^j = \mathrm{Ad}\big(\boldsymbol{H}^i_j\big)^\top \mathbf{w}^i \tag{2.31}$$

Note that this transformation uses the inverse transformation of Eq. 2.26

Momentum and rigid body dynamics

For the study of dynamic balance, the momentum and rigid body dynamics are considered in the screw theory framework. Consider the linear momentum $\boldsymbol{p}$ and angular momentum $\boldsymbol{\xi}$ around the origin of the reference frame, which is generated by a particle of $\mathrm{d}m$ mass located at $\boldsymbol{r}$, subject to a twist $\boldsymbol{t}^\top = [\boldsymbol{\omega}^\top, \boldsymbol{v}^\top]$

$$\boldsymbol{p} = \mathrm{d}m\dot{\boldsymbol{r}} = -\mathrm{d}m\boldsymbol{r} \times \boldsymbol{\omega} + \mathrm{d}m\boldsymbol{v}, \tag{2.32}$$

$$\boldsymbol{\xi} = \boldsymbol{r} \times \boldsymbol{p} = -\mathrm{d}m\boldsymbol{r} \times \boldsymbol{r} \times \boldsymbol{\omega} + \mathrm{d}m\boldsymbol{r} \times \boldsymbol{v} \tag{2.33}$$

Together the linear and angular momentum form a screw $\boldsymbol{h}$ which is termed momentum wrench in this thesis, or impulsive wrench by Ball [11]

$$\boldsymbol{h} = \begin{bmatrix} \boldsymbol{\xi} \\ \boldsymbol{p} \end{bmatrix} = \boldsymbol{M}\boldsymbol{t} \tag{2.34}$$

The mass matrix $\boldsymbol{M}$ of a rigid body is obtained by an integral over all particles of the body. Using Eq. 2.32 and Eq. 2.32 the following mass matrix is obtained

$$\boldsymbol{M} = \int_V \begin{bmatrix} -[\boldsymbol{r}\times]^2 & [\boldsymbol{r}\times] \\ -[\boldsymbol{r}\times] & \boldsymbol{I}_3 \end{bmatrix} \mathrm{d}m = \begin{bmatrix} \boldsymbol{G} - m[\boldsymbol{c}\times]^2 & m[\boldsymbol{c}\times] \\ -m[\boldsymbol{c}\times] & m\boldsymbol{I}_3 \end{bmatrix} \tag{2.35}$$

Here $m = \int_V \mathrm{d}m$ denotes the mass, $\boldsymbol{c}$ the location of the COM and $\boldsymbol{G}$ the second moment of inertia tensor around the COM, in short moment of inertia . A 3×3 identity matrix is denoted with $\boldsymbol{I}_3$

The mass matrix couples a twist with a wrench and therefore changes its frame of expression by following transformation rule

$$\boldsymbol{M}^j_\bullet = \mathrm{Ad}\big(\boldsymbol{H}^i_j\big)^\top \boldsymbol{M}^i_\bullet \mathrm{Ad}\big(\boldsymbol{H}^i_j\big) \tag{2.36}$$

This can also be deduced from the frame invariance of kinetic energy $K = 1/2\ \boldsymbol{t}^\top \boldsymbol{M}\boldsymbol{t}$.

[2] The Lie bracket is given by $[\boldsymbol{t}_i, \boldsymbol{t}_j] = [\boldsymbol{\omega}_i \times \boldsymbol{\omega}_j \quad \boldsymbol{\omega}_i \times \boldsymbol{v}_j - \boldsymbol{v}_i \times \boldsymbol{\omega}_j] = \mathrm{ad}(\boldsymbol{t}_i)\boldsymbol{t}_j$

By rotation and translation along its principal axes, the mass matrix may be diagonalized. The corresponding transformation can be found through eigenvalue decomposition. The resulting principal moments of inertia tensor $\boldsymbol{G}_p = \mathrm{diag}(\boldsymbol{g})$ is characterized by three principal moments of inertia $\boldsymbol{g} = \begin{bmatrix} g_1 & g_2 & g_3 \end{bmatrix}$. From Eq. 2.35 it can be shown that for all feasible – or constructible – bodies the principal moments of inertia are positive and that a triangle inequality holds. Together with the mass positivity the following set of inequality equations on the mass matrix are obtained

$$m \geq 0, \qquad \boldsymbol{g} \geq 0, \qquad g_i + g_j \geq g_k \tag{2.37}$$

For the process of dynamic balance it is essential that these positivity equations are respected in order to be able to construct the envisioned bodies and mechanism.

According Newton-Euler laws, the wrench acting on a body is the derivative of the momentum wrench (Eq. 2.34). Therefore the derivatives of both the twist and the mass matrix are needed. The derivative of the mass matrix of body i is found by transforming it into a body-fixed frame. In this frame it is constant $\dot{\boldsymbol{M}}_i^i = 0$ under the assumption of rigid body dynamics. Therefore the time derivative of the mass matrix becomes

$$\dot{\boldsymbol{M}}_i^0 = \frac{\partial}{\partial t}\left(\mathrm{Ad}\big(\boldsymbol{H}_0^i\big)\right)^\top \boldsymbol{M}_i^i \mathrm{Ad}\big(\boldsymbol{H}_0^i\big) + \mathrm{Ad}\big(\boldsymbol{H}_0^i\big)^\top \boldsymbol{M}_i^i \frac{\partial}{\partial t}\left(\mathrm{Ad}\big(\boldsymbol{H}_0^i\big)\right) \tag{2.38}$$

$$= -\mathrm{ad}(\boldsymbol{t}_i^{0,0})^\top \boldsymbol{M}_i^0 - \boldsymbol{M}_i^0 \mathrm{ad}(\boldsymbol{t}_i^{0,0}) \tag{2.39}$$

after inclusion of Eq. 2.36 and Eq. 2.27. From now on all elements are expressed with respect to the fixed inertial frame, unless specified otherwise, such that the superscripts are dropped. Following Featherstone [38], the wrench acting on body i becomes

$$\mathbf{w}_i = \dot{\boldsymbol{h}}_i = \boldsymbol{M}_i \dot{\boldsymbol{t}}_i - \mathrm{ad}(\boldsymbol{t}_i)^\top \boldsymbol{M}_i \boldsymbol{t}_i \tag{2.40}$$

in which the self-annihilation property of the adjoint twist matrix ($\mathrm{ad}(\boldsymbol{t})\boldsymbol{t} = 0$) eliminates the second part of Eq. 2.39. The first part of the wrench is due to the acceleration twist $\dot{\boldsymbol{t}}$. The second part, termed bias wrench, is a combination of the centripetal force and gyroscopic effects due to the misalignment of the angular velocity vector with the principal axes of the body. This shows that a free-floating body ($\mathbf{w} = 0$) can experience acceleration twists $\dot{\boldsymbol{t}} = \boldsymbol{M}^{-1}\mathrm{ad}(\boldsymbol{t})^\top \boldsymbol{M}\boldsymbol{t}$ even though the momentum wrench is constant.

With this, the introduction of the rigid body dynamics in screw theory framework is completed. The dynamic balance conditions in this formulation will be derived and integrated in the following section to show their nonholonomic character.

2.3 Nonholonomic moment balance conditions

Force balance of a general set of bodies is ensured by a condition on pose, namely by making the total COM of these bodies stationary, or moving with

a constant velocity. This allows for several analysis and synthesis tools for dynamic balance [10, 107]. Moment balance conditions on pose level alone do not exist in general, due to the nonhonomicity nature of angular momentum conservation [80]. The moment balance conditions of an arbitrary set of bodies are dependent on both pose and velocity of the bodies.

In this section, the implications of this property on dynamic balance will be investigated. Firstly, the integration of the dynamic balance conditions from shaking wrenches to conditions on pose is attempted. Secondly, an example is shown to illustrate that the nonholonomic behaviour allows for a wider choice of dynamically balanced trajectories than expected from the number of DOF and dynamic balance conditions.

Dynamic balance conditions

Dynamic balance requires zero shaking wrench $\mathbf{w}_\mathrm{s}$ of the system. The shaking wrench is the time derivative of the sum of the momentum wrenches in a system. For a system with n bodies the dynamic balance conditions therefore read

$$\mathbf{w}_\mathrm{s} = \sum_{i=1}^{n} \dot{\boldsymbol{h}}_i \equiv \mathbf{0} \tag{2.41}$$

Since these dynamic balance conditions depend only on a sum of derivatives, they may be integrated with respect to time t through through anti-differentiation

$$\int_0^t \mathbf{w}_\mathrm{s} = \sum \boldsymbol{h}_i(t) - \sum \boldsymbol{h}_i(0) \equiv \text{const.} \tag{2.42}$$

For convenience the summation bounds are dropped. By applying the proper boundary conditions the dynamic balance condition resolves to

$$\sum \boldsymbol{h}_i(t) \equiv \sum \boldsymbol{h}_i(0) \tag{2.43}$$

This shows that the sum of the momentum wrenches in the system has to be constant. If the system is initially at rest ($\dot{\boldsymbol{q}}_\mathrm{ini} = 0$, $\boldsymbol{h}_i(0) = 0$), the dynamic balance condition may be equated to zero

$$\sum \boldsymbol{h}_i(t) \equiv \mathbf{0} \tag{2.44}$$

The force and moment balance conditions are now separated (Eq. 2.34) to show that a second integration step leads to uniform conditions on pose for force balance

$$\sum \boldsymbol{p}_i = \sum m_i \dot{\boldsymbol{c}}_i \equiv \mathbf{0} \tag{2.45}$$

$$\sum \boldsymbol{\xi}_i = \sum \boldsymbol{G}_i \boldsymbol{\omega}_i + \sum m_i \boldsymbol{c}_i \times \dot{\boldsymbol{c}}_i \equiv \mathbf{0} \tag{2.46}$$

When the masses are assumed constant ($\dot{m}_i = 0$) Eq. 2.45 can be integrated a second time to yield the force condition on the centre of masses in the system

$$\sum m_i \boldsymbol{c}_i(t) \equiv \sum m_i \boldsymbol{c}_i(0) \tag{2.47}$$

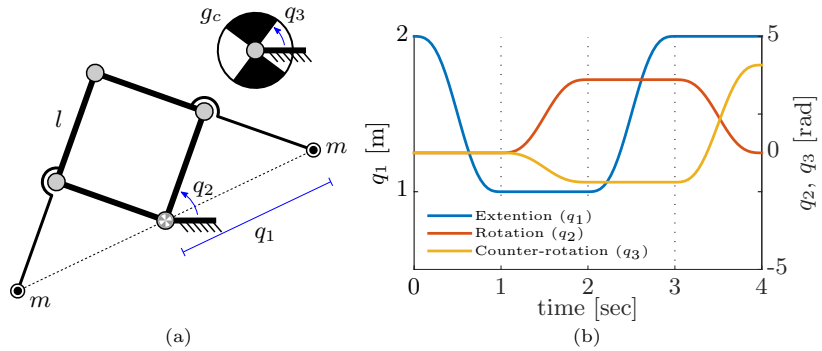

Figure 2.7: (a) A force balanced pantograph is dynamically balanced by a counter-rotating inertia wheel. (b) The nonholonomic behaviour of this system can be used to reach any pose in its configuration space in a dynamically balanced manner.

from which the force balance condition on the total centre of mass $\boldsymbol{c}_\mathrm{T}$ is deduced

$$\frac{1}{m_\mathrm{T}} \sum m_i \boldsymbol{c}_i = \boldsymbol{c}_\mathrm{T} \equiv \text{const.} \tag{2.48}$$

with m_T as the total mass of the system.

When the moment balance conditions (Eq. 2.46) are integrated in a similar fashion, the resulting condition will in general be dependent on both the pose $(\boldsymbol{c}_i, \boldsymbol{R}_i)$ and the velocities $(\dot{\boldsymbol{c}}_i, \boldsymbol{\omega}_i)$ of the bodies during motion. In other words, the moment balance condition cannot be integrated to obtain unique conditions on admissible orientations and positions of the bodies only. Therefore these conditions constrain paths and not poses, as shown by the falling cat example. For the cat any orientation could be obtained dependent on the choice of path.

Example: nonholonomic pantograph

This nonholonomic behaviour can also be exploited [81] to reach more poses in a dynamically balanced way. For example, consider a symmetric pantograph which can rotate around its base axis (Fig. 2.7a). For simplicity reasons it is assumed that its inertial properties can be modelled by two point masses at the ends of the pantograph. The first DOF, i.e., the extension and retraction q_1, is dynamically balanced since the point masses are equal and move in an opposite direction on a line. The second DOF q_2, the rotation of the pantograph as a whole, is dynamically balanced by actuation of a counter-rotation of an inertia wheel. The angular velocity of the wheel is $\dot{q}_3$.

The moment balance condition of this mechanism becomes

$$g_\mathrm{P}(q_1)\dot{q}_2 + g_\mathrm{c}\dot{q}_3 \equiv 0 \tag{2.49}$$

in which $g_\mathrm{c} = 5$ kg m^2 is the MOI of the counter-rotating wheel and $g_\mathrm{P}(q_1)$ is the MOI of the pantograph

$$g_p(q_1) = 2mq_1^2 \tag{2.50}$$

with $m = 1$ kg. Since the MOI of the pantograph is changing due to the extension and retraction, the velocity of the counter-rotating wheel has to be

$$\dot{q}_3 = -\frac{g_{\mathrm{p}}(q_1)}{g_{\mathrm{c}}}\dot{q}_2 \tag{2.51}$$

Although at each given moment only two DOFs of the system are dynamically balanced, all kinematically admissible combinations of q_1, q_2 and q_3 can be reached in a dynamically balanced manner by choosing the trajectory, (i.e. q_1, q_2, $\dot{q}_2$).

For example, by sequential extension ($\Delta q_1 = -1$ m), rotation ($\Delta q_2 = \pi$ rad), retraction ($-\Delta q_1 = 1$ m) and retrograde-rotation ($-\Delta q_2 = -\pi$ rad), the pantograph is back to its initial pose, as shown in Fig. 2.7b. The counter-rotating inertia wheel, on the other hand, must end up in a different orientation, as it has counter-acted a changed moment of inertia of the pantograph. The change of angle of the counter-rotating inertia wheel is computed as

$$\Delta q_3 = -\frac{2m}{g_{\mathrm{c}}}(2q_{1,\mathrm{ini}} + \Delta q_1)\Delta q_1 \Delta q_2 \tag{2.52}$$

in which $q_{1,\mathrm{ini}} = 2$ m is the initial opening of the pantograph. By repetitive application of this cycle, any value for q_3 can be obtained.

This shows that, thanks to its nonholonomic character, more poses could be reached than expected from the number DOF and number of constraints of the mechanism. This 'wiggling', 'cat-like' behaviour can be used for example in space to reorient a satellite without applying external torques, i.e. without using its thrusters.

Implications of nonholonomic conditions for synthesis methods

For the goal of deriving a comprehensive synthesis method, this nonholonomic character has the consequence that nonholonomic kinematics, such as rolling contacts, should be used in conjunction with parabola drawing devices, such as Van Schooten's linkage, to exactly trace the moment balance condition of an arbitrary set of bodies. This does not seem very practical as a large number of additional links and friction contacts are needed, potentially more costly and impractical than the common solution of an additional motor to actively generate moment balance. It should be mentioned that it is also possible to achieve dynamically balanced motion of an arbitrary force balanced linkage by inserting a spherical joint, or a revolute joint in the planar case, between the mechanism and the base at the location of the common COM. When this joint is free to move, the mechanism as a whole will counteract the inbalance of the internal motion. The disadvantage of this is that the absolute orientation of the linkage becomes uncontrollable.

When we wish to use conventional linkages, consisting of revolute or prismatic joints, an alternative approach is needed since conventional joints apply only holonomic constraints. They can therefore not be used to exactly trace the moment balance conditions of an arbitrary set of bodies. However, we can apply more 'superfluous' conditions to balance the motion of an arbitrary

set of bodies. Alternatively, we could make sure that we start from a set of bodies with specific dynamic properties. Either way, additional constraints are needed for the synthesis of dynamically balanced mechanisms. Although some approaches are presented in literature, such as symmetry or reduction of DOF, the exact nature of these additional constraints still remains elusive [96]. This underlines the need for investigation of the essential kinematic properties as formulated in Objective 2 of this thesis.

Frame-invariant dynamic balance conditions

On a side note, another difference between force and moment balance is revealed when the dynamic balance conditions Eq. 2.31 are transformed from one (fixed) reference frame (a) to another (b) Eq. 2.44. It shows that force balance (FB, Eq. 2.45) is a frame invariant property, whereas moment balance (MB, Eq. 2.46) is not frame invariant

$$\sum \boldsymbol{p}_i^b = (\boldsymbol{R}_b^a)^\top \underbrace{\sum \boldsymbol{p}_i^a}_{\text{FB}}, \tag{2.53}$$

$$\sum \boldsymbol{\xi}_i^b = (\boldsymbol{R}_b^a)^\top \underbrace{\sum \boldsymbol{\xi}_i^a}_{\text{MB}} - (\boldsymbol{R}_b^a)^\top \left[\boldsymbol{o}_b^a \times\right] \underbrace{\sum \boldsymbol{p}_i^a}_{\text{FB}} \tag{2.54}$$

From these equations it is deduced that if a system is force balanced when expressed in one frame (a), it is also force balanced when evaluated in any another frame of reference (b). This frame invariance does not hold for moment balance, that is for moment balance without force balance. Th residual shaking forces ($\sum \boldsymbol{p}_i^a$) will induce a shaking moment when evaluated around a different point ($\boldsymbol{o}_b^a$). This means that a system can simply be referred to a force balanced or dynamically balanced, while for moment balanced systems the point of application should always be mentioned. It might discussed that solely moment balance has some advantages when the application point is chosen favorable, for example if the point is chosen to be the elastic center of the base. However, according to the best knowledge of author no examples of moment balance without force balance are found in literature, whereas force balance without moment balance is prevalent. This is one of the reasons why in this thesis moment balance is not treated separately but always in conjunction with force balance.

2.4 Dynamic balance versus dynamic decoupling

Dynamic decoupling is a concept that is closely related to dynamic balance: a system is dynamically balanced when the internal motion of the mechanism does not induce shaking forces and shaking moments on the *fixed* base, whereas a system is dynamically decoupled when the *motion* of the base does not induce inertial forces and torques on the internal DOFs of the mechanism. As these dynamically decoupled mechanisms may be regarded as rigid bodies they can

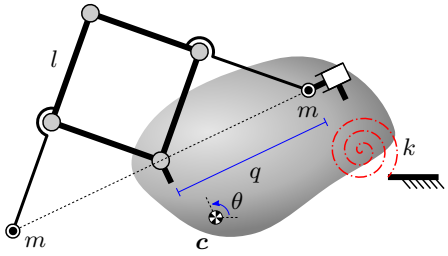

Figure 2.8: A dynamically balanced pantograph with a prismatic joint attached to a floating base. The red striped spiral denotes a torsional spring between the floating base and the inertial frame to simulate a base with a finite stiffness. Since we assume that the spring only induces a torsional stiffness, the location of attachment point has no influence and is chosen arbitrary.

be stacked and combined to form larger dynamically balanced structures, as done with several synthesis methods [86, 120].

Some literature seems to suggest that dynamic balance automatically leads to dynamic decoupling [97, 86, 120, 63]. However, dynamic balance is a necessary but not a sufficient conditions for dynamic decoupling, as shown in this section. Furthermore, it requires constant moments of inertia of the complete mechanism.

First, this section gives an example of a dynamically balanced mechanism which has a variable moment of inertia to show that dynamic decoupling and dynamic balance cannot be equated. this difference is then described more formally by providing the equations of motion of an arbitrary mechanism with a moving base. Lastly, this section closes with remarks on the definition of dynamic balance.

Example: a free-floating pantograph and a pantograph with a compliant base

For the purpose of showing the difference between dynamic balance and dynamic decoupling, consider a symmetrical, dynamically balanced pantograph with a prismatic joint attached to a free-floating base (Fig. 2.8). The pantograph is actuated by a linear motor governing the extension q of the pantograph. The mass distribution of the pantograph is chosen to be two point masses of 1 kg each, attached to its ends. This pantograph is dynamically balanced since the motion of the point masses are co-linear, opposite and equal, just as in the previous example (Section 2.3). Due to the varying distance between the two point masses, the system's total moment of inertia is not constant. The length of the segments of the pantograph l are all 1 m. The centre of mass of the complete system, i.e. base and pantograph, is located at $\boldsymbol{c}$. When fully collapsed ($q = 0$) the system has a moment of inertia of 1 kg m^2 around $\boldsymbol{c}$. The angle of the base with respect to the inertial reference frame is denoted by θ.

Three cases are simulated to show the effect of a moving base (Fig. 2.9)

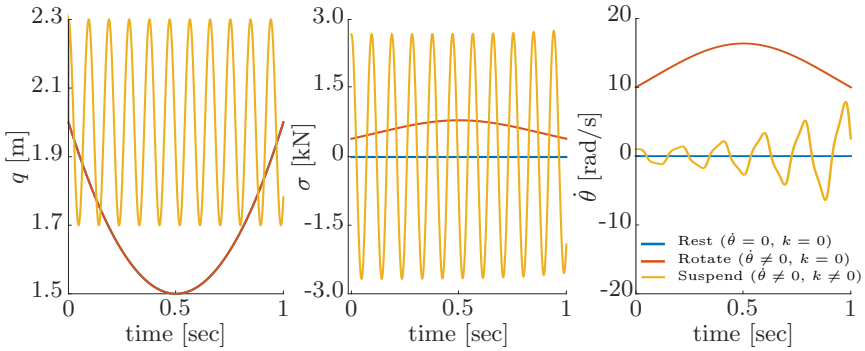

(a) Pantograph extension (b) Actuation force (c) Base velocity

Figure 2.9: Simulation results of a dynamically balanced slider pantograph with a varying total moment of inertia, which is placed on a floating base. Three cases are simulated; with a free-floating base $k = 0$ initially at rest $\dot{\theta}_{\text{ini}} = 0$ (*blue*), with initial angular velocity of the base $\dot{\theta}_{\text{ini}} \neq 0$ and $k = 0$ (*red*), and the base that is suspended by spring $k \neq 0$ with an initial vibration $\dot{\theta}_{\text{ini}} \neq 0$ (*yellow*).

on the internal motion of the mechanism. In the first two cases the base is free-floating: 1) with the base initially in rest ($\dot{\theta}_{\text{ini}} = 0$ rad/s) and 2) with an initial base velocity of $\dot{\theta}_{\text{ini}} = 10$ rad/s. In both cases the extension q of the pantograph is changed from 2 m to 1.5 m and back again (Fig. 2.9a). 3) In the third case the base is supported by a spring with a finite stiffness to show the effect of the combination of robot motion and base vibrations. A rotational spring is attached in $\boldsymbol{c}$ and has a spring constant of $k = 10^4$ Nm/rad. This yields a natural frequency of the complete system around 5.4 Hz for $q = 2$ m, depending on the pose of the pantograph. The base is given an initial velocity of $\dot{\theta}_{\text{ini}} = 1$ rad/s to initiate vibration. To show that a dynamic balance mechanism does affect the base vibration, the pantograph is actuated by a harmonic signal with an amplitude of 0.3 m at 10.8 Hz, twice the natural frequency of the system (Fig. 2.9a).

In the first case, when the base is initially at rest, it remains in rest, undisturbed by movement of the mechanism (Fig. 2.9c). This confirms the dynamic balance of the system. In the second case, the base has a non-zero, but also a non-constant angular velocity. The angular momentum of the base is therefore also not constant. The fact that the pantograph has a variable moment of inertia around $\boldsymbol{c}$ explains this velocity change of the base. The conservation of angular momentum of the whole system leads to a change in angular momentum of the base itself. Furthermore, when the base is rotating, the centripetal forces acting on pantograph require additional actuator forces as seen in Fig. 2.9b. The third case shows aggravation of the base vibrations due to inertial motion of the dynamically balanced pantograph. This shows that, although the internal motion with respect to a fixed base is dynamically balanced, it is not dynamically decoupled and thus it will not feel like a rigid body. This means that a dynamically balanced mechanism can in fact aggravate existing

base vibrations.

Governing equations

The difference between dynamic decoupling and dynamic balance can also be shown from the equations of motion. Consider a general mechanism consisting of n bodies attached to a free-floating base. The twist of each body can be broken down into a twist relative to the base $\boldsymbol{t}_i^{\mathrm{B}}$ and a twist of the base relative to the inertial frame of reference $\boldsymbol{t}_{\mathrm{B}}$. All twists and wrenches are expressed in the inertial frame such that this superscript is dropped. The twist of each body is therefore written as

$$\boldsymbol{t}_i = \boldsymbol{t}_{\mathrm{B}} + \boldsymbol{t}_i^{\mathrm{B}} \tag{2.55}$$

Assume that the system is initially at rest ($\boldsymbol{t}_i^{\mathrm{B}} = 0$, and $\boldsymbol{t}_{\mathrm{B}} = 0$), such that the dynamic balance condition (Eq. 2.44) becomes

$$\boldsymbol{h}_{\mathrm{I}} = \sum \boldsymbol{M}_i \boldsymbol{t}_i^{\mathrm{B}} \equiv \mathbf{0} \tag{2.56}$$

Now the base starts moving it with $\boldsymbol{t}_{\mathrm{B}}$. This means that the total momentum of the mechanism becomes

$$\boldsymbol{h} = \boldsymbol{M}_{\mathrm{T}} \boldsymbol{t}_{\mathrm{B}} + \sum \boldsymbol{M}_i \boldsymbol{t}_i^{\mathrm{B}} = \boldsymbol{h}_{\mathrm{B}} + \boldsymbol{h}_{\mathrm{I}} \tag{2.57}$$

Here $\boldsymbol{M}_{\mathrm{T}} = \boldsymbol{M}_{\mathrm{B}} + \sum \boldsymbol{M}_i$ is the total mass matrix of the mechanism and base. By taking the time derivative of the total momentum wrench through a chain rule with respect to base motion $\boldsymbol{t}_{\mathrm{B}}$ and internal motion q_i, the total wrench $\mathbf{w}$ exerted on the system is found

$$\mathbf{w} = \dot{\boldsymbol{h}}_{\mathrm{B}} + \dot{\boldsymbol{h}}_{\mathrm{I}} \tag{2.58}$$

$$= \underbrace{\boldsymbol{M}_{\mathrm{T}} \dot{\boldsymbol{t}}_{\mathrm{B}} - \mathrm{ad}(\boldsymbol{t}_{\mathrm{B}})^{\top} \boldsymbol{M}_{\mathrm{T}} \boldsymbol{t}_{\mathrm{B}}}_{\text{Rigid body}} + \underbrace{\sum \frac{\partial}{\partial q_i} \left(\boldsymbol{M}_{\mathrm{T}} \right) \boldsymbol{t}_{\mathrm{B}} \dot{q}_i}_{\text{Inertia change}} \underbrace{- \mathrm{ad}(\boldsymbol{t}_{\mathrm{B}})^{\top} \boldsymbol{h}_{\mathrm{I}} + \mathbf{w}_{\mathrm{I}}}_{\text{Dynamic balance}} \tag{2.59}$$

This is the sum of all wrenches acting on the system when the base and the mechanism is moving. Here $\mathbf{w}_{\mathrm{I}}$ denotes the shaking wrench due to internal motion of the mechanisms

$$\mathbf{w}_{\mathrm{I}} = \sum \frac{\partial}{\partial q_i} \left(\boldsymbol{h}_{\mathrm{I}} \right) \dot{q}_i \tag{2.60}$$

Three types of effects appear in Eq. 2.59

1. The first effect is due to the motion of the base and mechanism as a whole, i.e. when the mechanism and the base are rigid. This is therefore termed the 'rigid body effect' (Eq. 2.40). In dynamically decoupled systems only this wrench remains.

2. The second effect is attributed to a change of the total mass matrix of the mechanism by internal motion. This effect can be cancelled by making the total mass matrix constant.

3. The third effect is due to the change of internal momentum of the mechanism. This effect is cancelled by dynamic balance ($\boldsymbol{h}_{\mathrm{I}} = \mathbf{w}_{\mathrm{I}} = \mathbf{0}$)

For the system to be dynamically decoupled, effects 2 and 3 should be eliminated, leaving solely the rigid body effects. This means the system should be dynamically balanced and have a constant mass matrix ($\partial/\partial q_i(\boldsymbol{M}_{\mathrm{T}})\boldsymbol{t}_{\mathrm{B}} = 0$, for all i) with respect to the base.

A force-balanced mechanism has a constant total centre of mass with respect to the base by the definition of Eq. 2.48. The total inertia matrix $\boldsymbol{G}_{\mathrm{T}}$, on the other hand, is not necessary constant for dynamically balanced mechanisms, as illustrated by the pantograph example. Therefore, the partial derivative of total mass matrix becomes

$$\frac{\partial}{\partial q_i}(\boldsymbol{M}_{\mathrm{T}}) = \begin{bmatrix} \dfrac{\partial}{\partial q_i}(\boldsymbol{G}_{\mathrm{T}}) & \mathbf{0} \\ \mathbf{0} & \mathbf{0} \end{bmatrix} \tag{2.61}$$

This shows that indeed the forces and translations are decoupled by force balance, whereas moments and rotations are not necessarily decoupled by dynamic balance. For the latter, a constant total moment of inertia is required as well. This means that kinetic energy may be transferred between the base and a dynamically balanced mechanism, thereby affecting the internal motion of the mechanism. This illustrates a second fundamental difference between force balance and moment balance.

On the definition of dynamic balance

The difference between the claims in literature on the equality of dynamic balance and dynamic decoupling [97, 86, 120, 63], and the results presented here, is perhaps a matter of definition: dynamic balance may be defined with respect to 1) a fixed base or 2) to the inertial frame. In the first case, additional conditions are required to ensure dynamic decoupling, while in the second case the DOFs of the base have to be included in the moment balance condition.

The claims in literature suggest that the second definition is adopted in these papers. Yet none of these papers consider the effect of moving the base in the moment balance condition, and thereby implicitly adopt the first definition of dynamic balance. This also seems be the logical choice since dynamic balance is then a property of the mechanism only and does not depend on the (possible) movements of the base.

Part of the discrepancy in literature can be explained by the fact that three prominent dynamically balanced mechanisms, the two four-bars in [86] and the crank-slider [19], also have a constant moment of inertia [34] and hence are dynamically decoupled. A further explanation is that force balance leads to a decoupling of the translations and forces, whereas for moment balance an additional decoupling condition should be satisfied.

Theoretically, this means that dynamically balanced mechanisms can aggravate – but not induce – base vibrations, since kinetic energy can be exchanged with a moving base, as shown also by the simulation. Fortunately, most dynamically balanced robots will be supported by a sufficiently rigid frame, resulting

in negligible base velocities. Combined with an approximately constant total moment of inertia, it may be expected that the difference between dynamic decoupling and dynamic balance is of minor significance for this application. However, in other applications where the base undergoes larger movements, such as in satellite applications, the fundamental difference between dynamic balance and dynamic decoupling has a substantial influence. Also, when a dynamically balanced mechanism is to be used as a dynamically balanced module for synthesis purposes, the mechanism must additionally possess a constant total moment of inertia in the plane of movement [120].

2.5 Conclusion

In this chapter the screw theory framework is presented alongside two fundamental differences between force and moment balance. Screw theory enables a uniform treatment of the linear and angular domain. It furthermore provides a geometrical interpretation of the linear and angular velocities, and of the forces and moments acting on a rigid body. This enables a concise formulation of the dynamic balance conditions for investigation of the nonholonomic nature of the moment balance conditions and the difference between dynamic decoupling and dynamic balance.

The moment balance conditions, as opposed to the force balance conditions, cannot be formulated as conditions on pose alone. This condition will, in general, also be dependent on linear and angular velocities. This nonholonomic property of the angular momentum conservation complicates the search for synthesis methods, as the force balance methods cannot readily be generalized to moment balance. On the other hand, trajectory planning can be used to enable a larger dynamically balanced range of motion than expected from the instantaneous DOF of the system.

Dynamic balance does not automatically lead to a complete dynamic decoupling of the robot's internal motion from the base movements. With force balance, the translations of the base will not influence the relative motion of the system. For an additional decoupling of the rotations of the base, dynamic balance has to be combined with a constant total moment of inertia. This adds an additional constraint on the derivation of new synthesis methods that rely on stacking and recombination of dynamically decoupled modules.

Acknowledgment

This chapter has been compiled after discussions with dr. ir. Marcel Ellenbroek, dr. Yuanqing Wu and prof. dr. Marco Carricato. Many thanks to them for their insights. The author also would like to thank dr. ir. J.P. Meijaard for his insights and references on the 'falling cat problem'.

Chapter 3

A screw based methodology for instantaneous dynamic balance

Fast-moving industrial robots exert large varying reaction forces and moments on their base frame, inducing vibrations, wear and accuracy degeneration. These shaking forces and moments can be eliminated by a specific design of the mass distribution of the robot links, resulting in a dynamically balanced mechanism. Obtaining the conditions for dynamic balance proves to be a hurdle even for simple planar parallel mechanisms due to the required inclusion and inspection of the kinematic relations. In this chapter, a screw theory based methodology is presented, which gives and solves the necessary instantaneous dynamic balance conditions for planar and spatial mechanisms in a uniform and geometrical manner. Instantaneous dynamic balance yields a pose in which robot accelerations induce no shaking forces and moments. This is interpreted as an intersection point of multiple reactionless paths. This method is applied to a 2-DOF planar mechanism, named the Fuga I, for which it resulted in two perpendicularly intersecting reactionless paths, intersecting in the middle of the workspace. Experiments on this demonstrator validated the instantaneous dynamic balance by showing a reduction of approximately 95% of the peak-to-peak shaking forces and moments over the intersecting reactionless paths.

Dynamic balance through a direct application of screw theory and associated geometric interpretation is attempted in this chapter (Objective 1). Since screw theory is mainly confined to instantaneous properties such as velocities and forces, the resulting balancing method is also instantaneous, meaning it only holds for a single pose. This pose however can be conveniently chosen to be the reference pose in which the mechanism is defined, such that the loop-closure constraints are satisfied by definition and the dynamic balance conditions do not encompass the solution to the loop-closure constraint equations.

This chapter is a reprint with minor adaptations from: J. J. de Jong, J. van Dijk, J. L. Herder, A screw based methodology for instantaneous dynamic balance. *Mechanism and Machine Theory* (2019), vol. 141, pp. 267-282.

3.1 Introduction

Industrial manipulators moving with high speeds and accelerations induce strong shaking forces and shaking moments at the base frame, causing disturbing vibrations in the frame and the surroundings [55]. These disrupting shaking forces and shaking moments can be eliminated by design of robot kinematics and inertial parameters, i.e. the mass, center of mass, and moments of ineria[68, 5], resulting in a dynamically balanced robot. When only the shaking forces are canceled the mechanism is said to be force balanced, and moment balanced when the shaking moments are canceled [108]. Since the shaking forces and moments are the derivatives of the linear and angular momentum, dynamic balance is obtained when the linear and angular momentum are constant (or zero in practice) [116].

Commonly, force balance is considered prior to moment balance and is obtained by choice of counter-masses [15, 83]. Consecutively, moment balance is achieved by addition of reaction wheels [41], counter-mechanisms [17, 63] or idler loops [7], potentially leading to unfavorable complexity, additional mass and higher motor torques [108].

Fortunately, some parallel mechanisms, such the kite type and the anti-parallelogram type $4R$ planar four-bar, permit a dynamically balanced design without the need of additional counter-mechanisms [86]. Yet, the process to find these designs relies on manipulation and factorization of the dynamic balancing conditions, i.e the momentum equations, in minimal coordinates. The intrinsic complexity of the loop-closure equations makes this manual process increasingly difficult for higher-DOF and spatial mechanisms. Therefore, Gosselin et al. partially automated the factorization process through toric geometry [44], and later algebraic geometry [76]. These algebraic methods still require some case-by-case treatment, and are yet to be extended to multi-DOF mechanisms. Furthermore, the algebraic nature of the balance procedure hinders the derivation of intuition, which is desired from a designers point of view.

Synthesis methods partly overcome the inspection of equations through stacking and recombination of dynamically balanced elements. Ricard et al. [86], and later Wu et al. [120], used the dynamic balanced four-bar linkage as a building block for multi-DOF, planar and spatial, dynamic balanced mechanisms, resulting in rather complex structures with unfavorable mass to payload ratios [104]. Van der Wijk et al. developed Fishers principal vector method of describing human motion [40] into a synthesis method, which produces inherently force balance mechanisms [107]. Based on this method, the 3-DOF over-actuated DUAL V was presented [109]. Dynamic balance was achieved over two perpendicular paths by mirror symmetry of the design. Although this synthesis methodology yields new dynamically balanced mechanisms, it does not cover all the possible solutions [96], and is currently confined to planar linkages.

Alternatively, dynamically balanced behavior can be enforced by limiting the robot motion to reactionless paths [84, 126], or trajectories [61]. These methods are less restrictive on the choice of inertial parameters and enable ‘dynamic balance when needed’. For example, during the traveling phase of a

pick-and-place robot, when accuracy is not essential, the robot can follow any trajectory but just before and during the pick or placement phase the robot follows a reactionless path, in order to let vibrations die out and enable an accurate motion. Currently, only for specific kinematic structures it is known how to shape these reactionless paths by design of the robot [84, 109].

In pursuit of an intuitive method that yields all force and moment balanced designs for arbitrary, planar or spatial linkages, we propose to use screw theory. In this chapter, a screw theory based method is presented that yields instantaneous dynamic balance for arbitrary mechanisms. Instantaneous dynamic balance is a pose in which the accelerations of the robot will not induce shaking forces and moments. We will show that, with additional conditions, these poses form intersections of multiple reactionless paths. This enables the design of reactionless paths by choice of this pose. The current method relies on a unified, geometric interpretation of the angular and linear momentum, leading to a set of feasibility bounds on the selection of the dynamic balance solution. The validity of this method will be shown by design, construction and measurement of an experimental demonstrator named the Fuga I, which is completely force balanced over the whole workspace and moment balanced along two perpendicular paths, which intersect in the middle of the workspace.

The chapter is organized as follows: Firstly, the screw theory with its application to rigid body dynamics will be recapitulated. The dynamic balance conditions are given in the screw theory framework. Secondly, the dynamic balance conditions are solved in two steps; A) on mechanism level – posing conditions on a specific number of the bodies, and B) on body level – solving these conditions to obtain a range of inertial parameters for these bodies. Thirdly, this method is applied to a five-bar demonstrator, and validated by both simulations and experiments. This chapter is a generalization of the method presented in [32], which was confined to planar mechanisms consisting of revolute joints.

3.2 Screw based dynamic balancing method

Screw theory [11] provides a unified geometrical interpretation of the instantaneous spatial motion – termed twist – of a rigid body and of the force and torque – termed wrench – acting on this body. On one hand, screw theory leans on Mozzi-Chasles' theorem, which states that all rigid body motion can be interpreted as a rotation around an axis in space and a translation along that axis. Similarly, for forces and moments, Poinsot's theorem states that the sum of forces and moments acting on a body can be represented by a force along a line in space and a torque around that line. These spatial interpretations are termed screws. On the other hand, screw theory draws on Lie's theory of exponential mappings and manifolds – which can be interpreted as the configuration space of connected rigid bodies. This states that the admissible twists lie on the tangent space of this manifold. These screws are therefore differential and instantaneous properties. Screw theory has been applied to a wide variety of modeling and design problems including singularity analysis [129], kinematic synthesis methods [62], and robot dynamics [90, 85, 38]. The

extension of screw theory to a dynamic balancing procedure for multi-DOF, closed-loop mechanisms has not been attempted.

Screw theory

The angular and linear velocity, respectively $\boldsymbol{\omega}$ and $\boldsymbol{v}$ together form the twist $\boldsymbol{t}$ of a body. The twist is interpreted as the rotation around an instantaneous axis in the direction of $\boldsymbol{\omega}$, passing through point $\boldsymbol{r}_t$ and a translation along this axis, called the pitch λ_t (Fig. 3.1). The velocity $\boldsymbol{v}$ is defined velocity of the points passing through the origin

$$\boldsymbol{t} = \begin{bmatrix} \boldsymbol{\omega} \\ \boldsymbol{v} \end{bmatrix} \qquad \boldsymbol{v} = \boldsymbol{r}_t \times \boldsymbol{\omega} + \lambda_t \boldsymbol{\omega} \tag{3.1}$$

From a given twist the axis location and the pitch can be computed as

$$\boldsymbol{r}_t = \frac{\boldsymbol{\omega} \times \boldsymbol{v}}{\|\boldsymbol{\omega}\|^2} + \delta_t \boldsymbol{\omega} \qquad \lambda_t = \frac{\boldsymbol{v}^\top \boldsymbol{\omega}}{\|\boldsymbol{\omega}\|^2} \tag{3.2}$$

in which δ_t is the free variable along the twist axis. The equation of the pitch gives rise to two special cases if 1) $\lambda_t = 0$ or if 2) $\lambda_t = \infty$. The first occurs when $\boldsymbol{\omega}$ and $\boldsymbol{v}$ are perpendicular. This is interpreted as a pure rotation. The latter happens when $\boldsymbol{\omega} = 0$ and $\boldsymbol{v} \neq 0$ and is seen as a pure translation. Later in the balancing process, these special cases require special attention.

Similarly, the linear and angular momentum – respectively denoted with $\boldsymbol{p}$, and $\boldsymbol{\xi}$ – form a screw, the 'momentum' wrench (Fig. 3.1)

$$\boldsymbol{h} = \begin{bmatrix} \boldsymbol{\xi} \\ \boldsymbol{p} \end{bmatrix} \qquad \boldsymbol{\xi} = \boldsymbol{r}_h \times \boldsymbol{p} + \lambda_h \boldsymbol{p} \tag{3.3}$$

This momentum wrench $\boldsymbol{h}$ can be interpreted as a linear momentum in the direction of $\boldsymbol{p}$, passing through point $\boldsymbol{r}_h$ and an angular momentum around this axis, here called the momentum pitch λ_h

$$\boldsymbol{r}_h = \frac{\boldsymbol{p} \times \boldsymbol{\xi}}{\|\boldsymbol{p}\|^2} + \delta_h \boldsymbol{p} \qquad \lambda_h = \frac{\boldsymbol{\xi}^\top \boldsymbol{p}}{\|\boldsymbol{p}\|^2} \tag{3.4}$$

in which δ_h is the free variable along the wrench axis. It should be noted that the twist and wrench are dual properties. The screw axis of the twist is formed by its 'rotative' component, the angular velocity. Conversely, for the wrench its 'translative' part, the linear momentum or force, determines the screw axis. Therefore, a wrench is often denoted as a co-screw. Two special cases occur on the momentum wrench; if 1) the linear and angular momentum are perpendicular ($\lambda_h = 0$) or if 2) the momentum wrench is a pure angular momentum ($\lambda_h = \infty$).

The momentum wrench is formed by the product of a body's mass matrix $\boldsymbol{M}$ and its twist

$$\boldsymbol{h} = \boldsymbol{M}\boldsymbol{t} \tag{3.5}$$

The body's mass matrix is formed by the mass integral over all points $\boldsymbol{r}$ in the bodies volume V. This gives rise to a matrix build up with m as the body's mass, $\boldsymbol{c}$ the location of the COM and $\boldsymbol{G}$ the angular inertia matrix expressed around the COM

$$\boldsymbol{M} = \int_V \begin{bmatrix} -[\boldsymbol{r}\times]^2 & [\boldsymbol{r}\times] \\ -[\boldsymbol{r}\times] & \boldsymbol{I}_3 \end{bmatrix} \mathrm{d}m \qquad = \begin{bmatrix} \boldsymbol{G} - m[\boldsymbol{c}\times]^2 & m[\boldsymbol{c}\times] \\ -m[\boldsymbol{c}\times] & m\boldsymbol{I}_3 \end{bmatrix} \tag{3.6}$$

In here $[\boldsymbol{a}\times]$ denotes the skew symmetric matrix of a 3-vector. The angular inertia matrix $\boldsymbol{G}$ is parameterized by three moments of inertia g_{xx}, g_{yy}, and g_{zz}, and three products of inertia g_{xy}, g_{xz}, and g_{yz}. Altogether, the body's mass matrix is determined by 10 inertial parameters. The angular inertia matrix can be diagonalized $\boldsymbol{G}^{\mathrm{p}} = \mathrm{diag}(\boldsymbol{g})$ by rotating it along its principal axes. Here $\boldsymbol{g} = [g_1, g_2, g_3]$ denotes the vector of principal moments of inertia

$$\boldsymbol{G} = \begin{bmatrix} g_{xx} & g_{xy} & g_{xz} \\ g_{xy} & g_{yy} & g_{yz} \\ g_{xz} & g_{yz} & g_{zz} \end{bmatrix} = \boldsymbol{R}^\top \boldsymbol{G}^{\mathrm{p}} \boldsymbol{R} \tag{3.7}$$

This rotation matrix $\boldsymbol{R}$ can be found by eigenvalue decomposition. It should be noted eight orientations result in a diagonal inertia matrix, i.e. for each octant one. For simplicity sake we choose a sorted inertia vector. From the integral form of the mass matrix (Eq. 3.6) and the positivity of mass, it can be deducted that the principal moments of inertia must be non-negative, and form a triangle inequality. Therefore we get the following set of inequality conditions on the mass and inertia of a body

$$m \geq 0 \tag{3.8}$$
$$\boldsymbol{g} \geq 0 \tag{3.9}$$
$$g_2 + g_3 \geq g_1 \tag{3.10}$$
$$g_1 \geq g_2 \geq g_3 \tag{3.11}$$

The lower limits on in these conditions are formed by theoretical objects such as infinitely slender, flat, or perfectly axisymmetric objects.

Dynamic balance conditions in screw theory

Dynamic balance is obtained when the sum of the momentum wrenches of all n_{b} bodies in the mechanism is zero for all motion. In the current notation this reads

$$\sum_{i=1}^{n_{\mathrm{b}}} \boldsymbol{h}_i = \sum_{i=1}^{n_{\mathrm{b}}} \boldsymbol{M}_i \boldsymbol{t}_i \equiv 0 \tag{3.12}$$

For a closed-loop mechanism the body twists $\boldsymbol{t}_i$ are not independent as they are related through the differential loop-closure constraints. For each of the n_{d} DOF of the mechanism, whose coordinates are denoted by $\boldsymbol{u}$, a unique twist is associated to each body $\hat{\boldsymbol{t}}_{i,j}$. This unit twist (denoted with a hat) is defined as the twist of body i generated by a unit velocity actuation of DOF j. The

actual body twist $\boldsymbol{t}_i$ is formed by the weighted sum over the input velocities $\dot{u}_j$ of these unit twists

$$\boldsymbol{t}_i = \sum_{j=1}^{n_\mathrm{d}} \hat{\boldsymbol{t}}_{i,j} \dot{u}_j \tag{3.13}$$

These unit twist can be found readily by screw theory methods and are not discussed further, refer to for instance to [129]. Substituting these unit twist back into the balancing condition of Eq. 3.12, we can find the dynamic balancing conditions for each of the n_d DOFs

$$\sum_{i=1}^{n_\mathrm{b}} \hat{\boldsymbol{h}}_{i,j} \dot{u}_j = \sum_{i=1}^{n_\mathrm{b}} \boldsymbol{M}_i \hat{\boldsymbol{t}}_{i,j} \dot{u}_j \equiv 0 \tag{3.14}$$

in which $\hat{\boldsymbol{h}}_{i,j}$ is the unit momentum wrench of body i as a consequence of unit velocity of DOF j. Combination of these balance conditions using Eq. 3.13 provides a condition on the momentum wrench basis $\boldsymbol{M}_\mathrm{B}$

$$\boldsymbol{h} = \sum_{i=1}^{n_\mathrm{b}} \begin{bmatrix} \hat{\boldsymbol{h}}_{i,1} & \cdots & \hat{\boldsymbol{h}}_{i,n_d} \end{bmatrix} \dot{\boldsymbol{u}} = \boldsymbol{M}_\mathrm{B}(\boldsymbol{u}) \dot{\boldsymbol{u}} \equiv 0 \tag{3.15}$$

Clearly dynamic balance requires the sum of the unit momentum wrenches associated to the same DOF to be zero. As it is algebraically complex to obtain and solve the closed-form expression of $\boldsymbol{M}_\mathrm{B}(\boldsymbol{u})$ for all $\boldsymbol{u}$ — due to the complexity or unavailability of the solution to the loop-closure constraint equation — we confine ourselves to a reference configuration $\boldsymbol{u}_0$ in which the mechanism is defined. In this configuration the loop-closure equation is satisfied by this definition and we have no problem of obtaining $\boldsymbol{M}_\mathrm{B}$. Since Eq. 3.15 should hold for all possible velocities $\dot{\boldsymbol{u}}$ in this pose, $6 \times n_\mathrm{d}$ instantaneous dynamic balance conditions are obtained for the spatial case and $3 \times n_\mathrm{d}$ for the planar case

$$\boldsymbol{M}_\mathrm{B}(\boldsymbol{u}_0) \equiv 0 \tag{3.16}$$

If this not only holds for $\boldsymbol{u}_0$, but for all $\boldsymbol{u}$ in a specific assembly mode the mechanism is globally balanced. In the remainder of this section these equations are solved for the inertial parameters in the mass matrix as to yield instantaneous dynamic balance.

Approach to solve dynamic balance conditions

The instantaneous dynamic balance method presented here, consists of two steps. In Step A, the dynamic balance conditions (Eq. 3.14) are solved on mechanism level by requiring a specific relation between the twist and momentum wrench for n_d bodies, i.e. on a number of bodies equal to the DOF of the mechanisms. In Step B, this twist-momentum relation is solved to find the corresponding mass matrix of these n_d bodies. In both steps, special cases are identified and treated. In order to ensure that feasible inertial parameters (Eq. 3.8 - Eq. 3.10) are found in Step B, a detailed description of the attainable

momentum (momentum span) as function of the inertial parameters and twist is given. Therefore, in the next paragraphs the description of the two steps is interleaved with a screw based interpretation of the momentum span.

Step A. Dynamic balance solution on mechanism level

The $6 \times n_{\mathrm{d}}$ dynamic balancing conditions (Eq. 3.14) are solved by uniquely associating a momentum wrench and a twist to n_{d} mass matrices. From this twist-momentum relation the mass matrix is solved in Step B. Please note the difference between n_{d} and n_{b}, as the former is the number of DOF and the latter is the number of bodies.

The balancing procedure that we present here, relies on isolating and solving one mass matrix for each of the n_{d} balance conditions. This is done by virtually splitting the mechanism into two parts, a 'proximal' part and a 'distal part'. The proximal part consist of one or more base-grounded serial chains, whose joints will serve as the independent coordinates. The distal part which contains the remaining bodies and the dependent joints of the mechanism. In this approach the mass matrices of the proximal part shall be solved from the balancing conditions, whereas the distal mass matrices are the free parameters.

The proximal set should consist of n_{d} joints and bodies that together form serial or tree-like chains connected to the basis. These 'proximal' joints will function as the input or independent coordinates of the mechanism. The inertial parameters of the n_{d} proximal bodies, directly connected to these input joints, shall be determined as a function of the inertial parameters of the distal part, whose inertial parameters are free. Now, due to the hierarchy in serial or tree-like chains, the actuation of the last input joint j of such a serial chain will not induce a movement or momentum of the other proximal bodies, such that we have an isolated and solvable balance condition on the body connected to the last input joint. For this motion to be dynamically balanced, the momentum generated by this body should be equal and opposite to the momentum generated by the distal part of the mechanism

$$-\sum_{i\neq j}^{n_{\mathrm{b}}} \hat{\boldsymbol{h}}_{i,j} = \hat{\boldsymbol{h}}_{j,j} = \boldsymbol{M}_j \hat{\boldsymbol{t}}_{j,j} \tag{3.17}$$

As the other input joints and connected 'proximal' bodies are kept fixed, only the inertial parameters of the distal bodies show up in the left side of this equation. The inertial parameters $\boldsymbol{M}_j$ for this body can be solved via equations which are presented later. After this mass matrix is solved, the approach is repeated for the second to last link and so on, until all inertial parameters of the n_{d} proximal bodies are determined. As the choice of input joints is not unique, a variety of sequences can be used as long as no passive joints are in between the input joints and the base and the chosen input joints are single DOF joints whose parameterization does not result in a singular mechanism.

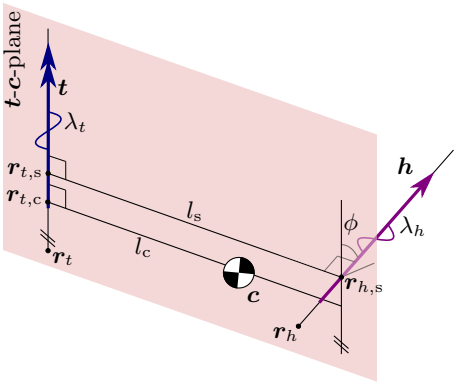

Figure 3.1: A geometrical representation of the momentum $\boldsymbol{h}$ generated by a twist $\boldsymbol{t}$ and body with a COM at $\boldsymbol{c}$.

Intermezzo: Screw theory interpretation of the linear and angular momentum to determine solution bounds

Before the mass matrices $\boldsymbol{M}_j$ are extracted from Eq. 3.17, we need to know which momentum wrench is produced from a given twist-mass matrix combination. Later on, this relation is inverted to find the mass matrix for a given momentum wrench and twist. Moreover, we wish to know how to ensure that feasibility bounds (Eq. 3.8 - Eq. 3.10) are respected by the solution. Furthermore, special cases need to be identified to see if additional conditions are required. In the first part, the twist-momentum relation is interpreted in a screw theory manner, following the work of Selig et al. [91]. In the second part, a detailed study on the effect of the body orientation on the generated angular momentum is conducted to ensure that the feasibility bounds on the moments of inertia are satisfied.

As we are concerned with the general geometric interpretation of the twist-momentum relation, we write the linear and angular momentum for and arbitrary body and twist, and hence drop the sub- and superscript notation. Using Eq. 3.3 and Eq. 3.6 the expression for the linear and angular momentum becomes

$$\boldsymbol{p} = -m\boldsymbol{c} \times \boldsymbol{\omega} + m\boldsymbol{v} \tag{3.18}$$

$$= m(\boldsymbol{r}_t - \boldsymbol{c}) \times \boldsymbol{\omega} + m\lambda_t \boldsymbol{\omega} \tag{3.19}$$

$$\boldsymbol{\xi} = \boldsymbol{G}\boldsymbol{\omega} + \boldsymbol{c} \times \boldsymbol{p} \tag{3.20}$$

Following the interpretation of [91], a plane may be constructed through the twist-line $\boldsymbol{t}$ and the COM location $\boldsymbol{c}$, the $\boldsymbol{t}$-$\boldsymbol{c}$-plane (Fig. 3.1). The point where the momentum wrench passes through this $\boldsymbol{t}$-$\boldsymbol{c}$-plane is termed $\boldsymbol{r}_{h,\mathrm{s}}$. In their paper, following the work of Ball [11], Selig et al. show that this point is simultaneously the shortest distance point between $\boldsymbol{t}$ and $\boldsymbol{h}$. The corresponding shortest distance point on the twist axis is $\boldsymbol{r}_{t,\mathrm{s}}$. Without any moment of inertia,

i.e. when the body is a point mass, the momentum wrench passes through $\boldsymbol{c}$. With increased angular momentum the wrench line moves further away from $\boldsymbol{t}$ and $\boldsymbol{c}$. The exact extent of the angular momentum span will be studied later in this section. The linear momentum vector is not always normal to the $\boldsymbol{t}$-$\boldsymbol{c}$-plane ($\cos(\phi) = m\lambda_t/\|\boldsymbol{p}\|$) due to the influence of the twist pitch (Eq. 3.19).

In the general finite twist pitch case, the momentum pitch is found to be

$$\lambda_h = \frac{\boldsymbol{\xi}^\top \boldsymbol{p}}{\|\boldsymbol{p}\|^2} = \frac{\lambda_t \boldsymbol{\omega}^\top \boldsymbol{G}\boldsymbol{\omega} + \boldsymbol{\omega}^\top \big[\boldsymbol{c} - \boldsymbol{r}_t\times\big]\boldsymbol{G}\boldsymbol{\omega}}{m\|\boldsymbol{\omega}\|^2(\lambda_t^2 + l_c^2)} \tag{3.21}$$

in here l_c is the distance between the COM and the twist axis.

Special cases

Special cases for the momentum occur when 1) the momentum pitch is zero, or 2) when the momentum pitch is infinite. The combination of twist and the mass of the body for which these special conditions occur are given here. We exclude trivial cases such as $m = 0$.

1. The zero pitch momentum ($\lambda_h = 0$) occurs when $\boldsymbol{p} \perp \boldsymbol{\xi}$. The momentum pitch (Eq. 3.21) is zero when the twist pitch has a specific relation with the angular velocity

$$\lambda_t = -\frac{\boldsymbol{\omega}^\top \big[\boldsymbol{c} - \boldsymbol{r}_t\times\big]\boldsymbol{G}\boldsymbol{\omega}}{\boldsymbol{\omega}^\top \boldsymbol{G}\boldsymbol{\omega}} \tag{3.22}$$

   Furthermore, when the twist pitch is infinite ($\lambda_t = \infty$), Eq. 3.20 and Eq. 3.18 reduce to

$$\boldsymbol{p} = m\boldsymbol{v} \qquad\qquad \boldsymbol{\xi} = \boldsymbol{c} \times \boldsymbol{p} \tag{3.23}$$

   such that in $\boldsymbol{p} \perp \boldsymbol{\xi}$, resulting in a zero momentum pitch.

2. An infinite pitch momentum ($\lambda_h = \infty$) appears when $\|\boldsymbol{p}\| = 0$. From Eq. 3.19 it is deduced that this is only the case when the body is in pure rotation ($\lambda_t = 0$) around the COM ($l_c = 0$).

This means that an infinite pitch twist always results in a zero pitch momentum and furthermore, an infinite pitch momentum can only be generated by a zero pitch twist. Refer to Table 3.1 for an overview of these conditions.

Angular momentum as function of body orientation

The angular momentum span is required to completely define the momentum limits for a given body. This will be used later on to determine feasible balance solutions. For brevity reasons, we group the influence of the COM on the angular momentum

$$\boldsymbol{\xi}_c = \boldsymbol{\xi} - \boldsymbol{c} \times \boldsymbol{p} = \boldsymbol{G}\boldsymbol{\omega} \tag{3.24}$$

Now, we are interested to see what values for $\boldsymbol{\xi}_c$ can be obtained for any given angular velocity, principal moments of inertia and orientations of the body

$$\boldsymbol{\xi}_c = \boldsymbol{R}^\top \boldsymbol{G}^{\mathrm{p}} \boldsymbol{R}\boldsymbol{\omega} \tag{3.25}$$

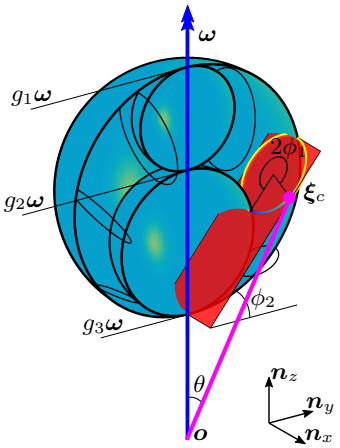

Figure 3.2: For all orientations of a body, the angular momentum $\boldsymbol{\xi}_c$ generated by angular velocity $\boldsymbol{\omega}$ will lie inside a sphere with two spherical cavities, of which the dimensions and position are determined by the bodies principal moments of inertia g_1, g_2, and g_3. Here the orientation of the body is parameterized by ϕ_1, ϕ_2, and ϕ_3 (currently $\phi_3 = 0$) around local $\boldsymbol{n}_z$, $\boldsymbol{n}_x$, and $\boldsymbol{n}_z$ axes.

Without loss of generality we choose $\boldsymbol{\omega}$ along the global z-axis and $\boldsymbol{R}$ with three consecutive rotations according the z-x-z convention

$$\boldsymbol{R} = \boldsymbol{R}_z(\phi_1)\boldsymbol{R}_x(\phi_2)\boldsymbol{R}_z(\phi_3) \tag{3.26}$$

Since $\boldsymbol{\omega}$ is invariant for $\boldsymbol{R}_z$ we have for the angular momentum the following product of matrices

$$\boldsymbol{\xi}_c = \boldsymbol{R}_z^\top(\phi_3)\boldsymbol{R}_x^\top(\phi_2)\boldsymbol{R}_z^\top(\phi_1)\boldsymbol{G}^{\mathrm{p}}\boldsymbol{R}_z(\phi_1)\boldsymbol{R}_x(\phi_2)\boldsymbol{\omega} \tag{3.27}$$

Which after expansion this becomes:

$$\begin{aligned}\boldsymbol{\xi}_c = g_3\boldsymbol{\omega} + \sin(\phi_2)\boldsymbol{R}_z^\top(\phi_3)\boldsymbol{R}_x^\top(\phi_2 + \tfrac{\pi}{2}) \\ \left(\frac{g_1 - g_2}{2}\boldsymbol{R}_y(2\phi_1)\boldsymbol{\omega} - \left(g_2 - g_3 + \frac{g_1 - g_2}{2}\right)\boldsymbol{\omega}\right)\end{aligned} \tag{3.28}$$

The effect of the angles ϕ_1, ϕ_2 and ϕ_3 on the angular momentum is depicted in Fig. 3.2. From the previous equation it follows that angular momentum $\boldsymbol{\xi}_c$ lies on circle – parameterized by $2\phi_1$ – which, in turn, lies on a plane passing through $g_3\boldsymbol{\omega}$. The angle of the plane with the y-axis is given by ϕ_2. The size and center of the circle scale with $\sin(\phi_2)$. This whole figure is rotated by ϕ_3 around the $\boldsymbol{n}_z$-axis. This means that, for all orientations, the angular momentum $\boldsymbol{\xi}_c$ will be contained inside a sphere with two spherical cavities. These three spheres touch at $g_1\boldsymbol{\omega}$, $g_2\boldsymbol{\omega}$, and $g_3\boldsymbol{\omega}$. From this interpretation,

three bounds on $\boldsymbol{\xi}_c$ can be deducted, which are respected for any orientation of the body

$$\|\boldsymbol{\xi}_c - 1/2(g_1 + g_3)\boldsymbol{\omega}\| \leq 1/2(g_1 - g_3) \tag{3.29}$$

$$\|\boldsymbol{\xi}_c - 1/2(g_1 + g_2)\boldsymbol{\omega}\| \geq 1/2(g_1 - g_2) \tag{3.30}$$

$$\|\boldsymbol{\xi}_c - 1/2(g_2 + g_3)\boldsymbol{\omega}\| \geq 1/2(g_2 - g_3) \tag{3.31}$$

These conditions should be respected later when selecting a dynamically balanced mass distribution. This also gives a critical maximal value for the principal moments of inertia, such that a given $\boldsymbol{\xi}_c$ lies on the surface of one of the spheres. The cosine law yields the maximal moment of inertia:

$$g_1 \leq g_{1,\text{crit}} = \frac{\boldsymbol{\xi}_c^\top (g_2\boldsymbol{\omega} - \boldsymbol{\xi}_c)}{\boldsymbol{\omega}^\top (g_2\boldsymbol{\omega} - \boldsymbol{\xi}_c)} \tag{3.32}$$

$$g_2 \leq g_{2,\text{crit}} = \frac{\boldsymbol{\xi}_c^\top (g_3\boldsymbol{\omega} - \boldsymbol{\xi}_c)}{\boldsymbol{\omega}^\top (g_3\boldsymbol{\omega} - \boldsymbol{\xi}_c)} \tag{3.33}$$

$$g_3 \leq g_{3,\text{crit}} = \frac{\boldsymbol{\xi}_c^\top (g_1\boldsymbol{\omega} - \boldsymbol{\xi}_c)}{\boldsymbol{\omega}^\top (g_1\boldsymbol{\omega} - \boldsymbol{\xi}_c)} \tag{3.34}$$

When the principal moments of inertia are chosen equal, i.e. $g_1 = g_2$ or $g_2 = g_3$, the angular momentum span collapses to the surface of a sphere. In case all principal moments of inertia are equal, i.e. $g_1 = g_2 = g_3$, the angular momentum span collapses to a point on the $\boldsymbol{\omega}$-axis.

Furthermore, from the interpretation of Fig. 3.2 and the positivity of the principal moments of inertia, it follows that the angle θ between the momentum and the angular velocity always smaller is than $\pi/2$. Therefore

$$\boldsymbol{\omega}^\top \boldsymbol{\xi}_c = \|\boldsymbol{\omega}\| \|\boldsymbol{\xi}_c\| \cos(\theta) > 0 \tag{3.35}$$

With this interpretation of the relation between the momentum wrench, twist and mass matrix we have obtained several conditions to which the balance solution should adhere for solvability and feasibility.

Step B. Dynamic balance solution on body level

Now that we have a geometric interpretation of the possible momentum for a given twist, we will extract the inertial parameters from the $6 \times n_\text{d}$ instantaneous dynamic balance condition (Eq. 3.17) as obtained in Step A. These conditions state that the momentum generated the body that is directly connected to the independent joint must be equal and opposite to the momentum of the rest of the mechanism. So we assume that we now know the twist $\hat{\boldsymbol{t}}_{j,j}$ and the momentum $\hat{\boldsymbol{h}}_{j,j}$ of a body but not yet the mass matrix $\boldsymbol{M}_j$ that couple these. This section aims to obtain these mass matrices. For each of the n_d bodies we have to satisfy 6 dynamic balance conditions, for which we can use 10 parameters. This means that in general we can choose 4 parameters (within bounds) and solve for the remaining 6 parameters. We will do this in three steps. First, the force balance conditions are solved. Second, the moment

balance solution are obtained. Third, the special cases such as the planar case are discussed. At last we will discuss the implications of this procedure for global dynamic balance and path balance (reactionless paths).

Force balance

From dynamic balance conditions, as found in Eq. 3.17, we can solve the mass and COM by recasting it into the form of Eq. 3.18

$$m = \frac{1}{\lambda_t} \frac{\boldsymbol{\omega}^\top \boldsymbol{p}}{\|\boldsymbol{\omega}\|^2}, \qquad \boldsymbol{c} = -\frac{[\boldsymbol{\omega}\times](m\boldsymbol{v} - \boldsymbol{p})}{m\|\boldsymbol{\omega}\|^2} + \delta\boldsymbol{\omega} \tag{3.36}$$

For brevity reasons we omit the subscripts of Eq. 3.17. It can be seen that mass is completely fixed and that the COM must lie on a line parametrized by a variable δ along $\boldsymbol{\omega}$. These equations furthermore show for that a positive mass ($m > 0$) it is required that $\boldsymbol{\omega}^\top \boldsymbol{p}$ and λ_t have the same sign.

Moment balance

Moment balance imposes three conditions Eq. 3.24, which are function of the 6 inertial parameters. We solve this undetermined set of equations by selecting the principal moments of inertia $\boldsymbol{g}$ and solving for the orientation of the body ($\boldsymbol{R}$ in Eq. 3.7). An equally valid approach would be to choose an orientation and then solve for the principal moments of inertia. However, in that case the incorporation of the feasibility constraints (Eq. 3.9 and Eq. 3.10) is much harder. It should be noted that $\boldsymbol{\xi}_c$ depends on $\boldsymbol{c}$ and therefore on the choice of δ. Furthermore, we have already seen that several special cases and bounds exist, that should be taken into account.

To solve the moment balance, firstly a local frame will be aligned with the principal axis of inertia. Secondly, the angular velocity as expressed in this local frame ($\boldsymbol{\omega}^{\mathrm{p}}$) will be determined. Thirdly, the rotation matrix – mapping the global to the local angular velocity $\boldsymbol{\omega}^{\mathrm{p}}$ – will be extracted. We have the following set of equations for which we wish to solve $\boldsymbol{R}$

$$\boldsymbol{\omega}^{\mathrm{p}} = \boldsymbol{R}\boldsymbol{\omega}, \qquad \boldsymbol{\xi}_c = \boldsymbol{R}^\top \boldsymbol{G}^{\mathrm{p}} \boldsymbol{\omega}^{\mathrm{p}} \tag{3.37}$$

It can be seen that three conditions hold for the local angular velocity vector

$$\|\boldsymbol{\omega}\|^2 = \|\boldsymbol{\omega}^{\mathrm{p}}\|^2 \tag{3.38}$$

$$\boldsymbol{\omega}^\top \boldsymbol{\xi}_c = (\boldsymbol{\omega}^{\mathrm{p}})^\top \boldsymbol{G}^{\mathrm{p}} \boldsymbol{\omega}^{\mathrm{p}} \tag{3.39}$$

$$\|\boldsymbol{\xi}_c\|^2 = (\boldsymbol{\omega}^{\mathrm{p}})^\top (\boldsymbol{G}^{\mathrm{p}})^2 \boldsymbol{\omega}^{\mathrm{p}} \tag{3.40}$$

This can be rewritten in matrix-vector form on the element-wise quadratic of the principal moments of inertia vector ($\boldsymbol{g}^{\circ 2} = [g_1^2, g_2^2, g_3^2]$) and of local angular velocity ($(\boldsymbol{\omega}^{\mathrm{p}})^{\circ 2} = [(\omega_1^{\mathrm{p}})^2, (\omega_2^{\mathrm{p}})^2, (\omega_3^{\mathrm{p}})^2]$)

$$\begin{bmatrix} \|\boldsymbol{\omega}\|^2 \\ \boldsymbol{\omega}^\top \boldsymbol{\xi}_c \\ \|\boldsymbol{\xi}_c\|^2 \end{bmatrix} = \begin{bmatrix} \mathbf{1} & \boldsymbol{g} & \boldsymbol{g}^{\circ 2} \end{bmatrix}^\top (\boldsymbol{\omega}^{\mathrm{p}})^{\circ 2} \tag{3.41}$$

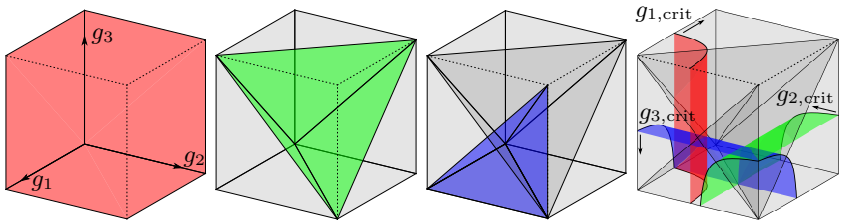

Figure 3.3: The four types of bounds on the selection of the principal moments of inertia in the balancing process. (a) positive principal moments of inertia $\boldsymbol{g} > 0$, (b) The triangle inequality $g_i \leq g_j + g_k$, (c) the sorting condition $g_1 \geq g_2 \geq g_3$ (d) and the critical principal moments of inertia (Eq. 3.32 - Eq. 3.32) for a given $\boldsymbol{\omega}$ and $\boldsymbol{\xi}_c$.

in here $\mathbf{1}$ denotes a 3-vector of ones. This leads to a solution of the local angular velocity vector as

$$(\boldsymbol{\omega}^{\mathrm{p}})^{\circ 2} = \begin{bmatrix} \mathbf{1} & \boldsymbol{g} & \boldsymbol{g}^{\circ 2} \end{bmatrix}^{-\top} \begin{bmatrix} \|\boldsymbol{\omega}\|^2 \\ \boldsymbol{\omega}^\top \boldsymbol{\xi}_c \\ \|\boldsymbol{\xi}_c\|^2 \end{bmatrix} \tag{3.42}$$

This matrix inversion can be done as long as all principal moments of inertia are different $g_1 \neq g_2 \neq g_3$. In the next section, equal principal moments of inertia will be investigated. Eight distinct solutions for $\boldsymbol{\omega}^{\mathrm{p}} = \mathrm{diag}([\pm 1, \pm 1, \pm 1])\sqrt{(\boldsymbol{\omega}^{\mathrm{p}})^{\circ 2}}$ are found, each corresponding to an octant. The positivity conditions $(\boldsymbol{\omega}^{\mathrm{p}})^{\circ 2} > 0$ are satisfied as long as $\boldsymbol{g}$ is chosen such that the previously determined angular momentum limits Eq. 3.29 - Eq. 3.31 are satisfied.

The rotation matrix $\boldsymbol{R}$ is found by recognizing that the following system of equations must hold

$$\boldsymbol{R} \begin{bmatrix} \boldsymbol{\omega} & \boldsymbol{\xi}_c & \boldsymbol{\omega} \times \boldsymbol{\xi}_c \end{bmatrix} = \begin{bmatrix} \boldsymbol{\omega}^{\mathrm{p}} & \boldsymbol{G}^{\mathrm{p}} \boldsymbol{\omega}^{\mathrm{p}} & \boldsymbol{\omega}^{\mathrm{p}} \times \boldsymbol{G}^{\mathrm{p}} \boldsymbol{\omega}^{\mathrm{p}} \end{bmatrix} \tag{3.43}$$

$$\boldsymbol{R}\boldsymbol{A} = \boldsymbol{B} \tag{3.44}$$

which can be inverted if $\boldsymbol{\omega}$ and $\boldsymbol{\xi}_c$ are not co-linear, yielding

$$\boldsymbol{R} = \boldsymbol{B}\boldsymbol{A}^{-1} \tag{3.45}$$

In this approach the principal moments of inertias are free to choose. However, we saw that for the resulting $(\boldsymbol{\omega}^{\mathrm{p}})^{\circ 2}$ to be positive, $\boldsymbol{g}$ must be selected such that Eq. 3.29 - Eq. 3.31 are respected. Furthermore, also the positive definiteness of the moment of inertia matrix (Eq. 3.9) must be respected in addition to the triangle inequality Eq. 3.10 and the sorting condition Eq. 3.11. These constraints can easily be incorporated by limiting the choice of $\boldsymbol{g}$. Giving a total set of 9 limiting conditions of the choice of $\boldsymbol{g}$. Fig. 3.3 gives a graphical interpretation of these conditions.

Now to summarize, feasible instantaneous dynamic balance solutions can be found as long as 1) the twist pitch λ_t and $\boldsymbol{\omega}^\top \boldsymbol{p}$ have the same sign (Eq. 3.36), and 2) $\boldsymbol{\omega}^\top \boldsymbol{\xi}_c > 0$ (Eq. 3.35). In general, there are four parameters to choose within bounds: δ on the COM and $\boldsymbol{g}$ on the moment of inertia matrix.

Special conditions

In several special conditions this general solution requires additional conditions. Firstly, when the principal moments of inertia are chosen equal and the inverse in Eq. 3.42 does not exist. Secondly, when $\boldsymbol{\omega}$ and $\boldsymbol{\xi}_c$ are collinear and the inverse in Eq. 3.45 does not exist. Thirdly, when the pitches of the twist or momentum wrench are either zero or infinite. Fourthly and lastly, in the planar case the out of plane components can be ignored leading to a reduced solution space.

1) In case an axisymmetric body is chosen such that $g_1 = g_2$ or $g_2 = g_3$ the solution to $\boldsymbol{\omega}^{\mathrm{p}}$ in Eq. 3.42 gains a freedom, allowing for different orientations of the body without changing the corresponding moment of inertia matrix. In that case, the values of the equal ($g_2 = g_{\mathrm{e}}$) principal moments of inertia cannot be chosen freely as $\boldsymbol{\xi}_c$ should lie on the surface of a sphere (Eq. 3.32 - Eq. 3.34) and therewith determining the remaining moment of inertia (g_{u})

$$g_2 = g_{\mathrm{e}} = \frac{\boldsymbol{\xi}_c^{\top}(g_{\mathrm{u}}\boldsymbol{\omega} - \boldsymbol{\xi}_c)}{\boldsymbol{\omega}^{\top}(g_{\mathrm{u}}\boldsymbol{\omega} - \boldsymbol{\xi}_c)} \tag{3.46}$$

Equal principal moments of inertia $g_1 = g_2 = g_3$ can only be chosen if $\boldsymbol{\xi}_c$ and $\boldsymbol{\omega}$ are co-linear, then $\boldsymbol{R}$ is a free choice that does not change the inertia matrix. For the g_i's the following condition must hold

$$g_1 = g_2 = g_3 = \frac{\|\boldsymbol{\xi}_c\|}{\|\boldsymbol{\omega}\|} \tag{3.47}$$

2) In general, when $\boldsymbol{\xi}_c$ and $\boldsymbol{\omega}$ are co-linear, both should be aligned along one of the principal axis, fixing only the corresponding principal moment of inertia. The other principal moments of inertia and the orientation around that principal axis are free to choose.

3) In previous sections several special cases of the twist and momentum wrench are identified. For the dynamic balance some of these require special attention. We have seen that both the twist and the required momentum wrench can be finite, infinite or zero pitched (co-) screws. This leads to 9 cases as shown in table Table 3.1. Based on twist pitch and momentum pitch equations, respectively Eq. 3.2 and Eq. 3.21, we discuss 3 conditions, from which the whole table can be deducted.

- In the limit case $\lambda_t = 0$, the body is in pure rotation. Therefore $\boldsymbol{\omega}$ and $\boldsymbol{p}$ should be perpendicular. This leaves m in Eq. 3.36 indeterminate and free to choose.

- In the limit case $\lambda_t = \infty$ the body is in pure translation $\boldsymbol{\omega} = 0$. Therefore, this requires $\boldsymbol{v} \parallel \boldsymbol{p}$. This bounds $\boldsymbol{c}$ to line due to $\boldsymbol{\xi} = \boldsymbol{c} \times \boldsymbol{p}$ in Eq. 3.20. The balancing equations become

$$m = \frac{\|\boldsymbol{p}\|}{\|\boldsymbol{v}\|} \qquad\qquad \boldsymbol{c} = \frac{\boldsymbol{p} \times \boldsymbol{\xi}}{\|\boldsymbol{p}\|^2} + \delta\boldsymbol{p} \tag{3.48}$$

  Therefore $\boldsymbol{\xi}$ and $\boldsymbol{p}$ should be perpendicular, requiring $\lambda_h = 0$. Other values for λ_h are not possible. Therefore, $\boldsymbol{G}$ is free to choose.

Table 3.1: For several special cases the general instantaneous dynamic balance conditions (G.C.) of Eq. 3.36 and Eq. 3.45 do not hold. Either the combination of twist and wrench are not possible (N.P.) or require additional conditions. Additional parameter freedom is denoted with a ¿.

	$\lvert\lambda_t\rvert = (0,\infty)$	$\lvert\lambda_t\rvert = 0$	$\lvert\lambda_t\rvert = \infty$
$\lvert\lambda_h\rvert = (0,\infty)$	G.C.	$\boldsymbol{\omega} \perp \boldsymbol{p}, \quad m = ¿$	N.P.
$\lvert\lambda_h\rvert = 0$	G.C.	$\boldsymbol{\omega} \perp \boldsymbol{p} \quad m = ¿$	$\boldsymbol{v} \parallel \boldsymbol{p}, \quad \boldsymbol{G} = ¿$
$\lvert\lambda_h\rvert = \infty$	N.P.	$\boldsymbol{p} = 0, \quad m = ¿$	N.P.

- The limit case $\lambda_h = \infty$ occurs only when $\boldsymbol{p} = 0$. This places $\boldsymbol{c} = \boldsymbol{r}_t + \delta\boldsymbol{\omega}$ on the twist axis. Therefore, it requires $\lambda_t = 0$. Other values for λ_t are not possible in this case.

4) In the planar case we can ignore the out of plane parts and we are left with a single inertia value g. We have two cases either $\lambda_t = 0$, in which m is indeterminate, or $\lambda_t = \infty$, in which g is indeterminate. In the first case Eq. 3.19 and Eq. 3.20 are solved by

$$\boldsymbol{c} = \boldsymbol{r}_t - \frac{1}{m}\frac{\boldsymbol{\omega} \times \boldsymbol{p}}{\|\boldsymbol{\omega}\|^2}, \tag{3.49}$$

$$g = \frac{\boldsymbol{\omega}^\top(\boldsymbol{\xi} - \boldsymbol{r}_t \times \boldsymbol{p})}{\|\boldsymbol{\omega}\|^2} - \frac{1}{m}\frac{\|\boldsymbol{p}\|^2}{\|\boldsymbol{\omega}\|^2} \tag{3.50}$$

In the second case $\lambda_t = \infty$ the body is in pure translation and we require $\boldsymbol{v} \parallel \boldsymbol{p}$, refer to Table 3.1. Therefore, similar to the spatial case m and $\boldsymbol{c}$ are determined according to Eq. 3.48 and g is undetermined.

All these special conditions impose additional requirements on $\boldsymbol{t}$ and $\boldsymbol{h}$. When following the hierarchical dynamic balancing procedure, as presented in this chapter, these additional constraints are inherited over to the bodies higher in the chain, limiting their choice of mass distribution.

Global dynamic balance

With approach we have solved a necessary subset of the dynamic balance conditions, the instantaneous dynamic balance in reference pose. Outside this particular pose the dynamic balance is not necessarily maintained. To extend this global dynamic balance, the previously derived dynamic balance solutions should be valid for all possible poses and motions. The homogenization of this step is outside the scope of this chapter.

Reactionless paths

When a multi-DOF mechanism is partially balanced, for example when only the shaking forces are canceled, a part of its motion can still be fully dynamically balanced by moving over a reactionless path [84, 126]. Such a path balance is generally possible when the mechanisms has more DOFs than unbalanced directions, i.e. directions in which shaking forces or shaking moments are felt.

In these cases a part of the DOFs may be chosen to compensate the unbalance caused by the other DOF.

These reactionless paths are computed, similar to [126], by choosing the coordinate velocities on the null-space of the momentum basis Eq. 3.15

$$\dot{\boldsymbol{u}} \in \ker(\boldsymbol{M}_{\mathrm{B}}) \tag{3.51}$$

and integrating these into paths. In general, this $\boldsymbol{M}_{\mathrm{B}}$ matrix is full rank and does not possess a null-space. However, in the case the mechanism has more DOF than unbalanced directions, a null-space appears, which can be integrated into reactionless paths. In an instantaneous dynamic balance pose, the momentum basis ($\boldsymbol{M}_{\mathrm{B}}$) is a null matrix, locally allowing for the full mobility to be used. This means that for a partially balanced mechanism, multiple reactionless paths meet in these poses. Furthermore that in these poses the shaking wrench is not influenced by the joint accelerations.

3.3 Design of a dynamically balanced five-bar mechanism

Kinematics and dynamics

To illustrate the presented instantaneous dynamic balancing methodology, and to show that instantaneous dynamic balance results in intersecting reactionless paths, we apply the method to a 2-DOF planar $5R$ mechanism. This five-bar mechanism is parameterized as two serial chains with revolute joints at $\boldsymbol{o}_1$ till $\boldsymbol{o}_4$, joined together at the end-effector $\boldsymbol{o}_5$, as shown in Fig. 3.4. The distance between the base joints $\boldsymbol{o}_1$ and $\boldsymbol{o}_3$ is length l_0. The length of the four moving bodies are l_1 till l_4. For later use in the differential kinematics, auxiliary angles β_{ij} between body i and body j are used. To each body, a mass m_i, and a moment of inertia g_i are associated. The center of mass $\boldsymbol{c}_i$ of each body is defined by a distance d_i and an angle γ_i.

For instantaneous dynamic balance, only the differential kinematics are required. The loop-closure equations are assumed to be satisfied, and not discussed here. According to the hierarchical balancing procedure, as described in previous sections, the two base joints q_1 and q_3 are chosen as the input joints. For each of the DOFs the mechanism will act as a four-bar mechanism. We will only apply this procedure for the first DOF (q_1). The second DOF (q_3) can be treated similarly. The angular velocity of the input link is the unit vector perpendicular to the plane of the robot $\hat{\boldsymbol{\omega}}_{1,1} = \boldsymbol{n}_z$. The twist of the bodies due unit velocity of joint 1 become

$$\hat{\boldsymbol{t}}_{1,1} = \begin{bmatrix} \boldsymbol{n}_z \\ \boldsymbol{o}_1 \times \boldsymbol{n}_z \end{bmatrix} \quad \hat{\boldsymbol{t}}_{2,1} = \begin{bmatrix} \hat{\boldsymbol{\omega}}_{2,1} \\ \boldsymbol{r}_{2,1} \times \hat{\boldsymbol{\omega}}_{2,1} \end{bmatrix} \quad \hat{\boldsymbol{t}}_{3,1} = \boldsymbol{0} \quad \hat{\boldsymbol{t}}_{4,1} = \begin{bmatrix} \hat{\boldsymbol{\omega}}_{4,1} \\ \boldsymbol{o}_4 \times \hat{\boldsymbol{\omega}}_{4,1} \end{bmatrix} \tag{3.52}$$

in which the angular velocities of link 2 and 4 are

$$\hat{\boldsymbol{\omega}}_{2,1} = \frac{l_1}{l_2} \frac{\sin(\beta_{14})}{\sin(\beta_{24})} \boldsymbol{n}_z, \qquad \hat{\boldsymbol{\omega}}_{4,1} = \frac{l_1}{l_4} \frac{\sin(\beta_{12})}{\sin(\beta_{24})} \boldsymbol{n}_z \tag{3.53}$$

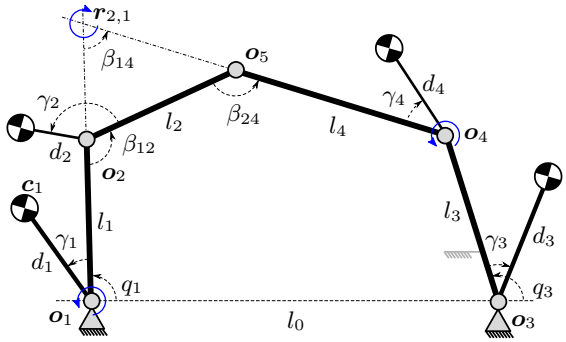

Figure 3.4: The kinematics of the $5R$ planar five-bar mechanism. The solid arrows indicate axis of rotation of moving bodies due to actuation of q_1 and fixation of q_3. For body 2, the axis of rotation lies at $\boldsymbol{r}_{2,1}$.

The instantaneous center of rotation of body $\boldsymbol{r}_{2,1}$ is on the intersection of the line through $\boldsymbol{o}_1$ and $\boldsymbol{o}_2$ and the line through $\boldsymbol{o}_4$ and $\boldsymbol{o}_5$

$$\boldsymbol{r}_{2,1} = \boldsymbol{o}_2 + \frac{l_4 \sin(\beta_{12})}{l_1 \sin(\beta_{14})}(\boldsymbol{o}_1 - \boldsymbol{o}_2) \tag{3.54}$$

Similar conditions can be derived for the second DOF, the rotation of base joint 3, yielding $\hat{\boldsymbol{t}}_{2,3}$, $\hat{\boldsymbol{t}}_{3,3}$, and $\hat{\boldsymbol{t}}_{4,3}$.

Dynamic balance conditions of a five-bar

Instantaneous dynamic balance is obtained by inspecting the two DOFs of the mechanism independently. In Fig. 3.5 this procedure is depicted graphically. For instantaneous dynamic balance of the first DOF, the momentum of the two distal bodies 2 and 4 should be equated to that of the proximal body 1

$$\hat{\boldsymbol{h}}_{1,1} = -\hat{\boldsymbol{h}}_{2,1} - \hat{\boldsymbol{h}}_{4,1} \tag{3.55}$$

Such that the linear and angular momentum generated by body 1 becomes

$$\hat{\boldsymbol{p}}_{1,1} = -\hat{\boldsymbol{p}}_{2,1} - \hat{\boldsymbol{p}}_{4,1} \qquad \hat{\boldsymbol{\xi}}_{1,1} = -\hat{\boldsymbol{\xi}}_{2,1} - \hat{\boldsymbol{\xi}}_{4,1} \tag{3.56}$$

with the linear and angular momentum (Eq. 3.19 and Eq. 3.20) of the distal bodies as

$$\hat{\boldsymbol{p}}_{2,1} = m_2(\boldsymbol{r}_{2,1} - \boldsymbol{c}_2) \times \hat{\boldsymbol{\omega}}_{2,1} \qquad \hat{\boldsymbol{p}}_{4,1} = m_4(\boldsymbol{o}_4 - \boldsymbol{c}_4) \times \hat{\boldsymbol{\omega}}_{4,1} \tag{3.57}$$

$$\hat{\boldsymbol{\xi}}_{2,1} = -g_2\hat{\boldsymbol{\omega}}_{2,1} - \boldsymbol{c}_2 \times \hat{\boldsymbol{p}}_{2,1} \qquad \hat{\boldsymbol{\xi}}_{4,1} = -g_4\hat{\boldsymbol{\omega}}_{4,1} - \boldsymbol{c}_4 \times \hat{\boldsymbol{p}}_{4,1} \tag{3.58}$$

Now, with the previously derived solutions to force and moment balance for planar linkages, respectively Eq. 3.49 and Eq. 3.50, we can find the moment of

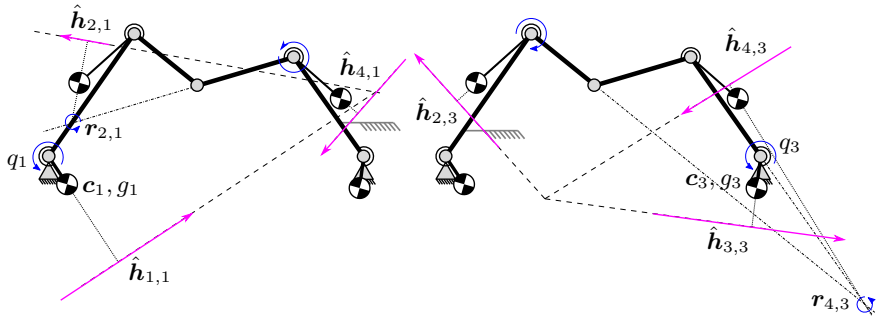

Figure 3.5: A graphical representation of the instantaneous dynamic balance procedure of a $5R$ planar five-bar. *Left* shows that the momentum wrenches of the bodies (straight arrows) due to the actuation of the first DOF (joint q_1) sum to zero. *Right* shows the zero sum of the momentum wrenches for the second DOF, the actuation of joint q_3.

inertia and COM of base links 1 and 3 as function the inertial parameters of links 2 and 4 and a choice of mass. For link 1 we have

$$\boldsymbol{c}_1 = \boldsymbol{o}_1 + \frac{\boldsymbol{n}_z \times (\hat{\boldsymbol{p}}_{2,1} + \hat{\boldsymbol{p}}_{4,1})}{m_1}, \tag{3.59}$$

$$g_1 = \boldsymbol{n}_z^\top \left(\boldsymbol{o}_1 \times (\hat{\boldsymbol{p}}_{2,1} + \hat{\boldsymbol{p}}_{4,1}) - \hat{\boldsymbol{\xi}}_{2,1} - \hat{\boldsymbol{\xi}}_{4,1} \right) - \frac{\|\hat{\boldsymbol{p}}_{2,1} + \hat{\boldsymbol{p}}_{4,1}\|^2}{m_1} \tag{3.60}$$

For link 3 similar conditions hold.

This means that the inertial parameters of link 2 and 4 and the masses of link 1 and 3 can be chosen freely as long as the resulting moments of inertia are positive. This positivity is ensured if the required momentum lines $\hat{\boldsymbol{h}}_{1,1}$ and $\hat{\boldsymbol{h}}_{3,3}$ pass counter-clock wise around their revolute joints. Already the solutions to six dynamic balance conditions are found; four force balance and two moment balance conditions.

Global force balance

From literature it is known that six constraints should be satisfied to obtain global force balance [83]. Since instantaneous dynamic balance is a necessary subset of global force balance, we have found and solved already four force balance conditions, such that only two additional constraints are required for global force balance. These are

$$d_4 = \frac{m_2 l_4}{m_4 l_2} d_2, \qquad \gamma_4 = \pi + \gamma_2 \tag{3.61}$$

Global dynamic balance of the five-bar mechanism is not possible without negative moments of inertia or counter rotations. This can be deducted from special kinematic conditions required for the dynamic balance of the four-bar mechanism [86].

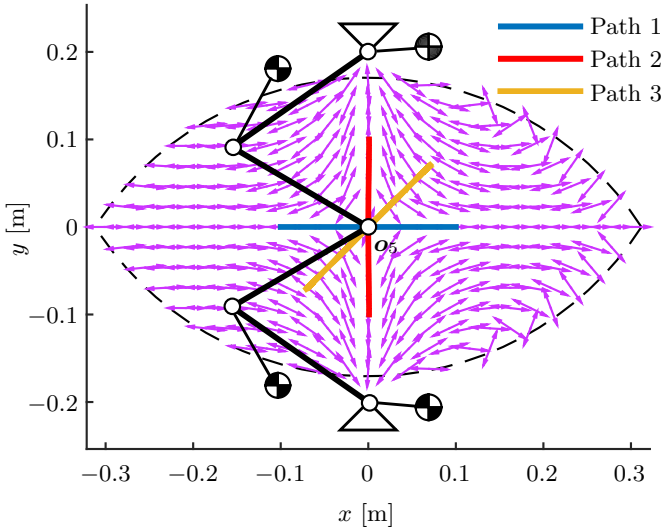

Figure 3.6: The designed mechanism permits one DOF of dynamically balanced movement, in each pose. The pink arrows indicate the corresponding traces of the end-effector $\boldsymbol{o}_5$. Path 1 and 2 are reactionless paths that in the middle of the workspace, the instantaneous dynamic balance pose. Path 3 is the non-moment balanced path. The dashed line denotes the workspace boundary.

Reactionless paths

Now that global force balance — and hence partial dynamic balance — is established for the five-bar mechanism, only one unbalanced dimension remains, the shaking moment. This means that rank $(\boldsymbol{M}_\mathrm{B}) = 1$ and that, in reference to Eq. 3.51, one of the DOFs can be used to render moment balance, i.e. counteract the unbalance of the other DOF. In each pose we therefore have at least one dynamically balanced motion freedom. This motion freedom is computed using the null space operation (Eq. 3.51) and plotted for a grid of end-effector positions (Fig. 3.6). Numerical integration of this null-space operation yields reactionless paths. In the points where the instantaneous dynamic balance conditions are satisfied (here in $[0, 0]$), multiple of these reactionless paths meet, locally allowing a two dynamically balanced DOF.

Design of demonstrator

Based on this result, a force balanced five-bar mechanism is designed that has two intersecting reactionless paths to demonstrate the existence of instantaneous dynamic balance. The system is designed to be placed on a 6-axis force/torque sensor to quantify its balance quality. The present dynamic balance conditions (Eq. 3.60 and Eq. 3.61) place conditions on $\boldsymbol{c}_1$,$\boldsymbol{c}_3$, $\boldsymbol{c}_4$, g_1, and g_3. This leaves a design freedom on kinematic parameters (l_0 - l_4) and the remaining inertial parameters (m_1 - $m_4, \boldsymbol{c}_2, g_2$ and g_4). These parameters can be

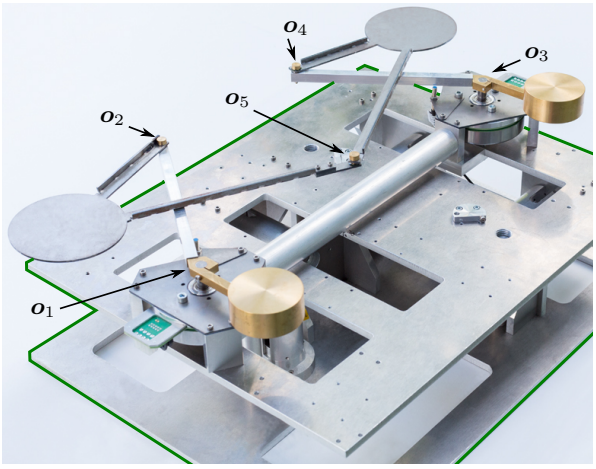

Figure 3.7: The 2-DOF dynamically balanced robot *Fuga I* mounted on a 6-DOF force/torque sensor (outlined) to measure the shaking forces and moments during motion.

chosen freely as long as all the masses and moments of inertia are positive. Here we aim to show that the current method opens a larger design freedom while permitting comparable reactionless paths as mechanisms obtained by existing methods, i.e by connecting two mirror symmetric dyads [19] or by the DUAL V [109].

Therefore, the final design of the robot is chosen based on the following aspects: 1) The reactionless paths should be perpendicular and as straight as possible. 2) The mechanism must be constructible e.g. links should have sufficient stiffness. 3) Workspace should be sufficiently large. 4) Motor torques should be minimal. 5) The demonstrator should fit on a 6-DOF force/torque sensor. 6) The center of mass of all links should be in a single plane to avoid out of plane torques.

Finally, an symmetric M-shaped design of the five-bar mechanism is selected and constructed Fig. 3.7. The base joints are 400 mm apart. The upper arms and the lower arms have a length of 190 mm and 180 mm, respectively. Refer to Table 3.2 for the other dimensions and design parameters. This gives the mechanism a singularity free workspace of with a diameter of approximately 380 mm. The instantaneous dynamic balance pose lies in the middle of the workspace. The first reactionless path is along the symmetry line and the second is approximately along the base link (Fig. 3.6). This second reactionless path is an approximate straight line with a deviation +/- 0.5% (0.9 mm deviation over a stroke of 200 mm). The exotically shaped upper arms are used for sufficient stiffness while providing the required moments of inertia. Direct drive brushless motors of Maxon EC-flat 90 are used. These have a peak torque of 7.4 Nm and a moment of inertia of 3060 g cm^2. A joint-space PID+ controller with computed torque control is used to steer the robot.

Table 3.2: The kinematic and inertial parameters of the Fuga I.

Name	Symbol	Value	Unit
Base width	l_0	400	mm
Upper arm length	l_1, l_3	190	mm
Lower arm length	l_2, l_4	180	mm
COM upper arm	d_1, d_3	69	mm
COM lower arm	d_2, d_3	140	mm
COM angle upper arm	γ_1, γ_3	150	deg
COM angle lower arm	γ_2, γ_4	90	deg
Mass upper arm	m_1, m_3	0.66	kg
Mass lower arm	m_2, m_4	0.21	kg
MOI upper arm	g_1, g_3	1.46	g m^2
MOI lower arm	g_2, g_4	1.66	g m^2

3.4 Evaluation of a dynamically balanced five-bar mechanism

Evaluation approach

To evaluate the instantaneous dynamic balance of this demonstrator, the shaking forces and moments were measured over three paths, which all intersect in theinstantaneous dynamic balance pose. The first two paths are the reactionless paths and the third is a non-moment balanced path. As shown in Fig. 3.6, the first path is over the x-axis, the symmetry line of the mechanism. The second path is over the y-axis. The third and unbalanced motion is a diagonal over the workspace. To show that in this pose the shaking moments are not affected by accelerations, a second-order motion profile is chosen such that the accelerations switch in this instantaneous dynamic balance pose. These paths have an equal length of 200 mm and the traveling time is 0.4 s. This gives a maximum end-effector velocity and acceleration of 1 m/s and 5 m/s^2, respectively. The measured shaking forces in the plane (x- and y-direction) and the measured shaking moment out of plane (z-direction) will be reported for these motions. The average of 15 runs are given. As the measurement setup and the mechanism showed an eigenfrequency around 27 Hz, a lowpass filter with a cut-off of 10 Hz was applied to the force/torque measurements.

The mechanism is modeled in a multibody dynamics software. The measured joint angles are fed into this model to simulate and explain the resulting force and moment measurements. Firstly, this gives an estimation of the bearing forces at the two base joints. In the perfectly force balanced case these two forces completely cancel out each other. Therefore, the measured residual shaking forces are compared to the modeled internal forces for reference. Secondly, the modeled shaking moments are a measure for the shaking moments caused by deviations from the reactionless paths, whereas the difference between the

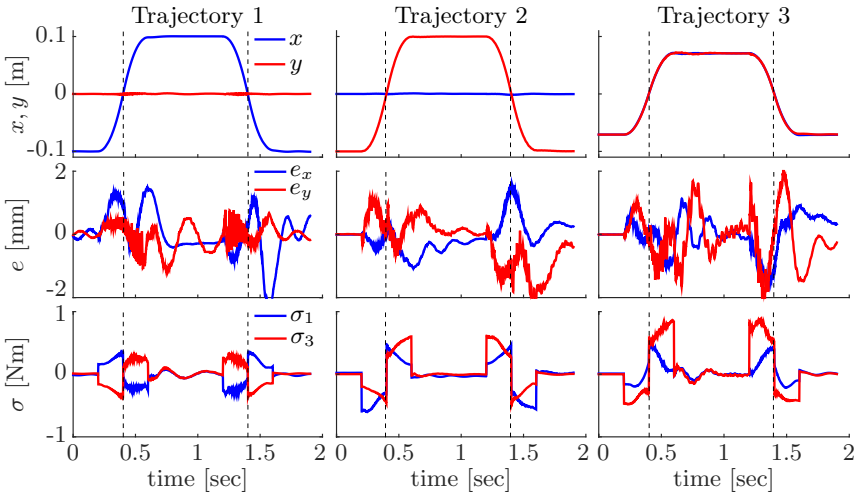

Figure 3.8: The x- and y-position of the end-effector (top row), the controller error e in end-effector coordinates (middle row) and the used motor torque σ (bottom row) for the three trajectories. Trajectory 1 and 2 follow the two reactionless paths through the center of the workspace. Trajectory 3 follows a non-moment balanced diagonal. The vertical lines indicate where the robot passes through the instantaneous dynamic balance pose.

modeled and the measured shaking moments gives a measure for construction and measurement errors.

Results

Fig. 3.9 shows the shaking moments and forces as measured for the three paths. The peak-to-peak shaking moment for the two reactionless paths are 0.06 and 0.04 Nm respectively, for the unbalanced path this is 0.80 Nm. This corresponds to a reduction of 93% and 95% of the shaking moment with respect to the unbalanced path. The difference between the measured and modeled shaking moment is maximally 0.04, 0.02 and 0.10 Nm for the three paths. In addition, the third trajectory shows instantaneous dynamic balance in the center of the workspace. In this pose, the switch of accelerations does not affect the shaking moments, as indicated by the arrows.

The shaking forces for the three paths have a peak-to-peak value of 0.26, 0.11 and 0.04 N respectively. When comparing these shaking forces to the estimated bearing forces, which are 5.93, 4.51, and 2.58 N, it shows that approximately 96, 98, and 99 % of the forces in the mechanism cancel out.

Fig. 3.8 shows that the paths could be followed up to an end-effector accuracy of 2 mm. This corresponds to 1% of the length of the path. This is computed by transforming the measured joint space error to the end-effector error under the assumption of perfect rigidity.

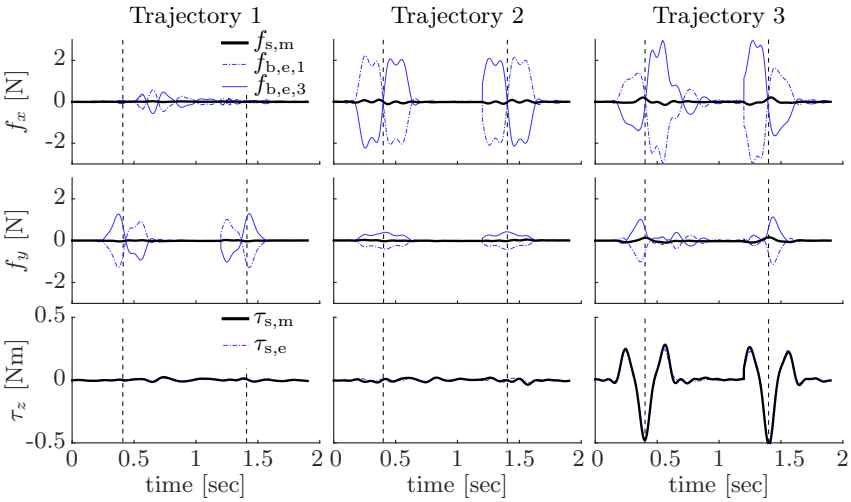

Figure 3.9: The measured shaking forces $f_{\mathrm{s,m}}$ (top and middle) and moments $\tau_{\mathrm{s,m}}$ (bottom) are shown with thick solid lines. For comparison the estimated bearing forces on the base joint are given in thin dashed and thin solid lines, respectively $f_{\mathrm{b,e,1}}$ and $f_{\mathrm{b,e,3}}$. In the bottom row the estimated shaking moment $\tau_{\mathrm{s,e}}$ is shown with a thin dashed line. The vertical lines indicate where the robot passes through the instantaneous dynamic balance pose.

From the difference between the measured and the modeled shaking moments it is deduced that for the two reactionless paths 23% and 57% of the residual unbalance can be explained by controller inaccuracies causing the robot to deviate from the reactionless path. Other causes for the difference between measured and modeled shaking moments can be internal vibrations, production tolerances and inaccuracies. High frequency internal vibrations required low pass filtering of the force/torque sensor signal to eliminate the measured high frequency vibration. It is expected that this filtering influences the comparison between measured and modeled shaking forces and moments.

3.5 Discussion

Instantaneous dynamic balance can be found when the momentum wrenches in a mechanism sum to zero for all velocities in a certain pose. By following a specific sequence through the chains, unique and solvable constraints are placed on the proximal part of the mechanism. From these conditions, the mass, COM and inertia matrix can be deduced for all cases. The remaining variables are the COM location along $\boldsymbol{\omega}$ axis and principal moments of inertia $\boldsymbol{g}$. This fixes the mass, COM, and the orientation of the body. The positivity of mass and inertia, the triangle inequality put bounds on the choice of inertia matrices. This requires that λ_t should have the same sign as $\boldsymbol{\omega}^\top \boldsymbol{p}$ and that $\boldsymbol{\omega}^\top \boldsymbol{\xi}_c > 0$. In several special cases, additional requirements on $\boldsymbol{t}$ and $\boldsymbol{h}$ are to be

satisfied (Table 3.1). These requirements are inherited over to bodies higher in the chain, limiting the choice of their inertial parameters. By satisfying these bounds, the mechanism can be constructed in theory. In practice, however, additional constraints on stiffness, shape, etc. will further limit the choice of inertial parameters.

The instantaneous dynamic balance conditions can be found for any robot, provided that resulting parameterization must be nonsingular and the proximal part solely consists of single DOF joints, as the method selects of a set of serially connected joints as independent coordinates. The method relies on the differential kinematics only, which are readily available through screw theory and does not require the solution to or inspection of the loop-closure equations.

The instantaneous balance pose and path balance might prove useful in pick-and-place applications where high precision is only needed at specific moments and poses. For example, precision is typically only of importance during the placement phase, whereas during the traveling phase it is not needed. By following a dynamically balanced trajectory shortly before and during placement, the base vibrations are given time to dampen out. This enables a high-precision end-effector motion when needed, while still providing for the whole workspace. Now, with the availability of the instantaneous dynamic balance pose a wider choice of trajectories is possible to reach a preselected pose of interest.

To extend the instantaneous dynamic balance to global dynamic balance, additional conditions are to be met. It requires not only that the momentum is zero in a certain pose, but also in all other poses. Harmonizing this step is beyond the scope of this chapter.

The Fuga I was constructed to demonstrate that the presented method results in instantaneous dynamic balance. Although its unusual mass distribution is not likely to be used in industry, its dynamic balanced paths are comparable to that of the DUAL V [109], yet is achieved through a design with two instead of four motors. Also, the COM does not have to lie on the line through the pivots, and the upper and lower link lengths can differ. This shows that with this method, novel dynamic balance solutions can found for mechanisms with reactionless paths, and that the location of their intersection points can be chosen freely. The shape of the reactionless paths is determined by the remaining parameters, the choice of which is outside the scope of this chapter. Here an iterative approach was adopted, which resulted in perpendicular, approximately straight paths.

The dynamic balance measures, as reported here, are dependent on the cycle time, motion profiles and the choice of paths. This is due to the velocity dependent terms in the shaking forces and moments and hence in the dynamic balance measures. Here, the worst and best the trajectories for this setup are compared. These are therefore regarded as representative of the robot.

3.6 Conclusion

For the first time, screw theory has been applied to derive a subset of the dynamic balance conditions for any planar or spatial, single or multi-DOF

mechanism in a general, geometrical manner, without requiring the closed-form solution to the loop-closure constraint equation.

The presented screw-based dynamic balance method provides and solves six conditions per DOF in spatial case, and three per DOF in the planar case. These conditions yield instantaneous dynamic balance, which is a prerequisite for global dynamic balance. This is interpreted as pose, in which multiple reactionless paths intersect. The freedom and bounds on the choice of masses, centers of mass, and moments of inertia where interpreted in a geometric manner.

This method is applied to a planar five-bar mechanism and gave six instantaneous dynamic balance conditions; four out of six conditions for global force balance and two conditions on instantaneous moment balance. The mechanism was designed such that two reactionless paths intersect in the middle of the workspace and are approximately perpendicular straight lines. Measurements and simulations showed that the shaking forces where at least 96% lower then the internal bearing forces, indicating force balance. The measurements also confirmed the existence of two intersecting reactionless paths. When comparing the non-moment balanced paths with the two reactionless paths, a shaking moment reduction in the order of 95 % was achieved. This shows the existence of an instantaneous dynamic balance pose in the middle of the workspace.

3

Chapter 4

Higher-order Taylor approximation of finite motions of mechanisms

Higher-order derivatives of kinematic mappings give insight into the motion characteristics of complex mechanisms. Screw theory and its associated Lie group theory have been used to find these derivatives of loop-closure equations up to an arbitrary order. In this chapter, this is extended to the higher-order derivatives of the solution to these loop-closure equations to provide an approximation of the finite motion of serial and parallel mechanisms. This recursive algorithm, consisting solely of matrix operations, relies on a simplified representation of the higher-order derivatives of open chains. The method is applied to a serial, a parallel and an overconstrained mechanism. In all cases adequate approximation is obtained over a large portion of the workspace.

4.1 Introduction

Screw theory is frequently used to analyze the instantaneous motion of spatial kinematics. This theory gives the instantaneous kinematic relations between the spatial angular and linear velocities of bodies (twists) and constraint forces and moments (constraint wrenches) acting on a mechanism. This differential analysis is only available in the pose of inspection, and in general does not give a description of the finite motion of a mechanism. On the other hand,

The dynamic balance conditions as derived in the previous chapter are only solved for a single 'reference' pose, the instantaneous dynamic balance pose. In order to extend dynamic balance over the whole workspace, the next chapter (Chapter 5) attempts to satisfy all higher-order partial derivatives of the dynamic balance condition. This chapter paves the way, by providing an algorithm that recursively yields the higher-order derivatives of the solution to the loop-closure equation that are required for this balancing approach. This higher-order kinematic approach thereby bypasses the need to solve the loop-closure constraint equations in closed-form whose solution might not be available or too involved for algorithmic treatment.

This chapter is a reprint from: J. J. de Jong, A. Müller, J. L. Herder, Higher-order Taylor approximation of finite motions in mechanisms. *Robotica* (2019) vol. 37 (7), pp. 1190-1201

closed-form solutions to the geometric closure equations are not always available or are intricate to obtain for more complex mechanisms. This hinders the use of algebraic methods for expressing the finite motion of a mechanisms. For synthesis and analysis purposes, attempts have been made to extend the infinitesimal screw analysis using higher-order derivatives. Bartkowiak and Woernle [12] used the higher-order derivatives of screws to find the conditions such that overconstrained single loop linkages have a single degree of freedom. Their numerical method yields an estimated maximum number of derivatives required to guarantee finite local mobility. Wohlhart [117, 118] coined the term 'order of shakiness'. It defines to which order an arbitrary input still satisfies the higher-order derivatives of the loop-closure equations. In [22] several mechanisms are discussed that do not possess a finite mobility but still exhibit a higher-order local differential mobility which in practice leads to an unexpected large range of motion. Derivatives up to an arbitrary order of loop-closure equations can be found by taking Lie brackets of instantaneous screw axes, which can be expressed as matrix multiplications of twists [87, 77]. This paves the way for algorithmic differentiation-free derivatives of the loop-closure equations [78].

However, higher-order derivatives and approximations of finite motion in closed-loop mechanisms were not yet reported. This involves finding the higher-order derivatives of the solution to implicit closure equations. These solutions can be an inverse kinematic model (IK), forward kinematic model (FK) or other types of mappings, relating the dependent and independent coordinates in the kinematic loop.

These higher-order derivatives and approximations of finite motion can be used for the analysis of admissible motions of mechanisms. It also can be used to enhanced numerical methods for the simulation of the kinematics and motions. Furthermore, the derivatives of the design criteria can be algebraically expressed as a function of geometric properties such as link lengths, potentially aiding the synthesis of specific kinematics, such as straight line mechanisms. Another possible application is the description of the derivatives of the dynamics of mechanisms, particularly to determine the conditions for dynamic balance in arbitrary mechanisms. A system is dynamically balanced when all shaking forces and moments vanish for all admissible motions [107]. This implies that the angular and linear momentum should be constant (for practical purposes usually zero) and all its derivatives should remain zero throughout motion. These higher-order derivatives of momentum should provide the geometric and dynamic conditions for dynamic balancing. For path planning, a sufficient smooth function in the actuator coordinates is required, i.e. necessitating a sufficient number of higher derivatives of kinematic mappings between the end-effector and actuators.

Unfortunately, processing these higher-order multivariate derivatives requires elaborate bookkeeping, as can be seen in the implementation of the higher-order chain rule, the Faa di Bruno's rule [69]. This renders it arduous to find the solution to the implicitly formulated higher-oder constraints.

In this chapter a simplified representation of the higher-order derivatives of the screw systems is presented, which directly follows from the product of exponentials of Brockett [20]. With Vetter's method for managing matrix deriv-

atives [112] this enables us to obtain a recursive, differentiation-free algorithm for higher-order derivatives of the solution to the closure equations. Using these resulting higher-order derivatives of the Jacobians, a Taylor approximation of open and closed-loop kinematics is performed. The method is illustrated with an approximation of the finite motion of three mechanisms: 1) a serial 6 DOF manipulator, 2) a parallel five-bar mechanism, 3) and an overconstrained but mobile Bennett linkage. A preliminary version of this work is presented in [29]

Before we introduce the higher-order derivatives of the loop-closure solution, the screw algebra is revisited and applied to an open chain (Section 4.2). Based on this, a simplified representation of the higher-order derivatives of an open chain is presented (Section 4.2). Subsequently, the loop-closure equations and the matrix derivatives are revisited (Section 4.2–4.2). Using these rules the algorithm for determining the higher-order derivatives of the loop-closure and its Taylor expansion are presented (Section 4.2) and its implementation is shown in three examples (Section 4.3–4.3).

4.2 Method

Concepts and notation

In the notation of screw theory, as used in this chapter, a reference frame ψ_i is associated to each rigid body i. Points in space $\boldsymbol{a}$ can be expressed with respect to this reference frame (denoted with superscript $\boldsymbol{a}^i$). In the homogeneous representation the $\boldsymbol{a}^i$-vector is appended with a 1. A change of reference frame from frame i to j follows from the homogeneous transformation matrix $\boldsymbol{H}_i^j$ which consists of a rotation matrix $\boldsymbol{R}$ and a translation vector $\boldsymbol{o}$

$$\boldsymbol{a}^j = \boldsymbol{H}_i^j \boldsymbol{a}^i \qquad\qquad \boldsymbol{H} = \begin{bmatrix} \boldsymbol{R} & \boldsymbol{o} \\ \boldsymbol{0} & 1 \end{bmatrix} \tag{4.1}$$

The time derivative of the transformation matrix is given by the twist $\boldsymbol{t}_i^{k,j}$, i.e. the generalized velocity of body i with respect to body j expressed in frame k. For clarity reasons the subscript and second superscript are omitted when unambiguous. The twist is a vector containing the angular $\boldsymbol{\omega}$ and translational $\boldsymbol{v}$ velocity $\boldsymbol{t}^\top = [\boldsymbol{\omega}^\top, \boldsymbol{v}^\top]$. The $\big[\boldsymbol{\omega}\times\big]$ denotes the skew symmetric matrix of $\boldsymbol{\omega}$

$$\dot{\boldsymbol{H}}_i^j = \big[\boldsymbol{t}_i^{j,j}\times\big]\boldsymbol{H}_i^j \qquad\qquad \big[\boldsymbol{t}\times\big] = \begin{bmatrix} \big[\boldsymbol{\omega}\times\big] & \boldsymbol{v} \\ \boldsymbol{0} & 0 \end{bmatrix} \tag{4.2}$$

The twist's 'frame of expression' changes with the adjoint transformation matrices here denoted with $\mathrm{Ad}\big(\boldsymbol{H}\big)$

$$\boldsymbol{t}^j = \mathrm{Ad}\big(\boldsymbol{H}_i^j\big)\boldsymbol{t}^i \qquad\qquad \mathrm{Ad}\big(\boldsymbol{H}\big) = \begin{bmatrix} \boldsymbol{R} & \boldsymbol{0} \\ \big[\boldsymbol{o}\times\big]\boldsymbol{R} & \boldsymbol{R} \end{bmatrix} \tag{4.3}$$

The time derivative of adjoint transformation matrix is given in terms of instantaneous transformation matrix $\mathrm{ad}\big(\boldsymbol{t}\big)$

$$\frac{\partial}{\partial t}\Big(\mathrm{Ad}\big(\boldsymbol{H}_i^j\big)\Big) = \mathrm{ad}\big(\boldsymbol{t}_i^{j,j}\big)\mathrm{Ad}\big(\boldsymbol{H}_i^j\big) \qquad \mathrm{ad}\big(\boldsymbol{t}\big) = \begin{bmatrix} \big[\boldsymbol{\omega}\times\big] & \boldsymbol{0} \\ \big[\boldsymbol{v}\times\big] & \big[\boldsymbol{\omega}\times\big] \end{bmatrix} \tag{4.4}$$

This matrix itself can be expressed in another reference frame according to a nested transform

$$\mathrm{ad}\big(\boldsymbol{t}^j\big) = \mathrm{ad}\Big(\mathrm{Ad}\big(\boldsymbol{H}_i^j\big)\boldsymbol{t}^i\Big) = \mathrm{Ad}\big(\boldsymbol{H}_i^j\big)\mathrm{ad}\big(\boldsymbol{t}^i\big)\mathrm{Ad}\big(\boldsymbol{H}_j^i\big) \tag{4.5}$$

Using these twists and their exponentials, a concise formulation for the forward kinematic mapping of an open chain is available in the form of Brockett's product of exponentials [20]

$$\boldsymbol{H}_n^0 = \prod_{i=0}^{n} \boldsymbol{H}_i^{i-1}(q_i) = \prod_{i=0}^{n} \exp(q_i \big[\boldsymbol{s}_i^0 \times\big])\boldsymbol{H}_n^0(0) \tag{4.6}$$

Here, the instantaneous screw vector $\boldsymbol{s}_i^0$, specifies the amount of twist of body i generated by the unit actuation of joint i expressed in global frame. This screw vector is therefore a purely geometric entity. As this screw vector is defined according the ordering of the chain — always with respect to the previous body — the second superscript is omitted. This also means that the instantaneous screw vectors of lower kinematic pairs are constant when expressed in the connecting frames, i.e., $d/dt(\boldsymbol{s}_i^{i-1}) = d/dt(\boldsymbol{s}_i^i) = \boldsymbol{0}$.

4

Derivatives of twist systems (open chain)

For an open chain, the higher-order partial derivatives can be found using the transformations of the previous section. A chain of transformations can be decomposed into a part which is constant and part which is varying with respect to this particular derivative. The nested transform (Eq. 4.5) of the twist gives a concise formulation of the derivative of a chain, provided that $i \leq n$

$$\frac{\partial}{\partial q_i}\left(\mathrm{Ad}\big(\boldsymbol{H}_n^0\big)\right) = \mathrm{Ad}\big(\boldsymbol{H}_{i-1}^0\big)\frac{\partial}{\partial q_i}\left(\mathrm{Ad}\big(\boldsymbol{H}_i^{i-1}\big)\right)\mathrm{Ad}\big(\boldsymbol{H}_n^i\big) \tag{4.7}$$

$$= \mathrm{Ad}\big(\boldsymbol{H}_{i-1}^0\big)\mathrm{ad}\big(\boldsymbol{s}_i^{i-1}\big)\mathrm{Ad}\big(\boldsymbol{H}_i^{i-1}\big)\mathrm{Ad}\big(\boldsymbol{H}_n^i\big) \tag{4.8}$$

$$= \mathrm{ad}\big(\boldsymbol{s}_i^0\big)\mathrm{Ad}\big(\boldsymbol{H}_n^0\big) \tag{4.9}$$

For the second-order, such a concise representation also exists. For the consecutive derivative with respect to joint j there exist two possibilities, it is either after body i in the chain (case 1) or before i in the chain (case 2), provided that $j \leq n$.

1. Case 1. $(i \leq j)$ In the case that joint j is higher in the chain than i, the twist is unaffected $(\partial/\partial q_j(\mathrm{ad}\big(\boldsymbol{s}_i^0\big)) = 0)$. Therefore, the second partial derivative becomes

$$\frac{\partial}{\partial q_j}\frac{\partial}{\partial q_i}\left(\mathrm{Ad}\big(\boldsymbol{H}_n^0\big)\right) = \mathrm{ad}\big(\boldsymbol{s}_i^0\big)\mathrm{ad}\big(\boldsymbol{s}_j^0\big)\mathrm{Ad}\big(\boldsymbol{H}_n^0\big) \tag{4.10}$$

2. Case 2. $(i \geq j)$ In the case that j is below i in the chain we use the nested transform property to split the chain into a dependent and independent

part. It may be verified that $\partial/\partial q_j(\mathrm{ad}(\boldsymbol{s}_i^j)\mathrm{Ad}(\boldsymbol{H}_n^j)) = 0$. Therefore

$$\frac{\partial}{\partial q_j}\frac{\partial}{\partial q_i}\left(\mathrm{Ad}(\boldsymbol{H}_n^0)\right) = \frac{\partial}{\partial q_j}\left(\mathrm{Ad}(\boldsymbol{H}_j^0)\mathrm{ad}(\boldsymbol{s}_i^j)\mathrm{Ad}(\boldsymbol{H}_n^j)\right) \tag{4.11}$$

$$= \frac{\partial}{\partial q_j}\left(\mathrm{Ad}(\boldsymbol{H}_j^0)\right)\mathrm{ad}(\boldsymbol{s}_i^j)\mathrm{Ad}(\boldsymbol{H}_n^j) \tag{4.12}$$

Using (Eq. 4.9) a chain of matrix products can be found and collected again using the nested transform Eq. 4.5

$$\frac{\partial}{\partial q_j}\frac{\partial}{\partial q_i}\left(\mathrm{Ad}(\boldsymbol{H}_n^0)\right) = \mathrm{ad}(\boldsymbol{s}_j^0)\mathrm{ad}(\boldsymbol{s}_i^0)\mathrm{Ad}(\boldsymbol{H}_n^0) \tag{4.13}$$

This leaves us with an expression similar to (Eq. 4.10), with the difference that sequence of multiplication is swapped. This also follows from the symmetry (commutativity) property of mixed partial derivatives.

A consecutive application of (Eq. 4.10) and (Eq. 4.13) gives us the geometrical higher-order partial derivatives of the adjoint transformation matrix. The mixed partial derivative with respect to the elements of $\boldsymbol{q}$ are denoted by $D_{\boldsymbol{q}}^{\boldsymbol{\alpha}} = \partial^k/(\partial q_1^{\alpha_1}\cdots\partial q_n^{\alpha_n})$. Vector $\boldsymbol{\alpha} = (\alpha_1, \ldots, \alpha_n)$ comprises the order of derivatives corresponding to $\boldsymbol{q}$, running from the base to the end-effector. $k = \alpha_1 + \ldots + \alpha_n = |\boldsymbol{\alpha}|$ is the total order (Appendix A). The mixed partial derivative of the adjoint transformation matrix is

$$\mathrm{D}_{\boldsymbol{q}}^{\boldsymbol{\alpha}}\left(\mathrm{Ad}(\boldsymbol{H}_n)\right) = \prod_{i=1}^{n}\mathrm{ad}(\boldsymbol{s}_i)^{\alpha_i}\mathrm{Ad}(\boldsymbol{H}_n) \tag{4.14}$$

and similarly for the higher partial derivatives of the instantaneous screw vectors

$$\mathrm{D}_{\boldsymbol{q}}^{\boldsymbol{\alpha}}(\boldsymbol{s}_n) = \prod_{i=1}^{n-1}\mathrm{ad}(\boldsymbol{s}_i)^{\alpha_i}\boldsymbol{s}_n \tag{4.15}$$

These results (Eq. 4.14 and Eq. 4.15) are similar to that of [77], with the difference that the index ranges — to distinguish between the sequence of derivatives — are taken into account by the ordering of $\boldsymbol{\alpha}$. From the commutative property of mixed partial derivatives it follows that for any sequence of differentiation the same results are obtained.

Loop-closure equations

The open-loop derivatives (Eq. 4.14 and Eq. 4.15) can be used for the derivatives of loop-closure equations, as a closed loop can be seen as a connection of open loops, e.g. a simple loop can be seen as an open chain of with the last link fixed to the base. The loop-closure constraint equation (lc) states how the members of the loop are constrained. It can be written in terms of locally validly chosen independent $\boldsymbol{u}$ and dependent coordinates $\boldsymbol{d}$, also termed input and output, respectively. The total set of coordinates we call $\boldsymbol{r}^\top = \begin{bmatrix}\boldsymbol{u}^\top & \boldsymbol{d}^\top\end{bmatrix}$

$$\mathrm{lc}(\boldsymbol{u}, \boldsymbol{d}) \equiv \boldsymbol{0} \tag{4.16}$$

The solution to this condition is denoted by km, which can be the inverse, forward, or any other kinematic model giving an exact relation between independent and dependent coordinates

$$\boldsymbol{d} = \mathrm{km}(\boldsymbol{u}) \tag{4.17}$$

The solution (km) to the loop-closure equation is not necessarily available for complex mechanisms. Therefore, we are looking for a Taylor expansion using higher-order derivatives of the constraint formulation and the open loop derivatives of section Section 4.2. We start with the first-order time derivative of the closure equation. This reads

$$\frac{\partial}{\partial t}\left(\mathrm{lc}\right) = \mathrm{D}_{\boldsymbol{u}}(\mathrm{lc})\,\dot{\boldsymbol{u}} + \mathrm{D}_{\boldsymbol{d}}(\mathrm{lc})\,\dot{\boldsymbol{v}} = \boldsymbol{U}\dot{\boldsymbol{u}} + \boldsymbol{V}\dot{\boldsymbol{d}} \equiv \boldsymbol{0} \tag{4.18}$$

Here $\mathrm{D}_{\boldsymbol{u}}(\mathrm{lc}) = \boldsymbol{U}$ and $\mathrm{D}_{\boldsymbol{d}}(\mathrm{lc}) = \boldsymbol{V}$ denote the matrix collection of all the first-order partial derivatives (Jacobians) of the constraint equations with respect to $\boldsymbol{u}$ and $\boldsymbol{d}$ while assuming independence of $\boldsymbol{u}$ and $\boldsymbol{d}$. This gives rise to the Jacobians $\boldsymbol{C}$ and $\boldsymbol{Q}$, respectively linking $\dot{\boldsymbol{d}}$ and $\dot{\boldsymbol{r}}$ to $\dot{\boldsymbol{d}}$

$$\dot{\boldsymbol{d}} = -\boldsymbol{V}^{-1}\boldsymbol{U}\dot{\boldsymbol{u}} = \boldsymbol{Q}\dot{\boldsymbol{u}} = \mathrm{D}_{\boldsymbol{u}}(\mathrm{km})\,\dot{\boldsymbol{u}} \qquad \dot{\boldsymbol{r}} = \boldsymbol{C}\dot{\boldsymbol{u}} = \begin{bmatrix}\boldsymbol{I}\\ \boldsymbol{Q}\end{bmatrix}\dot{\boldsymbol{u}} \tag{4.19}$$

We already have seen that closure equations can be written as a function of transformation matrices of the open chain. Therefore, the higher-order partial derivatives of the open loop equivalent ($\mathrm{D}^{\alpha}_{\boldsymbol{r}}(\mathrm{lc})$) are available. Now we are looking for a method of writing the higher-order derivatives of the constraint Jacobian $\boldsymbol{Q}_k = \mathrm{D}^k_{\boldsymbol{u}}(\mathrm{km})$.

Multivariate matrix derivatives using Kronecker product

The higher-order partial derivatives of matrices can be managed with the use of the Kronecker product [112]. Refer to Appendix A for definition and properties of the Kronecker product as used in this chapter. Different from [112], the higher-order derivatives of matrices are organized here as the concatenation of the derivatives of the columns $\boldsymbol{A} = \begin{bmatrix}\boldsymbol{a}_1 & \dots & \boldsymbol{a}_m\end{bmatrix}$

$$\mathrm{D}_{\boldsymbol{x}}(\boldsymbol{A}) = \begin{bmatrix}\mathrm{D}_{\boldsymbol{x}}(\boldsymbol{a}_1) & \dots & \mathrm{D}_{\boldsymbol{x}}(\boldsymbol{a}_m)\end{bmatrix} \tag{4.20}$$

$$\mathrm{D}^2_{\boldsymbol{x}}(\boldsymbol{A}) = \mathrm{D}_{\boldsymbol{x}}(\mathrm{D}_{\boldsymbol{x}}(\boldsymbol{A})) = \begin{bmatrix}\mathrm{D}^2_{\boldsymbol{x}}(\boldsymbol{a}_1) & \dots & \mathrm{D}^2_{\boldsymbol{x}}(\boldsymbol{a}_m)\end{bmatrix} \tag{4.21}$$

The partial derivatives of the product rule, the chain rule, Kronecker product, and the inverse matrix derivative are given as follows:

- Product rule of $\boldsymbol{A}(\boldsymbol{x}) \in \mathbb{R}^{n\times m}$ and $\boldsymbol{B}(\boldsymbol{x}) \in \mathbb{R}^{m\times q}$, with $\boldsymbol{x} \in \mathbb{R}^p$, in which $\boldsymbol{I}_p$ is the $p \times p$ identity matrix

$$\mathrm{D}_{\boldsymbol{x}}(\boldsymbol{AB}) = \mathrm{D}_{\boldsymbol{x}}(\boldsymbol{A})\,(\boldsymbol{B} \otimes \boldsymbol{I}_p) + \boldsymbol{A}\mathrm{D}_{\boldsymbol{x}}(\boldsymbol{B}) \tag{4.22}$$

- Chain rule of nested variables $\boldsymbol{b}$ and $\boldsymbol{c}$

$$\mathrm{D}_{\boldsymbol{c}}(\boldsymbol{A}(\boldsymbol{b}(\boldsymbol{c}))) = \mathrm{D}_{\boldsymbol{b}}(\boldsymbol{A})\,(\boldsymbol{I}_m \otimes \mathrm{D}_{\boldsymbol{c}}(\boldsymbol{b})) \tag{4.23}$$

- Derivatives of the Kronecker product can be given with the use of permutation matrices (refer to Appendix A)

$$\mathrm{D}_{\boldsymbol{x}}(\boldsymbol{A}\otimes\boldsymbol{B}) = (\mathrm{D}_{\boldsymbol{x}}(\boldsymbol{A})\otimes\boldsymbol{B})(\boldsymbol{I}_m\otimes\boldsymbol{P}_{q,p}) + \boldsymbol{A}\otimes\mathrm{D}_{\boldsymbol{x}}(\boldsymbol{B}) \tag{4.24}$$

- Derivative of matrix inversion

$$\mathrm{D}_{\boldsymbol{x}}\big(\boldsymbol{A}^{-1}\big) = -\boldsymbol{A}^{-1}\mathrm{D}_{\boldsymbol{x}}(\boldsymbol{A})\,(\boldsymbol{A}^{-1}\otimes\boldsymbol{I}_p) \tag{4.25}$$

Recursive application of these rules allows the extension of these derivatives to higher orders.

Higher-order derivatives of the constraint Jacobians

Using the rules from the previous section, the second-order derivatives (Hessian) of the solution to the constraint equations are found. This is done by consecutive application of the chain rule, the product rule, and the inverse matrix derivative to the constraint Jacobian (Eq. 4.19)

$$\begin{aligned}\boldsymbol{Q}_2 = \mathrm{D}_{\boldsymbol{u}}(\boldsymbol{Q}_1) &= -[\mathrm{D}_{\boldsymbol{r}}\big(\boldsymbol{V}^{-1}\big)\,(\boldsymbol{U}\otimes\boldsymbol{I}) - \boldsymbol{V}^{-1}\mathrm{D}_{\boldsymbol{r}}(\boldsymbol{U})](\boldsymbol{I}\otimes\boldsymbol{C}) &(4.26)\\ &= -\boldsymbol{V}^{-1}[\mathrm{D}_{\boldsymbol{r}}(\boldsymbol{V})\,(\boldsymbol{Q}_1\otimes\boldsymbol{I}) + \mathrm{D}_{\boldsymbol{r}}(\boldsymbol{U})](\boldsymbol{I}\otimes\boldsymbol{C}) &(4.27)\end{aligned}$$

After reordering the Kronecker products, we can find a concise formulation of the Hessian matrix

$$\boldsymbol{Q}_2 = -\boldsymbol{V}^{-1}\begin{bmatrix}\mathrm{D}_{\boldsymbol{r}}(\boldsymbol{V}) & \mathrm{D}_{\boldsymbol{r}}(\boldsymbol{U})\end{bmatrix}(\boldsymbol{C}\otimes\boldsymbol{C}) = -\boldsymbol{V}^{-1}\boldsymbol{F}_2\boldsymbol{L}_2 \tag{4.28}$$

in which $\boldsymbol{F}_2 = \mathrm{D}^2_{\boldsymbol{r}}(\mathrm{lc})$. A further derivation is applied to show that a similar structure as the Hessian can be found for the 3$^{\mathrm{rd}}$ derivative

$$\boldsymbol{Q}_3 = \mathrm{D}_{\boldsymbol{u}}(\boldsymbol{Q}_2) = -\boldsymbol{V}^{-1}\begin{bmatrix}\mathrm{D}_{\boldsymbol{r}}(\boldsymbol{V}) & \mathrm{D}_{\boldsymbol{r}}(\boldsymbol{F}_2) & \boldsymbol{F}_2\end{bmatrix}\begin{bmatrix}\boldsymbol{Q}_2\otimes\boldsymbol{C}\\ \boldsymbol{L}_2\otimes\boldsymbol{C}\\ \mathrm{D}_{\boldsymbol{u}}(\boldsymbol{L}_2)\end{bmatrix} = -\boldsymbol{V}^{-1}\boldsymbol{F}_3\boldsymbol{L}_3 \tag{4.29}$$

For higher orders this process can be repeated until the desired order is reached, giving us a recursive algorithm

$$\boldsymbol{Q}_k = -\boldsymbol{V}^{-1}\begin{bmatrix}\mathrm{D}_{\boldsymbol{r}}(\boldsymbol{V}) & \mathrm{D}_{\boldsymbol{r}}(\boldsymbol{F}_{k-1}) & \boldsymbol{F}_{k-1}\end{bmatrix}\begin{bmatrix}\boldsymbol{Q}_{k-1}\otimes\boldsymbol{C}\\ \boldsymbol{L}_{k-1}\otimes\boldsymbol{C}\\ \mathrm{D}_{\boldsymbol{u}}(\boldsymbol{L}_{k-1})\end{bmatrix} = -\boldsymbol{V}^{-1}\boldsymbol{F}_k\boldsymbol{L}_k \tag{4.30}$$

This algorithm consist of three steps:

1. The higher-order derivatives of $\boldsymbol{V}$ and $\boldsymbol{U}$ are substituted into the proper location of $\boldsymbol{F}_k$. These can be found a priori by higher-order screw derivatives of the open-loop equivalent.
2. The $\boldsymbol{L}_k$ matrix is filled with precursory, lower-order results.
3. The combination of the three matrices gives the subsequent partial derivative of the constraint Jacobian.

It should be noted that repeating terms occur which could be combined to mitigate the computational burden. The simplification of this recursive formulation is outside the scope of this chapter.

Higher-order Taylor approximation of closure equation

The Taylor approximation of the loop-closure solution can now be written using the partial derivatives of the constraint Jacobians up to the k-th order. We assume that at the evaluation point the closure constraint is satisfied, and that the evaluation point is at zero such that the Taylor series becomes a Maclaurin series. The input for the independent variables is given as a power (denoted with $^{\otimes i}$) of Kronecker products [112]

$$\boldsymbol{d}(\boldsymbol{u}) \approx \boldsymbol{d}(\boldsymbol{0}) + \boldsymbol{Q}_1\boldsymbol{u} + \frac{1}{2!}\boldsymbol{Q}_2(\boldsymbol{u}\otimes\boldsymbol{u}) + \frac{1}{3!}\boldsymbol{Q}_3(\boldsymbol{u}\otimes\boldsymbol{u}\otimes\boldsymbol{u}) + \cdots = \sum_{i=0}^{k} \frac{1}{i!}\boldsymbol{Q}_i\boldsymbol{u}^{\otimes i} \quad (4.31)$$

4.3 Examples

To show the performance of this procedure for single- and multi-DOF mechanisms, three examples are presented here. In the first example, the Taylor approximation along a trajectory of a serial robot is investigated to see its performance close to the workspace boundary. In the second example, a multi-DOF approximation of a parallel manipulator is shown. In the third example, the method is applied to a Bennett linkage to compare two approaches to deal with overconstrained mechanisms.

The computation times for these examples are recorded and reported in Table 4.1. The time reported is for an average over 10 trails with 200 evaluation poses each. These computations were done with Matlab 2014b running on a PC with an Intel Core i7 4800MQ running at 2.70GHz.

Approximate solution of the inverse kinematics of a 6 DOF serial manipulator

The inverse kinematic model of general serial linkages are not readily available. For a 6 DOF serial manipulator the IK is found by Husty et al. [50] by invoking algebraic methods to find and solve a univariate polynomial of order 16. In this first example we will show the procedure to find the higher-order derivatives and Taylor approximation of a 6 DOF serial manipulator following a straight line, rendering it a single DOF expansion.

This manipulator consists of 6 bodies with 6 joints and an end-effector which should follow a straight line in the y-direction. Therefore the constraints are written as

$$\text{lc} : \boldsymbol{H}_6^0(\boldsymbol{q})\boldsymbol{H}_{\text{ee}}^6 = \boldsymbol{H}_{\text{des}}^0(y_{\text{des}})$$

in which $\boldsymbol{H}_{\text{ee}}^6$ describes the location of the end-effector expressed in the 6^{th} body fixed frame, and $\boldsymbol{H}_{\text{des}}^0$ the desired end-effector pose in global frame. The independent coordinate is the the y-position along the straight line $\boldsymbol{u} = y_{\text{des}}$. The dependent coordinates are the set of joint angles $\boldsymbol{d} = \boldsymbol{q}$.

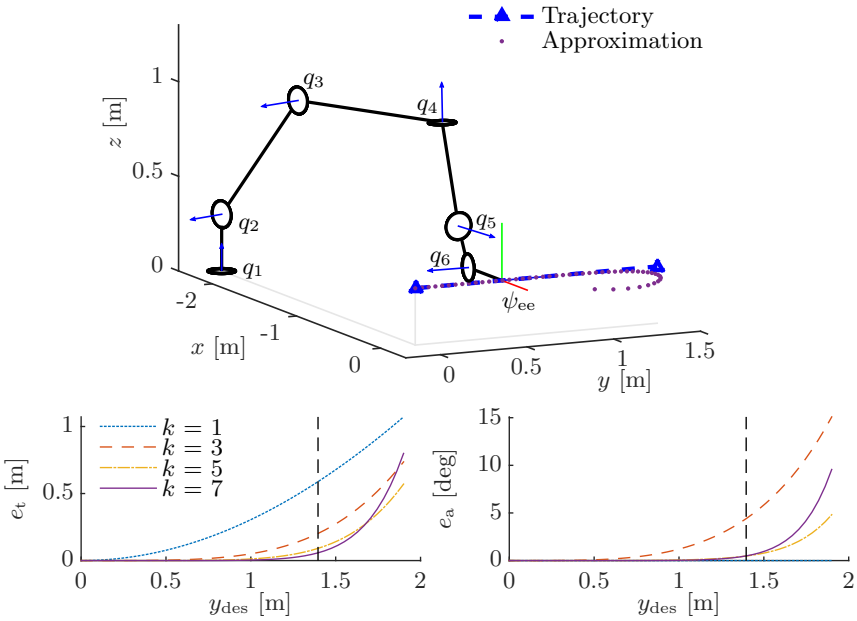

Figure 4.1: *Top* The 7^{th}-order Taylor expansion of the inverse kinematic model of a 6 DOF serial manipulator (solid black) over a desired horizontal trajectory y_{des}. The evaluation point is $[0, 0, 0.3]$. The trajectory is approximated well until close to the end of the workspace at $[0, 1.4, 0.3]$. *Bottom left and right* The approximation error for translation e_{t} and orientation e_{a}, respectively. The vertical line denotes the end of the workspace.

Based on these constraint equations, the first- and second-order derivatives the open loop Jacobains are given

$$\mathrm{D}_{\boldsymbol{u}}(\mathrm{lc}) = \boldsymbol{U} = \boldsymbol{s}_{\text{des}} \qquad \mathrm{D}_{\boldsymbol{d}}(\mathrm{lc}) = \boldsymbol{V} = \begin{bmatrix} \boldsymbol{s}_1 & \cdots & \boldsymbol{s}_6 \end{bmatrix}$$
$$\mathrm{D}_{\boldsymbol{r}}(\boldsymbol{U}) = \boldsymbol{0} \qquad \mathrm{D}_{\boldsymbol{r}}(\boldsymbol{V}) = \begin{bmatrix} \boldsymbol{0} & \mathrm{D}_{\boldsymbol{r}}(\boldsymbol{s}_2) & \cdots & \mathrm{D}_{\boldsymbol{r}}(\boldsymbol{s}_6) \end{bmatrix}$$

in which the product of sequence (Eq. 4.15) is used to fill the higher-order Jacobains

$$\begin{aligned} \mathrm{D}_{\boldsymbol{r}}(\boldsymbol{s}_i) &= \begin{bmatrix} \boldsymbol{0} & \frac{\partial}{\partial q_1}(\boldsymbol{s}_i) & \cdots & \frac{\partial}{\partial q_{i-1}}(\boldsymbol{s}_i) & \boldsymbol{0} \end{bmatrix} \\ &= \begin{bmatrix} \boldsymbol{0} & \mathrm{ad}(\boldsymbol{s}_1)\boldsymbol{s}_i & \cdots & \mathrm{ad}(\boldsymbol{s}_{i-1})\boldsymbol{s}_i & \boldsymbol{0} \end{bmatrix} \end{aligned}$$

The Taylor approximation is made up to the 7^{th} order. The result of this approximation can be seen in Fig. 4.1. In the initial pose — in which the end-effector is in [0,0,0.3] — the robot lies in the xz-plane. The desired trajectory is a motion from this initial pose until 2 m in the y-direction which is beyond the workspace boundary. The workspace ends at 1.4 m.

For higher orders it can be seen that tracking converges to the desired path until the boundary of the workspace. Beyond this point the trajectory estimate is no longer adequate and the approximation starts to diverge. In this case the radius of convergence coincides with the edge of workspace.

Approximate solution of a five-bar mechanism's motion

The higher-order derivatives and Taylor expansion technique is applied to approximate the inverse kinematic solution of a $5R$ five-bar mechanism. We choose to describe the five-bar as a connection of two open chains a and b, with joints q_1 and q_2, and q_3 and q_4 respectively. The interconnection point is the end-effector $\boldsymbol{x}^0$. This point has to satisfy the constraint equation from both sides (a and b) calculated in local frame $\boldsymbol{x}_a^0 = \boldsymbol{H}_2^0(\boldsymbol{q}_{1,2})\boldsymbol{x}^2$ and $\boldsymbol{x}_b^0 = \boldsymbol{H}_4^0(\boldsymbol{q}_{3,4})\boldsymbol{x}^4$. The closure equation can be written as

$$\text{lc} : \boldsymbol{0} = \begin{bmatrix} \boldsymbol{x}^0 - \boldsymbol{x}_a^0 \\ \boldsymbol{x}^0 - \boldsymbol{x}_b^0 \end{bmatrix} \tag{4.32}$$

4

Using the end-effector coordinates $\boldsymbol{u} = \boldsymbol{x}^0$ as input and the 4 joint angles $\boldsymbol{d} = \begin{bmatrix} q_1 & \dots & q_4 \end{bmatrix}^\top$ as output, the first-order partial derivatives of the closure equation become

$$\mathrm{D}_{\boldsymbol{u}}(\text{lc}) = \boldsymbol{U} = \begin{bmatrix} \boldsymbol{I} \\ \boldsymbol{I} \end{bmatrix} \quad \mathrm{D}_{\boldsymbol{d}}(\text{lc}) = \boldsymbol{V} = \begin{bmatrix} \left[\boldsymbol{s}_1^0\times\right]\boldsymbol{x}_a^0 & \left[\boldsymbol{s}_2^0\times\right]\boldsymbol{x}_a^0 & \boldsymbol{0} & \boldsymbol{0} \\ \boldsymbol{0} & \boldsymbol{0} & \left[\boldsymbol{s}_3^0\times\right]\boldsymbol{x}_b^0 & \left[\boldsymbol{s}_4^0\times\right]\boldsymbol{x}_b^0 \end{bmatrix}$$

The higher-order partial derivatives can be found by using the twist derivatives from Section 4.2 and recursive equations from Section 4.2.

The Taylor approximation is computed up to the 7^{th} order for 200 positions of the end-effector $\boldsymbol{x}^0$ forming 4 paths over the x- and y-axes and over the diagonals, with the aim of finding an approximation of the corresponding joint displacement of the joints $[q_1 \dots q_4]$. For the evaluation of the quality of the Taylor approximation, the end-effector position is approximated from the left $\boldsymbol{x}_a^0$ and right $\boldsymbol{x}_b^0$ side, and plotted together with input paths.

The result of the Taylor approximation (Fig. 4.2) shows that in a large portion of the workspace around the evaluation point $\boldsymbol{x}^0 = \boldsymbol{0}$ the approximation converges to the target trajectory indicating a correct estimation of finite joint displacement. However, further from the evaluation point and closer to workspace boundary the accuracy is less as can be seen in the insert.

The Bennett linkage, an overconstrained linkage

An overconstrained linkage has a redundant set of loop-closure constraints. That is, the number of dependent coordinates $\boldsymbol{d}$ is smaller than the number of constraints. This poses a problem for proposed method — as apparent from Eq. 4.19 — since it requires inversion of the matrix $\boldsymbol{V}$, which was so far assumed to be square and nonsingular. Among others, there are two ways to find the higher-order derivatives of the loop-closure solution: 1) By selection of a *subset* of constraint conditions to make a square system 2) or by replacing the inverse

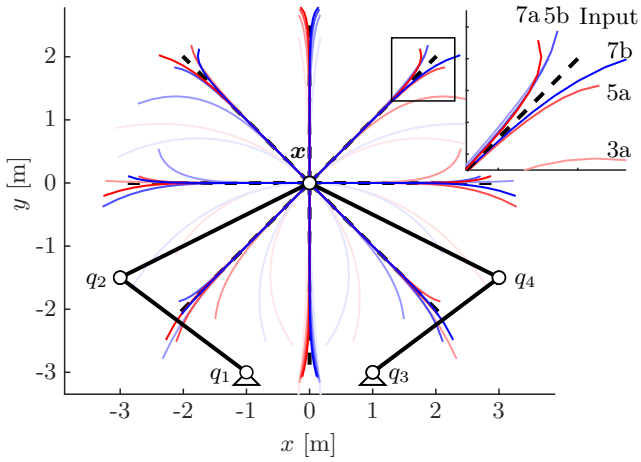

Figure 4.2: The Taylor approximation of the inverse kinematic model of a five-bar (solid grey) around evaluation point at $\boldsymbol{x}^0 = [0, 0]$ up to the 7^{th} order for 4 different trajectories. It shows the left (a, red) and right (b, blue) estimation of end-effector trajectory (dashed black) for the order 1, 3, 5, and 7. The insert shows convergence for higher-order estimations far from the evaluation point.

with a left *pseudo inverse* in Eq. 4.19. This can be done when the columns of $\boldsymbol{V}$ are independent, otherwise the mechanism is in a singular pose where its instantaneous DOF increases. Using the left pseudo inverse, the solution is then

$$\boldsymbol{Q}_k = -(\boldsymbol{V}^\top \boldsymbol{V})^{-1} \boldsymbol{V}^\top \boldsymbol{F}_k \boldsymbol{L}_k = -\boldsymbol{V}^+ \boldsymbol{F}_k \boldsymbol{L}_k \tag{4.33}$$

For the subset method (method 1), the corresponding constraint equation will be indicated with lc_s. A possible disadvantage of this method is that the constraint equations can be selected sub-optimally, which may induce parameterization singularities, and thus limiting the Taylor approximation.

An example of such an overconstrained mechanism is the Bennett linkage [13]. The Bennett linkage consists of a single spatial loop compromising 4 non-parallel revolute joints which do not intersect in a single point. According to the Chebychev-Grübler-Kutzbach's criterion such a spatial linkage with 4 bodies and 4 joints should have a mobility of -2. However, the mechanism is mobile when specific kinematic conditions are satisfied [9, 12]:

1. Equality of the opposite link lengths $l_1 = l_3$, $l_2 = l_4$
2. Equality of the opposite angles between joint axes $\alpha_1 = \alpha_3$, $\alpha_2 = \alpha_4$
3. The Bennett condition $l_1 / \sin(\alpha_1) = l_2 / \sin(\alpha_2)$

The joint angles relate according to: $q_1 + q_3 = q_2 + q_4 = 2\pi$ with q_1 and q_2 as

$$\sin(\alpha_1/2 - \alpha_3/2) \tan(q_1/2) \tan(q_2/2) = \sin(\alpha_1/2 + \alpha_3/2) \tag{4.34}$$

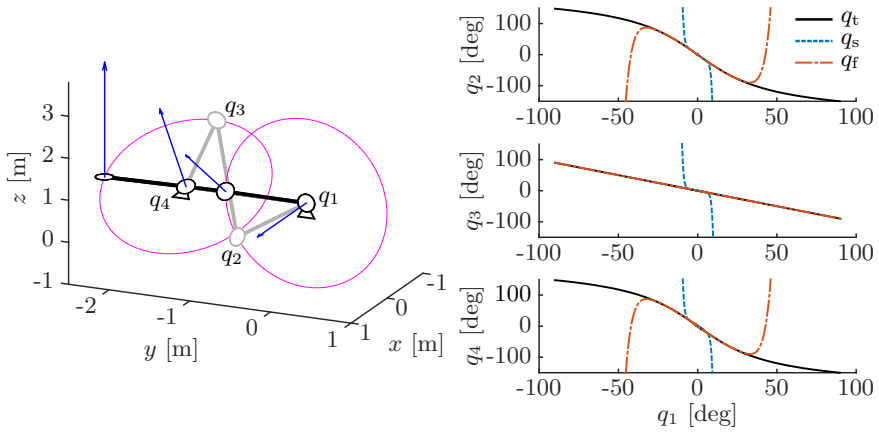

Figure 4.3: Comparison between the two Taylor approximations of the Bennett linkage (10^{th} order); 1) using a subset of constraints, and 2) using the pseudo inverse of the full set. *Left* shows the Bennett linkage as used, in gray a typical pose and in black the evaluation pose, which is close to co-linearity. The blue arrows indicate the joint axes ($\boldsymbol{n}_i$). The magenta circles indicate the motion of the coupler link. *Right* shows a comparison between the theoretical joint angles q_t, and the approximated joint angles using the selection method q_s and the pseudo inverse method (q_f).

4

To show the Taylor approximation, we assume no prior knowledge of joint angle relations, and we will write the closure equations in terms of transformation matrices. We do need the kinematic conditions to ensure full mobility. We use $\alpha_1 = 0.6$ rad, $\alpha_2 = 1$ rad, $l_1 = 1$ m, and $l_2 = 1.5$ m. The Bennett linkage is treated as two open chains, the first linkage consisting of bodies 1 till 3 and a second linkage consisting solely of body 4. Both body 1 and body 4 are hinged with the base. For the loop closure, body 3 is considered rigidly attached to the fourth body. Joint 1 is treated as the independent coordinate $\boldsymbol{u} = q_1$. There exist three dependent coordinates $\boldsymbol{d}^\top = \begin{bmatrix} q_2 & q_3 & q_4 \end{bmatrix}$. Together with the 6 constraints this makes the mechanism three times overconstrained. The effect of both strategies will be shown in and around a special configuration of the robot.

With the selection strategy only the angular constraints are taken into account. For the complete constraint also the translational constraints are used

$$\text{lc}_\text{s} : \boldsymbol{R}_0^3(\boldsymbol{q}_{1-3})\boldsymbol{R}_4^0(q_4) = \text{const.} \qquad \text{lc}_\text{f} : \boldsymbol{H}_0^3(\boldsymbol{q}_{1-3})\boldsymbol{H}_4^0(q_4) = \text{const.} \tag{4.35}$$

For the Bennett linkage there exist two special configuration when the mechanism is fully collapsed onto a line. In that configuration all the joint axes ($\boldsymbol{n}_i$) are perpendicular to the same line, as shown in Fig. 4.3. As lc_s is selected to be consisting of the angular constraints, the system is in a parameterization singularity and the corresponding $\boldsymbol{V}_\text{s} = \begin{bmatrix} \boldsymbol{n}_2 & \boldsymbol{n}_3 & -\boldsymbol{n}_4 \end{bmatrix}$ matrix is singular. When the full set of constraints is taken into account $\boldsymbol{V}_\text{f} = \begin{bmatrix} \boldsymbol{s}_2 & \boldsymbol{s}_3 & -\boldsymbol{s}_4 \end{bmatrix}$ has a rank of 3 and its left pseudo inverse still exists.

Table 4.1: The mean execution time in seconds of the Taylor expansion for the three examples. For the overconstrained Bennett linkage the results of the selection (s) and full (f) method are given.

Order	Serial	Five-bar	Bennett (s)	Bennett (f)
1	0.56×10^{-3}	49×10^{-6}	2.1×10^{-3}	2.1×10^{-3}
2	6.9×10^{-3}	1.5×10^{-3}	3.6×10^{-3}	3.4×10^{-3}
3	11×10^{-3}	3.1×10^{-3}	4.7×10^{-3}	3.4×10^{-3}
4	28×10^{-3}	11×10^{-3}	11×10^{-3}	11×10^{-3}
5	85×10^{-3}	47×10^{-3}	27×10^{-3}	19×10^{-3}
6	0.35	0.47	38×10^{-3}	48×10^{-3}
7	2.6	5.4	81×10^{-3}	85×10^{-3}

Also close to this special configuration the Taylor approximation using the selection strategy ($\mathrm{lc_s}$) on angular constraints suffers from this parameterization singularity as can be seen in Fig. 4.3. Here, a Taylor approximation up to 10^{th} order is made for both strategies. The evaluation pose is close (+0.4 deg of input joint) to the special configuration. It can be seen that the Taylor expansion using the selected constraints, follows until roughly 6 deg. With the full set of constraints an approximation up to 30 deg could be obtained. This regression can be explained by numerical round off errors accumulating due to the ill-conditioned matrix inverse of $\boldsymbol{V}_{\mathrm{s}}$.

It should be noted that although the Bennett linkage has no singularities, there is a radius of convergence around its evaluation point. This is due to the fact that the relation between the input and the output angle follows an arctan relation in Eq. 4.34.

4.4 Discussion

In all three examples it can be seen that the Taylor approximation is confined to a region of convergence. One limiting cause is the existence of the singularities. Additionally, as seen in the Bennett linkage, the underlying closure solution can pose boundaries on the Taylor approximation. Therefore, in the case the closure solution is not known beforehand, one cannot discriminate between both causes of bounded convergence, based on a single Taylor approximation.

This method is restricted to lower kinematic pairs by the assumption that the screw vector associated with the joints is constant when expressed in the frames of the connecting bodies. For most practical applications this is sufficient.

For the calculation of higher-order partial derivatives, the proposed method uses Kronecker products of matrices, which can lead to very large matrices for larger systems and higher orders, as can be seen in Table 4.1. This possibly poses practical limits on the applicability of this procedure. Sparse matrices and the aggregation of mixed partial derivatives can be used to mitigate computer memory usage and reduce the number of matrix operations. Also, as seen

in the Bennett linkage example, an expansion close to singularity leads to ill-conditioned matrices reducing the numerical accuracy significantly.

The method presented here generates higher-order derivatives of motion by matrix multiplications without the need of taking derivatives analytically. This method allows to investigate the finite motion of open- and closed-loop linkages without the need to solve the closure equations while maintaining algebraic insight between the geometrical parameters. This opens up a potential of algebraic investigation and synthesis of motion of closed-loop linkages.

4.5 Conclusion

In this chapter, a recursive method was presented which gives the higher-order partial derivatives of open- and closed-loop mechanisms consisting of lower kinematic pairs. This method relies on a combination of a simplified representation of the higher-order twist derivatives, also presented here, and the matrix derivatives of Vetter. This enables the Taylor approximation of kinematic mappings over a given trajectory and workspace, as shown by three examples. The method showed to be applicable to open- and closed-loop mechanisms with multi-DOF and to overconstrained mechanisms, yielding an algebraic expression for the derivatives and the approximation of finite motion.

Chapter 5

Higher-order derivatives of rigid body dynamics with application to dynamic balance

The fluctuating reaction forces and moments induced by high-speed robots may lead to undesired base vibrations, noise and a loss of the end-effector accuracy. Dynamic balance aims to eliminate these shaking forces and moments by adding counter-rotating inertia wheels or duplicate, mirrored mechanisms, which may also lead to an unwanted increase of complexity and motor effort. Alternatively, dynamically balanced can be obtained for a small number of closed-loop mechanisms solely by a specific design of the masses, centers of mass and moments of inertia of the moving links whose solution is potentially a more simple and cost-effective. Yet, the extension of this set of mechanisms is hindered by the intricacy of the dynamic balance conditions, as these conditions typically contain closed-form kinematic models, needed to express them in minimal coordinates. This chapter presents a novel higher-order dynamic balance method that yields the all dynamically balanced designs of given nonsingular mechanism. This method relies on the higher-order partial derivatives of the rigid body dynamics, thus avoiding the need for finite kinematic models. The resulting necessary and sufficient dynamic balance conditions are linear in the inertial parameters such that general null space procedures, either numeric or symbolic, yield all dynamically balanced masses, centers of mass and moments of inertia. The method is illustrated by known examples, leading to a novel dynamically balanced, spatially moving 3-RSR linkage that is dynamically balanced for motion over three planes of symmetry.

This chapter aims to expands the dynamic balance solution of Chapter 3 over the whole workspace by finding and solving a sufficient number of higher-order partial derivatives of the dynamic balance conditions (Objective 1). The aim is to arrive at algorithm a that is applicable to any given planar or spatial, serial or parallel, single-DOF or multi-DOF linkage of which a closed-form kinematic model might not be readily available. Therefore the higher-order kinematic approach of the previous chapter is expended to the dynamics and the dynamic balance conditions.

5.1 Introduction

Fluctuating reaction forces and moments generated by fast moving robots cause unwanted base vibrations and accuracy loss at the end-effector [68]. These shaking forces and moments may be reduced or even eliminated by a specific design of the robot's structure and inertial parameters [5]. Such mechanisms, that emit neither shaking forces nor shaking moments, are termed dynamically balanced, or force-balanced when only the shaking forces are zero. This feature may be achieved by the addition of supplementary counter-mechanisms to a given mechanism, such as counter-rotating wheels [14, 47] or idler loops [6, 127, 19]. Alternatively, various synthesis methods combine and recombine elementary dynamically balanced modules such four-bars [86, 120] or panthograph-like structures [40, 107, 109] into larger DOF, force balanced or dynamically balanced mechanisms. These elementary modules and synthesis approached, on the other hand, were obtained by analysis (inspection) of the dynamic balance conditions, resulting in a range of mass distributions, i.e. masses, centers of mass, and moments of inertia that balance these mechanisms [86, 74, 75].

For the viability of dynamic balance it is essential to find simple and low-weight mechanisms that still fulfill the desired kinematic task. In this view, the addition of counter-mechanisms seem undesirable since it will increases the mass, complexity and the required motor torque. The synthesis approaches, on the other hand, have proven to be versatile for force balance, yet, incomplete for dynamic balance [96]. To expand the scope of the dynamic balance designs and to enable new synthesis methods the focus of this chapter lies in the improvement and automation of the analysis approach.

The necessary and sufficient dynamic balance conditions are a constant linear and angular momentum. This sets their derivatives, the shaking forces and moments, to zero [116]. In practice, when the system is initially at rest, a zero linear and angular momentum suffices. A combination of inertial parameters that satisfy these conditions is termed a dynamically balanced solution, whereas the set of all solutions is termed the design space of dynamically balanced inertial parameters, or design space for brevity reasons. It should be noted that serial mechanisms cannot be dynamically balanced without additional counter-mechanisms as they would require zero or negative MOIs [47]. For parallel mechanisms is not trivial to obtain the complete design space as the dynamic balance conditions are to be expressed in minimal coordinates [43]. This involves the incorporation of kinematic loop-closure models, which may be intricate, even for relatively simple parallel linkages [86], or unavailable in closed-form for more complex mechanisms [49].

This complexity of the balance conditions is partly overcome by the Linear Independent Vector Method [15] and derived methods [57, 23, 60] for force balance, and the Inertia Flow Method [125], which dynamically balance planar mechanisms with counter-mechanisms. These methods eliminate only a subset of dependent coordinates, leading to simpler balancing conditions while

This chapter is submitted to *Machines and Mechanism Theory* under the title: 'Higher-order derivatives of rigid body dynamics with application to dynamic balance' by J. J. de Jong, A. Müller, and J. L. Herder

still yielding the complete design space in general. However, in special kinematic cases, such as parallelograms, these incomplete kinematic models lead to spurious force or moment balance conditions and therefore to an incomplete description of the design space [43]. Moreover, Ricard and Gosselin [86] showed that two special kinematic cases of the planar $4R$ four-bar linkage, the kite-type and antiparallogram-type, may be fully dynamically balanced by a specific mass distribution, i.e. without the need for counter-mechanisms. This gives rise to some of the aforementioned synthesis methods [86, 120].

To prove that the two special cases of the four-bar linkage [86] are indeed the only dynamically balanced solutions, Moore et al. factorized the balance conditions and loop-closure equations by toric geometry and Laurent polynomials [44]. Subsequently, through a similar algebraic approach, they showed that the spherical four-bar linkage cannot be dynamically balanced without additional structures [76]. This shows that dynamic balance by mass distribution require very specific kinematic conditions. Currently, these algebraic methods still requires tailored inspection per mechanism and are yet to be extended to multi-DOF mechanisms. An alternative method to deal with the kinematic complexity of the loop-closure equations was adopted in [33]. There, screw theory was applied to find instantaneous dynamic balance, yielding a single pose in which robot accelerations will not induce shaking forces and moments. Since outside this pose the balance quality is not guaranteed, this method yields and solves only necessary, but not sufficient, conditions for dynamic balance.

To summarize; in literature several systematic analysis methods were presented that solve the dynamic balance conditions for given linkages. Yet, no method yields the complete dynamically balanced design space of arbitrary linkages without a tailored manipulation of loop-closure equations. Such a method is desired to advance our understanding of dynamic balance and to find new, simple and lightweight solutions.

In this chapter, this longstanding problem is tackled by extending the instantaneous approach of [33] over the complete workspace by including and solving a sufficiently number of higher-order derivatives of the dynamic balance conditions. The loop-closure conditions are automatically satisfied since this operation is performed in the reference pose, i.e. the pose in which the mechanisms dimensions are defined, therefore no closed-form kinematic models are needed. This method leads to the necessary and (we conjecture) sufficient dynamic balance conditions, and an automatic and complete characterization of all dynamically balanced designs of any given nonsingular mechanism consisting of lower kinematic pairs.

To this end, a screw theory based (Section 5.2) recursive algorithm is presented that, for the first time, yields all higher-order derivatives of the linear and angular momentum equations (the dynamic balancing conditions) of serial and parallel kinematics (Section 5.3). This algorithm strongly leans on the higher-order kinematic models as derived in [28]. The resulting higher-order momentum equations are recast into the parameter-linear form [58, 24] to provide dynamic balance conditions that are linear in the inertial parameters and solvable by null space algorithms (Section 5.4). General null space algorithms, i.e. singular value decomposition or Gaussian elimination, yield a complete descrip-

tion of all dynamically balanced mass distributions. The resulting description however, may be strongly mixed in the inertial parameters, causing a loss of interpretation and design intuition. Therefore, an alternative, meaningful description of the design space of serial and parallel linkages is presented. This basis is derived from the concept of inertia transfer and the multipole representation of the inertial parameters, as used in the field parameter identification [88] (Section 5.5). This interpretation, here termed the multipole-rod representation, is shown to aid the feasibility study of dynamic balanced mechanisms. It is furthermore shown that for serial mechanisms only derivatives up to the second order are needed for dynamic balance. For parallel linkages such an upper-bound is found to be case dependent. Case studies of a 6-DOF serial robot, a $4R$ planar four-bar linkage, and a 3-RSR mechanism illustrate the higher-order dynamic balance method (Section 5.6). This results in a novel 3-RSR mechanism design that is dynamically balanced for the 2-DOF that lie on three mirror symmetric planes.

5.2 Synopsis, concepts and notation

In this section the groundwork is laid for the higher-order derivatives of rigid body dynamics in a screw theory framework. It starts with a synopsis of the method to guide the reader through the following sections. Thereafter the kinematics and higher-order derivatives of kinematics in screw theory is introduced, followed by a recapitulation of the rigid body dynamics including the multipole-rod representation of the mass matrix.

Synopsis of the higher-order dynamic balance method

The general dynamic balance conditions (as we will show in Eq. 5.50) may be written in the form of

$$\bar{\boldsymbol{h}}(\boldsymbol{u}, \boldsymbol{d}, \bar{\boldsymbol{z}}) \equiv \boldsymbol{0} \tag{5.1}$$

in which $\boldsymbol{u}$ are the independent coordinates, $\boldsymbol{d}$ the dependent coordinates and $\bar{\boldsymbol{z}}$ the collection of all inertial parameters of the mechanism, i.e. masses, centers of mass, and moments of inertia. To design a dynamically balanced mechanism we which to find $\bar{\boldsymbol{z}}$, such that the balancing condition holds for all independent $\boldsymbol{u}$ and corresponding dependent coordinates $\boldsymbol{d}$.

The conventional approach would be to write the dynamic balance conditions in minimal coordinates, i.e. write Eq. 5.1 in terms of $\boldsymbol{u}$ and $\bar{\boldsymbol{z}}$ only, by invoking the loop-closure equation

$$\mathrm{lc}(\boldsymbol{u}, \boldsymbol{d}) \equiv \boldsymbol{0} \qquad \Rightarrow \qquad \boldsymbol{d} = \mathrm{km}(\boldsymbol{u}) \tag{5.2}$$

This however is shown to be a tedious approach as there is in general no solution to the loop-closure equation, i.e. km is not always known. Furthermore, if the solution is found nevertheless, it is typically a set of complex equations which are hard to use in the balancing procedure.

In this chapter we take a different approach. Here we place the mechanism in the reference configuration ($\boldsymbol{u}_0$ and $\boldsymbol{d}_0$) in which the mechanism is defined. In this pose the loop-closure equation (lc) are satisfied by definition of the mechanism. Now we use the fact that the Taylor approximation of Eq. 5.1 around this pose should be also be zero for dynamic balance. With a slight abuse of notation this reads

$$\begin{aligned}\bar{\boldsymbol{h}}(\boldsymbol{u},\boldsymbol{d},\bar{\boldsymbol{z}}) \approx \bar{\boldsymbol{h}}(\boldsymbol{u}_0,\boldsymbol{d}_0,\bar{\boldsymbol{z}}) + \mathrm{D}_{\boldsymbol{u}}\big(\bar{\boldsymbol{h}}(\boldsymbol{u}_0,\boldsymbol{d}_0,\bar{\boldsymbol{z}})\big)\,(\boldsymbol{u}-\boldsymbol{u}_0) \\ + \frac{1}{2!}\mathrm{D}^2_{\boldsymbol{u}}\big(\bar{\boldsymbol{h}}(\boldsymbol{u}_0,\boldsymbol{d}_0,\bar{\boldsymbol{z}})\big)\,(\boldsymbol{u}-\boldsymbol{u}_0)^2 + \cdots \equiv \boldsymbol{0}\end{aligned} \tag{5.3}$$

This should hold for all motion, i.e. for all $\boldsymbol{u}$, necessitating all Taylor coefficients (the higher partial derivatives $\mathrm{D}^k_{\boldsymbol{u}}\big(\bar{\boldsymbol{h}}\big)$) to be zero. Therefore we obtain the following necessary conditions

$$\mathrm{D}^k_{\boldsymbol{u}}\big(\bar{\boldsymbol{h}}(\boldsymbol{u}_0,\boldsymbol{d}_0,\bar{\boldsymbol{z}})\big) \equiv \boldsymbol{0} \tag{5.4}$$

which are the derivatives with respect to the independent coordinates $\boldsymbol{u}$ that take the dependency of $\boldsymbol{d}$ into account. This dependency is readily available from recursive application of the implicit function theorem, as done through the procedure described in [33]. Now we have arrived at a set of conditions that are pose independent and do not require an explicit solution to the loop-closure equations (Section 5.3). We furthermore conjecture that with enough (but finite number) of these partial derivatives, these necessary conditions become also a sufficient set of conditions.
Moreover, it will be shown that the inertial parameter vector $\bar{\boldsymbol{z}}$ is linear in these Taylor coefficients (Eq. 5.4), such that they, with the help of a regression matrix $\boldsymbol{X}_k$, can be written in the form of

$$\boldsymbol{X}_k(\boldsymbol{u}_0,\boldsymbol{d}_0)\bar{\boldsymbol{z}} \equiv \boldsymbol{0} \tag{5.5}$$

and solved using methods from linear algebra (Section 5.4)

$$\bar{\boldsymbol{z}} \in \ker\left(\boldsymbol{X}_k\right) \tag{5.6}$$

Leading to a complete description of all dynamically balanced mass distributions. Subsequently, we systematically partition and interpret the resulting design space in order to retain some insight in design dependency and feasibility of the solution (Section 5.5). At last we illustrate the method on known and new examples (Section 5.6).

Serial and parallel kinematics in screw theory

Screw theory is used throughout this work as it gives a concise representation of the higher-order derivatives of kinematics and dynamics. This screw theory framework draws on the fact that the motion of a body may be interpreted as a combination of an angular velocity $\boldsymbol{\omega}$ around an axis in space, passing through point $\boldsymbol{r}_{\mathrm{t}}$, and a linear velocity along that axis, termed the pitch λ_{t}

$$\boldsymbol{t} = \begin{bmatrix}\boldsymbol{\omega}\\ \boldsymbol{v}\end{bmatrix} = \begin{bmatrix}\boldsymbol{\omega}\\ \boldsymbol{r}_{\mathrm{t}} \times \boldsymbol{\omega}\end{bmatrix} + \lambda_{\mathrm{t}}\begin{bmatrix}\boldsymbol{0}\\ \boldsymbol{\omega}\end{bmatrix} \tag{5.7}$$

This combination of linear $\boldsymbol{v}$ and angular velocity $\boldsymbol{\omega}$, is termed twist $\boldsymbol{t}$. The linear velocity $\boldsymbol{v}$ is the velocity of the particles of the body that instantaneously pass through the origin of the reference frame. Two special cases exist: 1) a pure rotation, i.e. the angular velocity is orthogonal to the linear velocity, resulting in a zero pitch ($\lambda_\mathrm{t} = 0$), and 2) a pure translation, when the angular velocity is zero and the pitch is infinite ($\lambda_\mathrm{t} = \infty$).

The twist of a link in a serial mechanism is linearly dependent on the joint velocities $\dot{\boldsymbol{q}}$ of the joints lower in the chain. The twist basis vector $\boldsymbol{s}_j$ associated to each joint j is termed unit twists or instantaneous screw axis (ISA). The joints in a single chain are numbered from 1 to n_d, from the base to the end-effector. Together these ISAs form the serial chain Jacobian $\boldsymbol{J}_i$ of body i

$$\boldsymbol{t}_i = \boldsymbol{J}_i \dot{\boldsymbol{q}} = \begin{bmatrix} \boldsymbol{s}_1 & \cdots & \boldsymbol{s}_i & \boldsymbol{0} \end{bmatrix} \dot{\boldsymbol{q}}, \qquad \boldsymbol{s} = \begin{bmatrix} \boldsymbol{n} \\ \boldsymbol{r}_\mathrm{s} \times \boldsymbol{n} \end{bmatrix} + \lambda_\mathrm{s} \begin{bmatrix} \boldsymbol{0} \\ \boldsymbol{n} \end{bmatrix} \tag{5.8}$$

These ISA are pure geometric quantities that solely dependent on the joint location $\boldsymbol{r}_\mathrm{s}$, orientation of the joint, encoded by unit vector $\boldsymbol{n}$, and the pitch of the joint λ_s. In this case we treat the three single DOF lower pairs: revolute (R) i.e. $\lambda_\mathrm{s} = 0$, helical (H), or prismatic (P) i.e. $\lambda_\mathrm{s} = \infty$. For the prismatic joint $\boldsymbol{n} = 0$ whereas the joint direction is given by the unit vector $\lambda_s \boldsymbol{n} = \boldsymbol{n}_\infty$. The higher DOF pairs are treated as instantaneously identical to s set of serially connected single DOF pairs.

For parallel mechanisms, the body twists may by found by regarding each loop as a connection of multiple serial chains. A single loop for example is opened by cutting an arbitrary body, resulting into two serial chains of which the last 'virtual' bodies have the same twists. These loop-closure conditions constrain the twists the bodies, as encoded by matrix $\boldsymbol{K}$, such that the set of joint coordinates $\boldsymbol{q}$ is no longer independent. By selecting a suitable (nonsingular) set of n_d input coordinates $\boldsymbol{u}$, this system can be solved and all dependent joint coordinates determined

$$\mathrm{D}_{\boldsymbol{q}}(\mathrm{lc})\, \dot{\boldsymbol{q}} = \boldsymbol{K}\bar{\boldsymbol{J}}\dot{\boldsymbol{q}} \equiv 0, \qquad \dot{\boldsymbol{q}} \in \ker(\boldsymbol{K}\bar{\boldsymbol{J}}), \qquad \dot{\boldsymbol{q}} = \boldsymbol{C}\dot{\boldsymbol{u}} \tag{5.9}$$

The mechanisms Jacobian $\bar{\boldsymbol{J}}^\top = [\boldsymbol{J}_1^\top \cdots \boldsymbol{J}_{n_\mathrm{b}}^\top]$ is the collection of all n_b body Jacobians. The $n_\mathrm{b} \times n_\mathrm{d}$ $\boldsymbol{C}$-matrix denotes the first-order solution to the loop-closure equations.

To express finite motion, a reference frame ψ_i is associated to each body i. A transformation matrix $\boldsymbol{H}_i$, consisting of a rotation matrix $\boldsymbol{R}_i$ and a translation vector $\boldsymbol{o}_i$, express a point $\boldsymbol{a}$ from a body-fixed frame into the inertial frame of reference $\boldsymbol{a}^0 = \boldsymbol{H}_i \boldsymbol{a}^i$. In this convention the $\boldsymbol{a}^i$ vector consist of four values; 3 Cartesian coordinates and a 1. The superscripts denote the frames of expression of the point. These transformation matrices relate again to the ISAs in chain by product of matrix exponentials, leading to the general forward kinematics of serial chains [20]

$$\boldsymbol{H}_i = \prod_{j=1}^{i} \exp(q_j \left[\boldsymbol{s}_j \times\right]), \qquad \boldsymbol{H} = \begin{bmatrix} \boldsymbol{R} & \boldsymbol{o} \\ \boldsymbol{0} & 1 \end{bmatrix}, \tag{5.10}$$

in which $\exp(q_j \left[\boldsymbol{s}_j \times\right])$ denotes the matrix exponential of the 4×4 semi-skew symmetric matrix of the ISA in the initial configuration ($\boldsymbol{q} = \boldsymbol{0}$),

$$\left[\boldsymbol{s}\times\right] = \begin{bmatrix} \left[\boldsymbol{n}\times\right] & \boldsymbol{r}_\mathrm{s} \times \boldsymbol{n} + \lambda_\mathrm{s}\boldsymbol{n} \\ \boldsymbol{0} & 0 \end{bmatrix} \tag{5.11}$$

and $\left[\boldsymbol{n}\times\right]$ the 3×3 skew symmetric matrix of $\boldsymbol{n}$.

A local ISA $\boldsymbol{s}_i^i$ is expressed in the inertial frame of reference by the adjoint transformation matrix $\mathrm{Ad}\big(\boldsymbol{H}\big)$

$$\boldsymbol{s}_i^0 = \mathrm{Ad}\big(\boldsymbol{H}_i\big)\boldsymbol{s}_i^i, \qquad \mathrm{Ad}\big(\boldsymbol{H}\big) = \begin{bmatrix} \boldsymbol{R} & \boldsymbol{0} \\ \left[\boldsymbol{o}\times\right]\boldsymbol{R} & \boldsymbol{R} \end{bmatrix} \tag{5.12}$$

The time derivative of the transformation matrix relates to the body twist through the matrix form of the adjoint twist transformation, here termed adjoint twist matrix $\mathrm{ad}(\boldsymbol{t}_i)$

$$\frac{d}{dt}(\mathrm{Ad}\big(\boldsymbol{H}_i\big)) = \mathrm{ad}(\boldsymbol{t}_i)\mathrm{Ad}\big(\boldsymbol{H}_i\big), \qquad \mathrm{ad}(\boldsymbol{t}) = \begin{bmatrix} \left[\boldsymbol{\omega}\times\right] & \boldsymbol{0} \\ \left[\boldsymbol{v}\times\right] & \left[\boldsymbol{\omega}\times\right] \end{bmatrix} \tag{5.13}$$

5

Higher-order derivatives of kinematics

For parallel mechanisms a closed-form solution to the kinematic loop-closure equations does not exist in general. Yet, a higher-order approximation of the motion is available by treating the closed loop as a connection of several serial chains. For such a connection the higher-order derivatives of the loop-closure equations are found and solved yielding a Taylor approximation of finite motion [28]. In that approach, the higher-order partial derivatives of the body twists are found from the adjoint twist matrices corresponding to the ISA that are lower in the serial chain equivalent [79]. Since each ISA is constant when expressed in a local body-fixed frame, all these derivatives follow from a repetitive application of Eq. 5.13 to Eq. 5.12, such that

$$\mathrm{D}_{\boldsymbol{q}}^{\boldsymbol{\alpha}}(\boldsymbol{s}_i) = \prod_{j=1}^{i-1} \mathrm{ad}\big(\boldsymbol{s}_j\big)^{\alpha_j} \boldsymbol{s}_i \tag{5.14}$$

In here the higher-order partial derivatives with respect to the elements of $\boldsymbol{q}$ are denoted by $\mathrm{D}_{\boldsymbol{q}}^{\boldsymbol{\alpha}}(\boldsymbol{A}) = \partial^k / \partial q_1^{\alpha_1} \cdot \ldots \cdot \partial q_n^{\alpha_n}(\boldsymbol{A})$. Vector $\boldsymbol{\alpha} = (\alpha_1, \ldots, \alpha_n)$ comprises the order of the derivatives corresponding to $\boldsymbol{q}$, running from the base to the end-effector. Hence we assume an ordered sequence, i.e. α_i corresponds to the joint q_i. The $k = \alpha_1 + \ldots + \alpha_n = |\boldsymbol{\alpha}|$ is the total order. The joints higher in the chain have no contribution to the motion of the lower joints, such that this derivative (Eq. 5.14) is set to zero when i.e. $\alpha_j \neq 0$ for $j \geq i$. By this, all the higher-order partial derivatives of the body Jacobians $\mathrm{D}_{\boldsymbol{q}}^{\boldsymbol{\alpha}}(\boldsymbol{J}_i)$ are available.

This procedure is used for the solution of the higher-order closed-loop constraints [28] by recasting it into the matrix derivative framework of Vetter for

bookkeeping [112]. In this notation the collection of all first-order partial derivatives of matrix $\boldsymbol{A} = [\boldsymbol{a}_1 \quad \cdots \quad \boldsymbol{a}_m]$ are sorted according to[1]

$$\mathrm{D}_{\boldsymbol{q}}(\boldsymbol{A}) = \left[\mathrm{D}_{\boldsymbol{q}}(\boldsymbol{a}_1) \quad \cdots \quad \mathrm{D}_{\boldsymbol{q}}(\boldsymbol{a}_m)\right], \tag{5.15}$$

$$\mathrm{D}_{\boldsymbol{q}}(\boldsymbol{a}_i) = \left[\partial/\partial q_1(\boldsymbol{a}_i) \quad \cdots \quad \partial/\partial q_n(\boldsymbol{a}_i)\right] \tag{5.16}$$

With this, the derivatives of the loop-closure solution $\mathrm{D}_{\boldsymbol{u}}(\boldsymbol{C})$ are found through application of the chain rule and product rule (Appendix A) to Eq. 5.9. The collection of second-order loop-closure constraints read

$$\mathrm{D}_{\boldsymbol{q}}\left(\boldsymbol{K}\bar{\boldsymbol{J}}\right)(\boldsymbol{C}\otimes\boldsymbol{C}) + \boldsymbol{K}\bar{\boldsymbol{J}}\mathrm{D}_{\boldsymbol{u}}(\boldsymbol{C}) \equiv 0 \tag{5.17}$$

In here $\boldsymbol{A}\otimes\boldsymbol{B}$ denotes the Kronecker product of two matrices (Appendix A). From this equation $\mathrm{D}_{\boldsymbol{u}}(\boldsymbol{C})$ is solved. A recursive application leads to the k-th order constraints

$$\mathrm{D}^k_{\boldsymbol{u}}\left(\boldsymbol{K}\bar{\boldsymbol{J}}\boldsymbol{C}\right) = \sum_{i=1}^{n_b}\left[\mathrm{D}^k_{\boldsymbol{q}}\left(\boldsymbol{K}\bar{\boldsymbol{J}}\right) \quad \cdots \quad \boldsymbol{K}\bar{\boldsymbol{J}}\right]\bar{\boldsymbol{C}}_k \equiv 0, \tag{5.18}$$

$$\left(\bar{\boldsymbol{C}}_k\right)^\top = \left[\left(\boldsymbol{C}^{\otimes k}\right)^\top \quad \cdots \quad \mathrm{D}^k_{\boldsymbol{u}}(\boldsymbol{C})^\top\right] \tag{5.19}$$

from which $\mathrm{D}^k_{\boldsymbol{u}}(\boldsymbol{C})$ may be solved through the algorithm presented in [28]. The Kronecker power is denoted by a $\otimes k$ superscript. The exact composition of the $\bar{\boldsymbol{C}}_k$ collection matrix is found through repetitive application of the chain and product rules, but is omitted due to space limitation.

5

Rigid body dynamics

The rigid body dynamics of spatially moving objects and linkages is concisely written with the use of screw theory [11, 90]. This section briefly introduces of rigid body dynamics in screw theory, followed by the presentation of the multipole-rod representation, used in the interpretation of the dynamically balanced solution later on.

Momentum wrench and mass matrix

The momentum of a body is the product of the body's spatial mass matrix $\boldsymbol{M}$ and the twist $\boldsymbol{t}$ associated to it. The momentum is a co-screw or a wrench-like entity and therefore termed momentum wrench hereafter

$$\boldsymbol{h} = \begin{bmatrix}\boldsymbol{\xi}\\ \boldsymbol{p}\end{bmatrix} = \boldsymbol{M}\boldsymbol{t} \tag{5.20}$$

The mass matrix of a body is formed by the integral over all mass-weighted particles $\boldsymbol{r}$ of the body

$$\boldsymbol{M} = \int_V \begin{bmatrix}-\left[\boldsymbol{r}\times\right]^2 & \left[\boldsymbol{r}\times\right]\\ -\left[\boldsymbol{r}\times\right] & \boldsymbol{I}_3\end{bmatrix}\mathrm{d}m = \begin{bmatrix}\boldsymbol{E} & \left[m\boldsymbol{c}\times\right]\\ -\left[m\boldsymbol{c}\times\right] & m\boldsymbol{I}_3\end{bmatrix} \tag{5.21}$$

[1] Please note the two distinct uses of the differentiation operator. When the superscript is a vector $\mathrm{D}^{\boldsymbol{\alpha}}_{\boldsymbol{q}}$ it denotes a sequence of partial derivatives, but when the superscript is a scalar $\mathrm{D}^k_{\boldsymbol{q}}$ it is a collection of partial derivatives of order k (Chapter A).

This gives rise to the classical description with a mass m, a center of mass $\boldsymbol{c}$ and inertia matrix $\boldsymbol{E}$ with respect to the inertial frame of reference. The inertia matrix $\boldsymbol{E}$ contains 3 moments and 3 products of inertia, respectively on its diagonal $\boldsymbol{e}_{\mathrm{d}}^{\top} = [e_1 \quad e_2 \quad e_3]$ and its off diagonal $\boldsymbol{e}_{\mathrm{o}}^{\top} = [e_4 \quad e_5 \quad e_6]$. Due to the frame invariance of kinetic energy $K = 1/2\boldsymbol{t}^{\top}\boldsymbol{M}\boldsymbol{t}$, the mass matrix transforms with an adjoint transformation matrix on the right and its transposed on the left. Any mass matrix can be diagonalized by expressing it in a body-fixed reference frame that is located at the center of mass and aligned with the principal axis of the body. The corresponding transformation matrix is $\mathrm{Ad}\big(\boldsymbol{H}_{\mathrm{p}}\big)$. This gives rise to three principal MOIs g_1, g_2, and g_3

$$\boldsymbol{M} = \mathrm{Ad}\big(\boldsymbol{H}_{\mathrm{p}}\big)^{-\top}\mathrm{diag}(g_1, g_2, g_3, m, m, m)\mathrm{Ad}\big(\boldsymbol{H}_{\mathrm{p}}\big)^{-1} \tag{5.22}$$

In this body-fixed frame, the mass matrix is constant, i.e. $\dot{m}$ and $\dot{g}_i = 0$, due to the rigid body assumption. Since the mass matrix is formed by a collection of positive mass particles, the mass matrix itself is symmetric positive definite, leading to 7 inequality conditions on the mass and the principal MOIs

$$m > 0, \qquad g_i > 0, \qquad g_i + g_j > g_k \tag{5.23}$$

Momentum wrench basis

Similar to the twist basis, we define a mechanism's momentum basis that spans all possible momentum wrenches at a given pose. The basis vectors, termed the instantaneous momentum wrenches (IMW) and denoted with $\hat{\boldsymbol{h}}_i$, are the momentum wrenches generated by unit actuation of each joint. The total momentum wrench of a serial mechanism is therefore given by

$$\boldsymbol{h} = \sum \boldsymbol{M}_i\boldsymbol{t}_i = \bar{\boldsymbol{M}}\bar{\boldsymbol{J}}\dot{\boldsymbol{q}} = \begin{bmatrix}\hat{\boldsymbol{h}}_1 & \cdots & \hat{\boldsymbol{h}}_n\end{bmatrix}\dot{\boldsymbol{q}}, \qquad \hat{\boldsymbol{h}}_i = \sum_{j=i}^{n_{\mathrm{b}}} \boldsymbol{M}_j\boldsymbol{s}_i \equiv 0 \tag{5.24}$$

In here $\bar{\boldsymbol{M}} = [\boldsymbol{M}_1 \quad \cdots \quad \boldsymbol{M}_n]$ denotes the collection of all mass matrices in the chain. For dynamic balance all the IMWs should be zero for arbitrary motion. For parallel linkages the momentum wrench basis is computed by applying the first order loop-closure solution $\boldsymbol{C}$ to the serial chain equivalent

$$\boldsymbol{h} = \bar{\boldsymbol{M}}\bar{\boldsymbol{J}}\boldsymbol{C}\dot{\boldsymbol{u}} \equiv 0 \tag{5.25}$$

Multipole-rod interpretation of the mass matrix

In the current dynamic balancing procedure we will use the fact that the balancing conditions are linear in the elements of the mass matrix such that they can be solved through a set of linear operations. For the interpretation of the resulting design space the conventional mass matrix parameterisation conssisting of masses m, COMs $\boldsymbol{c}$ and principal MOIs $\boldsymbol{g}$ is not suitable since it is not linear in the elements of the mass matrix. Therefore we will use a slight adaptation of the multipole concept of Ros et al. [88], termed the multipole-rod representation (Fig. 5.1). This interpretation relies on the fact that a mass matrix can be decomposed into three primitive elements; 1) a single point mass the at $\boldsymbol{r}$,

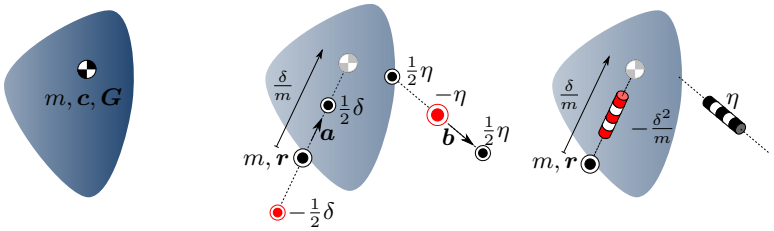

(a) Conventional (b) Multipole (c) Multipole-rod

Figure 5.1: Three representations of the inertial parameters of a body. (a) The conventional representation with a mass m, a center of mass $\boldsymbol{c}$ and an inertia matrix $\boldsymbol{G}$ around $\boldsymbol{c}$. (b) The multipole representation [88] with parameters that are linear in the mass matrix; a monopole m at $\boldsymbol{r}$, a dipole δ in the direction $\boldsymbol{a}$, and a quadripole η in the direction of $\boldsymbol{b}$. One monopole, three dipoles and six quadripoles are sufficient to describe arbitrary bodies. (c) The multipole-rod representation reduces the number of graphical elements by interpreting the quadripole as an infinitely long, slender rod, termed 'pure-inertia rod' and depicting it a striped bar. The monopole is termed 'point mass', whereas the dipole is treated as a 'displacement' of the point mass with negative pure-inertia rod in the same direction.

5

denoted with a subscript m, 2) a *displacement* of the point mass in the direction of a unit vector $\boldsymbol{a}$ combined with a pure-inertia rod of opposite magnitude, denoted with a subscript δ, and 3) a pure-inertia rod in the direction of a unit vector $\boldsymbol{b}$, denoted with a subscript η. These pure-inertia rods are interpreted as infinitely long slender rods in the direction of the unit vector. Since these rods are infinitely slender, their mass is zero whereas only the rotational velocity component in a perpendicular direction generates angular momentum. A rotation around their longitudinal axis generates no angular momentum. The sole difference with the method of [88] is the graphical representation to reduces the larger number of point masses (poles), which might otherwise congest the figures.

Now, any mass matrix can be represented by choice of 10 of these primitive elements, one point mass, three displacements, and six pure-inertia rods, as long as the spanning vectors $\boldsymbol{a}_i$ and $\boldsymbol{b}_i$ are unique

$$\boldsymbol{M} = m\boldsymbol{M}_m(\boldsymbol{r}) + \sum_{i=1\cdots3} \delta_i \boldsymbol{M}_\delta(\boldsymbol{a}_i, \boldsymbol{r}) + \sum_{i=1\cdots6} \eta_i \boldsymbol{M}_\eta(\boldsymbol{b}_i) \tag{5.26}$$

The zeroth, first, and second moment of mass of these elements are given by

$$\begin{aligned} m_\mathrm{m} &= 1, \quad & (m\boldsymbol{c})_\mathrm{m} &= \boldsymbol{r}, \quad & \boldsymbol{E}_\mathrm{m} &= -\big[\boldsymbol{r}\times\big]^2, \\ m_\delta &= 0, \quad & (m\boldsymbol{c})_\delta &= \boldsymbol{a}, \quad & \boldsymbol{E}_\delta &= 1/2\big[\boldsymbol{r}-\boldsymbol{a}\times\big]^2 - 1/2\big[\boldsymbol{r}+\boldsymbol{a}\times\big]^2, \\ m_\eta &= 0, \quad & (m\boldsymbol{c})_\eta &= \boldsymbol{0}, \quad & \boldsymbol{E}_\eta &= -\big[\boldsymbol{b}\times\big]^2 \end{aligned} \tag{5.27}$$

For the planar case, this representation requires one point mass, two displace-

ments and one pure-inertia rod, of which the elements reduce to

$$\begin{aligned} m_{\mathrm{m}} &= 1, & (m\boldsymbol{c})_{\mathrm{m}} &= \boldsymbol{r}, & e_{\mathrm{m}} &= \|\boldsymbol{r}\|^2, \\ m_\delta &= 0, & (m\boldsymbol{c})_\delta &= \boldsymbol{a}, & e_\delta &= 2\boldsymbol{a}^\top \boldsymbol{r}, \\ m_\eta &= 0, & (m\boldsymbol{c})_\eta &= \boldsymbol{0}, & e_\eta &= 1 \end{aligned} \tag{5.28}$$

For feasibility of each body, they must consist of at least one positive point mass, and three non-coplanar positive pure-inertia rods (Eq. 5.23), since two pure-inertia rods represent an infinitely flat object. A negative pure-inertia rod requires at least 3 arbitrarily oriented positive pure-inertia rods (or two positive coplanar pure-inertia rods) of sufficient magnitude to represent a feasible body. A closed-form feasibility description of an arbitrary collection of these elements can be found through eigendecomposition of the resulting mass matrix, but lies outside the scope of this chapter.

5.3 Higher-order derivatives of the momentum equations and the dynamic balance conditions

The previously presented higher-order analysis of the kinematics is extended to rigid body dynamics in this section. We aim is to find and solve the necessary and sufficient dynamic balance conditions of arbitrary mechanisms without invoking the finite, closed-form solution to the loop-closure equations. For dynamic balancing purposes this study is confined to the change of rigid body momentum. Other effects such as gravity, elasticity, or external forces are not taken into account. The dynamic balance conditions are obtained from the partial derivatives of the mass matrices and momentum equations of serial mechanisms, which are extended thereafter to parallel mechanisms by including the higher-order derivatives of the loop-closure solution. It should be noted that although serial mechanisms cannot be dynamically balanced without additional counter-mechanisms, their description are important for dynamic balance since parallel mechanisms can be regarded as connected serial chains.

Derivatives of the mass matrix in a serial chain

The mass matrix of a body i in a serial chain depends on the pose of the joints that are lower in the kinematic chain according to Eq. 5.10 and Eq. 5.22. Therefore, the partial derivative with respect to a joint j, lower in a serial chain ($j \leq i$), is found by applying Eq. 5.13 to Eq. 5.22

$$\frac{\partial}{\partial q_j}(\boldsymbol{M}_i) = -\mathrm{ad}\big(\boldsymbol{s}_j\big)^\top \boldsymbol{M}_i - \boldsymbol{M}_i \mathrm{ad}\big(\boldsymbol{s}_j\big) \tag{5.29}$$

Here we have used the fact that the mass matrix is constant in the body-fixed frame. For all partial derivatives with respect to joints higher in the chain ($j > i$) this derivative is zero.

A second partial derivative is either with respect to a joint higher ($j \leq l \leq i$) or joint lower ($l \leq j \leq i$) in the chain. In the first case ($j \leq l \leq i$) the partial

derivative becomes

$$\frac{\partial}{\partial q_l}\frac{\partial}{\partial q_j}\left(\boldsymbol{M}_i\right) = \mathrm{ad}\big(\boldsymbol{s}_l\big)^\top \Big(\mathrm{ad}\big(\boldsymbol{s}_j\big)^\top \boldsymbol{M}_i + \boldsymbol{M}_i \mathrm{ad}\big(\boldsymbol{s}_j\big)\Big) + \Big(\mathrm{ad}\big(\boldsymbol{s}_j\big)^\top \boldsymbol{M}_i + \boldsymbol{M}_i \mathrm{ad}\big(\boldsymbol{s}_j\big)\Big)\,\mathrm{ad}\big(\boldsymbol{s}_l\big) \tag{5.30}$$

Here the Jacobi identity $\partial/\partial q_l(\mathrm{ad}\big(\boldsymbol{s}_j\big)) = \mathrm{ad}(\mathrm{ad}\big(\boldsymbol{s}_l\big)\boldsymbol{s}_j) = \mathrm{ad}\big(\boldsymbol{s}_l\big)\mathrm{ad}\big(\boldsymbol{s}_j\big) - \mathrm{ad}\big(\boldsymbol{s}_j\big)\mathrm{ad}\big(\boldsymbol{s}_l\big)$ is used. For the second case ($l \leq j \leq i$) only the derivative of the mass matrix has to be taken into account as a higher joint does not influence a lower ISA ($\partial/\partial q_l(\mathrm{ad}\big(\boldsymbol{s}_j\big)) = 0$). This results in a similar equation as Eq. 5.30, with the sole difference that the indices j and l are swapped. This also follows from the symmetry of partial derivatives. This nested structure, i.e. the pre- and postmultiplication of adjoint twist matrices, is preserved for the higher orders, leading to a recursive formula for all partial derivatives of the mass matrix

$$\frac{\partial}{\partial q_j}(\mathrm{D}_{\boldsymbol{q}}^{\boldsymbol{\alpha}}(\boldsymbol{M}_i)) = -\mathrm{ad}\big(\boldsymbol{s}_j\big)^\top \mathrm{D}_{\boldsymbol{q}}^{\boldsymbol{\alpha}}(\boldsymbol{M}_i) - \mathrm{D}_{\boldsymbol{q}}^{\boldsymbol{\alpha}}(\boldsymbol{M}_i)\,\mathrm{ad}\big(\boldsymbol{s}_j\big) \tag{5.31}$$

in here j is the lowest joint to which a partial derivative is taken, i.e. $\alpha_l = 0$ for all $l < j$. In case $\alpha_l \neq 0$ for any $l > i$, this equation is set to zero. These derivatives may be summed to form the partial derivatives of the aggregated mass matrices (Eq. 5.24).

5

Derivatives of the momentum wrench in a serial chain

Now that the derivatives of the mass matrix up to arbitrary order are available, we consider the partial derivatives of the momentum wrench with the aim of obtaining all higher-order dynamic balance conditions. Consider the momentum wrench generated by the j-th body due to actuation of joint i, which is lower in the chain. Two types of non-zero partial derivatives appear. Either joint l — with respect to which the derivative is taken — is below the joint i, or between the joint i and the j-th body. In the first case ($l \leq i \leq j$), the partial derivative of both the mass matrix and the ISA have to be taken into account, partially canceling out

$$\frac{\partial}{\partial q_l}\left(\boldsymbol{M}_j \boldsymbol{s}_i\right) = \frac{\partial}{\partial q_l}\left(\boldsymbol{M}_j\right)\boldsymbol{s}_i + \boldsymbol{M}_j \frac{\partial}{\partial q_l}\left(\boldsymbol{s}_i\right) = -\mathrm{ad}\big(\boldsymbol{s}_l\big)^\top \boldsymbol{M}_j \boldsymbol{s}_i \tag{5.32}$$

In the second case ($i < l \leq j$), the partial derivative of the ISA vanishes $\partial/\partial q_l(\boldsymbol{s}_i) = 0$. Therefore, the partial derivative of the momentum wrench becomes

$$\frac{\partial}{\partial q_l}\left(\boldsymbol{M}_j \boldsymbol{s}_i\right) = \frac{\partial}{\partial q_l}\left(\boldsymbol{M}_j\right)\boldsymbol{s}_i = -(\mathrm{ad}\big(\boldsymbol{s}_l\big)^\top \boldsymbol{M}_j + \boldsymbol{M}_j \mathrm{ad}\big(\boldsymbol{s}_l\big))\boldsymbol{s}_i \tag{5.33}$$

The higher-order partial derivatives are found similarly by making a split between the partial derivatives related to joints lower than the momentum generating ISA, and the ones related to the joints between the ISA and the

body. Therefore. a second multi-index defined by $\beta_l = \alpha_l$ for all $i < l \leq j$ and $\beta_l = 0$ for all $l \leq i$ and $l > j$. The partial derivatives of the momentum wrench are found from Eq. 5.31 according to

$$\mathrm{D}_{\boldsymbol{q}}^{\boldsymbol{\alpha}}(\boldsymbol{M}_j \boldsymbol{s}_i) = \prod_{l=1}^{i} \left(-\mathrm{ad}\big(\boldsymbol{s}_l\big)^{\top}\right)^{\alpha_l} \mathrm{D}_{\boldsymbol{q}}^{\boldsymbol{\beta}}(\boldsymbol{M}_j)\, \boldsymbol{s}_i \tag{5.34}$$

Again this equation is set to zero if $\alpha_l \neq 0$ for any $l > j$. These partial derivatives may be summed to obtain the derivatives of the total momentum of the mechanism. Notice that in this equation the momentum derivatives are formulated as a sequence of matrix operations, which are linear in the mass matrix.

Derivatives of the dynamic balance conditions of a serial chain

The dynamic balance conditions dictate that the momentum wrench of a mechanism is zero for all motion. Therefore also all higher-order derivatives of the momentum wrench must be zero. We conjecture that with a large enough number of derivatives k_{max} these are not only the necessary but also the sufficient dynamic balance conditions for nonsingular mechanisms. In fact, here it will be shown that for serial mechanisms only derivatives up to the second order are needed ($k_{\max} \leq 2$). When these are satisfied, all the higher-order dynamic balance conditions satisfied, and the mechanism is dynamically balanced for finite motion.

For zeroth-order dynamic balance, 6 conditions (Eq. 5.24) are placed on each aggregated mass matrix

$$\hat{\boldsymbol{h}}_i = \sum_{j=i}^{n_{\mathrm{b}}} \boldsymbol{M}_j \boldsymbol{s}_i = \tilde{\boldsymbol{M}}_i \boldsymbol{s}_i \equiv 0, \qquad \tilde{\boldsymbol{M}}_i = \begin{bmatrix} \tilde{\boldsymbol{E}}_i & \big[\widetilde{m_i \boldsymbol{c}_i}\times\big] \\ -\big[\widetilde{m_i \boldsymbol{c}_i}\times\big] & \tilde{m}_i \boldsymbol{I}_3 \end{bmatrix} \tag{5.35}$$

The aggregated mass matrix $\tilde{\boldsymbol{M}}_i$ is sum of the mass matrices belonging to bodies higher in the chain than $\boldsymbol{s}_i$. Consider now the following momentum derivatives of $\hat{\boldsymbol{h}}_j$ and $\hat{\boldsymbol{h}}_l$, involving any triplet $\boldsymbol{s}_l$, $\boldsymbol{s}_j$, and $\boldsymbol{s}_i$ of non-infinite pitch ISA, which are arranged in ascending order ($l \leq j \leq i$)

$$\frac{\partial}{\partial q_i}\left(\hat{\boldsymbol{h}}_j\right) = \frac{\partial}{\partial q_i}\left(\tilde{\boldsymbol{M}}_i\right)\boldsymbol{s}_j \equiv 0, \qquad \frac{\partial}{\partial q_i}\left(\hat{\boldsymbol{h}}_l\right) = \frac{\partial}{\partial q_i}\left(\tilde{\boldsymbol{M}}_i\right)\boldsymbol{s}_l \equiv 0 \tag{5.36}$$

$$\frac{\partial}{\partial q_l}\frac{\partial}{\partial q_i}\left(\hat{\boldsymbol{h}}_j\right) = -\mathrm{ad}\big(\boldsymbol{s}_l\big)^{\top}\frac{\partial}{\partial q_i}\left(\hat{\boldsymbol{h}}_j\right) - \frac{\partial}{\partial q_i}\left(\tilde{\boldsymbol{M}}_i\right)\mathrm{ad}\big(\boldsymbol{s}_l\big)\boldsymbol{s}_j \equiv 0 \tag{5.37}$$

Notice that these dynamic balancing conditions place constraints on the same aggregated mass matrix $\tilde{\boldsymbol{M}}_i$ since $\boldsymbol{q}_i$ is the highest joint of the partial derivatives and $\partial/\partial q_i(\boldsymbol{M}_j) = 0$ for $j \leq i$. As the first-order balancing conditions (Eq. 5.36) ensures that $\partial/\partial q_i(\hat{\boldsymbol{h}}_j) = 0$, the second-order dynamic balance conditions (Eq. 5.37) reduce to

$$\frac{\partial}{\partial q_i}\left(\tilde{\boldsymbol{M}}_i\right)\mathrm{ad}\big(\boldsymbol{s}_l\big)\boldsymbol{s}_j \equiv 0 \tag{5.38}$$

A recursive application shows that this extends to the higher orders, such that all balance conditions are in the form of

$$\frac{\partial}{\partial q_i}\left(\tilde{\boldsymbol{M}}_i\right)\prod_{l=j}^{i}\left(\mathrm{ad}\left(\boldsymbol{s}_l\right)^{\top}\right)^{\alpha_l}\boldsymbol{s}_j \equiv 0 \tag{5.39}$$

Moreover, the zeroth-order balance conditions (Eq. 5.35) satisfies all higher-order force balancing conditions since $\partial/\partial q_i(\tilde{\boldsymbol{M}}_i)$ is a function of the linear momentum and the mass is assumed to be constant

$$\frac{\partial}{\partial q_i}\left(\widetilde{m_i\boldsymbol{c}_i}\right) = \hat{\boldsymbol{p}}_i \equiv 0, \qquad \frac{\partial}{\partial q_i}\left(\tilde{m}_i\right) = 0 \tag{5.40}$$

Therefore, only the following first- and second-order moment balance conditions remain:

$$\frac{\partial}{\partial q_i}\left(\tilde{\boldsymbol{E}}_i\right)\boldsymbol{n}_j \equiv 0, \qquad \frac{\partial}{\partial q_i}\left(\tilde{\boldsymbol{E}}_i\right)\boldsymbol{n}_l \equiv 0, \qquad \frac{\partial}{\partial q_i}\left(\tilde{\boldsymbol{E}}_i\right)\left[\boldsymbol{n}_l\times\right]\boldsymbol{n}_j \equiv 0 \tag{5.41}$$

In the general case, when $\boldsymbol{n}_j \nparallel \boldsymbol{n}_l$, this imposes 9 independent constraints on the derivative of the inertia matrix, requiring $\partial/\partial q_i(\tilde{\boldsymbol{E}}_i) = 0$, thus directly satisfying all higher-order partial derivatives (Eq. 5.39). This shows that derivatives of a higher order than $k_{\max} = 2$ impose no new dynamic balance conditions for serial linkages.

When, in the special case, all non-infinite pitch ISA lower in the chain are aligned, i.e. $\boldsymbol{n}_j \parallel \boldsymbol{n}_i$ for all $j < i$, the moment balance conditions (Eq. 5.41) vanish or become equivalent. Then, only three higher-order constraints are imposed on the aggregated inertia matrix $\tilde{\boldsymbol{E}}_i$. Prismatic joints (infinite pitch ISA) lower in the chain impose no higher-order moment balance conditions as their angular velocities $\boldsymbol{n}_j$ are zero.

To summarize, for serial linkages the zero-order force and moment balance condition (Eq. 5.35) and the first- and second-order moment balance conditions (Eq. 5.41) are necessary and sufficient, leading to a $k_{\max} = 2$.

Derivatives of the dynamic balance conditions of parallel mechanisms

The dynamic balance conditions of parallel mechanisms dictate a zero momentum wrench (Eq. 5.25) for all independent velocities $\dot{\boldsymbol{u}}$. Therefore the zeroth-order balancing conditions read

$$\bar{\boldsymbol{M}}\bar{\boldsymbol{J}}\boldsymbol{C} \equiv 0 \tag{5.42}$$

Also all higher-order partial derivatives with respect to $\boldsymbol{u}$ should be zero for dynamic balance. These conditions are found by repetitive application of the chain rule, the product rule and derivatives of the Kronecker product, similar to Eq. 5.19. The first-order dynamic balancing conditions become

$$\mathrm{D}_{\boldsymbol{u}}\left(\bar{\boldsymbol{M}}\bar{\boldsymbol{J}}\boldsymbol{C}\right) = \mathrm{D}_{\boldsymbol{q}}\left(\bar{\boldsymbol{M}}\bar{\boldsymbol{J}}\right)\left(\boldsymbol{C}\otimes\boldsymbol{C}\right) + \bar{\boldsymbol{M}}\bar{\boldsymbol{J}}\mathrm{D}_{\boldsymbol{u}}(\boldsymbol{C}) \equiv 0, \tag{5.43}$$

This generalizes to higher-orders by a repetitive application of the chain and product rules

$$\mathrm{D}_{\boldsymbol{u}}^{k}\big(\bar{\boldsymbol{M}}\bar{\boldsymbol{J}}\boldsymbol{C}\big) = \big[\mathrm{D}_{\boldsymbol{q}}^{k}\big(\bar{\boldsymbol{M}}\bar{\boldsymbol{J}}\big) \quad \cdots \quad \bar{\boldsymbol{M}}\bar{\boldsymbol{J}}\big]\,\bar{\boldsymbol{C}}_k \equiv 0 \tag{5.44}$$

It should be noted that these higher-order dynamic balance conditions are linear in the mass matrices and can be obtained through a series of matrix multiplications and linear operations.

We conjecture that after sufficient number of derivatives ($k_{\max}$) these are not only the necessary but also the sufficient conditions for the dynamic balance of parallel mechanisms in a general, nonsingular poses. The proof of this is not given here, yet, this assertion is supported by the fact that kinematic relations and momentum conditions are described by trigonometric analytic functions that are smooth in nonsingular robot configurations.

5.4 Dynamic balance solution using the parameter-linear form

Now, to solve these higher-order dynamic balance conditions for arbitrary mechanisms, they will be recast in the parameter-linear form [58, 24]. This enables null space procedures to extract all dynamically balanced mass distributions.

Parameter-linear form

Since the zeroth m, first $m\boldsymbol{c}$ and second moment of mass $\boldsymbol{E}$ are linear in the momentum equation, the following parameter-linear form holds

$$\boldsymbol{h} = \boldsymbol{M}\boldsymbol{t} = \big[\boldsymbol{t}*\big]\boldsymbol{z}, \qquad \boldsymbol{z}^{\top} = \begin{bmatrix} m & m\boldsymbol{c}^{\top} & \boldsymbol{e}_{\mathrm{d}}^{\top} & \boldsymbol{e}_{\mathrm{o}}^{\top} \end{bmatrix} \tag{5.45}$$

in which the $\boldsymbol{z}$-vector is formed by the inertial parameters of the body. The twist dependent 'regression' matrix given by

$$\big[\boldsymbol{t}*\big] = \begin{bmatrix} \boldsymbol{0} & -\big[\boldsymbol{v}\times\big] & \mathrm{diag}(\boldsymbol{\omega}) & \big[\boldsymbol{\omega}*\big] \\ \boldsymbol{v} & \big[\boldsymbol{\omega}\times\big] & \boldsymbol{0} & \boldsymbol{0} \end{bmatrix}, \qquad \big[\boldsymbol{\omega}*\big] = \begin{bmatrix} \omega_5 & \omega_6 & 0 \\ \omega_4 & 0 & \omega_6 \\ 0 & \omega_4 & \omega_5 \end{bmatrix}. \tag{5.46}$$

Notice that the ordering of the inertial parameter slightly differs from [24]. In this notation the point mass, displacement and pure-inertia rod elements of the multipole-rod representation (Eq. 5.27) are respectively denoted by $\boldsymbol{z}_m(\boldsymbol{r})$, $\boldsymbol{z}_\delta(\boldsymbol{r},\boldsymbol{n})$, and $\boldsymbol{z}_\eta(\boldsymbol{n})$. The parameter-linear form of the momentum basis of a serial mechanisms is directly computed from Eq. 5.24

$$\bar{\boldsymbol{h}} = \mathrm{vec}(\bar{\boldsymbol{M}}\bar{\boldsymbol{J}}) = \begin{bmatrix} \hat{\boldsymbol{h}}_1 \\ \vdots \\ \hat{\boldsymbol{h}}_n \end{bmatrix} = \begin{bmatrix} \big[\boldsymbol{s}_1*\big] & \cdots & \big[\boldsymbol{s}_1*\big] \\ \vdots & \ddots & \vdots \\ 0 & \cdots & \big[\boldsymbol{s}_n*\big] \end{bmatrix} \begin{bmatrix} \boldsymbol{z}_1 \\ \vdots \\ \boldsymbol{z}_n \end{bmatrix} = \boldsymbol{W}\bar{\boldsymbol{z}} \tag{5.47}$$

in here $\bar{\boldsymbol{h}}$ and $\bar{\boldsymbol{z}}$ denote the concatenation of all IWM and all inertial parameters in the chain, respectively.

To obtain the parameter-linear form of parallel linkages, the vectorization of matrix products (Appendix A) is applied to Eq. 5.42

$$\bar{\boldsymbol{h}} = \mathrm{vec}(\bar{\boldsymbol{M}}\bar{\boldsymbol{J}}\boldsymbol{C}) = (\boldsymbol{C}^\top \otimes \boldsymbol{I}_6)\boldsymbol{W}\bar{\boldsymbol{z}} = \boldsymbol{X}\bar{\boldsymbol{z}} \tag{5.48}$$

Higher-order dynamic balance conditions in the parameter-linear form

The parameter-linear form also applies to higher-order derivatives of the balance conditions as they are formed through a sequence of matrix operations, which are linear the inertial parameters. The higher-order serial chain regression matrices $\boldsymbol{W}_k$ can be found accordingly, i.e. by the application of Eq. 5.45 to Eq. 5.31 and Eq. 5.34), resulting in the following condition

$$\mathrm{vec}\left(\mathrm{D}^k_{\boldsymbol{q}}(\bar{\boldsymbol{h}})\right) = \boldsymbol{W}_k\bar{\boldsymbol{z}} \equiv \boldsymbol{0} \tag{5.49}$$

For parallel linkages the parameter-linear form is found by applying the matrix vectorization to Eq. 5.44, such that

$$\mathrm{vec}\left(\mathrm{D}^k_{\boldsymbol{q}}(\bar{\boldsymbol{h}})\right) = (\bar{\boldsymbol{C}}_k^\top \otimes \boldsymbol{I}_6)\bar{\boldsymbol{W}}_k\bar{\boldsymbol{z}} = \boldsymbol{X}_k\bar{\boldsymbol{z}} \equiv 0 \tag{5.50}$$

in which $\bar{\boldsymbol{W}}_k^\top = \begin{bmatrix}\boldsymbol{W}_1^\top & \cdots & \boldsymbol{W}_k^\top\end{bmatrix}$ and $\boldsymbol{I}_6$ is a 6×6 identity matrix. Now we have arrived at the parameter-linear form of the higher-order derivatives of the momentum equations of serial and parallel linkages. It should be observed that all these steps solely rely on matrix operations suitable for algorithmic treatment.

Dynamic balance solution

Dynamic balance requires inertial parameters $\bar{\boldsymbol{z}}$ that are on the intersection of the null spaces of all the $\boldsymbol{X}_i$ matrices

$$\bar{\boldsymbol{z}} \in \ker \boldsymbol{X}_i, \qquad \bar{\boldsymbol{z}} \in \ker(\bar{\boldsymbol{X}}_{k_{\max}}), \qquad \bar{\boldsymbol{z}} = \boldsymbol{N}\boldsymbol{y} \tag{5.51}$$

in which $\bar{\boldsymbol{X}}_{k_{\max}}^\top = \begin{bmatrix}\boldsymbol{X}_1^\top & \cdots & \boldsymbol{X}_{k_{\max}}^\top\end{bmatrix}$ is the collection of all regression matrices up to order $k_{\max}$. The columns of the $\boldsymbol{N}$ matrix form a basis that span this null space and therewith describe the full design space of the dynamically balanced inertial parameters. This $\boldsymbol{N}$ matrix is termed the basis of the design space and may be found through numeric or symbolic null space algorithms such as Gauss-Jordan elimination or singular value decomposition. The corresponding design parameters are $\boldsymbol{y}$. With this the complete set of dynamically balanced inertial parameters of any given nonsingular linkages may be found.

5.5 Partitioning and interpretation of the design space of dynamically balanced inertial parameters

The application of conventional null space algorithms to the dynamic balance problem (Eq. 5.51) may result in a design space description that is strongly

mixed in the inertial parameters, compromising structure and design intuition. To aid the designer, a partitioning of the design space with respect to the joint topology is presented alongside a multipole-rod representation (Fig. 5.1) of these partitions. It will be shown that 6 types of inertia transfer matrices completely describe the design space of serial linkages. These inertia transfer matrices contain all inertial parameters that can be transferred between two hinged bodies, i.e. subtracted from one body and added to the other, without changing the momentum of the linkage. This partitioning will lead to a general description of the design space of serial mechanisms that, more importantly, also covers a large part of the design space of parallel mechanisms.

Partitioning the design space of serial linkages

The dynamic balancing conditions of serial linkages (Eq. 5.35 and Eq. 5.41) are formulated in terms of aggregated mass matrices $\tilde{\boldsymbol{M}}_i$. Before presenting the general solution it may already be observed this solution will therefore also be in terms these aggregated mass matrices. From these aggregated solutions each individual mass matrix can be found accordingly

$$\boldsymbol{M}_i = \tilde{\boldsymbol{M}}_i - \tilde{\boldsymbol{M}}_{i+1}, \qquad \boldsymbol{z}_i = \boldsymbol{N}_i \boldsymbol{y}_i - \boldsymbol{N}_{i+1} \boldsymbol{y}_{i+1} \tag{5.52}$$

Therefore, the complete design space basis $\boldsymbol{N}$ of a serial chain (Eq. 5.51) may be partitioned as a band diagonal matrix

$$\begin{bmatrix} \boldsymbol{z}_1 \\ \boldsymbol{z}_2 \\ \vdots \\ \boldsymbol{z}_{n-1} \\ \boldsymbol{z}_n \end{bmatrix} = \begin{bmatrix} \boldsymbol{N}_1 & -\boldsymbol{N}_2 & & \cdots & \boldsymbol{0} \\ & \boldsymbol{N}_2 & -\boldsymbol{N}_3 & & \vdots \\ & & \ddots & \ddots & \\ \vdots & & & \boldsymbol{N}_{n-1} & -\boldsymbol{N}_n \\ \boldsymbol{0} & \cdots & & & \boldsymbol{N}_n \end{bmatrix} \begin{bmatrix} \boldsymbol{y}_1 \\ \boldsymbol{y}_2 \\ \boldsymbol{y}_3 \\ \vdots \\ \boldsymbol{y}_{n-1} \\ \boldsymbol{y}_n \end{bmatrix} \tag{5.53}$$

in here the submatrix $\boldsymbol{N}_i$ describe all inertial parameters that can be exchanged between the two bodies hinged at joint i without changing the dynamic behavior of the chain. These $\boldsymbol{N}_i$ matrices are therefore termed inertia transfer matrices. The second next subsection shows that there exist 6 types of inertia transfer matrices depending on the type of joint and alignment with the joint axes lower in the chain.

It should be noted that a similar concept is used in the context of parameter identification to describe the set of unidentifiable inertial parameters [88, 115]. Inertial parameters are said to be unidentifiable if they do not contribute to the kinetic energy of the mechanism. The serial design space, as found here, constitutes of these unidentifiable inertial parameters as zero momentum also implies zero kinetic energy. This also shows that the inertial parameters in this serial design space do not affect the required motor effort of the mechanism.

Partitioning the design space of parallel linkages

We have already seen that parallel linkages can be converted into serial chains by opening the loop. Therefore, the dynamic balance conditions, and hence the

solutions, for serial mechanisms are also valid for parallel mechanisms. Yet, this is not necessarily the complete design space, since the loop-closure equations allow for dynamically balanced mass distributions, which lie outside the design space of serial mechanisms since rank $\left(\bar{\boldsymbol{X}}\right) \leq \text{rank}\left(\bar{\boldsymbol{W}}\right)$. The design space of parallel mechanisms can therefore be partitioned in a part dealing with the equivalent serial chains $\boldsymbol{N}_{\text{S}}$ and a remainder $\boldsymbol{N}_{\text{P}}$ associated to the loop closure, termed parallel design space basis

$$\boldsymbol{N} = \begin{bmatrix} \boldsymbol{N}_{\text{S}} & \boldsymbol{N}_{\text{P}} \end{bmatrix}, \qquad \boldsymbol{N}_{\text{S}} = \begin{bmatrix} \boldsymbol{N}_I & \cdots & \boldsymbol{N}_N \end{bmatrix} \tag{5.54}$$

The serial equivalent design space basis $\boldsymbol{N}_{\text{S}}$ is found by cutting the loops of a parallel mechanism such that a set of N chains are found. The serial design space basis $\boldsymbol{N}_I$ associated to chain I has the band-diagonal form of Eq. 5.53. The complete serial design space is the union of the serial design spaces of the chains into which the mechanism is decomposed. The serial design spaces of the individual chains are not necessarily disjoint, e.g. two design spaces bases $\boldsymbol{N}_I$ and $\boldsymbol{N}_{II}$ of a single loop may cover the same design freedom. This means that the rank of the serial design space is equal to, or smaller than, the sum of the rank of the individual serial design spaces. Furthermore it should be noted that the serial design space is invariant to where a loop is opened, although the basis might be different.

A meaningful parallel design space basis is found by introducing of a suitable test matrix $\boldsymbol{T}$, whose inertial parameters are not in the span of the serial design space. The null space basis $(\bar{\boldsymbol{X}}\boldsymbol{T})^{\perp}$ of the resulting higher-order momentum wrenches $\bar{\boldsymbol{X}}\boldsymbol{T}$ yields an interpretable design space basis $\boldsymbol{N}_{\text{P}}$

$$\boldsymbol{N}_{\text{P}} = \boldsymbol{T}(\bar{\boldsymbol{X}}\boldsymbol{T})^{\perp} \tag{5.55}$$

Interpretation, the concept of inertia transfer

In Section 5.3, it is shown that dynamic balance impose two conditions on the aggregated mass matrices of serial linkages: Firstly, each aggregated mass matrix $\tilde{\boldsymbol{M}}_i$ should be chosen such that its IMW vanishes ($\tilde{\boldsymbol{M}}_i \boldsymbol{s}_i \equiv 0$). Secondly, each aggregated inertia matrix should either generate no changing angular momentum ($\partial/\partial q_i(\tilde{\boldsymbol{E}}_i)\boldsymbol{n}_i \equiv 0$) — in case all lower ISA of non-infinite pitch are parallel ($\boldsymbol{n}_j \parallel \boldsymbol{n}_i$, for all $j < i$) — or be constant ($\partial/\partial q_i(\tilde{\boldsymbol{E}}_i) \equiv 0$) — in case one or more the lower ISA are not parallel ($\boldsymbol{n}_j \nparallel \boldsymbol{n}_i$, for any $j < i$). From the first condition three cases arise; zero, finite or infinite pitch ISA, while for the second condition two cases exist; either the axes are parallel or skew. This gives rise to 6 types of solution for the aggregated mass matrices of 1-DOF lower kinematic pairs, and, consequently, 6 types of inertia transfer spaces $\boldsymbol{N}_i$. For higher-DOF joints and joints in planar linkages a similar representation exist as shown thereafter.

Six inertia transfer matrices

Here, the multipole-rod representation of these 6 inertia transfer matrices are given (Fig. 5.2). The dimensions of these inertia transfer matrices are in Table 5.1.

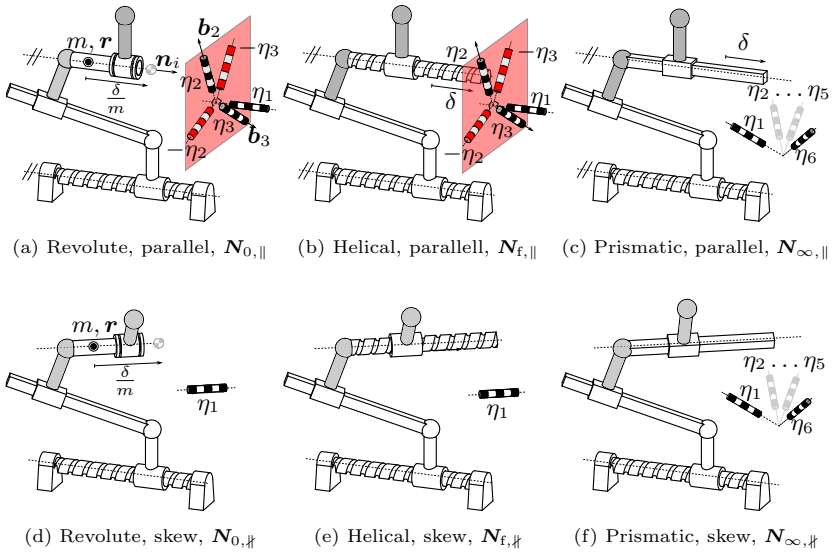

Figure 5.2: The interpretation of the 6 sets of inertial parameters that can be exchanged between the two (grey) links attached to joint i without changing the dynamic behavior of the chain as a whole. These six cases arise from the three types of 1-DOF lower pairs, and parallelism with all preceding revolute and helical joints. The alignment of the preceding prismatic joints have no influence. It should be noted that for clarity sake the effect of the displacement on the MOIs is not shown, as it can be compensated by, or absorbed in η_1. Since the pure-inertia rods have no application point, they are displayed at an arbitrary location.

1.a. In case the inertia transfer matrix belongs to a zero pitch ISA that is parallel to all preceding zero and finite pitch ISA, there are 5 inertial parameter that can be exchanged between the two bodies hinged by the joint. These are: 1) a point mass on the joint axis $\boldsymbol{z}_{\mathrm{m}}$, 2) a displacement of this point $\boldsymbol{z}_{\delta}$ in the direction of the joint axis $\boldsymbol{n}$, 3) a pure-inertia rod η_1 in the direction of the joint axis $\boldsymbol{n}$ and 4,5) two perpendicular pairs of pure-inertia rods, which are all four perpendicular to $\boldsymbol{n}$. These pure-inertia rods are of pair-wise opposite magnitudes η_2, and η_3.

The reason for these freedoms is that the actuation of a joint with a point mass m anywhere on its axis does not induce any linear or angular momentum nor change the IWM of lower joints (Eq. 5.41). This yields the design freedoms $\boldsymbol{z}_{\mathrm{m}}$ and $\boldsymbol{z}_{\delta}$. The five pure-inertia rods allow for a modification of the inertia tensor. Since the pure-inertia rod η_1 is in the direction of the joint axis it generates no angular momentum. The first of pure-inertia rod pairs η_2 is in the direction of $\boldsymbol{b}_2$, which is perpendicular to $\boldsymbol{n}$. The angular momentum induced by $\boldsymbol{b}_2$ is canceled by an equal and negative pure-inertia rod in a direction perpendicular

to both $\boldsymbol{n}$ and $\boldsymbol{b}_2$ (Fig. 5.2). This also holds for a second pair η_3 with corresponding $\boldsymbol{b}_3$. The inertia transfer matrix is therefore parameterized according to

$$\begin{aligned}\boldsymbol{N}_{0,\parallel}(\boldsymbol{s}) = \big[\boldsymbol{z}_m(\boldsymbol{r}_s) \quad \boldsymbol{z}_\delta(\boldsymbol{n},\boldsymbol{r}_s) \quad \boldsymbol{z}_\eta(\boldsymbol{n}) \\ \boldsymbol{z}_\eta(\boldsymbol{b}_2) - \boldsymbol{z}_\eta(\boldsymbol{n}\times\boldsymbol{b}_2) \quad \boldsymbol{z}_\eta(\boldsymbol{b}_3) - \boldsymbol{z}_\eta(\boldsymbol{n}\times\boldsymbol{b}_3)\big]\end{aligned} \tag{5.56}$$

1.b. In case the lower joint axes are not parallel, the zero pitch joint inertia transfer matrix loses the two pure-inertia rod pairs, since a rotation of these perpendicular pairs cause a change of the aggregated inertia matrix. This results in the following inertia transfer matrix

$$\boldsymbol{N}_{0,\nparallel} = \big[\boldsymbol{z}_m(\boldsymbol{r}_s) \quad \boldsymbol{z}_\delta(\boldsymbol{n},\boldsymbol{r}_s) \quad \boldsymbol{z}_\eta(\boldsymbol{n})\big] \tag{5.57}$$

2.a. For finite pitch and parallel joint axes, the point mass will generate a linear momentum through its pitching motion. The mass should therefore equate to zero. The displacement is massless and therefore induce no linear momentum. The remainder of the inertia transfer matrix is equal to Eq. 5.56

$$\boldsymbol{N}_{\mathrm{f},\parallel} = \big[\boldsymbol{z}_\delta(\boldsymbol{n},\boldsymbol{r}_s) \quad \boldsymbol{z}_\eta(\boldsymbol{n}) \quad \boldsymbol{z}_\eta(\boldsymbol{b}_2) - \boldsymbol{z}_\eta(\boldsymbol{n}\times\boldsymbol{b}_2) \quad \boldsymbol{z}_\eta(\boldsymbol{b}_3) - \boldsymbol{z}_\eta(\boldsymbol{n}\times\boldsymbol{b}_3)\big] \tag{5.58}$$

2.b. For the finite pitch, non-parallel case the displacement and both perpendicular pairs cause a change in IWM and are therefore omitted

$$\boldsymbol{N}_{\mathrm{f},\nparallel} = \boldsymbol{z}_\eta(\boldsymbol{n}) \tag{5.59}$$

3.a. The size of the inertia transfer matrix is 7 for a prismatic joint whose axis is parallel to all preceding zero and finite ISAs. The matrix is characterized by a displacement in the direction of the joint axis and a free second mass moment $\boldsymbol{E}$ giving rise to 6 pure-inertia rods

$$\boldsymbol{N}_{\infty,\parallel} = \big[\boldsymbol{z}_\delta(\boldsymbol{n}_\infty,\boldsymbol{n}_\infty) \quad \boldsymbol{z}_\eta(\boldsymbol{b}_1) \quad \cdots \quad \boldsymbol{z}_\eta(\boldsymbol{b}_6)\big] \tag{5.60}$$

3.b. When the preceding zero-pitch or finite-pitch joint axis are non-parallel to the prismatic joint axis $\boldsymbol{n}_\infty$, they will cause changing $\boldsymbol{n}_\infty$ and a changing displacement direction. To maintain a constant IWM of the lower joints, this displacement is therefore omitted, leaving solely the second mass moment free to choose

$$\boldsymbol{N}_{\infty,\nparallel} = \big[\boldsymbol{z}_\eta(\boldsymbol{b}_1) \quad \cdots \quad \boldsymbol{z}_\eta(\boldsymbol{b}_6)\big] \tag{5.61}$$

Multi-DOF joints

This approach also holds for multi-DOF joints that can locally be modeled as a serial connection of 1-DOF joints, e.g., cylindrical, planar, universal or spherical joints. These multi-DOF joints can transmit inertial parameters, which are

Table 5.1: The size of the 6 inertial transfer matrices. Each joint i in a serial chain extends the design space depending on the type of joint; revolute (R), helical (H), or prismatic (P) and the alignment with all non-prismatic joints $j < i$ lower in the chain; a) aligned or b) not aligned. *With a prismatic joint, the prismatic joint direction applies $\boldsymbol{n}_i = \boldsymbol{n}_{i,\infty}$

	type	λ_i	a ($\boldsymbol{n}_j \parallel \boldsymbol{n}_i$)	b ($\boldsymbol{n}_j \nparallel \boldsymbol{n}_i$)
1	R	0	5	3
2	H	finite	4	1
3	P^*	∞	7	6

given by the intersection of the inertia transfer matrices corresponding to the lower kinematic pair analog. For example, a cylindrical joint can be modeled as prismatic and a revolute joint in series such that its inertia transfer matrix becomes the intersection of $\boldsymbol{N}_0$ and $\boldsymbol{N}_\infty$, which is the inertia transfer associated to a helical joint $\boldsymbol{N}_\mathrm{f}$. Depending on the alignment of the lower joints, either type a or b is to be selected. A planar joint is serial connection of two prismatic joints such that its inertia transfer is $\boldsymbol{N}_\infty$. Universal and spherical joints locally behave as a serial connection of multiple non-parallel, intersecting revolute joints. The associated inertia transfer is therefore a point mass ($\boldsymbol{z}_\mathrm{m}(\boldsymbol{r})$) on the intersection point $\boldsymbol{r}$ of these axes.

Joints in planar linkages

In the planar case only zero and infinite pitch ISA exist. Therefore, three types of inertia transfer matrices appear, 1) the ISA is revolute and therefore automatically parallel to all other revolute joints, 2) the ISA and all lower ISA are prismatic joints or 3) the ISA is prismatic but at least one of the lower joints is a revolute joint

$$\boldsymbol{N}_0 = \boldsymbol{z}_m(\boldsymbol{r}_\mathrm{s}), \qquad \boldsymbol{N}_{\infty,\parallel} = \begin{bmatrix} \boldsymbol{z}_\delta(\boldsymbol{n}_\infty) & \boldsymbol{z}_\eta \end{bmatrix}, \qquad \boldsymbol{N}_{\infty,\nparallel} = \boldsymbol{z}_\eta \tag{5.62}$$

In the first case, the point mass should be on the revolute joint and the MOI around that point should be zero. In the second case, the body solely translates, therefore the mass should be zero and the first and second moments of mass are free, as parameterized by a displacement and a pure-inertia rod. In the third case, when the ISA under inspection is prismatic and one or more lower joints are revolute, this displacement will causes a changing MOI associated to the rotation of the lower joints. This the displacement should therefore be zero.

With this description of the inertia transfer matrices $\boldsymbol{N}_i$ of common joints, the dynamically design space of any serial linkage is found. Also for parallel linkages, the serial equivalent design space basis $\boldsymbol{N}_\mathrm{S}$ is completely determined, generalizing [125] to spatial linkages. It should be noted that the serial linkages cannot be dynamically balanced without addition of counter-mechanisms. This can also be established from the inertia transfer matrices as none of them permit

both a positive mass and positive MOIs. Therefore, a specific $\boldsymbol{N}_\mathrm{P}$ is required to render a feasible dynamically balanced design space. The existence of this additional design space is found on a case-by-case basis in the next section.

5.6 Case studies

The higher-order dynamic balance approach is illustrated here with case studies of a serial 6-DOF mechanism, a planar $4R$ four-bar linkage and a 3-RSR mechanism. In all cases an interpretation of the parallel design space bases $\boldsymbol{N}_\mathrm{P}$ will be given, if present.

Serial 6-DOF robot

Here we study here a 6-DOF robot to show how a serial design space basis is found. We consider a $HPRS$-robot (Fig. 5.3) of which the first joint axis is aligned with the third joint axis $\boldsymbol{n}_1 = \boldsymbol{n}_3$. The second, prismatic joint has no particular alignment. The fourth, spherical joint is modeled as three intersecting twists $\boldsymbol{s}_4$, $\boldsymbol{s}_5$, and $\boldsymbol{s}_6$ with no intermediate bodies. Therefore this linkages consists of four bodies in total. The zeroth-order regression matrix with the associated design space basis become

$$\boldsymbol{W}_0 = \begin{bmatrix} [\boldsymbol{s}_1 *] & \begin{bmatrix}\boldsymbol{s}_1 *\\ \boldsymbol{s}_2 *\end{bmatrix} & \begin{bmatrix}\boldsymbol{s}_1 *\\ \boldsymbol{s}_2 *\\ \boldsymbol{s}_3 *\end{bmatrix} & \begin{bmatrix}\boldsymbol{s}_1 *\\ \boldsymbol{s}_2 *\\ \boldsymbol{s}_3 *\\ \boldsymbol{s}_4 *\\ \boldsymbol{s}_5 *\\ \boldsymbol{s}_6 *\end{bmatrix} \\ & & & \end{bmatrix}, \quad \boldsymbol{N} = \begin{bmatrix} \boldsymbol{N}_1 & -\boldsymbol{N}_2 & & \boldsymbol{0} \\ & \boldsymbol{N}_2 & -\boldsymbol{N}_3 & \\ & & \boldsymbol{N}_3 & -\boldsymbol{N}_4 \\ & & & \boldsymbol{N}_4 \end{bmatrix} \tag{5.63}$$

This zeroth-order regression matrix has $\operatorname{rank}(\boldsymbol{W}_0) = 23$. Through application of the algorithm presented in Section 5.4, it is found that the regression matrix terminates at $k_\mathrm{max} = 1$ with $\operatorname{rank}\left(\bar{\boldsymbol{W}}_{k_\mathrm{max}}\right) = 24$ leaving $\boldsymbol{n}_\mathrm{b} \times 10 - \operatorname{rank}\left(\bar{\boldsymbol{W}}_{k_\mathrm{max}}\right) = 16$ design parameters free. That is because only the derivative $\partial/\partial q_2(\tilde{\boldsymbol{M}}_1 \boldsymbol{s}_1) = \partial/\partial q_2(\tilde{\boldsymbol{M}}_2)\boldsymbol{s}_1$ place additional dynamic balancing conditions. All other derivatives are covered by the zeroth- or first-order condition. Therefore the relevant rows of the first-order regression matrix are

$$\boldsymbol{W}_1 = -\begin{bmatrix}\boldsymbol{0} & \left[\operatorname{ad}(\boldsymbol{s}_2)\boldsymbol{s}_1 *\right] + \operatorname{ad}(\boldsymbol{s}_2)^\top \left[\boldsymbol{s}_1 *\right] & \cdots & \left[\operatorname{ad}(\boldsymbol{s}_2)\boldsymbol{s}_1 *\right] + \operatorname{ad}(\boldsymbol{s}_2)^\top \left[\boldsymbol{s}_1 *\right]\end{bmatrix} \tag{5.64}$$

It should be noted that the first 10 columns are zero, due to $\partial/\partial q_2(\boldsymbol{M}_1) = 0$. Since $\boldsymbol{s}_2$ is not aligned with $\boldsymbol{s}_1$, the actuation of q_2 will cause a displacement of the COM leading to a change of the aggregated mass matrix felt by $\boldsymbol{s}_1$. For the rest, the prismatic joint does not affect the momentum generated by the joint higher in the chain. As the other joints are either aligned or spherical, no additional constraints are placed. The corresponding inertia transfer matrices are therefore

$$\boldsymbol{N}_1 = \boldsymbol{N}_{\mathrm{f},\parallel}(\boldsymbol{s}_1), \quad \boldsymbol{N}_2 = \boldsymbol{N}_{\infty,\nparallel}(\boldsymbol{s}_2), \quad \boldsymbol{N}_3 = \boldsymbol{N}_{0,\parallel}(\boldsymbol{s}_3), \quad \boldsymbol{N}_4 = \boldsymbol{z}_m(\boldsymbol{r}_4) \tag{5.65}$$

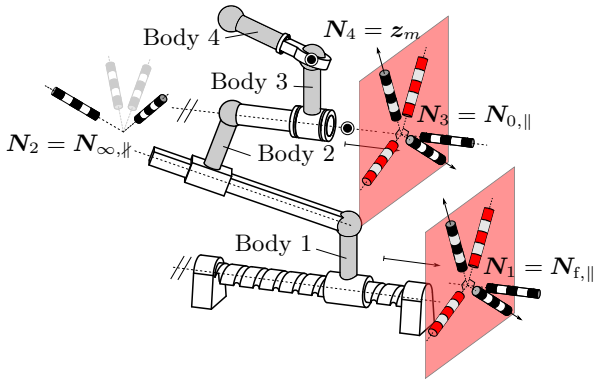

Figure 5.3: The 16 dynamically balanced design parameters of the *HPRS* 6-DOF serial chain. Each of the four joints permits a transfer of inertial parameters $\boldsymbol{N}_i$.

The first joint is a helical joint fixed to the base such that it inertia transfer matrix has rank $\left(\boldsymbol{N}_{\mathrm{f},\parallel}\right) = 4$ (Eq. 5.58). The second joint is a prismatic joint whose axis is not aligned with joint 1 such that it transmits rank $\left(\boldsymbol{N}_{\infty,\nparallel}\right) = 6$ design freedoms (Eq. 5.61). In fact, if only the zeroth-order balancing condition would be taken into account $\boldsymbol{N}_2$ would gain an additional 'displacement' such that it would be $\boldsymbol{N}_{\infty,\parallel}$. The revolute joint, joint 3, is aligned and stays aligned with the preceding finite pitch ISA (joint 1) such that it has an inertia transfer matrix of rank $\left(\boldsymbol{N}_{0,\parallel}\right) = 5$ (Eq. 5.56). The spherical joint is seen as the intersection of three perpendicular revolute joints such that it solely transmits a point mass at the intersection point $\boldsymbol{r}_4$. This leads to a total design freedom of rank $(\boldsymbol{N}) = 16$. This corresponds with the order of the regression matrix $\bar{\boldsymbol{W}}_{k_{\max}}$, which is found through the algorithm.

Planar four-bar

The planar $4R$ four-bar linkage is a classical example in the dynamic balance literature. Although widely studied for decades [14], a solution that does not rely on additional counter-mechanisms was only found in the year 2000 by Ricard and Gosselin [86]. Thereafter, this mechanism has been used as dynamic balancing module to obtain 3-DOF and 6-DOF dynamically balanced mechanisms [120]. Here, this linkage is studied to show that the current method replicates the results from literature.

The linkage consist of four revolute joints at $\boldsymbol{o}_1$ up to $\boldsymbol{o}_4$. The first and last joints are attached to the base (Fig. 5.4). The moving links have lengths l_1, l_2, and l_3 and the base length is l_4. We analyze this linkage by cutting the third link between joint 3 and 4. Two kinematic branches I and II are obtained, consisting of joint 1, 2 and 3 and joint 4, respectively. Therefore, the serial equivalent design space basis becomes

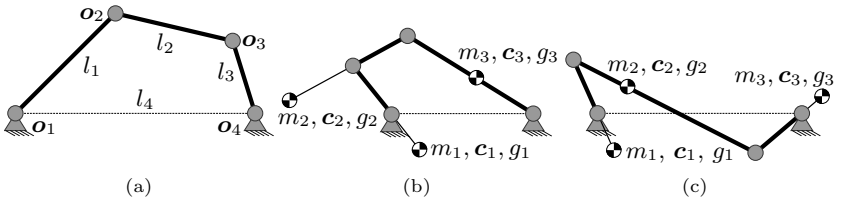

Figure 5.4: (a) The kinematic definition of the planar four-bar linkage, with the two dynamically balanced types (b) the kite and (c) the antiparallelogram.

$$\boldsymbol{N}_{\mathrm{S}} = \begin{bmatrix} \boldsymbol{N}_I & \boldsymbol{N}_{II} \end{bmatrix}, \quad \boldsymbol{N}_I = \begin{bmatrix} \boldsymbol{N}_1 & -\boldsymbol{N}_2 & \boldsymbol{0} \\ \boldsymbol{0} & \boldsymbol{N}_2 & -\boldsymbol{N}_3 \\ \boldsymbol{0} & \boldsymbol{0} & \boldsymbol{N}_3 \end{bmatrix}, \quad \boldsymbol{N}_{II} = \begin{bmatrix} \boldsymbol{0} \\ \boldsymbol{0} \\ -\boldsymbol{N}_4 \end{bmatrix} \tag{5.66}$$

Since all joints are revolute joints, the inertial transfer matrices consist of a point mass at the joint location (Eq. 5.62), i.e. $\boldsymbol{N}_i = \boldsymbol{N}_0 = \boldsymbol{z}_m(\boldsymbol{r}_i)$. This shows that the inertial parameter of link three, at which the cut has been made, will lie on the span of $\boldsymbol{N}_3$ and $\boldsymbol{N}_4$. The loop opening can also be performed at another link resulting in another basis for the same null space. Therefore, $\operatorname{rank}(\boldsymbol{N}_{\mathrm{S}}) = 4$.

Through application of the higher-order derivatives algorithm, the $\bar{\boldsymbol{X}}$-matrix is obtained. Inspection of the rank $\bar{\boldsymbol{X}}$-matrix reveals that in the general case, this matrix has a maximum rank of $\operatorname{rank}\left(\bar{\boldsymbol{X}}_{k_{\max}}\right) = 8$ and requires $k_{\max} = 3$ derivatives to reach this limit. Since there are 12 inertial parameters, this linkage has a design freedom $\operatorname{rank}(\boldsymbol{N}) = 4$. This shows that with the loop-opening method the complete design space of the general four-bar linkage has been found. This serial equivalent design space has no feasible solutions, since the addition of a positive point mass to one link requires a negative point mass on the connecting link. A feasible link with a positive MOI requires at least two positive point masses, which is not supported by this general solution.

Fortunately, there exist two special kinematic conditions in which the dimension of the design space increases and the linkage permits feasible dynamically balanced solutions [86, 75]. These are the anti-parallelogram ($l_1 = l_3$, $l_2 = l_4$) and the kite-type four-bar linkage ($l_1 = l_2$, $l_3 = l_4$), as shown in Fig. 5.4. In both cases, the base link has to be wider than two equal moving links. Here we study only the anti-parallelogram case, for which the rank of the $\bar{\boldsymbol{X}}$ matrix drops to $\operatorname{rank}\left(\bar{\boldsymbol{X}}\right) = 7$, and the design space is extended with a basis

$$\boldsymbol{N}_{\mathrm{P}}^{\top} = \begin{bmatrix} \boldsymbol{z}_\eta^{\top} & -\boldsymbol{z}_\eta^{\top} & \boldsymbol{z}_\eta^{\top} \end{bmatrix} \tag{5.67}$$

This may be interpreted as three pure-inertia rods in which the inertia connected to the coupler is opposite to the other two [34]. This solution arises since the links of the mechanism follow a linear relation on the angular velocities $\boldsymbol{\omega}_1 - \boldsymbol{\omega}_2 + \boldsymbol{\omega}_3 = 0$ [17]. The solution is parameterized by y_1 up to y_5. The first four parameters deal with the serial equivalent $\boldsymbol{N}_{\mathrm{S}}$, while the y_5 is variable

associated to $\boldsymbol{N}_{\mathrm{P}}$. The resulting body masses and local MOIs become

$$m_i = y_i - y_{i+1}, \qquad g_i = l_i^2 \left(1 - \frac{y_i}{m_i}\right) y_i + (-1)^{i+1} y_5 \tag{5.68}$$

From the mass positivity condition (Eq. 5.23) it follows that the design parameters should be selected decreasingly through the chain

$$y_1 > y_2 > y_3 > y_4 \tag{5.69}$$

The positivity of the MOI places upper and lower bounds on the choice of y_5

$$y_5 > l_1^2 \left(1 - \frac{y_1}{m_1}\right) y_1, \quad y_5 < l_2^2 \left(1 - \frac{y_2}{m_2}\right) y_2, \quad y_5 > l_1^2 \left(1 - \frac{y_3}{m_3}\right) y_3 \tag{5.70}$$

A similar result emerges for the kite-type four-bar linkage, with the sole difference that equal length crank and coupler have a positive moment inertia whereas the rocker has a negative pure-inertia rod. With this example we have shown that dynamic balancing results from literature could be replicated using the proposed higher-order dynamic balancing method. Furthermore we have shown an example in which the serial, loop opening solution aids in interpreting the whole dynamic balance solution and the feasibility conditions. The special kinematic cases, as found by Moore and Gosselin [75], may also be derived from rank reduction of $\bar{\boldsymbol{X}}$-matrix, but this lies outside the scope of this chapter.

3-*RSR* spatial parallel mechanism

To show that this procedure also holds for multi-DOF mechanisms we investigate a symmetric 3-RSR mechanism [16]. In this section we will show that the design space of the 3-RSR does not contain feasible designs when considering the whole of its workspace. Fortunately, it permits a dynamically balanced solution for 2-DOF movements over one plane of symmetry and with some additional constraints on three planes of symmetry.

Kinematic definition

The 3-RSR under investigation (Fig. 5.5) consist of three arms whose upper and lower links are of equal length $l_{\mathrm{u}} = l_{\mathrm{l}}$. The platform and the base have identical dimensions $l_{\mathrm{b}} = l_{\mathrm{p}}$. The first arm consist of two revolute joints 1 and 3, respectively hinged at the base at $\boldsymbol{r}_1$ and at the platform at $\boldsymbol{r}_3$. Their joint axes $\boldsymbol{n}_1$ and $\boldsymbol{n}_3$ are co-linear in the reference configuration. The spherical joint, which connect link 1 and 2, is located at $\boldsymbol{r}_2$. Arms 2 and 3, consisting of joints 4 - 9 and links 3 - 6 are similar yet rotated with ϕ and $-\phi$ around the vertical axis. The platform is link 7. The three base joints are chosen to be the independent coordinates u_1, u_2, and u_3. Throughout motion the mechanism is mirror symmetric with respect to a plane Π_{s} passing through the three S-joints [16, 121]. Due to this symmetry, the platform of this robot remains tangential to a variable sized sphere whose south pole is fixed at the origin of the robot.

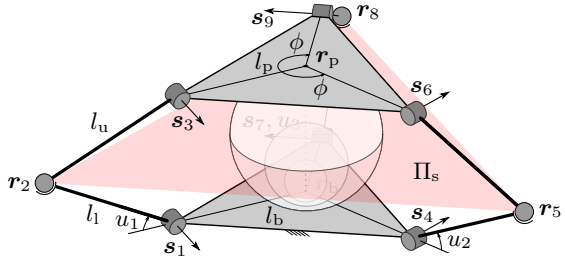

Figure 5.5: The kinematic definition of the 3-*RSR*. During motion the end-effector stays tangential to an expanding sphere touching the platform center and the base center [16]. This mechanism further exhibits a mirror symmetry with respect to a plane Π_s passing thorough the spherical joints located at $\boldsymbol{r}_2$, $\boldsymbol{r}_5$, and $\boldsymbol{r}_8$.

General dynamic balance solution

Similar to previous example, the serial equivalent design space is found by cutting the three kinematic loops at the platform leaving three *RSR* chain, respectively consisting of joints 1 - 3, 4 - 6 and 7 - 9. The corresponding design space basis is

$$\boldsymbol{N}_S = \begin{bmatrix} \boldsymbol{N}_1 & -\boldsymbol{N}_2 & \boldsymbol{0} & & & & & & \\ \boldsymbol{0} & \boldsymbol{N}_2 & -\boldsymbol{N}_3 & & & & & & \\ & & & \boldsymbol{N}_4 & -\boldsymbol{N}_5 & \boldsymbol{0} & & & \\ & & & \boldsymbol{0} & \boldsymbol{N}_5 & -\boldsymbol{N}_6 & & & \\ & & & & & & \boldsymbol{N}_7 & -\boldsymbol{N}_8 & \boldsymbol{0} \\ & & & & & & \boldsymbol{0} & \boldsymbol{N}_8 & -\boldsymbol{N}_9 \\ \boldsymbol{0} & \boldsymbol{0} & \boldsymbol{N}_3 & \boldsymbol{0} & \boldsymbol{0} & \boldsymbol{N}_6 & \boldsymbol{0} & \boldsymbol{0} & \boldsymbol{N}_9 \end{bmatrix}, \quad (5.71)$$

with

$$\begin{aligned} \boldsymbol{N}_1 &= \boldsymbol{N}_{0,\parallel}(\boldsymbol{s}_1), & \boldsymbol{N}_2 &= \boldsymbol{z}_m(\boldsymbol{r}_2), & \boldsymbol{N}_3 &= \boldsymbol{N}_{0,\nparallel}(\boldsymbol{s}_3) \\ \boldsymbol{N}_4 &= \boldsymbol{N}_{0,\parallel}(\boldsymbol{s}_4), & \boldsymbol{N}_5 &= \boldsymbol{z}_m(\boldsymbol{r}_5), & \boldsymbol{N}_6 &= \boldsymbol{N}_{0,\nparallel}(\boldsymbol{s}_6) \\ \boldsymbol{N}_7 &= \boldsymbol{N}_{0,\parallel}(\boldsymbol{s}_7), & \boldsymbol{N}_8 &= \boldsymbol{z}_m(\boldsymbol{r}_8), & \boldsymbol{N}_9 &= \boldsymbol{N}_{0,\nparallel}(\boldsymbol{s}_9) \end{aligned} \quad (5.72)$$

The base revolute joints have fixed axes while the platform joints have moving axes, giving rise to their respective inertia transfer matrices. Since a spherical joint (S) locally behaves as three perpendicular intersecting revolute joints, its inertia transfer matrix $\boldsymbol{N}_i$ is a point mass at the joint location $\boldsymbol{r}_i$, for $i = 2$, 5 and 8. This yields a serial equivalent design space with a rank of $3\times(5+1+3) = 27$. The $\bar{\boldsymbol{X}}$-matrix, which is found through the presented algorithm, terminates at $k_{\max} = 2$ and has a rank $\left(\bar{\boldsymbol{X}}_{k_{\max}}\right) = 43$. With 7 moving links and 70 inertial parameters to determine, it is shown that the complete design space is given by the serial equivalent design space ($70 = 43 + 27$) and no parallel design space exists. Therefore, additional counter-mechanisms are required for dynamic balance of the 3-*RSR* mechanisms.

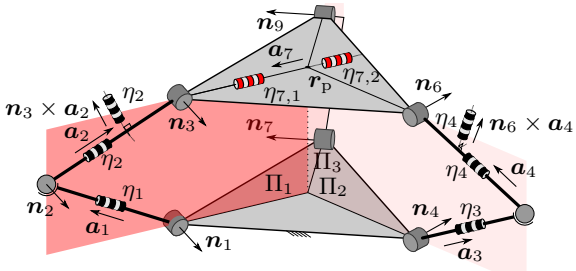

Figure 5.6: The 3-RSR mechanism exhibits a larger design space when moving over planes of symmetry. For movement over the first plane, indicated by Π_1, two additional design spaces appear. The first design freedom is an addition of pure-inertia rods to the first arm η_1 and η_2 a negative pure-inertia rod to the platform $\eta_{7,1}$. The second design freedom is an extra pure-inertia rods η_3, η_4 on the arm 2 and a negative pure-inertia rod on the platform $\eta_{7,2}$. Although not shown here, arm 3 has to be identical to arm 2. Later the balance for the other planes Π_2 and Π_3 is solved.

Dynamic balance for 2-DOF motion on planes of symmetry

Fortunately, the mechanism can be dynamically balanced when only a part of the workspace is considered. Here we will investigate the case when the platform center $\boldsymbol{r}_\mathrm{p}$ moves over a plane of mirror symmetry Π_1, normal to joint axis $\boldsymbol{n}_1$. This occurs when the two other base joints move in unison $u_2 = u_3$ (Fig. 5.6). Furthermore we will show that this permits a symmetric mass distrubution over the 3 arms and platform such that the mechanism is also dynamically balanced when moving over the other 2 planes of symmetry, i.e Π_2, when $u_1 = u_3$ and Π_3 when $u_1 = u_2$.

When the mechanisms is constrained to the first plane Π_1, the rank of the regression matrix drops by 8 to rank $\left(\bar{\boldsymbol{X}}_{k_\mathrm{max}}\right) = 35$, yielding a design space of size 35. A part of this enlarged design space can be explained by the fact that the S-joint of arm 1 now behaves as a revolute joint ($\boldsymbol{n}_1 \parallel \boldsymbol{n}_2 \parallel \boldsymbol{n}_3$) enlarging the serial design space by 6. Now the first arm's inertia transfer matrices (Eq. 5.72) become

$$\boldsymbol{N}_2 = \boldsymbol{N}_{0,\parallel}(\boldsymbol{s}_2) \qquad \boldsymbol{N}_3 = \boldsymbol{N}_{0,\parallel}(\boldsymbol{s}_3) \tag{5.73}$$

Furthermore, two additional parallel design freedoms appear, which are closely associated to the kite-type planar four-bar linkage (Section 5.6). When the first joint (u_1) is actuated and the others ($\dot{u}_2 = \dot{u}_3 = 0$) are fixed, the first arm and the platform moves as a kite-type four-bar linkage due to the mirror symmetry with respect to the plane Π_s through the S-joints. Due to this symmetry for all poses, the angular velocities of the bodies have a particular linear relation $\boldsymbol{\omega}_1 + \boldsymbol{\omega}_2 = \boldsymbol{\omega}_7$. The first parallel dynamic balance design freedom is therefore

$$\boldsymbol{N}_{\mathrm{P},1}^\top = \begin{bmatrix} \eta_1 \boldsymbol{z}_\eta^\top(\boldsymbol{a}_1) & \eta_2(\boldsymbol{z}_\eta^\top(\boldsymbol{a}_2) + \boldsymbol{z}_\eta^\top(\boldsymbol{n}_3 \times \boldsymbol{a}_2)) & \boldsymbol{0} & \eta_{7,1}\boldsymbol{z}_\eta^\top(\boldsymbol{a}_7) \end{bmatrix} \tag{5.74}$$

with

$$\eta_1 = 2\eta_2 = -\eta_{7,1} = 1 \tag{5.75}$$

For the second DOF $u_2 = u_3$ a second mirror symmetry is of importance; the mirror symmetry with respect to the plane Π_1 perpendicular to $\boldsymbol{n}_1$ and passing through the center of the base (Fig. 5.6). This is encoded in an angular velocity relation $\boldsymbol{\omega}_1 + \boldsymbol{\omega}_2 + \boldsymbol{\omega}_7 = \boldsymbol{\omega}_3 + \boldsymbol{\omega}_4 + \boldsymbol{\omega}_5 + \boldsymbol{\omega}_6$. Since arms 2 and 3 move in mirror symmetry with this plane, the second design freedom is found to be

$$\begin{aligned}\boldsymbol{N}_{\mathrm{P},2}^{\top} = \big[\mathbf{0} \quad \mathbf{0} \quad \eta_3 \boldsymbol{z}_\eta^{\top}(\boldsymbol{a}_3) \quad \eta_4(\boldsymbol{z}_\eta^{\top}(\boldsymbol{a}_4) + \boldsymbol{z}_\eta^{\top}(\boldsymbol{n}_6 \times \boldsymbol{a}_4)) \\ \eta_5 \boldsymbol{z}_\eta^{\top}(\boldsymbol{a}_5) \quad \eta_6(\boldsymbol{z}_\eta^{\top}(\boldsymbol{a}_6) + \boldsymbol{z}_\eta^{\top}(\boldsymbol{n}_9 \times \boldsymbol{a}_6)) \quad \eta_{4,2} \boldsymbol{z}_\eta^{\top}(\boldsymbol{a}_7)\big]\end{aligned} \tag{5.76}$$

with

$$\eta_3 = 2\eta_4 = \eta_5 = 2\eta_6 = 1, \qquad \eta_{7,2} = -1/2\cos(2\phi) - 3/2 \tag{5.77}$$

So arms 2 and 3 move in opposite directions with respect to this additional symmetric plane Π_1 (Fig. 5.6), canceling the angular momentum components in this plane. In the perpendicular direction ($\boldsymbol{n}_1$) the angular momentum is compensated by the negative pure-inertia rods of the platform.

5

Feasibility conditions

The resulting 35-dimensional solution space contains a range of feasible solutions. These solutions compensate the negative pure-inertia rods ($\eta_{7,1}$ and $\eta_{7,2}$) of the moving platform by addition of positive point masses to the shoulder, i.e the $\boldsymbol{z}_m(\boldsymbol{r}_i)$ in the corresponding inertia transfer matrix $\boldsymbol{N}_i$, for $i = 3$, 6, and 9. We will illustrate this on a mechanisms with a rotational symmetric base and platform ($\phi = 2/3\pi$). For demonstration purposes we reduce the rather large design space by choosing 1) all three arms to have an equal mass distribution ($y_{34} = y_{35}$, $\boldsymbol{y}_{16\ldots24} = \boldsymbol{y}_{25\ldots33}$), 2) the COMs to be inline with the arms, 3) an axisymmetric platform, and 4) the principal axis to be aligned with the links. This last simplification is ensured by choosing the first perpendicular pairs of $\boldsymbol{N}_1$, $\boldsymbol{N}_2$ and $\boldsymbol{N}_3$ to be aligned with the platform ($\boldsymbol{b}_{i,2} = \boldsymbol{a}_7$ for $i = 1, 2, 3$) and of equal magnitude ($y_4 = y_9 = y_{14}$). This choice allows a modification of the platforms MOIs without affecting the equality of the arms, since the platform inertia is directly transferred to the base. For the second and third arm these perpendicular pairs are set to be zero ($y_{19} = y_{28} = 0$). The second perpendicular pairs is aligned with the connecting link $\boldsymbol{b}_{i,3} = \boldsymbol{a}_j$. In this way all pure-inertia rods are on three mutually perpendicular axes, facilitating the selection of feasible MOIs.

The remaining parameters may be chosen freely as long as the mass and inertia feasibility conditions are satisfied (Eq. 5.23). The mass of the links become the sum of the point mass transfers

$$m_1 = m_3 = m_5 = y_1 - y_6, \quad m_2 = m_4 = m_6 = y_6 - y_{11}, \quad m_7 = 3y_{11} \tag{5.78}$$

The principal MOIs follow from the summation of the pure-inertia rods. Here the first principal axis is $\boldsymbol{n}_1$, the second is $\boldsymbol{a}_1$, and the third is $\boldsymbol{a}_1 \times \boldsymbol{n}_1$. The

Table 5.2: Geometric parameters of the simulated 3-RSR mechanisms

Name	Symbol	Value	Unit
Base width	l_b	3.00	[m]
Platform width	l_p	3.00	[m]
Lower arm length	l_l	1.00	[m]
Upper arm length	l_u	1.00	[m]
Arm angle	ϕ	$3/2\pi$	[rad]

principal MOIs of the first link are

$$g_{1,1} = y_{34} + l_\mathrm{l}^2 y_1 \left(1 - \frac{y_1}{m_1}\right), \quad g_{1,2} = y_3 - y_5 - y_8, \quad g_{1,3} = g_{1,1} + g_{1,2} + 2y_5, \tag{5.79}$$

For the second link the principal axes are oriented similarly; in the directions of $\boldsymbol{n}_3$, $\boldsymbol{a}_2$, and $\boldsymbol{n}_3 \times \boldsymbol{a}_2$, respectively

$$g_{2,1} = y_{34} + l_\mathrm{u}^2 y_6 \left(1 - \frac{y_6}{m_2}\right), \quad g_{2,2} = y_8 - y_{13} + \frac{1}{2} y_{34}, \quad g_{2,3} = g_{2,1} + g_{2,2} - y_{34} \tag{5.80}$$

The MOIs of the links of the other two arms are equal $\boldsymbol{g}_1 = \boldsymbol{g}_3 = \boldsymbol{g}_5$ and $\boldsymbol{g}_2 = \boldsymbol{g}_4 = \boldsymbol{g}_5$. The MOIs of the platform are formed by the parallel design space basis y_{34}, the added point masses at the shoulder y_{11}, the inertia transfer y_{13} over the connecting joints (i.e. in the direction of $\boldsymbol{n}_i$ for $i = 3$, 6, and 9), and the modification of by inertia transfer over the first chain y_{14}. The first principal MOI is around $\boldsymbol{a}_7$, the second around $\boldsymbol{n}_3$ and in the third out-of-plane direction $\boldsymbol{n}_3 \times \boldsymbol{a}_7$

$$g_{7,1} = \frac{3}{2}(l_\mathrm{p}^2 y_{11} + y_{13}) - \frac{1}{2} y_8 - y_{14} \tag{5.81}$$

$$g_{7,2} = \frac{3}{2}(l_\mathrm{p}^2 y_{11} + y_{13} - y_8) - \frac{9}{4} y_{34} \tag{5.82}$$

$$g_{7,3} = g_{7,1} + g_{7,2} + 2y_{14} \tag{5.83}$$

Now the platform is chosen axisymmetric $g_{7,1} = g_{7,2}$ by setting

$$y_8 = y_{14} - \frac{9}{4} y_{34}, \tag{5.84}$$

This axisymmetric solution extends the dynamically balance motion over the two other planes of mirror symmetry Π_2 and Π_3, which are perpendicular to the base joints $\boldsymbol{n}_4$ and $\boldsymbol{n}_7$, respectively. It should further be noted that the resulting mechanism is force balanced for its complete workspace.

By invoking the feasibility conditions (Eq. 5.23) we obtain the following set of feasibility conditions for the 3-RSR mechanism moving in a single plane

Table 5.3: The design parameters of the dynamically balanced 3-RSR mechanism as used in the numerical example.

Subspace		Range		Value				
Arm 1	$\boldsymbol{N}_I$	$\boldsymbol{N}_1$	$\boldsymbol{y}_{1\ldots5}$	2.00	0.00	-2.10	-0.05	-0.30
		$\boldsymbol{N}_2$	$\boldsymbol{y}_{6\ldots10}$	0.40	0.00	-2.30	-0.05	0.00
		$\boldsymbol{N}_3$	$\boldsymbol{y}_{11\ldots15}$	0.20	0.00	-2.40	-0.05	0.00
Arm 2	$\boldsymbol{N}_{II}$	$\boldsymbol{N}_4$	$\boldsymbol{y}_{16\ldots20}$	2.00	0.00	0.20	0.00	-0.30
		$\boldsymbol{N}_5$	y_{21}	0.40				
		$\boldsymbol{N}_6$	$\boldsymbol{y}_{22\ldots24}$	0.20	0.00	-0.10		
Arm 3	$\boldsymbol{N}_{III}$	$\boldsymbol{N}_7$	$\boldsymbol{y}_{25\ldots29}$	2.00	0.00	0.20	0.00	-0.30
		$\boldsymbol{N}_8$	y_{30}	0.40				
		$\boldsymbol{N}_9$	$\boldsymbol{y}_{31\ldots33}$	0.20	0.00	-0.10		
Parallel	$\boldsymbol{N}_{\mathrm{P}}$		$\boldsymbol{y}_{34\ldots35}$	1.00	1.00			

Π_1. It should be noted that several shadowing inequality conditions have been removed

$$0 < y_{11} < y_6 < y_1, \qquad y_{13} < y_8 < y_3, \qquad y_5 < 0, \qquad y_{14} < 0, \tag{5.85}$$

$$2l_{\mathrm{u}}^2 \frac{y_6 y_{11}}{m_2} < y_{34}, 0 < y_{34} + y_5 + l_{\mathrm{u}}^2 y_1 \left(1 - \frac{y_1}{m_1}\right), \tag{5.86}$$

$$0 < l_{\mathrm{p}}^2 y_{11}^2 + y_{13} + y_{14} - \frac{3}{2} y_{34} \tag{5.87}$$

It should be noted that similar feasibility conditions, yet more complex, can be obtained for the full 35-dimensional design. Furthermore, the satisfaction of the feasibility conditions does guarantee a practical implementation of the resulting balance solution. The solution for example may require very slender links, or centers of mass at a long distance from the joint, which are hard to realize in practice.

Numerical study

Based on these findings a geometry and design parameters $\boldsymbol{y}$ are selected for simulation (Table 5.2, and 5.3). The corresponding mass distribution is found in Table 5.4. In here the COM location of the arms are defined as $\boldsymbol{c}_i = \boldsymbol{r}_i - c_i \boldsymbol{a}_i$. Whereas c_i denote the distance to the connecting joint (Fig. 5.7). The COM of platform is at the center of the platform $\boldsymbol{c}_7 = \boldsymbol{r}_{\mathrm{p}}$.

Simulations of this mechanism in a multi-body software package confirm the dynamically balanced mass distribution by showing shaking forces and moments are effectively zero (Fig. 5.8) for movement over the three symmetric planes. The remaining shaking force and moments are attributed to round off errors.

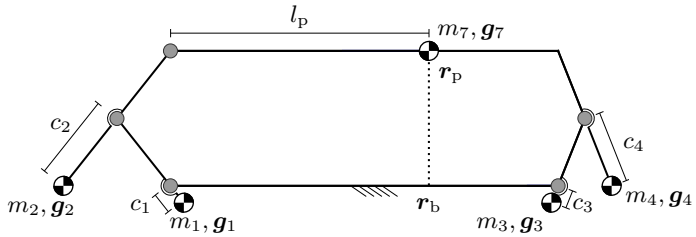

Figure 5.7: A side view (of Π_1) of the dynamically balanced 3-*RSR* as used in the simulation.

5.7 Discussion

The proposed method relies on the conjecture that the total momentum wrench remains constant for arbitrary motion if all higher-order partial derivatives of the momentum wrench are zero. Mathematically speaking this holds for all functions except for the flat functions. Such functions have one or more points in which all derivatives are zero but the function itself is not zero. In such 'flat' poses, in which the mechanisms motion governed by flat functions, this method will result in the necessary but not sufficient conditions for dynamic balance. These singular poses are therefore excluded.

In this chapter it is proven that for serial linkages two derivatives ($k_\mathrm{max} = 2$) are required to ensure the termination of the $\bar{\boldsymbol{X}}$-matrix, i.e. yielding the

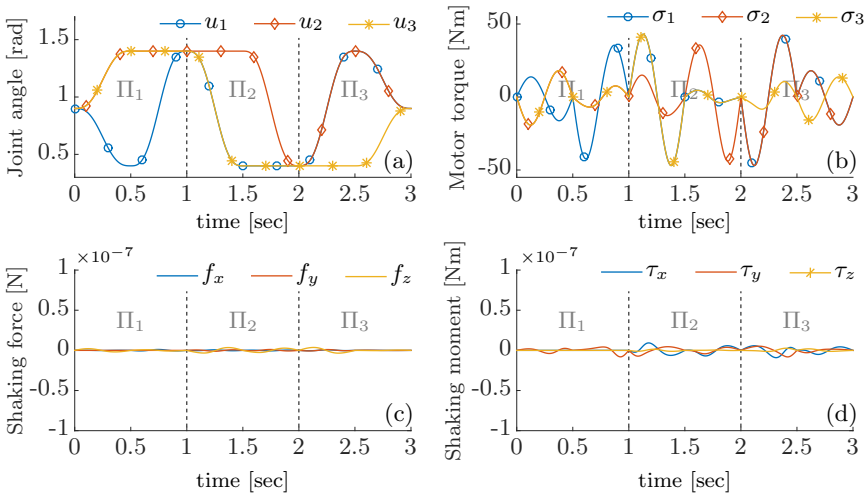

Figure 5.8: A simulation of the 3-*RSR* mechanism for a trajectory (a, b) over the three symmetric planes Π_i confirm dynamic balance as the resulting shaking forces (c) and shaking moments (d). The remaining shaking forces and moments are attributed to round-off errors in the simulations.

Table 5.4: The resulting masses, COM locations and MOIs of the 3-*RSR* as used in simulation

Name	Symbol	1	2	3	4	5	6	7	Unit
Mass	m_i	1.60	0.20	1.60	0.20	1.60	0.20	0.60	kg
COM	c_i	0.25	1.00	0.25	1.00	0.25	1.00	0.00	m
MOI 1	$g_{i,1}$	0.40	0.20	0.40	0.20	0.40	0.20	0.30	kg m^2
MOI 2	$g_{i,2}$	0.50	0.60	0.50	0.60	0.50	0.60	0.30	kg m^2
MOI 3	$g_{i,3}$	0.50	0.60	0.50	0.60	0.50	0.60	0.50	kg m^2

nessecary and sufficient conditions for dynamic balance. For parallel linkages such an upper-bound on the number of derivatives is not found. It currently relies on a case-by-case inspection of the $\bar{\boldsymbol{X}}$-matrix, as done in the examples. Although a constant rank of the $\bar{\boldsymbol{X}}$-matrix for higher orders it is a strong indicator, verification of the balancing solution is still formally required, for example by numerical simulations. Different mechanisms, but also different geometries have different $k_{\max}$ values. For example, for the general planar four-bar $k_{\max} = 3$ while for the (anti-)parallelogram geometry $k_{\max} = 2$.

By selection of a submatrix of the $\bar{\boldsymbol{X}}$-matrix, a larger design space will appear and exact dynamic balance is relaxed in favor of other requirements. For example, force balance only may be obtained by selecting only the relevant rows. Alternatively, approximate balancing may obtained by satisfying only derivatives up to a certain order, yielding dynamic balance in a neighborhood of the reference pose. Paths balance may be obtained by regarding paths or planes through the reference pose, as shown by the 3-*RSR* example. This method therefore generalizes the result of [33].

The feasibility conditions (Eq. 5.23) dictate whether or not a desired mass distribution can be constructed. To check the feasibility an eigenvalue problem is to be solved. The nonlinear nature of the eigenvalue problem prevents a closed-form treatment for arbitrary linkages. Currently this study is done on an individual basis. Yet, for simple linkages the partitioning and multipole-rod representation allowed for an interpretation and feasibility study without eigenvalues decomposition. Furthermore, even though some of the mechanisms studied here have no feasible design space, the complete characterization of the design space is expected to assist in the selection of the most favorable application dependent solution, i.e. with minimal motor torque and/or minimal number of counter-mechanisms.

5.8 Conclusion

This chapter presented a higher-order dynamic balancing method that yields and solves the necessary and sufficient dynamic balance conditions for arbitrary, serial or parallel, planar or spatial linkages in nonsingular, non-flat configurations. This method relies on a recursive algorithm to obtain the higher-order derivatives of rigid body dynamics up to an arbitrary order. In the parameter-

linear form these higher-order derivatives furnish the dynamic balance conditions that arise from a rank deficiency of the converged regression matrix. This enables generic null space procedures to yield all sets of dynamically balanced inertial parameters, i.e. the complete dynamically balanced design space of a given mechanism. It was shown that for serial linkages derivatives up to the second order yield the necessary and sufficient balance conditions. For such linkages the even higher-order partial derivatives will pose no new dynamic balance conditions. For parallel mechanisms such an upper bound was found per case. Partitioning and interpretation of the design space of serial linkages was presented based on the concept of inertia transfer. Six inertia transfer matrices where found that, depending on the alignment of the joints and the types of joints in the chain, allow for an exchange of inertial parameters without affecting the momentum generated by the mechanism as a whole. For general parallel mechanisms this serial equivalent design space fully describe the dynamically balanced design space, resulting in non-feasible designs due to negative masses or MOIs. Fortunately, in special kinematic cases a larger design space are found. Also, a larger design space is found when only a part of the workspace is to be dynamically balanced. For the 3-RSR mechanism, for instance, three dynamically balanced planes of symmetric 2-DOF motion were obtained without resorting to counter-mechanisms.

With this method a systematic, closed-form dynamic balance algorithm is presented that provides a uniform framework to study mechanisms that require no or a minimal number of counter-mechanisms, paving the way for the dynamic balance of high-speed robots.

Chapter 6

A pure-inertia method for the dynamic balance of symmetric planar mechanisms

In this chapter, we present a novel method for the dynamic balance of planar mechanisms, by transforming a mechanism into a dynamically equivalent form where all links have zero mass but non-zero moment of inertia. The dynamic balance of such pure-inertia systems is shown to be governed by mirror symmetry that cancels out the system's total angular momentum. Our method not only covers well-known dynamically balanced 1-DOF mechanisms, such as the slider-crank and four-bar linkages, but also leads to the discovery of a novel dynamically balanced 2-DOF planar mechanism.

6.1 Introduction

For robots and machines operating at high speeds, dynamic balance is desired to eliminate varying reaction forces and moments (also termed shaking forces and moments), which are known to be a major source of wear, noise and accuracy degradation [86]. The necessary and sufficient condition for dynamic balancing is that both the linear and angular momenta of the mechanism are constant. A mechanism is force balanced when only the linear momentum is constant, which in practice comes down to having a fixed center of mass of the system.

The previous chapters present methods and algorithms to find the dynamic balance solutions for a given mechanism. Furthermore, Chapter 5 confirms that the choice of kinematics largely determine whether a mechanism can be dynamically balanced without additional counter-mechanisms. However, this method do not indicate which mechanisms are favourable for dynamic balance and should be tested by these method. Rendering the search for dynamic balance a trial-and-error process. This chapter therefore aims to shed some light on the essential kinematic conditions that permit dynamic balance (Objective 2) by investigating a class of mirror symmetric parallel mechanisms.

This chapter is a reprint from: J. J. de Jong, Y. Wu, M. Carricato, J. L. Herder, A pure-inertia method for dynamic balancing of symmetric planar mechanisms. In: *Advances in Robot Kinematics* (2018), vol. 5. pp.1-8.

In principle, dynamic balance can be found by symbolically solving the kinematic and balancing equations for unknown kinematic and inertial parameters. A solution is in general not guaranteed, or otherwise very difficult to find, due to high algebraic complexity [86, 75]. Alternatively, one may construct dynamically balanced mechanisms from primitive functional modules which, either are dynamically balanced [120] or have the dynamic balance conditions that are easy to obtain symbolically [19, 106, 107]. The dynamic balance equations can be simplified by reducing the number of parameters through dynamic equivalence [31]. Two mechanisms with equal kinematics, but different mass distributions, are said to be dynamically equivalent or equimomental [89] if their linear and angular momenta are equal when undergoing a common arbitrary motion. Consequently, the two mechanisms will always have the same shaking forces and moments even though their masses, COMs, and moments of inertia are different.

A fruitful source of dynamically balanced mechanisms is the class of linkages, such as the pantograph [107], the slider-crank [19], and the four-bar [86], whose geometric structures exhibit a mirror symmetry about a plane moving with half magnitude (hence also half velocity) of that of the end-effector for full-cycle motion. Recently, the second and third author of this chapter made an addendum to this class of mechanisms by systematically investigating plane and line symmetry of a class of parallel mechanisms known as symmetric subspace motion generators [66, 121].

The main contribution of this chapter is twofold. Firstly, we propose a dynamic balance method via dynamic equivalence to massless systems with only moments of inertia. This approach, called pure-inertia method (PIM), provides a unified understanding of several existing dynamically balanced mechanisms that were previously synthesized by solving complex algebraic equations. Secondly, the PIM is applied to a novel 2-DOF planar symmetric mechanism proposed in [121]. Numerical simulation confirms that the mechanism is dynamically balanced.

6.2 Pure-inertia method

The pure-inertia method relies on the dynamic equivalence of all links in a mechanism to a zero mass with non-zero moment of inertia. A pure inertia may be interpreted as dynamically equivalent to an infinitely large and thin ring.

The principle of dynamic equivalence is illustrated in Fig. 6.1. A range of dynamically equivalent links can by found via *point mass redistribution* [31]. The initial inertial parameters comprise mass m_o, COM $\boldsymbol{c}_\mathrm{o}$, and moment of inertia g_o (Fig. 6.1a), whereas for the dynamic equivalent set we have: m_f, $\boldsymbol{c}_\mathrm{f}$, and g_f (Fig. 6.1b). If we start with a link hinged at $\boldsymbol{o}$, we may transfer a point mass of arbitrary value a — located at the hinge — from the link to the base and vice versa, without changing the link's momentum and shaking forces and moments. In the same manner, the link may exchange a point mass with any body i hinged to it by a revolute joint at a location denoted by $\boldsymbol{o}_i$. This is a valid dynamic equivalent operation, since the linear velocities of both

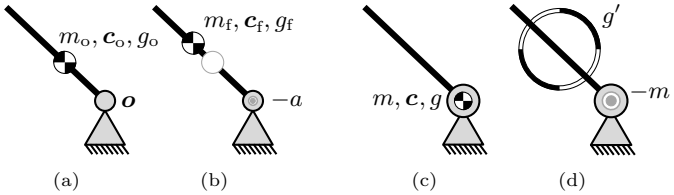

Figure 6.1: Dynamic equivalence via point mass redistribution. (a) a simple pendulum; (b) a dynamic equivalent of (a) by adding or subtracting a point mass at the hinge; (c) a pendulum with COM located at the hinge; (d) a dynamic equivalent of (c) with a pure moment of inertia.

connecting bodies are equal at a revolute joint, therefore an exchange of a point mass does not affect the mechanism's momentum. We have the following equations:

$$\begin{gathered} m_f = m_o + \sum_{i=1}^{n} a_i, \qquad m_f \boldsymbol{c}_f = m_o \boldsymbol{c}_o + \sum_{i=1}^{n} a_i \boldsymbol{o}_i, \\ g_f = g_o - m_f \|\boldsymbol{c}_f - \boldsymbol{c}_o\|^2 + \sum_{i=1}^{n} a_i \|\boldsymbol{o}_i - \boldsymbol{c}_o\|^2 \end{gathered} \tag{6.1}$$

To ensure dynamic equivalence, the point mas added to body i should be subtracted from body j, which we refer to as *mass continuity*. If both $m_f = 0$ and $m_f \boldsymbol{c}_f = \boldsymbol{0}$, i.e, if $m_o = -\sum_{i=1}^{n} a_i$ and $m_o \boldsymbol{c}_o = -\sum_{i=1}^{n} a_i \boldsymbol{o}_i$, the dynamics of the body is completely determined by a pure moment of inertia (Fig. 6.1d). This pure moment of inertia — or for brevity; pure inertia — shall be denoted with a prime: g'. When this holds for all bodies in the mechanism, the mechanism is said to be a pure-inertia mechanism.

A pure-inertia body is not physically feasible, but it can be transformed back into a feasible one by applying the reverse process of *point mass recomposition* [31], i.e., by adding point masses at the revolute joints. For the purpose of this chapter, we shall consider bodies connected with at most two revolute joints, and therefore all vectors in Eq. 6.1 can be treated as scalars. We treat here the recomposition of a pure-inertia body, e.g. $m_o = 0$, $m_o c_o = 0$, and $g_o = g'$. By assuming that one of the joints is located at the origin and the other at a distance l, the following relations hold for the mass, COM and moment of inertia:

$$m_f = a_1 + a_2, \qquad m_f c_f = a_2 l, \qquad g_f = g' + \frac{a_1 a_2}{a_1 + a_2} l^2 \tag{6.2}$$

The links generated from dynamically equivalent pure-inertia bodies, remain physically feasible if the equivalent mass m_f and moment of inertia g_f satisfy the following positivity constraints:

$$m_f > 0 \Leftrightarrow a_1 > -a_2, \qquad g_f > 0 \Leftrightarrow \frac{g'}{l^2} > -\frac{a_1 a_2}{a_1 + a_2} \tag{6.3}$$

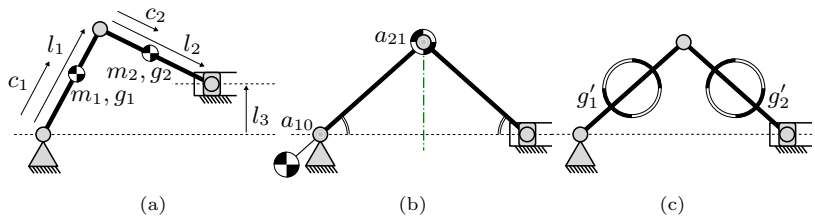

Figure 6.2: Dynamic balance conditions for a slider-crank mechanism. (a) The kinematic and inertial parameters. (b) The conventional dynamic balance conditions for a symmetric slider-crank. The symmetry line is represented by the green dash-dotted line. (c) The pure-inertia equivalent of the dynamically balanced slider-crank

which implies that a pure inertia, denoted g', is allowed to have a negative value. The limits on a_1 and a_2 are carried over to adjacent bodies due to mass continuity. See [31] for more details about the mass redistribution method. It should be noted that a pure-inertia mechanism has a fixed COM with respect to the base and is therefore necessarily force balanced. However, the reverse does not hold in general.

Dynamic balance

6

In the literature, force balance conditions are usually inspected prior to moment balancing. In comparison, for a pure-inertia mechanism, force balance conditions are automatically satisfied and therefore only the angular momentum, denoted ξ, needs to be canceled out to achieve dynamic balance:

$$\xi = \sum_{i=1}^{n} g_i' \omega_i \equiv 0 \tag{6.4}$$

It should be noted that the moments of inertia g_i' are pose independent. The angular velocities ω_i, on the other hand, imposes conditions on the geometry of the mechanism [86].

Dynamic balance of the slider-crank linkage using the PIM

We shall now illustrate the PIM by considering the dynamic balance of a slider-crank linkage, as shown in Fig. 6.2. According to [19], a slider-crank linkage can be dynamically balanced under symmetric kinematic conditions $l_1 = l_2$, $l_3 = 0$. Furthermore the total COM is required to be located at the base revolute joint, and links' inertial parameters should satisfy:

$$c_2 = 0, \qquad m_1 c_1 = -m_2 l_1, \qquad g_1 = g_2 - m_2 \left(\frac{m_2}{m_1} + 1 \right) l_1^2 \tag{6.5}$$

It is apparent that the symmetry condition $l_1 = l_2$ constrain link 1 and 2 to move with equal and opposite angular velocities: $\omega_1 = -\omega_2$. In reference to

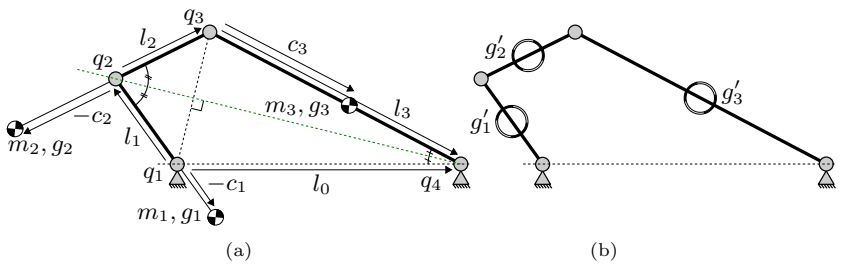

Figure 6.3: (a) The dynamically balanced four-bar linkage. (b) A pure-inertia dynamic equivalent of the linkage shown in (a). The green dash-dotted line shows the symmetric plane, bisecting the kite through joint q_2 and q_4.

Eq. 6.4, the dynamic balance condition for the slider-crank linkage reduces to:

$$g_2' = g_1' \tag{6.6}$$

We shall now show that this newly derived balance condition Eq. 6.6 is exactly equivalent to the conditions given in Eq. 6.5. Via the mass recomposition — refer to Eq. 6.2 — we have:

$$\begin{aligned} &m_1 = a_{10} - a_{21}, \quad && m_1 c_1 = -a_{21} l_1, \quad && g_1 = g_1' - a_{21}\left(\frac{a_{21}}{a_{10} - a_{21}} + 1\right) l_1^2 \\ &m_2 = a_{21}, && m_2 c_2 = 0, && g_2 = g_1' = g_2' \end{aligned} \tag{6.7}$$

We remark that the dynamics of the slider can be easily included in the above process. Since it only translates and generates no angular momentum, it is dynamically equivalent to a point mass which can be included in the dynamic balance conditions via point mass recomposition, as in Eq. 6.1.

Dynamic balance of the four-bar linkage using the PIM

Gosselin and Ricard [86] showed that two types of symmetric four-bar linkages can be dynamically balanced. The first one is the kite type, shown in Fig. 6.3. It is symmetric about a plane passing through joint q_2 and q_4. The second type, the anti-parallelogram, is symmetric about a plane which bisects the angle formed by lines through body l_1 and l_3.

We shall focus on the first type here (the same procedure can be applied to the anti-parallelogram). The kinematic symmetry conditions are: $l_1 = l_2$, and $l_0 = l_3$, whereas the dynamic balance conditions are[120]:

$$\begin{aligned} & && g_1 = g_{c1} + m_1 c_1 (l_1 - c_1) \\ &m_2 c_2 = m_1 c_1 + m_2 l_1, && g_2 = g_{c1} + m_2 c_2 (l_1 - c_2) \\ &m_3 c_3 = \frac{l_3}{l_1}\left(c_2 m_2 + l_1 m_3\right), && g_3 = -g_{c1} - m_3 c_3 (l_3 - c_3) \end{aligned} \tag{6.8}$$

in which g_{c1} is a useful collection of inertial parameters introduced in [120]. The corresponding pure-inertia mechanism can be generated by considering

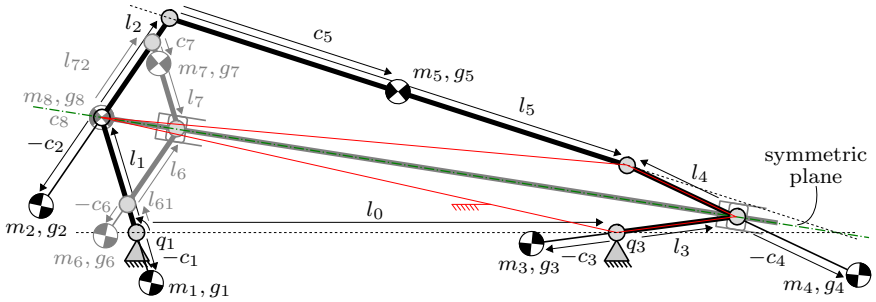

Figure 6.4: The dynamically balanced 2-DOF planar symmetric mechanism (a variant of the M_{2A}-type symmetric mechanism proposed in [121]). The angle bisecting pantograph-slide on the symmetry plane is shown in gray. When fixing one of the base joints the mechanism acts as a symmetric four-bar mechanism (red).

the following mass redistribution:

$$\begin{aligned} a_{21} &= a_{10} - m_1, \qquad a_{32} = a_{21} - m_2, \qquad a_{03} = a_{32} - m_3 \\ m_1'c_1' &= m_2'c_2' = m_1(c_1 - l_1) + a_{10}l_1, \qquad m_3'c_3' = \frac{l_3}{l_1}m_1'c_1' \end{aligned} \tag{6.9}$$

The link masses can then be canceled out by setting $a_{10} = -m_1/l_1(c_1 - l_1)$, thus resulting in the following pure-inertia dynamic balance conditions:

$$g_1' = g_2' = -g_3' = g_{c1} \tag{6.10}$$

which offers a novel interpretation of g_{c1}. It should be noted that these conditions can also be derived from the relation between the angular velocities $\omega_1 + \omega_2 = \omega_3$. Based on these pure-inertia conditions, we can find a range of dynamically equivalent mechanisms, as long as the selection of inertial parameters g_1', a_{10}, a_{21}, a_{32}, and a_{03} respect the positivity constraint $m_i > 0$ and $g_i > 0$.

6.3 Dynamic balance of a novel 2-DOF symmetric mechanism using the PIM

A novel 2-DOF symmetric planar mechanism, capable of generating finite rotations about any axis on its symmetric plane, was recently proposed in [121]. A variant is illustrated in Fig. 6.4. It comprises two RRR chains acting in-parallel on the end-effector and an angle-bisecting device (gray links in Fig. 6.4) to ensure a symmetric motion. The angle-bisecting device consists of a pantograph, attached via two revolute joints to two collinear slider joints on the symmetric plane. The symmetric plane bisects both "elbow" angles of the two RRR chains for full-cycle motion. Due to the *half-angle property* [122], the symmetric plane also bisects the angle between the base and the end-effector.

We shall apply the PIM to dynamically balance this novel mechanism in two steps. In the first step, the mass and moment of inertia of the angle-bisecting

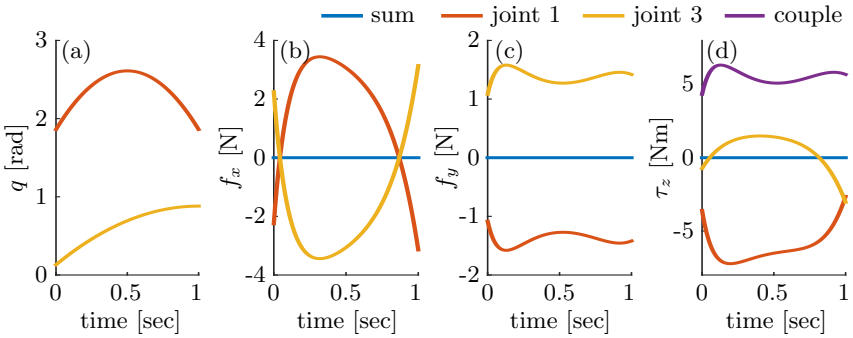

Figure 6.5: Simulation results of the novel 2-DOF manipulator. The figure shows the input angles (a), shaking forces in x and y direction (b, and c respectively) and the shaking moment (d). The shaking forces are the *sum* of reaction forces on the base joints (*joints 1 and 3*). The shaking moment is the *sum* of motor torques and the *couple* induced by base joint forces.

device are ignored (but assuming that the geometric constraint is still effective). We set base joints (q_1 and q_3) as the input variables. Because of the symmetry conditions, the angular velocity $\omega_{i,j}$ of body i with respect to the actuator $j = \{1, 3\}$ can be written as:

$$\begin{aligned} \omega_{1,1} + \omega_{2,1} &= \omega_{4,1} = \omega_{5,1} \\ \omega_{3,3} + \omega_{4,3} &= \omega_{2,3} = \omega_{5,3} \end{aligned} \tag{6.11}$$

Both relations are in fact equivalent to those of the kite-type four-bar linkage: when one of the base joints is locked, the platform and its adjacent link move as a single rigid link, thus similar to a kite-shaped four-bar linkage. Consequently, dynamic balance conditions can be derived from Eq. 6.10 as:

$$g'_1 = g'_2 = -g'_4 - g'_5, \qquad g'_3 = g'_4 = -g'_2 - g'_5 \tag{6.12}$$

In the second step, the entire mechanism is dynamically balanced. First, note that links l_6 and l_7 of the pantograph (the angle-bisecting device in Fig. 6.4) have the same angular velocity as that of links l_2 and l_1, respectively. Their moments of inertia can then be easily lumped together in the dynamic balance conditions derived in the first step. Secondly, due to the half-angle property, the angular velocity of the connecting link l_8, is exactly half the angular velocity of the end-effector. Thus we have:

$$\omega_6 = \omega_2, \qquad \omega_7 = \omega_1, \qquad \omega_8 = 0.5\omega_5 \tag{6.13}$$

The dynamic balance conditions for the entire mechanism are then given by:

$$g'_1 + g'_7 = g'_2 + g'_6, \qquad g'_3 = g'_4, \qquad g'_5 + 0.5g'_8 = -g'_2 - g'_4 \tag{6.14}$$

A simulation of the dynamically balanced 2-DOF mechanism was performed to validate the PIM. The numerical values chosen for the lengths, COM, masses

and moments of inertia can be found in Table 6.1 - 6.4. The simulation results, as shown in Fig. 6.5, confirm that the sum of the shaking forces and moments are zero for arbitrary motion.

6.4 Conclusion

All dynamically balanced mechanisms discussed in this chapter share the same property of kinematic symmetry and dynamical equivalence to pure-inertia mechanisms. The pure-inertia method provides a simplified approach for achieving dynamic balance for two reasons: (i) Force balance conditions are automatically satisfied; (ii) in the planar case, moments of inertia are pose invariant and can be treated as scalars, reducing the dynamic balance conditions to linear kinematic relations between angular velocities. These relations, in the class of mechanisms shown here, are linear due to kinematic symmetry conditions. Based on this new understanding, a new dynamically balanced 2-DOF mechanism was presented.

Table 6.1: Geometric parameters for the 2-DOF symmetric mechanism as used in the simulation.

Name	Symbol	Value	Unit
Base length	l_0	4.0	m
Arm length	l_1, l_2, l_3, l_4	1.0	m
Platform length	l_5	4.0	m
Pantograph length	l_6, l_7	0.75	m
Pantograph offset	l_{61}, l_{71}	0.25	m

Table 6.2: Pure moments of inertia.

Name	Symbol	Value	Unit
Left arm PI	g_1', g_2'	1.000	kg m^2
Right arm PI	g_3', g_4'	1.010	kg m^2
Platform PI	g_5'	-2.025	kg m^2
Pantograph PI	g_6', g_7', g_8'	10.00×10^{-3}	kg m^2

Table 6.3: Point mass redistribution.

Name	Symbol	Value	Unit
Left base joint	a_{10}	1.93	kg
Left elbow joint	a_{21}	-0.570	kg
Right base joint	a_{30}	-1.18	kg
Right elbow joint	a_{43}	-0.490	kg
Platform joints	a_{52}, a_{54}	-0.260	kg
Pantograph-arm joints	a_{61}, a_{72}, a_{81}	-10.0×10^{-3}	kg
Internal pantograph joints	a_{76}	-3.00×10^{-3}	kg

Table 6.4: Inertial parameters as used in the simulation of the dynamically balanced 2-DOF mechanism.

Name	Mass	kg	COM	m	MOI	kg m^2
Left lower arm	m_1	1.3	c_1	-0.43	g_1	0.17
Left upper arm	m_2	0.30	c_2	-0.89	g_2	0.50
Right lower arm	m_3	0.69	c_3	-0.71	g_3	0.17
Right upper arm	m_4	0.23	c_4	-1.1	g_4	0.46
Platform	m_5	0.52	c_5	2.0	g_5	55×10^{-3}
Lower pantograph arm	m_6	7.0×10^{-3}	c_6	-0.32	g_6	7.6×10^{-3}
Upper pantograph arm	m_7	13×10^{-3}	c_7	-0.17	g_7	11×10^{-3}
Symmetric bisector	m_8	10×10^{-3}	c_8	0.00	g_8	10×10^{-3}

Chapter 7

Discussion

This thesis aims to strengthen the mathematical basis for dynamic balance and provide three new methods to find new dynamically balanced mechanisms. The first two methods where aimed at solving the dynamic balance conditions in a uniform manner, whereas the third method attempts to shed light the kinematics that are required for effective balance solutions. Looking back on this work the question arises; to what extent have the objectives been fulfilled? And, further zooming out, what implications does this research have for the dynamic balancing field and beyond?

7.1 Reflection on the results

Holistic analysis method

Objective 1: *To develop a holistic analysis method that provides all dynamically balanced mass distributions for any planar or spatial parallel linkage with single or multi-DOF.*

Chapter 3 and 5 present two dynamic balancing methods aimed at fulfilling Objective 1. The instantaneous dynamic balance method (Chapter 3) yielded and solved the necessary zeroth-order conditions for dynamic balance in a geometric manner. This approach is uniform for all linkages and yields a single, instantaneously dynamically balanced pose in which the linkage is exactly dynamically balanced. That means that in this pose the accelerations robot will not induce shaking forces and moments. Close to this pose the balance quality is high, whereas further away it worsens. How severe this quality drop depends strongly on each case. The combination with path balance gives this pose more significance as it is found to be the intersection of multiple dynamically balanced paths. For this 'path balance', additional conditions are to be satisfied, which are found on a case-by-case basis. The Fuga I, for example, satisfies two force balance conditions in addition to the instantaneous dynamic balance conditions. This resulted in a mechanism which is dynamically balanced over two paths, intersecting in the middle of the workspace.

The higher-order dynamic balance method (Chapter 5) extends this approach to arbitrary order and thereby to the conditions that are necessary and

(we conjecture) sufficient for the dynamic balance of nonsingular linkages. By addition of the first-, second- and higher-order derivatives of the total momentum wrench, more conditions are found and solved, until exact dynamic balance extends over the whole workspace of the mechanism. It should be noted that also path balance, force balance, or partial balance, can be found by selection of subset of these conditions. For example, a 3-RSR linkage is found that is dynamically balanced for 2-DOF movement on three symmetric planes.

Both methods rely on the intrinsically spatial screw theory and treat force and moment balance simultaneously. The provided interpretation of the solution space is different for the two methods: Chapter 3 employs a conventional parameterization using masses and principal moments of inertia. This facilitates the feasibility study to ensure positive masses and moments of inertia. Chapter 5 uses a different parameterization, based on the multipole representation [52] originating from the prior art on parameter identification. Although this parameterization is linear in the linear and angular momenta, it is nonlinear in the feasibility conditions, precluding a closed-form feasibility check for arbitrary mechanisms. Therefore, the feasibility check is carried out on an individual basis as demonstrated in the case studies.

The higher-order dynamic balance method showed two distinct design spaces of dynamically balanced inertial parameters for parallel mechanisms. The first design space is associated with the serial chains into which a parallel mechanism can be decomposed. This may therefore be seen as the extension of the 'mass/inertia flow concept' [125] to the general spatial case. The second design space appears only in specific kinematic conditions, such as when the links' linear or angular velocities are subject to a linear relation [43, 17]. Since serial linkages always require bodies with negative or zero masses or moments of inertia for dynamic balance, this second, parallel design space is essential to enable feasible designs that do not require counter-rotating devices.

Essential kinematic conditions

Objective 2: *To understand the underlying principles needed to achieve dynamic balance through mass distribution design.*

From Chapter 5 — the higher-order dynamic balance approach — two types of essential kinematic conditions arise. Firstly, the linear and angular velocities should have a special relation whereby a parallel design space opens up. Secondly, this additional design space should be such that, in combination with the serial design space, it allows for feasible masses and moments of inertia of all bodies. Currently, it is not known how these rather abstract conditions can be turned into concrete mechanisms. Therefore, this method functions more as a check of whether a mechanism can be dynamically balanced, and if so, under what conditions.

The first type of essential kinematic conditions may potentially be found for a given mechanism by investigating the kinematic coupling matrix $\bar{\boldsymbol{X}}$. When its rank drops, i.e. when the determinant of a sufficiently large submatrix vanishes, an additional design space appears. The problem of deriving these conditions lies in the fact that this coupling matrix $\bar{\boldsymbol{X}}$ highly nonlinear is in the kinematic

parameters. Here, the algebraic balancing methods of Moore et al. [74, 75, 76] form a potential approach. The second type of conditions, on the feasibility, is potentially even harder to guarantee in closed form as it involves a set of inequality conditions.

Chapter 5 also revealed a similarity between the loop-closure constraints and the mass matrix. Comparison of the loop-closure condition (Eq. 5.19) with the dynamic balance condition (Eq. 5.44) shows that as long as the mass matrices remain within the constrained space, the mechanism is dynamically balanced. The consequence of this fact is not fully investigated but it may allow for an inverse design approach: to find kinematic constraints that permit feasible mass matrices.

Chapter 6 takes another route to fulfill this objective. It shows that two elementary dynamically balanced linkages from literature possess a specific relation on the linear and angular velocities, i.e. mirror symmetry with respect to a moving plane. Furthermore, it shows that the masses and moments of inertia of these linkages can be represented with a single pure moment of inertia per link. This enables a third dynamic balance method, termed the pure-inertia method. This method is applied to a class of linkages termed symmetric subspace motion generators, leading to a novel 2-DOF dynamically balanced linkage. It should, however, be noted that not all dynamically balanced linkages in literature are purely symmetric and furthermore, that not all symmetric subspace motion generators can be dynamically balanced, as shown by the 3-RSR in Chapter 5. These symmetric linkages are nevertheless expected to provide a promising source of linkages which may be dynamically balanced in the future.

In relation to the literature

Although it is impossible to relate the current work to the full width of the literature on dynamic balance, several observations can be made. The first point is a comparison of the algebraic dynamic balance methods [74, 75, 76] with the methods in this thesis. These algebraic methods have proven successful in obtaining the essential kinematic conditions for planar and spherical four-bar linkages, of which the spherical variant turned out not to be 'balanceable'. With the methods in this thesis it is not yet possible to obtain these essential kinematic conditions. The algebraic methods on the other hand did not produce an intuitive description of design space and required a tailored treatment of different single DOF linkages. As stated earlier, a natural next step would be to combine the higher-order balancing method with these algebraic methods to enable a systematic study of essential kinematic conditions of multi-DOF linkages.

The linearly independent vector method [15] and derived analysis methods [10, 60, 124] provide a simple set of conditions for force balance, although being too strict in special cases [43]. For the higher-order dynamic balance method, generality, completeness and moment balance of spatial mechanism come at the cost of mathematical transparency. Although a part of this complexity seem to be inherent in the dynamics of spatial mechanisms with multiple DOF, the multipole-rod representation of the inertial parameters and partitioning accord-

ing the joint topology recovered some of the interpretation which is essential from a designer's point of view.

Lastly, several systemic synthesis methods have been presented in the past. Among these, the method of principal vector linkages has resulted in a wide variety of force balanced planar linkages [107, 100] and several force balanced spatial linkages [101, 102]. Systematic moment balance, on the other hand, seems to require a different approach [96], as Chapter 2 confirms. This thesis did not present a full synthesis method but explores the prerequisites of such a method. It shows that synthesis through stacking requires dynamically decoupled modules. That means that, beside dynamic balance, also a constant total moments of inertia is required. It shows furthermore that synthesis through kinematically tracing the dynamic balance conditions, as done in the force balance methods, will either enforce more conditions then necessary, will require complex nonholonomic tracing mechanisms or will work only for a specific class of linkages. As a consequence, the Chapter 3, 5, and 6 were aimed at retrieving the nature of the essential kinematic conditions which resulted in two symmetric dynamically balanced 2-DOF linkages. A systematic study of these essential kinematic conditions is expected to pave the way for new systematic synthesis methods.

7.2 Future of dynamic balance

This thesis is confined to theoretical methods with the aim of finding new dynamically balanced mechanisms that have low complexity, mass and inertia. Yet there are more hurdles to be tackled before dynamic balance can fulfil its promise and advance high-precision, high-speed robots to the factory floor.

Towards practice

A common assumption in the dynamic balance literature is that all robot links are perfectly rigid, while the base frame is the sole source of vibrations. In practice, however, the robot links are not rigid and will deflect, causing internal vibrations and a loss of precision of the robot. Furthermore, the eigenfrequencies associated with these vibrations limit the controller bandwidth and thereby the performance of the robot. The addition of countermasses, as typically used in dynamic balance, is likely to lower these eigenfrequencies, compromising the performance of the system. Currently it is not clear how these conflicting effects of dynamic balance are to be harmonized. The little existing literature on this topic focuses on machines with fixed input speeds and is confined mainly to the time domain [113, 123, 128], with notable exceptions of [71, 72]. Recently, we published a preliminary frequency domain study of a 2-DOF planar manipulator with non-rigid, realistic link stiffnesses [30]. Two opposing effects became apparent: 1) a strong reduction of the shaking forces in the frequency domain below the first eigenfrequency, and 2) a lowering of first parasitic eigenfrequence and controller bandwidth due to the added mass. An optimal mass distribution was found that allows for a reduction of the shaking forces in the low-frequency region without compromising controller bandwidth. Further investigation of this topic is crucial, so as to tailor dynamic balance to practical applications.

Another assumption is that dynamically balanced mechanisms are also dynamically decoupled, and thus behave as a single rigid body while emitting zero vibrations. Chapter 2 shows that dynamic balance is a necessary but not a sufficient condition for dynamic decoupling; also a constant total moment of inertia of the mechanism is required. This means that it is in principle possible to aggravate existing rotational base vibrations by specific motion of a dynamically balanced mechanism. Yet, in practice, when the mechanism is fixed to a sufficiently stiff base frame, these vibrations are expected to be of minor significance when compared to the elimination of shaking moments due to dynamic balance and the remaining internal vibrations.

Other practical effects such as a varying payload [103, 26] parameter uncertainty [109], and backlash [14] have also received limited attention in literature. It is likely that this will result in some deviation from perfect balance, but by how much, and under what conditions? A study of these practical aspects may yield insight into the efficacy of, and novel design criteria for dynamically balanced robots.

This thesis reaffirms that dynamic balance by design of the mass distribution requires a very specific choice of robot kinematics. More solutions are expected by further study of dynamic balance, yet it is unlikely that after the long history of research, a multitude of dynamically balanced robots will be found that do not require some form of additional counter-structures. Some specific applications which are in nature symmetric, such as gripping, might profit from new synthesis techniques. For other non-symmetric applications, such as pick-and-place, passive or active counter-acting mechanisms might be indispensable [125, 19, 108, 105]. Nevertheless, a complete inventory of all dynamically balanced solutions, as supplied through the methods in this thesis, potentially enables designs that have a minimal amount of counter-acting elements, leading to more practical designs.

In most practical applications, a reduction of the shaking forces and moments suffices. Optimal dynamic balance strategies try to combine the best of both worlds by relaxing the exact dynamic balance conditions in a trade-off for lower motor torques, lower bearing loads, higher controller bandwidth or lower total mass. For this optimization to work, representative trajectories, starting values, boundary conditions, solvers and weighting factors between the objectives have to be chosen. Typically, also the kinematic structure and its geometry are chosen prior to the optimization. These initial choices on the kinematics directly limit the optimization potential, as certain kinematics are more suitable for dynamic balance than others. The results and intuition from exact dynamic balancing, such as treated in this thesis, may aid these choices and form a starting point for the optimization procedure. The higher-order approach as presented in Chapter 5 can potentially be extended to include optimality conditions. This would allow for a systematic weighting of poses, velocities and accelerations, making it less dependent on the trajectory choice, while retaining some intuition of the solution space.

A judicious weighting of shaking forces and shaking moments is indispensable for optimal dynamic balance. However, it is not directly clear how these translational and rotational domains relate to each other and to the effect-

iveness of the robot. For a case study on a Delta-like robot, we proposed to quantify dynamic balance based on the floor contact forces and end-effector accuracy by taking the geometry and stiffness of the base frame of the robot into account [27]. The results show that force balance only slightly improved these measures. The reason was found to be that, depending on the trajectory and frame-design, the shaking moments are the dominant source of vibrations. Therefore, a combined treatment of the shaking forces and moments and physically meaningful weighting factors are essential for the effectiveness of optimal dynamic balance.

Recommendation for further research

The recommendations for future research, as discussed so far, may be grouped into two research branches. One branch leads towards a systemic, exact dynamic balance method through synthesis, while the other branch of research guides dynamic balance towards practical implementation.

1. In this vision, a future synthesis method will grant robot designers with the guidelines to design effective and low-cost balancing solutions. By considering dynamic balance at the beginning a range of suitable mechanisms might be synthesized through an intuitive manipulation and recombination of elements, such that the most promessing one can be selected for detailing. Alternatively, such a synthesis method would a starting point for optimal balancing techniques and further the other branch, the practical implementation. To derive such a synthesis method more insight is needed into the essential kinematic conditions, as identified previously. Currently it not known what types of spatial mechanisms exhibit a feasible design space. The higher-order balancing method as presented in in this thesis might form a fruitful starting point. On the one hand, algebraic methods can be applied to isolate the essential kinematic conditions. On the other hand, a range of mechanisms can be quickly tested for balancablity and therewith build a library such mechanisms. One lead for this, as identified in this thesis, is mirror symmetry. The limited number of examples in this thesis confirm that symmetry has balancing potential, but also that it is not the only ingredient. Once the essential kinematic conditions become more palpable it is likely that new synthesis procedures follow suit.

2. In order to move dynamic balance towards practice, it is essential to identify the expected yield of dynamic balance in terms of end-effector precision and reduction of floor vibration. This requires the investigation the effects that appear in implementation, such as robot rigidity, frame design, play, tolerances, payload etc. It is therefore desired to design several representative demonstrators that no only show the reduction of shaking forces and moments, but also the effect on end-effector precision and floor vibrations. This might lead to new design heuristics and proofs of the effectiveness of dynamic balance of robots. Optimal dynamic balance techniques such as presented in [36, 111], provides an appropriate framework to weigh the design criteria and include expected effects of implementation into the design process.

7.3 Design through model inversion

Stepping away from dynamic balance, it can be seen that some of the methods in this thesis are applicable to other design problems. Modern day design processes, such as controller design or mechanical design, typically follow a design-model-evaluate-iterate paradigm. In this process an initial design is modelled, simulated and evaluated using mathematical models, such as FEM. If the design does not satisfy the design criteria, the design is changed and the process is repeated. Typically this new design is based on experience and heuristics. If the designer is lucky, the model provides some clues on how to improve the design. Optimization software automates this process by introducing a feedback loop, thereby requiring a properly defined design criterion and boundary conditions as well as a large number of evaluations. Another approach, also used for dynamic balance, is the reversal of this design process by inverting the model, or at least by making the model more transparent. In this thesis, for example, the higher-order derivatives of the dynamic model were used to extract necessary, sufficient and solvable conditions on the inertial parameters of a mechanism. This model inversion can potentially be extended to other related fields that have exact design criteria. For example, the design of statically balanced mechanisms [46] or of approximate path mechanisms [12] might benefit. By including elasticity [48] into the higher-order derivatives, this method might be applied to the design of flexure mechanisms and the control of robotic systems.

Chapter 8

Conclusion

This thesis presents two analysis methods to strengthen the mathematical basis of dynamic balance and one method working towards dynamic balance through synthesis. The first method unifies force and moment balance and provides a uniform description and interpretation of spatial dynamics through screw theory. The second method deals with the intrinsic algebraic complexity of kinematic equations by using higher-order derivatives of dynamic balance conditions. This yielded a complete description of dynamically balanced mass distributions for any given nonsingular linkage. Finding the kinematics that are favourable for dynamic balance is the aim of the third method. This method exploits and balances a specific class of kinematics, the planar symmetric subspace motion generators.

8.1 Instantaneous dynamic balance

In the first method, screw theory allowed for the the combined treatment of force and moment balance. This spatial method provides a geometrical and graphical interpretation of the dynamic balance conditions for arbitrary linkages without requiring the finite solution to the loop-closure equations. Furthermore, it provides a range of mass distributions that are necessary but not sufficient for the dynamic balance. These mass distributions result in pose that is instantaneously dynamically balanced. When the mechanism is placed in such a pose, the acceleration will yield no shaking forces or moments. Moving away from this pose, the dynamic balance quality reduces. It is shown that, in conjunction with path balance, these poses form an intersection of multiple reactionless paths.

This resulted in a 2-DOF planar mechanism, the Fuga I, which is force balanced over the complete workspace and moment balanced over two perpendicularly intersecting lines. A demonstrator showed a shaking moments reduction in the order of 95 % in comparison to a non-moment balanced trajectory. Force balance showed an equal quality when comparing the bearing forces with the shaking forces. The residual shaking forces and moments are attributed to practical implementations such as measurement noise, design tolerances and controller errors.

8.2 Higher-order dynamic balance

The second method, extends dynamic balance over the workspace by satisfying a sufficient number of higher-order derivatives of the momentum equations. It is conjectured this method thereby provides the complete design space of dynamically balanced inertial parameters of any given nonsingular linkage. These higher-order derivatives of the dynamic balance conditions were found by a screw theory-based algorithmic treatment that consist solely of matrix operations. The inertial parameters of the links are linear in these conditions, such that the complete dynamically balanced design space could be extracted by a nullspace operation. To retain design intuition, a systematic partitioning of the resulting design space was provided together with its multipole-rod interpretation. For serial mechanisms the dynamically balanced design space permits a partitioning associated to each joint, i.e. each joint in the chain adds design freedoms according to its type and its alignment with respect to previous joints in the chain. Six types of design spaces completely determine all types of serial linkages. For serial mechanisms this design space always includes zero or negative moments of inertia, necessitating counter-mechanisms for implementation.

As parallel linkages may be regarded as a set of connected serial linkages, the previously identified design space for serial linkages is valid also for parallel linkages. In the case of general parallel linkages, this design space — associated to the serial chains into which the parallel linkages can be decomposed — is the complete design space. However, in specific kinematic cases, such as kinematic mirror symmetry, an additional solution space opens up. This enlarged design freedom reduces the number of (or even eliminating the need for) counter-rotations required to implement dynamic balance. This enables designs that are potentially more light-weight and economically viable. As an example, a 3-RSR mechanism was presented that is dynamically balanced over 2-DOF motion on three planes of symmetry, indicating the possibilities of this method.

The basis for this higher-order dynamic balance method lies in the higher-order derivatives of the kinematics of serial and parallel linkages, as presented in Chapter 4. There an algorithm was presented that, for the first time, yields derivatives up to arbitrary order of different types of forward or inverse kinematic mappings. This method relies on recursively applying the implicit function theorem to arrive at a local solution to the loop-closure constraint equations. It enabled a Taylor-based motion approximation of arbitrary linkages, as shown by the examples of a serial 6-DOF robot, a planar five-bar mechanisms and the overconstrained Bennett linkage.

8.3 Symmetric and pure inertia mechanisms

These two dynamic balance methods give the, or a part of the, dynamic balance solution for a given mechanism but not tell which mechanisms are favourable for dynamic balance. The aim of the third dynamic balance method was to provide such clues and find mechanisms that can be dynamically balanced by sole design of the mass distribution. It was observed that several dynamically balanced mechanisms from literature share kinematic mirror symmetry. In the case of

the planar crank-slider linkage ($3RP$) and the planar four-bar linkage ($4R$) the essential kinematic conditions — required for dynamic balance — result in a linear relation between the angular velocity of the links. Therefore, these linkages are dynamically balanced when the links are chosen to be dynamically equivalent to pure moments of inertia. These insights on kinematic symmetry and the pure moment of inertia equivalent led to the development of a novel dynamically balanced 2-DOF planar manipulator.

8.4 Overarching conclusions

The three proposed dynamic balance methods provide the means and directions in the search for new dynamically balanced mechanisms. On the one hand, this thesis presents a method that computes the complete dynamically balanced design space for arbitrary linkages, being planar or spatial, open or closed loop linkages. This allows for a systematic check of whether a mechanism can be dynamically balanced by design of the mass distribution, i.e. without the need for counter-mechanisms. On the other hand, this thesis reaffirms that the kinematic choices dictate whether a mechanism can be dynamically balanced. Up to now it remains unknown what the exact nature of these essential kinematic conditions are. Nevertheless, the intuition that kinematic symmetry provides novel possibilities is strengthened by two novel dynamically balanced mechanisms that rely on symmetry. The combined use of the presented methods unlocks a systematic investigation into the nature of the essential kinematic conditions, which is of the utmost importance for the development of new dynamically balanced mechanisms.

Appendix A

Multivariate matrix derivatives using Kronecker product

The higher-order partial derivatives of matrices are managed in this thesis with the use of the Kronecker product [112]. In this appendix the Kronecker product notation and some elementary properties are listed along with the application to the bookkeeping of the higher-order partial derivatives. The differences between the sequence $(\mathrm{D}^k_{\boldsymbol{x}}(\boldsymbol{A}))$ and the collection $(\mathrm{D}^{\boldsymbol{\alpha}}_{\boldsymbol{x}}(\boldsymbol{A}))$ of higher-order partial derivatives are highlighted.

A.1 Kronecker product

The Kronecker product is defined as the collection of the element-wise multiplication of all elements in the respective matrices. Consider the following set of matrices: $\boldsymbol{A} \in \mathbb{R}^{n\times m}, \boldsymbol{B} \in \mathbb{R}^{p\times q}$

$$\boldsymbol{A} \otimes \boldsymbol{B} = \begin{bmatrix} a_{11}\boldsymbol{B} & \dots & a_{1m}\boldsymbol{B} \\ \vdots & \ddots & \vdots \\ a_{n1}\boldsymbol{B} & \dots & a_{nm}\boldsymbol{B} \end{bmatrix} \tag{A.1}$$

The mixed-product property is used to recombine normal matrix products and Kronecker products

$$(\boldsymbol{AB}) \otimes (\boldsymbol{CD}) = (\boldsymbol{A} \otimes \boldsymbol{C})(\boldsymbol{B} \otimes \boldsymbol{D}) \tag{A.2}$$

A sequence of the Kronecker product is swapped with pre- and postmultiplication of permutation matrices

$$\boldsymbol{A} \otimes \boldsymbol{B} = \boldsymbol{P}_{p,n}\boldsymbol{B} \otimes \boldsymbol{A}\boldsymbol{P}_{m,q} \tag{A.3}$$

These permutation matrices $\boldsymbol{P}_{n,m}$ are binary, orthogonal, square $nm \times nm$ matrices consisting of $m \times n$ sub-matrices. These sub-matrices $(\boldsymbol{P}^{i,j}_{n,m} \in \mathbb{N}^{m\times n})$ have only one 1 on a specific location $(\boldsymbol{P}^{i,j}_{n,m}(j,i) = 1)$

$$\boldsymbol{P}_{n,m} = \begin{bmatrix} \boldsymbol{P}^{1,1}_{n,m} & \dots & \boldsymbol{P}^{1,n}_{n,m} \\ \vdots & \ddots & \vdots \\ \boldsymbol{P}^{m,1}_{n,m} & \dots & \boldsymbol{P}^{m,n}_{n,m} \end{bmatrix} \tag{A.4}$$

The vectorization of matrix products is written by means of the Kronecker product

$$\mathrm{vec}(\boldsymbol{ABC}) = (\boldsymbol{C}^\top \otimes \boldsymbol{A})\mathrm{vec}(\boldsymbol{B}) \tag{A.5}$$

A.2 Collection of the higher-order partial derivatives

The collection of partial derivatives of a given vector $\boldsymbol{a}$ with respect to $\boldsymbol{x} \in \mathbb{R}^r$ are organized according to

$$\mathrm{D}_{\boldsymbol{x}}(\boldsymbol{a}) = \begin{bmatrix} \dfrac{\partial}{\partial x_1}(\boldsymbol{a}) & \cdots & \dfrac{\partial}{\partial x_r}(\boldsymbol{a}) \end{bmatrix} \tag{A.6}$$

The higher partial derivatives of vectors follow the same ordering

$$\mathrm{D}_{\boldsymbol{x}}(\mathrm{D}_{\boldsymbol{x}}(\boldsymbol{a})) = \begin{bmatrix} \mathrm{D}_{\boldsymbol{x}}\left(\dfrac{\partial}{\partial x_1}(\boldsymbol{a})\right) & \cdots & \mathrm{D}_{\boldsymbol{x}}\left(\dfrac{\partial}{\partial x_r}(\boldsymbol{a})\right) \end{bmatrix} \tag{A.7}$$

in which the i-th element is

$$\mathrm{D}_{\boldsymbol{x}}\left(\frac{\partial}{\partial x_i}(\boldsymbol{a})\right) = \begin{bmatrix} \dfrac{\partial}{\partial x_1}\dfrac{\partial}{\partial x_i}(\boldsymbol{a}) & \cdots & \dfrac{\partial}{\partial x_r}\dfrac{\partial}{\partial x_i}(\boldsymbol{a}) \end{bmatrix} \tag{A.8}$$

This is extended to the partial derivatives of a matrix $\boldsymbol{A} = \begin{bmatrix} \boldsymbol{a}_1 & \cdots & \boldsymbol{a}_m \end{bmatrix}$, which are organized according

$$\mathrm{D}_{\boldsymbol{x}}(\boldsymbol{A}) = \begin{bmatrix} \mathrm{D}_{\boldsymbol{x}}(\boldsymbol{a}_1) & \cdots & \mathrm{D}_{\boldsymbol{x}}(\boldsymbol{a}_m) \end{bmatrix}, \tag{A.9}$$

$$\mathrm{D}^2_{\boldsymbol{x}}(\boldsymbol{A}) = \mathrm{D}_{\boldsymbol{x}}(\mathrm{D}_{\boldsymbol{x}}(\boldsymbol{A})) = \begin{bmatrix} \mathrm{D}^2_{\boldsymbol{x}}(\boldsymbol{a}_1) & \cdots & \mathrm{D}^2_{\boldsymbol{x}}(\boldsymbol{a}_m) \end{bmatrix} \tag{A.10}$$

$$\mathrm{D}^k_{\boldsymbol{x}}(\boldsymbol{A}) = \begin{bmatrix} \mathrm{D}^k_{\boldsymbol{x}}(\boldsymbol{a}_1) & \cdots & \mathrm{D}^k_{\boldsymbol{x}}(\boldsymbol{a}_m) \end{bmatrix} \tag{A.11}$$

This may be extended in a similar manner to arbitrary order.

A.3 Sequences of higher-order partial derivatives

A sequence of higher-order partial derivatives is denoted with a vector in the superscript $\mathrm{D}^{\boldsymbol{\alpha}}_{\boldsymbol{x}}(\boldsymbol{A}) = \partial^k/(\partial x_1^{\alpha_1} \cdots \partial x_n^{\alpha_n})$. Consider for example the following sequence of partial derivatives

$$\frac{\partial}{\partial x_1}\frac{\partial^3}{\partial x_2^3}\frac{\partial^2}{\partial x_5^2}(\boldsymbol{A}) = \mathrm{D}^{\boldsymbol{\alpha}}_{\boldsymbol{x}}(\boldsymbol{A}) \qquad \text{with} \qquad \boldsymbol{\alpha} = [1, 3, 0, 0, 2] \tag{A.12}$$

The $\boldsymbol{\alpha}$-vector is an ordered multi-index corresponding to $\boldsymbol{x}$. The total order of this sequence is given by $\sum_i \alpha_i = |\boldsymbol{\alpha}|$. These sequences of higher-order partial derivatives clearly form the elements (rows and submatrices) of the collection of higher-order partial derivatives $\mathrm{D}^k_{\boldsymbol{x}}(\boldsymbol{A})$, i.e. $\mathrm{D}^k_{\boldsymbol{x}}(\boldsymbol{A})$ is formed by all sequences of $\boldsymbol{\alpha}$ for which $|\boldsymbol{\alpha}| = k$.

A.4 Partial derivatives of the matrix-vector product

The partial derivatives of a matrix-vector product with $\boldsymbol{b} \in \mathbb{R}^m$ become

$$\mathrm{D}_{\boldsymbol{x}}(\boldsymbol{Ab}) = \left[\frac{\partial}{\partial x_1} (\boldsymbol{Ab}) \quad \dots \quad \frac{\partial}{\partial x_r} (\boldsymbol{Ab}) \right] \tag{A.13}$$

in which the i-th column is

$$\frac{\partial}{\partial x_i} (\boldsymbol{Ab}) = \frac{\partial}{\partial x_i} (\boldsymbol{a_1}) \, b_1 + \ldots + \frac{\partial}{\partial x_i} (\boldsymbol{a_m}) \, b_m, \tag{A.14}$$

$$= \left[\frac{\partial}{\partial x_i} (\boldsymbol{a_1}) \quad \dots \quad \frac{\partial}{\partial x_i} (\boldsymbol{a_m}) \right] \boldsymbol{b} \tag{A.15}$$

In order to comply with the ordering of Eq. A.9 the multiplications have to be arranged, such that

$$\mathrm{D}_{\boldsymbol{x}}(\boldsymbol{Ab}) = \begin{bmatrix} \mathrm{D}_{\boldsymbol{x}}(\boldsymbol{a}_1) & \cdots & \mathrm{D}_{\boldsymbol{x}}(\boldsymbol{a}_m) \end{bmatrix} \begin{bmatrix} b_1 \boldsymbol{I}_r \\ \vdots \\ b_m \boldsymbol{I}_r \end{bmatrix} = \mathrm{D}_{\boldsymbol{x}}(\boldsymbol{A}) \, (\boldsymbol{b} \otimes \boldsymbol{I}_r) \tag{A.16}$$

in which $\boldsymbol{I}_r$ is the $r \times r$ identity matrix.

A.5 Matrix derivative relations

This leads to following matrix derivatives entities:
Product rule of $\boldsymbol{A}(\boldsymbol{x}) \in \mathbb{R}^{n \times m}$, $\boldsymbol{B}(\boldsymbol{x}) \in \mathbb{R}^{m \times q}$ and $\boldsymbol{x} \in \mathbb{R}^r$

$$\mathrm{D}_{\boldsymbol{x}}(\boldsymbol{AB}) = \mathrm{D}_{\boldsymbol{x}}(\boldsymbol{A}) \, (\boldsymbol{B} \otimes \boldsymbol{I}_r) + \boldsymbol{A} \mathrm{D}_{\boldsymbol{x}}(\boldsymbol{B}) \tag{A.17}$$

Chain rule of $\boldsymbol{A}(\boldsymbol{b}(\boldsymbol{c}))$ with nested variables $\boldsymbol{b}$ and $\boldsymbol{c}$

$$\mathrm{D}_{\boldsymbol{c}}(\boldsymbol{A}(\boldsymbol{b}(\boldsymbol{c}))) = \mathrm{D}_{\boldsymbol{b}}(\boldsymbol{A}) \, (\boldsymbol{I}_m \otimes \mathrm{D}_{\boldsymbol{c}}(\boldsymbol{b})) \tag{A.18}$$

Derivatives of the Kronecker product

$$\mathrm{D}_{\boldsymbol{x}}(\boldsymbol{A} \otimes \boldsymbol{B}) = (\mathrm{D}_{\boldsymbol{x}}(\boldsymbol{A}) \otimes \boldsymbol{B})(\boldsymbol{I}_m \otimes \boldsymbol{P}_{q,r}) + \boldsymbol{A} \otimes \mathrm{D}_{\boldsymbol{x}}(\boldsymbol{B}) \tag{A.19}$$

Derivative of matrix inversion

$$\mathrm{D}_{\boldsymbol{x}}\left(\boldsymbol{A}^{-1}\right) = -\boldsymbol{A}^{-1} \mathrm{D}_{\boldsymbol{x}}(\boldsymbol{A}) \, (\boldsymbol{A}^{-1} \otimes \boldsymbol{I}_r) \tag{A.20}$$

A recursive application of these equations allow for the extension of these derivatives up to arbitrary order.

A

Nomenclature

Abbreviations

COM	Centre of mass
DOF	Degree of freedom
FK	Forward kinematic model
IK	Inverse kinematic model
IMW	Instantaneous momentum wrench
ISA	Instantaneous screw axis
MOI	Second moment of inertia

Joint types

H	Helical joint
P	Prismatic joint
R	Revolute joint
S	Spherical joint

Mathematical notation

x	Scalar
$\boldsymbol{x}$	Vector
$\boldsymbol{X}$	Matrix
x	Function
$\bullet \times \bullet$	Cross product
$[\bullet, \bullet]$	Lie bracket
$\bullet \otimes \bullet$	Kronecker product
$\bullet \circ \bullet$	Element wise product
$\bar{\bullet}$	Collection of vectors or matrices
$\tilde{\bullet}$	Matrix aggregation
$\hat{\bullet}$	Normalized vector

$\check{\bullet}$	Vector appended with a one
$\dot{\bullet}$	First derivative with of $\bullet$ respect to time
$\ddot{\bullet}$	Second derivative with of $\bullet$ respect to time
$\bullet^\top$	Transpose
$\bullet^{-1}$	Matrix inverse
$\bullet^+$	Left pseudo inverse
$\bullet^{\circ 2}$	Element wise quadratic
$\bullet^{\otimes n}$	Kronecker product to the power n
$\bullet^\perp$	Null space basis
$\| \bullet \|$	Euclidean norm
$\left[\bullet\times\right]$	Skew symmetric matrix
$\left[\bullet*\right]$	Regression matrix of the parameter-linear form
$\frac{\partial}{\partial x}(\bullet)$	Partial derivative with respect to x
$\mathrm{D}^{\boldsymbol{\alpha}}_{\boldsymbol{x}}(\bullet)$	Mixed higher partial derivative with respect to $\boldsymbol{x}$ with corresponding multi-index $\boldsymbol{\alpha}$ to encode the order
$\mathrm{D}^{k}_{\boldsymbol{x}}(\bullet)$	Collection of higher partial derivatives with respect to $\boldsymbol{x}$ of order k
$\mathrm{ad}(\bullet)$	Adjoint representation of a twist
$\mathrm{Ad}(\bullet)$	Adjoint representation of a transformation matrix
$\mathrm{diag}(\bullet)$	Diagonal matrix form of a vector
$\ker(\bullet)$	Null space of $\bullet$
$\mathrm{vec}(\bullet)$	Vectorization of a matrix

Latin symbols

a	Point mass redistribution parameters
d	Distance
e	Error
g	Moment of inertia taken at the COM
g'	Pure moment of inertia
g_i	Principal moment of inertia around the i-th principal axis, taken at the COM
g_{ij}	Moment of inertia or product of inertia taken at the COM

k	Order of derivative
$k_{\max}$	Maximum order of derivative
km	Solution to the loop-closure constraint equation (kinematic model)
l	Length
lc	Loop closure constraint equation
m	Mass
q	Joint coordinate
t	Time
x	End-effector coordinate in x-direction
y	End-effector coordinate in y-direction
$\boldsymbol{a}$	Auxiliary point or vector
$\boldsymbol{b}$	Auxiliary point or vector
$\boldsymbol{c}$	Centre of mass
$\boldsymbol{d}$	Dependent coordinates
$\boldsymbol{e}$	Vector collection of the moments of inertia and products of inertia around the origin of the reference frame
$\boldsymbol{f}$	Force
$\boldsymbol{g}$	Principal moments of inertia vector
$\boldsymbol{h}$	Momentum wrench
$\hat{\boldsymbol{h}}_{i,j}$	Unit momentum wrench generated body i due to unit actuation of DOF j
$\boldsymbol{n}$	Unit vector and joint axis
$\boldsymbol{o}$	Origin of reference frame or reference point
$\boldsymbol{p}$	Linear momentum
$\boldsymbol{q}$	Vector of joint coordinates
$\boldsymbol{r}$	Auxiliary point or vector
$\boldsymbol{r}$	Total set of coordinates (Chaper 4 only)
$\boldsymbol{s}$	Instantaneous screw axis
$\boldsymbol{t}_i^{j,k}$	Twist of frame i with respect to frame j expressed in frame k
$\hat{\boldsymbol{t}}_{i,j}$	Unit twist of frame i due to unit actuation of DOF j
$\boldsymbol{u}$	Independent coordinates

$\boldsymbol{v}$	Velocity of the origin of the reference frame (linear velocity)
$\mathbf{w}$	Wrench
$\boldsymbol{x}$	End-effector coordinates
$\boldsymbol{y}$	Vector of design parameters of dynamically balanced designs
$\boldsymbol{z}$	Parameter-linear form of the mass matrix
K	Kinetic energy
P	Power
$\boldsymbol{A}$	Auxiliary matrix
$\boldsymbol{B}$	Auxiliary matrix
$\boldsymbol{C}$	Solution to the differential loop-closure constraints or loop-closure Jacobian
$\boldsymbol{E}$	Moment of inertia inertia tensor taken at the origin of the reference frame
$\boldsymbol{F}$	Collection of higher-order derivatives of the loop-closure equation
$\boldsymbol{G}$	Moment of inertia inertia tensor taken at the COM
$\boldsymbol{H}_i^j$	Transformation matrix of expressing frame i in frame j
$\boldsymbol{I}_n$	Identity matrix of size n
$\boldsymbol{J}$	Jacobian
$\boldsymbol{K}$	Differential loop-closure constraints
$\boldsymbol{L}$	Collection of precursory higher-order derivatives of the solution to the loop-closure equation
$\boldsymbol{M}$	Mass matrix
$\boldsymbol{M}_\mathrm{B}$	Momentum basis in minimal coordinates
$\boldsymbol{N}$	Null space basis of dynamically balanced inertial parameters
$\boldsymbol{N}_\mathrm{P}$	Null space basis vectors associated to the loop-closure
$\boldsymbol{N}_\mathrm{S}$	Null space basis of the equivalent serial chain
$\boldsymbol{N}_{0,\nparallel}$	Inertia transfer matrix of a revolute joint which is not parallel to all non-prismatic joints lower in the chain
$\boldsymbol{N}_{0,\parallel}$	Inertia transfer matrix of a revolute joint which is parallel to all non-prismatic joints lower in the chain
$\boldsymbol{N}_{\infty,\nparallel}$	Inertia transfer matrix of a helical joint which is not parallel to all non-prismatic joints lower in the chain

$\boldsymbol{N}_{\infty,\parallel}$ Inertia transfer matrix of a prismatic joint which is parallel to all non-prismatic joints lower in the chain

$\boldsymbol{N}_{\mathrm{f},\nparallel}$ Inertia transfer matrix of a helical joint which is not parallel to all non-prismatic joints lower in the chain

$\boldsymbol{N}_{\mathrm{f},\parallel}$ Inertia transfer matrix of a helical joint which is parallel to all non-prismatic joints lower in the chain

$\boldsymbol{Q}$ Higher-order derivative of the solution to the loop-closure constraint equation

$\boldsymbol{R}$ Rotation matrix

$\boldsymbol{T}$ Basis of the test space

$\boldsymbol{U}$ Jacobian of the loop-closure constraint equation with respect to the independent coordinates

$\boldsymbol{V}$ Jacobian of the loop-closure constraint equation with respect to the dependent coordinates

$\boldsymbol{W}$ Regression matrix of the equivalent serial chain

$\boldsymbol{X}$ Regression matrix of parallel mechanisms

Greek symbols

α Auxiliary variable

β Auxiliary angle

γ Auxiliary angle

δ Displacement

η Pure-inertia rod

θ Auxiliary angle

λ Pitch of a screw

ϕ Auxiliary angle

ψ Reference frame

$\boldsymbol{\alpha}$ Ordered multi-index

$\boldsymbol{\sigma}$ Actuation torque/force

$\boldsymbol{\xi}$ Angular momentum

$\boldsymbol{\xi}_c$ Angular momentum due to a pure rotation around the COM

$\boldsymbol{\tau}$ Moment

$\boldsymbol{\omega}$ Angular velocity

Π Symmetric plane

Bibliography

[1] S. K. Agrawal and A. Fattah. Reactionless space and ground robots: novel designs and concept studies. *Mechanism and Machine Theory*, 39(1):25–40, Jan. 2004.

[2] V. Arakelian, M. Dahan, and M. Smith. A historical review of the evolution of the theory on balancing of mechanisms. In *International Symposium on History of Machines and Mechanisms Proceedings HMM 2000*, pages 291–300, 2000.

[3] V. Arakelian and S. Sargsyan. On the design of serial manipulators with decoupled dynamics. *Mechatronics*, 22(6):904–909, Sept. 2012.

[4] V. H. Arakelian and M. R. Smith. Erratum: "Shaking Force and Shaking Moment Balancing of Mechanisms: A Historical Review With New Examples". *Journal of Mechanical Design*, 127(5):1034–1035, 2005.

[5] V. H. Arakelian and M. R. Smith. Shaking Force and Shaking Moment Balancing of Mechanisms: A Historical Review With New Examples. *Journal of Mechanical Design*, 127(2):334–338, 2005.

[6] C. Bagci. Shaking force balancing of planar linkages with force transmission irregularities using balancing idler loops. *Mechanism and Machine Theory*, 14(4):267–284, 1979.

[7] C. Bagci. Complete Shaking Force and Shaking Moment Balancing of Link Mechanisms Using Balancing Idler Loops. *Journal of Mechanical Design*, 104(2):482–493, 1982.

[8] C. Bagci. Complete balancing of linkages using complete dynamical equivalents of floating links: CDEL method. In *Proceedings of the Flexible Mechanisms, Dynamics, and Analysis*, pages 477–488, 1992.

[9] J. E. Baker. The Bennett, Goldberg and Myard linkages — in perspective. *Mechanism and Machine Theory*, 14(4):239–253, 1979.

[10] S. Balasubramanian and C. Bagci. Design equations for the complete shaking force balancing of 6R 6-bar and 6-bar slider-crank mechanisms. *Mechanism and Machine Theory*, 13(6):659–674, 1978.

[11] R. S. Ball. *A treatise on the theory of screws*. Cambridge University Press, UK, Cambridge, 1900.

[12] R. Bartkowiak and C. Woernle. Necessary and sufficient mobility conditions for single-loop overconstrained nH mechanisms. *Mechanism and Machine Theory*, 103:65–84, 2016.

[13] G. T. Bennett. A new mechanism. *Engineering*, 76(12):777–778, 1903.

[14] R. S. Berkof. Complete force and moment balancing of inline four-bar linkages. *Mechanism and Machine Theory*, 8(3):397–410, 1973.

[15] R. S. Berkof and G. G. Lowen. A new method for completely force balancing simple linkages. *Journal of Engineering for Industry*, 91(1):21–26, 1969.

[16] I. Bonev. *Geometric analysis of parallel mechanisms.* PhD thesis, Université Laval, Canada, 2003.

[17] S. Briot and V. Arakelian. Complete shaking force and shaking moment balancing of in-line four-bar linkages by adding a class-two RRR or RRP Assur group. *Mechanism and Machine Theory*, 57:13–26, Nov. 2012.

[18] S. Briot, V. Arakelian, and J.-P. Le Baron. Shaking force minimization of high-speed robots via centre of mass acceleration control. *Mechanism and Machine Theory*, 57:1–12, Nov. 2012.

[19] S. Briot, I. A. Bonev, C. M. Gosselin, and V. Arakelian. Complete shaking force and shaking moment balancing of planar parallel manipulators with prismatic pairs. In *Proceedings of the Institution of Mechanical Engineers, Part K: Journal of Multi-body Dynamics*, volume 223, pages 43–52, Mar. 2009.

[20] R. W. Brockett. Robotic manipulators and the product of exponentials formula. *Mathematical Theory of Networks and Systems SE - 9*, 58:120–129, 1984.

[21] M. Carricato and C. M. Gosselin. A Statically Balanced Gough/Stewart-Type Platform: Conception, Design, and Simulation. *Journal of Mechanisms and Robotics*, 1(3):031005, 2009.

[22] C. Chen. The order of local mobility of mechanisms. *Mechanism and Machine Theory*, 46(9):1251–1264, 2011.

[23] N. X. Chen. The complete shaking force balancing of a spatial linkage. *Mechanism and Machine Theory*, 19(2):243–255, 1984.

[24] A. Codourey and E. Burdet. A Body-oriented Method for Finding a Linear Form of the Dynamic Equation of Fully Parallel Robots. In *International Conference on Robotics and Automation, Albuquerque*, number April, pages 1612–1618, 1997.

[25] J.-F. Collard and C. M. Gosselin. Optimal Synthesis of a Planar Reactionless Three-Degree-of-Freedom Parallel Mechanism. *Journal of Mechanisms and Robotics*, 3(4):041009, 2011.

[26] J. J. de Jong and J. L. Herder. A comparison between five principle strategies for adapting shaking force balance during varying payload. In *14th IFToMM World Congress in Mechanism and Machine Science*, pages 25–30, 2015.

[27] J. J. de Jong, J. P. Meijaard, and V. van der Wijk. The influence of partial force balancing on the shaking moments, contact forces, and precision of a delta robot-Like manipulator in a compliant frame. In *Proceedings 2018 ASME IDETC/CIE*, pages 1–7, 2018.

[28] J. J. de Jong, A. Müller, and J. L. Herder. Higher-order Taylor approximation of finite motions in mechanisms. *Robotica*, 37(7):1190–1201, 2019.

[29] J. J. de Jong, A. Müller, J. van Dijk, and J. L. Herder. Differentiation-free taylor approximation of finite motion in closed loop kinematics. In

Computational Kinematics. Mechanisms and Machine Science, vol 50. Springer, Cham, volume 50, pages 577–584, 2018.

[30] J. J. de Jong, B. E. M. Schaars, and D. M. Brouwer. The influence of flexibility on the force balance quality: a frequency domain approach. In *Proceedings of the 19th international EUSPEN conference & exhibition*, number June, pages 2–5, 2019.

[31] J. J. de Jong, J. van Dijk, and J. L. Herder. On the Dynamic Equivalence of Planar Mechanisms, an Inertia Decomposition Method. In *New Trends in Mechanism and Machine Science*, volume 408, pages 51–59, 2017.

[32] J. J. de Jong, J. van Dijk, and J. L. Herder. A Screw-Based Dynamic Balancing Approach, Applied to a 5-Bar Mechanism. In J. Lenarcic and J.-P. Merlet, editors, *Advances in Robot Kinematics 2016. Springer Proceedings in Advanced Robotics*, pages 33–41. Springer, Cham, 2018.

[33] J. J. de Jong, J. van Dijk, and J. L. Herder. A screw based methodology for instantaneous dynamic balance. *Mechanism and Machine Theory*, 141:267–282, 2019.

[34] J. J. de Jong, Y. Q. Wu, M. Carricato, and J. L. Herder. A pure-inertia method for dynamic balancing of symmetric planar mechanisms. In *Advances in Robot Kinematics*, volume 5, pages 1–8, 2018.

[35] B. Demeulenaere. *Dynamic balancing of reciprocating machinery with application to weaving machines.* PhD thesis, Katholieke Universiteit Leuven, Belgium, 2004.

[36] B. Demeulenaere, E. Aertbeliën, M. Verschuure, J. Swevers, and J. De Schutter. Ultimate limits for counterweight balancing of crank-rocker four-bar linkages. *Journal of Mechanical Design*, 128(6):1272–1284, 2006.

[37] FANUC. Heavy payload 6 axis robot with very high structural rigidity and a wide envelope for large part handling. `https://www.fanuc.eu/at/en/robots/robot-filter-page/m-900-series`. Accessed: June 2019.

[38] R. Featherstone. *Rigid Body Dynamics Algorithms.* Springer, Boston, MA, US, 2008.

[39] A. A. Ferri. Friction Damping and Isolation Systems. *Journal of Mechanical Design*, 117(B), 1995.

[40] O. Fischer. *Theoretische Grundlagen für eine Mechanik der lebenden Körper.* Teubner, Leipzig, 1906.

[41] S. Foucault and C. M. Gosselin. On the development of a planar 3-DOF reactionless parallel mechanism. *ASME 2002 International Design Engineering Technical Conferences and Computers and Information in Engineering Conference*, pages 1–9, 2002.

[42] C. Gosselin. Gravity compensation, static balancing and dynamic balancing of parallel mechanisms. In *Smart Devices and Machines for Advanced Manufacturing*, pages 27–48. 2008.

[43] C. M. Gosselin. Note sur les conditions d'équilibrage de Berkof et Lowen. In *Congrès Canadien de Mécanique Appliquée*, volume 1, pages 497–498, 1997.

[44] C. M. Gosselin, B. Moore, and J. Schicho. Dynamic balancing of planar

mechanisms using toric geometry. *Journal of Symbolic Computation*, 44(9):1346–1358, Sept. 2009.

[45] C. M. Gosselin and F. Vollmer. Synthesis and design of reactionless three-degree-of-freedom parallel mechanisms. *IEEE Transactions on Robotics and Automation*, 20(2):191–199, 2004.

[46] J. L. Herder. *Energy-free systems: theory, conception, and design of statically balanced spring mechanisms*. PhD thesis, Technische Universiteit Delft, The Netherlands, 2001.

[47] J. L. Herder and C. M. Gosselin. A counter-rotary counterweight (CRCW) for light-weight dynamic balancing. In *Proceedings of ASME DETC*, pages 1–9, 2004.

[48] A. G. L. Hoevenaars, C. M. Gosselin, P. Lambert, and J. L. Herder. A Systematic Approach for the Jacobian Analysis of Parallel Manipulators with Two End-E ff ectors. *Mechanism and Machine Theory*, 109(October 2016):171–194, 2017.

[49] M. L. Husty. An algorithm for solving the direct kinematics of general Stewart-Gough platforms. *Mechanism and Machine Theory*, 31(4), 1996.

[50] M. L. Husty, M. Pfurner, and H. P. Schröcker. A new and efficient algorithm for the inverse kinematics of a general serial 6R manipulator. *Mechanism and Machine Theory*, 42(1):66–81, 2007.

[51] International federation of Robotics. Executive Summary World Robotics 2018 Industrial Robots Robot. Technical report, 2018. `https://ifr.org/downloads/press2018/Executive_Summary_WR_2018_Industrial_Robots.pdf`, Accessed: Dec. 2019.

[52] X. Iriarte, J. Ros, V. Mata, and A. Plaza. Multibody model reduction by parameter elimination. *Proceedings of the ECCOMAS Thematic Conference on Multibody Dynamics 2015, Multibody Dynamics 2015*, 2015.

[53] V. A. Kamenskii. On the problem of the number of counterweights in the balancing of plane linkages. *Journal of Mechanisms*, 3(4):323–333, 1968.

[54] T. Kane and M. Scher. A dynamical explanation of the falling cat phenomenon. *International Journal of Solids and Structures*, 5(7):663–670, 1969.

[55] J. Karidis, G. McVicker, J. Pawletko, L. Zai, M. Goldowsky, R. Brown, and R. Comulada. The Hummingbird minipositioner-providing three-axis motion at 50 g's with low reactions. In *Proceedings 1992 IEEE International Conference on Robotics and Automation*, pages 685–692. IEEE Comput. Soc. Press, 1992.

[56] D. Karnopp. Active and Semi-Active Vibration Isolation. In *Current Advances in Mechanical Design and Production*, pages 409–423, 1996.

[57] R. E. Kaufman and G. N. Sandor. Complete Force Balancing of Spatial Linkages. *Journal of Engineering for Industry*, 93(2):620–626, 1971.

[58] W. Khalil and F. Bennis. Symbolic Calculation of the Base Inertial Parameters of Closed-Loop Robots. *The International Journal of Robotics Research*, 14(2):112–128, 1995.

[59] I. Kochev. General theory of complete shaking moment balancing of

B

planar linkages: a critical review. *Mechanism and Machine Theory*, 35(11):1501–1514, Nov. 2000.

[60] I. S. Kochev. General method for full force balancing of spatial and planar linkages by internal mass redistribution. *Mechanism and Machine Theory*, 22(4):333–341, 1987.

[61] I. S. Kochev. Full shaking moment balancing of planar linkages by a prescribed input speed fluctuation. *Mechanism and Machine Theory*, 25(4):459–466, 1990.

[62] X. Kong and C. M. Gosselin. *Type synthesis of parallel mechanisms*. Springer, Berlin-Heidelberg, 2007.

[63] T. Laliberté and C. M. Gosselin. Synthesis, optimization and experimental validation of reactionless two-DOF parallel mechanisms using counter-mechanisms. *Meccanica*, 51(12):3211–3225, 2016.

[64] A. Lecours and C. M. Gosselin. Reactionless Two-Degree-of-Freedom Planar Parallel Mechanism With Variable Payload. *Journal of Mechanisms and Robotics*, 2(4):041010, 2010.

[65] W. Lewin. Demonstration of a bicycle wheel gyroscope. `https://youtu.be/1fWl2LNpcak`. Accessed: Sept. 2019.

[66] O. Loos. *Symmetric spaces*. Benjamin edition, 1969.

[67] G. G. Lowen and R. S. Berkof. Survey of investigations into the balancing of linkages. *Journal of Mechanisms*, 3(4):221–231, 1969.

[68] G. G. Lowen, F. R. Tepper, and R. S. Berkof. Balancing of linkages—an update. *Mechanism and Machine Theory*, 18(3):213–220, 1983.

[69] T. W. Ma. Higher chain formula proved by combinatorics. *Electronic Journal of Combinatorics*, 16(1):1–7, 2009.

[70] D. G. Manzer, J. P. Karidis, K. M. Wiley, D. C. Bruen, C. W. Cline, C. Hendricks, R. N. Wiggin, and Y.-Y. Yu. High-speed electrical testing of multichip ceramic modules. *IBM Journal of Research and Development*, 49(4.5):687–697, 2005.

[71] A. Martini, M. Troncossi, and A. Rivola. Elastodynamic effects of mass-balancing: Experimental investigation of a four-bar linkage. *Advances in Mechanical Engineering*, 2013, 2013.

[72] J. P. Meijaard and V. van der Wijk. On the Dynamic Balance of a Planar Four-Bar Mechanism with a Flexible Coupler. In *Advances in Mechanism and Machine Science*, volume 73, pages 2611–2620, 2019.

[73] H. F. Menschaar, A. B. G. Ariens, J. L. Herder, and B. M. Bakker. Five-bar mechanism with dynamic balancing means and method for dynamically balancing a five-bar mechanism, 2006. WO2006080846.

[74] B. Moore and J. Schicho. Two methods for force balancing of Bennett linkages. *Computational Kinematics*, 2009.

[75] B. Moore, J. Schicho, and C. M. Gosselin. Determination of the complete set of shaking force and shaking moment balanced planar four-bar linkages. *Mechanism and Machine Theory*, 44(7):1338–1347, July 2009.

[76] B. Moore, J. Schicho, and C. M. Gosselin. Dynamic balancing of spherical

4R linkages. *Journal of Mechanisms and Robotics*, 2(2):021002, 2010.

[77] A. Müller. Higher derivatives of the kinematic mapping and some applications. *Mechanism and Machine Theory*, 76:70–85, June 2014.

[78] A. Müller. Recursive higher-order constraints for linkages with lower kinematic pairs. *Mechanism and Machine Theory*, 100(April):33–43, June 2016.

[79] A. Müller. An overview of formulae for the higher-order kinematics of lower-pair chains with applications in robotics and mechanism theory. *Mechanism and Machine Theory*, 142:103594, 2019.

[80] R. M. Murray, Z. Li, and S. S. Sastry. *A Mathematical Introduction to Robotic Manipulation*. Boca Raton, FL., CRC Press edition, 1994.

[81] K. Nanos and E. Papadopoulos. On the use of free-floating space robots in the presence of angular momentum. *Intelligent Service Robotics*, 4(1):3–15, Dec. 2010.

[82] G. S. Natal, A. Chemori, and F. Pierrot. Dual-space control of extremely fast parallel manipulators: Payload changes and the 100G experiment. *IEEE Transactions on Control Systems Technology*, 23(4):1520–1535, 2015.

[83] P. Ouyang, Q. Li, and W. Zhang. Integrated design of robotic mechanisms for force balancing and trajectory tracking. *Mechatronics*, 13(8-9):887–905, Oct. 2003.

[84] E. Papadopoulos and A. Abu-Abed. Design and motion planning for a zero-reaction manipulator. *Proceedings of the 1994 IEEE International Conference on Robotics and Automation*, 7:1554–1559, 1994.

[85] G. R. Pennock and P. J. Meehan. Geometric Insight Into the Dynamics of a Rigid Body Using the Spatial Triangle of Screws. *Journal of Mechanical Design*, 124(4):684–689, 2002.

[86] R. Ricard and C. M. Gosselin. On the development of reactionless parallel manipulators. In *ASME 2000 Design Engineering Technical Conferences and Computers and Information in Engineering Conference*, volume 1, pages 1–10, Baltimore, Maryland, 2000.

[87] J. Rico, J. Gallardo, and J. Duffy. Screw theory and higher order kinematic analysis of open serial and closed chains. *Mechanism and Machine Theory*, 34(4):559–586, 1999.

[88] J. Ros, X. Iriarte, and V. Mata. 3D inertia transfer concept and symbolic determination of the base inertial parameters. *Mechanism and Machine Theory*, 49:284–297, 2012.

[89] E. J. Routh. *No An elementary treatise on the dynamics of a system of rigid bodies*. Macmillan, London, UK, 1877.

[90] J. Selig. Applying screw theory to robot dynamics. *Journal of Applied Mathematics and Mechanics*, 55(3):159–167, 1991.

[91] J. M. Selig and D. Martins. On the line geometry of rigid-body inertia. *Acta Mechanica*, 225(11):3073–3101, 2014.

[92] M. R. Smith and L. Maundert. Inertia forces in a four-bar linkage. *Journal of Mechanical Engineering Science*, 9(3):218–225, 1967.

[93] F. R. Tepper and G. G. Lowen. General Theorems Concerning Full Force Balancing of Planar Linkages by Internal Mass Redistribution. *Journal of Engineering for Industry*, 94(3):789–796, 1972.

[94] D. Tjepkema. *Active hard mount vibration isolation for precision equipment*. PhD thesis, University of Twente, The Netherlands, 2012.

[95] L. B. van de Ridder. *Vibration isolation for Coriolis mass-flow meters*. PhD thesis, University of Twente, The Netherlands, 2015.

[96] V. van der Wijk. Shaking-moment balancing of mechanisms with principal vectors and momentum. *Frontiers of Mechanical Engineering*, 8(1):10–16, Jan. 2013.

[97] V. van der Wijk. *Methodology for analysis and synthesis of inherently force and moment-balanced mechanisms - theory and applications*. PhD thesis, University of Twente, The Netherlands, 2014.

[98] V. van der Wijk. Mass equivalent dyads. *Recent Advances in Mechanism Design for Robotics, Mechanisms and Machine Science*, 33:35–45, 2015.

[99] V. van der Wijk. Mass equivalent triads. In *The 14th IFToMM World Congress, Taipei, Taiwan*, 2015.

[100] V. van der Wijk. On the grand 4R four-bar based inherently balanced linkage architecture. In *New Trends in Mechanism and Machine Science*, volume 7, pages 473–480, 2017.

[101] V. van der Wijk. Inherently Balanced Double Bennett Linkage. In *Computational Kinematics 2017.*, pages 1–8, 2018.

[102] V. van der Wijk. Spatial Orientations of Principal Vector Planes for Inherent Dynamic Balancing. In *Lenarcic J., Parenti-Castelli V. (eds) Advances in Robot Kinematics 2018. ARK 2018. Springer Proceedings in Advanced Robotics, vol 8. Springer, Cham*, pages 302–309, 2019.

[103] V. van der Wijk and J. L. Herder. Force balancing of variable payload by active force-balanced reconfiguration of the mechanism. In *ASME/IFToMM International Conference on Reconfigurable Mechanism and Robots, London*, pages 323–330, 2009.

[104] V. van der Wijk and J. L. Herder. Guidelines for low mass and low inertia dynamic balancing of mechanisms and robotics. In *Advances in Robotics Research*, pages 21–30. Springer, 2009.

[105] V. van der Wijk and J. L. Herder. Active dynamic balancing unit for controlled shaking force and shaking moment balancing. In *Proceedings of the ASME 2010 IDETC/CIE, Montreal ,Quebec, Canada*, 2010.

[106] V. van der Wijk and J. L. Herder. Dynamic balancing of a single crank-double slider mechanism with symmetrically moving couplers. In C. B. isla D., Ceccarelli M., Husty M., editor, *New Trends in Mechanism Science. Mechanisms and Machine Science*, number Vol 5, pages 413–420. 2010.

[107] V. van der Wijk and J. L. Herder. Synthesis method for linkages with center of mass at invariant link point — Pantograph based mechanisms. *Mechanism and Machine Theory*, 48:15–28, Oct. 2011.

[108] V. van der Wijk, J. L. Herder, and B. Demeulenaere. Comparison of

Various Dynamic Balancing Principles Regarding Additional Mass and Additional Inertia. *Journal of Mechanisms and Robotics*, 1(4):041006, 2009.

[109] V. van der Wijk, S. Krut, F. Pierrot, and J. L. Herder. Design and experimental evaluation of a dynamically balanced redundant planar 4-RRR parallel manipulator. *The International Journal of Robotics Research*, 32(6):744–759, June 2013.

[110] Verein Deutscher Ingenieure. Getriebedynamik Starrkörper-Mechanism (Transmission dynamics rigid body mechanisms). Technical Report October, 2008.

[111] M. Verschuure, B. Demeulenaere, E. Aertbeliën, J. Swevers, and J. De Schutter. Optimal counterweight balancing of spatial mechanisms using voxel-based discretizations. In *Proceedings - ISMA International Conference on Noise and Vibration Engineering*, pages 2159–2174, 2008.

[112] W. J. Vetter. Matrix Calculus Operations and Taylor Expansions. *Society for Industrial and Applied Mathematics*, 15(2):352–369, 1973.

[113] M. J. Walker and R. S. Haines. An experimental study of the effects of counterweights on a six-bar chain. *Mechanism and Machine Theory*, 17(6):355–360, 1982.

[114] M. J. Walker and K. Oldham. A general theory of force balancing using counterweights. *Mechanism and Machine Theory*, 13(2):175–185, 1978.

[115] P. M. Wensing, G. Niemeyer, and J.-J. E. Slotine. Observability in Inertial Parameter Identification. 2017.

[116] J. Wiederrich and B. Roth. Momentum Balancing of Four-Bar Linkages. *Journal of Engineering for Industry*, 98(4):1289–1295, 1976.

[117] K. Wohlhart. Degrees of shakiness. *Mechanism and Machine Theory*, 34(7):1103–1126, 1999.

[118] K. Wohlhart. From higher degrees of shakiness to mobility. *Mechanism and Machine Theory*, 45(3):467–476, Mar. 2010.

[119] A. Wright. Pauli and Bohr watch a spinning top. `https://www.nature.com/milestones/milespin/images/milespin03-i1.jpg`, 2008. Accessed: Aug. 2019.

[120] Y. Wu and C. M. Gosselin. Synthesis of Reactionless Spatial 3-DoF and 6-DoF Mechanisms without Separate Counter-Rotations. *The International Journal of Robotics Research*, 23(6):625–642, June 2004.

[121] Y. Q. Wu and M. Carricato. Symmetric Subspace Motion Generators. *IEEE Transactions on Robotics*, 34(3):716–735, 2018.

[122] Y. Q. Wu, H. Löwe, M. Carricato, and Z. Li. Inversion Symmetry of the Euclidean Group: Theory and Application to Robot Kinematics. *IEEE Transactions on Robotics*, 32(2):312–326, 2016.

[123] F. Xi and R. Sinatra. Effect of dynamic balancing on four-bar linkage vibrations. *Mechanism and Machine Theory*, 32(6):715–728, 1997.

[124] J. Yao and M. R. Smith. An improved complex mass method for force balancing of planar linkages. *Mechanism and Machine Theory*, 28(3):417–425, 1993.

[125] Z. Ye and M. Smith. Complete balancing of planar linkages by an equivalence method. *Mechanism and Machine Theory*, 29(5):701–712, July 1994.

[126] K. Yoshida, K. Hashizume, and S. Abiko. Zero reaction maneuver: flight validation with ETS-VII space robot and extension to kinematically redundant arm. In *International Conference on Robotics and Automation, Seoul, Korea*, pages 441–446, 2001.

[127] Y. Q. Yu. Research on Complete Shaking Force and Shaking Moment Balancing of Spatial Linkages. *Mechanism and Machine Theory*, 22(I):27–37, 1987.

[128] Y.-Q. Yu and B. Jiang. Analytical and experimental study on the dynamic balancing of flexible mechanisms. *Mechanism and Machine Theory*, 42(5):626–635, May 2007.

[129] M. Zoppi, D. Zlatanov, and R. Molfino. On the velocity analysis of interconnected chains mechanisms. *Mechanism and Machine Theory*, 41(11):1346–1358, Nov. 2006.

B

Scientific output

The following work has been published in the context of dynamic balance research:

Journal publications

J. J. de Jong, A. Müller, J. L. Herder, Higher-order Taylor approximation of finite motions in mechanisms. *Robotica* (2019) vol. 37 (7), pp. 1190-1201

J. J. de Jong, J. van Dijk, J. L. Herder, A screw based methodology for instantaneous dynamic balance. *Mechanism and Machine Theory* (2019), vol. 141, pp. 267-282.

J. J. de Jong, A. Müller, J. L. Herder, Higher-order derivatives of rigid body dynamics with application to dynamic balance. Submitted to *Mechanism and machine theory*.

Conference publications

J. J. de Jong, J. L. Herder, A comparison between five principle strategies for adapting shaking force balance during varying payload. In *Proceedings of the 14th IFToMM World Congress*, (2015) 446-454 .

J. J. de Jong, J. van Dijk, J. L. Herder, A screw-based dynamic balancing approach, applied to a 5-bar mechanism. In *Advances in Robot Kinematics* (2016), pp. 33-41.

J. J. de Jong, J. van Dijk, J. L. Herder, On the dynamic equivalence of planar mechanisms, an inertia decomposition method. In *New Trends in Mechanism and Machine Science* (2017), vol. 408, pp. 51-59.

J. J. de Jong, A. Müller, J. van Dijk, J. L. Herder, Differentiation-free Taylor approximation of finite motion in closed loop kinematics. In *Computational Kinematics. Mechanisms and Machine Science* (2018), vol. 50, pp. 577-584.

J. J. de Jong, Y. Wu, M. Carricato, J. L. Herder, A pure-inertia method for dynamic balancing of symmetric planar mechanisms. In *Advances in Robot Kinematics* (2018), vol. 5. pp.1-8.

J. J. de Jong, J.P. Meijaard, V. van der Wijk, The influence of partial force balancing on the shaking moments, contact forces, and precision of a Delta robot-like manipulator in a compliant frame. In *Proceedings of the ASME IDETC/CIE* (2018), V05BT07A026.

J. J. de Jong, B. E. M. Schaars, D. M. Brouwer, The influence of flexibility on the force balance quality: a frequency domain approach. In *Proceedings of the 19th EUSPEN International Conference & Exhibition*, (2019), pp. 546-549.

Dankwoord

Now this is not the end. It is not even the beginning of the end. But it is, perhaps, the end of the beginning.

— Winston Churchill, *November 1942*[1]

Voor u ligt een boekje waaruit de bekwaamheid van een zelfstandig onderzoeker zou moeten blijken. Een zelfstandig onderzoeker is echter zeker niet hetzelfde als een alleenstandig onderzoeker. Er zijn namelijk tamelijk veel mensen betrokken geweest bij de totstandkoming van dit boekje, daarvan wil ik er sommigen speciaal bedanken.

In de eerste plaats mijn protoren: Just en Volkert, dank voor de mogelijkheid om aan dit onderzoek te beginnen en Dannis, bedankt dat ik het[2] kon afmaken. Ondanks de organisatorische, persoonlijke en financiële stormen rondom dit project, hebben jullie een luwte gecreëerd waarin dit onderzoek in relatieve rust kon plaatsvinden. Just, ik wil je bedanken voor de ontspannen en stimulerende begeleiding en schrandere observaties. Volkert, dank voor je enthousiasme, creatieve geest en de aansporing om door te gaan; je bent zelf een taaie tiller. Dannis, het is erg leuk om te zien hoe je dingen terugbrengt tot de essentie, de rest laat vallen en van daaruit nieuwe dingen gaat opbouwen, dat is erg leerzaam. Johannes, helaas was je me te vlug af, maar als oud-begeleider hoor jij ook thuis in dit rijtje. Behalve een hoop control heb ik ook geleerd dat krachttermen, naast de Newtoniaanse, nog een heel andere toepassing kennen.

Graag zou ik ook enkelen speciaal willen bedanken voor hun bijdragen aan dit proefschrift. I wish to thank Andreas for his support of this research by guiding me through the dark waters of the higher-order differential kinematics and dynamics. Marco and Troy, many thanks for hosting us in *la grassa*, *la rossa* and, perhaps most importantly, *la dotta*. Thanks for your insights into symmetric mechanisms and questioning some very basic and essential questions, which led to two chapters in this thesis. Marcel, hartelijk dank voor het doorvragen, totdat jij weet dat ik begrijp wat andere mensen niet begrijpen als ik het uitleg zoals ik het uitleg wat jij toch al snapte, zoiets. Er is veel liefde voor de wetenschap en een open geest nodig om zo door taaie stof heen te bijten.

Dank ook voor de studenten waarmee ik afgelopen jaren samen mocht werken. Vinayak, Lennart, Gregorio, Arjan, Teun, Hans, Bram, Arjan, Adriaan,

[1] Een proefschrift is niet compleet zonder één quote, een beetje een misplaatste in dit geval.
[2] De 'balansonzin'.

Patrick, Wijnand, Koen, Florian en Adriaan, ik hoop dat het net zo leuk en leerzaam was voor jullie als voor mij.

Ook mijn (oud-) kamergenoten: Bert, Ger, Marijn, Mark, Tschiersky (de illustere M^3), Luis, Iqbal, de collega's van BW, WA, TM, PE en DEMCON: Wessels, Fluit, Kostas, Arvid, Alex, Bob, Jaap, Ronald, Gert-willem, Wouter, Koen, Hakan, Jos, Jurnan, Boukje, Matthias, Nia, Leo, Axel, Debbie, Martina, Rick, Sytze, Arnoud, Peter en niet te vergeten het BW/BSS voetbalteam waar ik als spion aan mee mocht doen, wil ik bedanken. Zonder jullie geleuter, gezeur, gebrul, geregel, gerammel, gelunch, geroddel, en getreuzel, zonder de koffiepauzes, sportpauzes en LEGO-pauzes, zonder de vrijdagmiddag-, donderdagmiddag- en andere middagborrels was het ongetwijfeld een stroeve en droeve bedoening geweest.

Vrienden en familie, volgens mij wisten jullie niet echt wat ik al die jaren daar op de UT uitspookte, niet omdat het top-secret was maar omdat ik er niets over vertelde. Nu hebben jullie het boekje en kunnen jullie het zelf lezen, succes. Ik ben erg blij en dankbaar voor de steun en de afleiding van afgelopen tijd, bijvoorbeeld onbenullig hard een pukkel op fietsen en om dan vervolgens te moe te zijn voor de volgende, of twee biertjes drinken en dan de volgende dag brak zijn omdat we gewoon burgers zijn, wat ook wel weer erg fijn is. Albert, nog speciaal bedankt voor de omslag, je stuurt nog de rekening hè? Molletjes, pappa (ik weet dat u erbij bent) mamma, Marijke en Klaas, Fedde, Reitse en Janneke en al het jonge gespuis, dank voor gewoon alles.

Uiteindelijke komt het allemaal terug bij het lieve thuisfront. Sarie, je hebt nu nog geen idee hoe fijn het is om weer bij jou thuis te komen. Annelies, dank dat je me bij elkaar houdt en soms weer in elkaar zet, jij weet hoe het past. Zonder jou was dit nooit gelukt.

Base vibrations are detrimental to the precision of high-speed robots. When a robot accelerates it induces opposing reaction forces and moments on the supporting base frame. The frame will deflect, vibrate and transmit these vibrations to the robot's end-effector, the floor and the equipment in the surroundings.

Dynamic balancing targets these disruptive vibrations by a specific design of the moving links, such that the reaction forces and moments become constant. As a consequence, the robot will induce no, or limited, vibrations in the base frame, improving the performance of both the robot and the systems in the vicinity. Parallel mechanisms are especially suited for dynamic balance, in comparison to their serial counterparts, as they permit more simple, light-weight and economically viable solutions. However, their kinematic and dynamic models are also more complex, which impedes a straightforward solution. Moreover, current systematic approaches are either not applicable to spatial mechanisms with multiple degrees of freedom or do not yield all possible solutions.

This thesis presents three screw theory based methods to systematically determine the complete dynamic balance solution for arbitrary, nonsingular mechanisms with lower kinematic pairs. Based on these methods three novel robot designs are presented, demonstrating that the dynamic balance of spatially moving parallel robots is within reach.

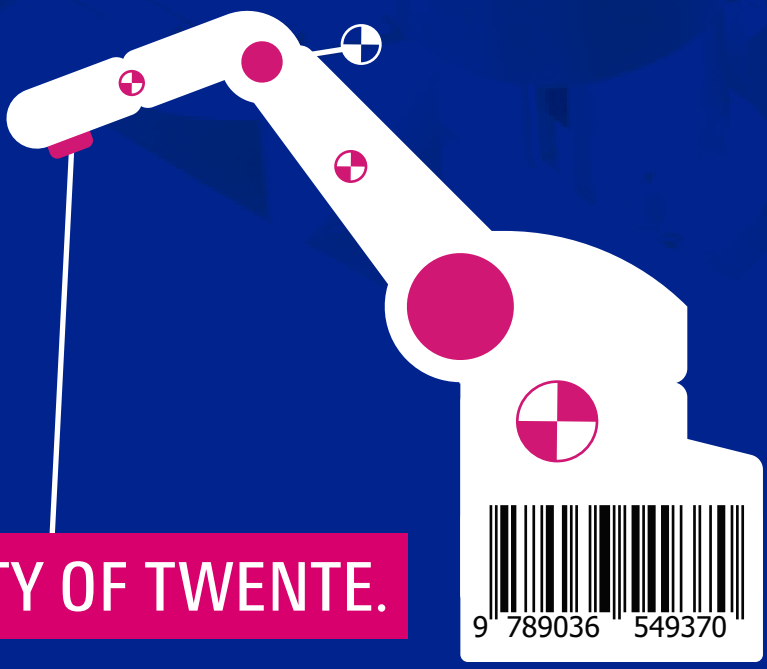

UNIVERSITY OF TWENTE.

9 789036 549370